THE ROLE OF ARID1A IN ENDOMETRIOSIS-RELATED INFERTILITY

By

Ryan Michael Marquardt

A DISSERTATION

Submitted to
Michigan State University
in partial fulfillment of the requirements
for the degree of

Cell and Molecular Biology —Doctor of Philosophy

2022

PUBLIC ABSTRACT

THE ROLE OF ARID1A IN ENDOMETRIOSIS-RELATED INFERTILITY

By

Ryan Michael Marquardt

Endometriosis occurs when endometrium-like tissue, normally limited to the inner lining of the uterus, forms lesions outside the uterus. This condition afflicts about 1-in-10 women of reproductive age and frequently causes severe pain and difficulty conceiving. Many cases of endometriosis-related infertility implicate endometrial dysfunction as the cause. The endometrium is composed of distinct epithelial and stromal cell types that coordinate to maintain endometrial homeostasis and prepare a receptive window for embryo implantation. However, endometriosis-related infertility is associated with dysregulation of epigenetic factors such as ARID1A that impairs endometrial function. ARID1A expression is decreased in endometrial tissue samples from infertile women with endometriosis, and past research in mice demonstrates that endometrial ARID1A loss causes infertility. This dissertation evaluates the contribution of ARID1A loss to endometriosis-related infertility by studying its roles in lesion development and in causing a non-receptive endometrium. Using genetically engineered mice, a non-human primate model of endometriosis, and endometrial samples from infertile women with endometriosis, the studies in this dissertation show that ARID1A loss contributes to endometriosis-related infertility by exacerbating endometriotic lesion formation, causing endometrial gland dysfunction, and precipitating extraordinary uterine inflammation during early pregnancy.

ABSTRACT

THE ROLE OF ARID1A IN ENDOMETRIOSIS-RELATED INFERTILITY

By

Ryan Michael Marquardt

The inner lining of the uterus, the endometrium, is composed of a luminal epithelial cell layer supported by an underlying stroma which contains epithelial gland structures. These distinct cell types coordinate with complex and dynamic molecular crosstalk tightly controlled by ovarian steroid hormones to regulate a healthy menstrual cycle and support the initiation and maintenance of a healthy pregnancy. Endometriosis occurs when endometrium-like tissue forms lesions outside the uterine cavity, and this painful disease afflicts about 10% of reproductive-age women, an estimated 176 million worldwide. Up to 50% of these individuals also experience infertility, and many cases cannot be explained by morphological or ovarian defects, which implicates a uterine environment that is non-receptive to embryo implantation. The molecular basis for the correlation between endometriotic lesion presence and a non-receptive endometrium is unclear, but available evidence suggests that dysregulation of epigenetic regulators may play a role. Expression of AT-rich interaction domain 1A (ARID1A), a chromatin remodeling factor, is lost in some endometriotic lesions and markedly reduced in endometrial biopsies from infertile women with endometriosis, but it is essential in the uterus for fertility. This dissertation evaluates the overarching hypothesis that ARID1A loss connects endometriosis and infertility by causing increased lesion development and a non-receptive endometrium. Chapter 1 provides a review of the current literature on the topics of normal ovarian steroid hormone regulation of endometrial function, the dysregulation that occurs in endometriosis with its clinical implications and therapeutic options, and the specific involvement of ARID1A in endometrial pathophysiology.

Chapter 2 delineates a critical role for endometrial epithelial ARID1A in uterine gland function for fertility. Chapter 3 reports the need for endometrial epithelial ARID1A to maintain uterine immune homeostasis during early pregnancy. Chapter 4 explores the involvement of endometrial ARID1A loss in a mouse model of endometriosis-related infertility. Chapter 5 describes a method for in vivo photoacoustic imaging of this endometriosis mouse model through the application of nanoparticle labeling. Finally, Chapter 6 summarizes the findings, discusses conclusions from the synthesized data in the context of the current literature, and provides ideas for future studies of related topics. Together, the studies herein make the case that endometrial ARID1A loss contributes to endometriosis-related infertility by exacerbating endometriotic lesion formation and compromising the ability of the endometrium to maintain the gland function and immune homeostasis necessary for the establishment and maintenance of pregnancy. Continued investigation through studies like these is key to understanding endometrial pathophysiology at the molecular level in order to enable development of targeted treatment options for women suffering the devastating effects of endometriosis and related infertility.

ACKNOWLEDGEMENTS

No one else in my professional life has had more of an impact on my success in this dissertation work than my mentor, Dr. Jae-Wook Jeong. I want to thank him for training me on the whole spectrum of what it means to do academic science: designing experiments, analyzing data, grantsmanship, peer review, navigating the field of reproductive biology, and the list goes on. I have grown immensely in these areas during my PhD training, and most of it is due to his patience and diligence in committing the time and attention necessary to mentor me. I am grateful to Dr. Jeong for giving me the opportunity to contribute to an incredibly interesting and worthwhile project, for pushing me to work hard, and for being understanding and flexible with my family responsibilities. I could not be where I am today without his encouragement and generosity in securing funding for the project as well as promoting my work to others in the field.

In addition to Dr. Jeong's grants from the Eunice Kennedy Shriver National Institute of Child Health & Human Development (NICHD R01HD084478 and R01HD101243), the work in this dissertation was also funded by a Ruth L. Kirschstein Predoctoral Individual National Research Service Award (NICHD F31HD101207), the Michigan State University (MSU) Reproductive and Developmental Sciences Training Program (RDSP; NICHD T32HD087166), MSU AgBio Research, and Michigan State University. I thank all these funding sources and the taxpayers who funded their budgets.

The colleagues I worked with in the lab were nothing short of critical to my success. No one was more helpful in teaching me techniques, covering for me on lab work, and solving problems for me than Dr. Tae Hoon Kim, Assistant Professor in Dr. Jeong's lab and co-author on all the studies in this dissertation. Tae Hoon was always happy to answer my questions or check

on my mice even though he was usually busier than me, and I could not be more grateful. I also want to thank the other lab members who helped with experiments, genotyping, tech support, and giving feedback on my work at various points in my time at MSU including Hanna Teasley, Hak Hyun Ka, Brandon Lee, Yeon Jeong Hwang, Gi-Jun Sung, Dinh Nam Tran, Ji Yeon Ahn, Krystina Dunston, and Harriet Omenge (and Erin Vegter and Samantha Hrbek in Dr. Asgi Fazleabas's lab).

I want to give special thanks also to my guidance committee members Drs. Asgi Fazleabas, Margaret Petroff, John Risinger, and David Arnosti, who each contributed their unique expertise and devoted their precious time to ensure my success as a PhD student. I especially want to highlight Dr. Fazleabas's contribution to my success as a close research collaborator and co-sponsor to my NIH F31 fellowship and Dr. Petroff's additional contributions as a research collaborator and as Director of the Cell and Molecular Biology (CMB) program at the time of my completion. I also thank the many other research collaborators inside MSU and outside who have contributed to my research including Drs. Ripla Arora, Taeho Kim, Md Nafiyjjaman, Ron Chandler, Jake Reske, Soo Hyun Ahn, Bruce Lessey (Wake Forest), Steven Young (University of North Carolina), Tom Spencer (University of Missouri), and Franco DeMayo (NIEHS).

Additionally, I want to thank the others in CMB who have helped me along the way including Dr. Susan Conrad, Director when I entered the program, Alaina Burghart, essential administrative guru, and the students who make up the CMB Graduate Student Organization. I am incredibly thankful to the MSU Department of Obstetrics, Gynecology and Reproductive Biology for being my department home and giving financial support along the way. In addition to committee members already named, I owe a debt of gratitude to Dr. Rick Leach, Harmony Van Valkenberg, Amanda Sterling, Jenna French, and all the other faculty and trainees who gave their support during my time in the department.

I would be remiss not to mention the RDSP program, co-directed by Dr. Fazleabas and Dr. Keith Latham, for all the opportunities it opened for training and growth in addition to the funding it provided. Thank you to the MSU Broadening Experiences in Scientific Training (BEST) program led by Drs. Julie Rojewski and Stephanie Watts, together with my externship hosts Erin Gorman at Health Colleges Research Services and Dr. Stephanie Ogren at Grand Rapids Public Museum, for allowing me the opportunity to explore careers both inside and outside academia and gain unique training experiences. Thank you to the MSU BioMolecular Science program and Director Dr. John LaPres for admitting me to MSU in the first place, funding my first year, and getting me set up with my classes and rotation labs. Thank you also to my undergraduate mentors Drs. Kaleb Pauley and Heather Kuruvilla at Cedarville University and Dr. Steven Crone at Cincinnati Children's Hospital for giving me the chance to experience research early as a student and supporting me in my pursuit of graduate studies. And thank you to the Society for the Study of Reproduction and the Society for Reproductive Investigation for giving me opportunities to present my work to the field, volunteer, and win trainee research awards.

None of this work would have been possible without the love and constant support of my family. I cannot begin to describe my gratitude for my lovely wife Brianna, four adorable and crazy kids (three of whom were born during my PhD training!), and faithful parents, who have each in their unique way grounded me, covered for me, and encouraged me through this work and training. And finally, my church family at Calvary Baptist has uniquely provided a larger community of support and displayed the abundant love of Jesus to me. I want to end by thanking Him, the Creator and Ruler of the biological processes I get to study, the One who gives me the gifts, abilities, and opportunities to do the work, and the Savior who created new life in me. I am a blessed man.

TABLE OF CONTENTS

LIST OF TABLES

LIST OF FIGURES

KEY TO ABBREVIATIONS

17βHSD2	17β-hydroxysteroid dehydrogenase type 2
ACK	Ammonium-chloride-potassium
AKT	Protein Kinase B
ANOVA	Analysis of variance
APTES	3- aminopropyltriethoxysilane
AREG	Amphiregulin
ARID1A	AT-rich interaction domain 1A
$AuCl_3$	Gold(III) chloride
BAF	BRG1-associated factors
BCL6	B cell CLL/lymphoma 6
BDNF	Brain-derived neurotrophic factor
BMP2	Bone morphogenetic protein 2
C/EBPβ	CCAAT enhancer binding protein beta
c-MYC	Myc proto-oncogene protein
C3	Complement component 3
CCDC170	Coiled-coil domain containing 170
CCL2	Monocyte chemoattractant protein-1; MCP-1
CCND1	Cyclin D1
CCR2	C-C motif chemokine receptor 2
CCR4	C-C motif chemokine receptor 4
CD11b	Cluster of differentiation molecule 11B

CD24	Cluster of differentiation 24
CD64	Cluster of differentiation 64
CDH1	Cadherin 1; E-CAD; E-cadherin
CDKN2B-AS1	LncRNA cyclin-dependent kinase inhibitor 2B antisense RNA 1
cDNA	Complementary DNA
ChIP	Chromatin immunoprecipitation
ChIP-seq	ChIP followed by sequencing
Clca3	Chloride channel accessory 3
COC	Combined oral contraceptive
COUP-TFII	Chicken ovalbumin upstream promoter-transcription factor II; NR2F2
COX-2	Cyclooxygenase-II
CRISPLD2	Cysteine rich secretory protein LCCL domain containing 2
CSF2	Colony-stimulating factor 2
CSF3	Colony-stimulating factor 3
CTAB	Hexadecyltrimethylammonium bromide
CXCL15	Chemokine (C-X-C motif) ligand 15
DAB	Diaminobenzidine
DBA	Dolichos biflorus
DEG	Differentially expressed gene
DIO2	Iodothyronine deiodinase 2
DNA	Deoxyribonucleic acid
DNG	Dienogest
E2	Estrogen; estradiol

EGR1	Early growth response 1
ELISA	Enzyme-linked immunosorbent assay
ERK	Extracellular signal-regulated kinase
ESR1	Estrogen receptor 1; ERα
ESR2	Estrogen receptor 2; ERβ
EZH2	Enhancer of zeste homolog 2
F4/80	EGF-like module-containing mucin-like hormone receptor-like 1
FBS	Fetal bovine serum
FDR	False discovery rate
FGF	Fibroblast growth factor
FGF-9	Fibroblast growth factor 9
FITC	Fluorescein isothiocyanate
FKBP52	FK506 binding protein prolyl isomerase 4
FN1	Fibronectin 1
FOXA2	Forkhead box A2
FOXO1	Forkhead box O1
FSHB	Follicle stimulating hormone subunit beta
G2	Gap 2
GAPDH	Glyceraldehyde-3-phosphate dehydrogenase
GATA2	GATA binding protein 2
GD	Gestation day
GEO	Gene Expression Omnibus
GLI1	Glioma-associated oncogene homolog 1

GnRH	Gonadotropin-releasing hormone
Gp130	Glycoprotein 130
GREB1	Growth regulating estrogen receptor binding 1
H&E	Hematoxylin and eosin
HAND2	Heart and neural crest derivatives expressed 2
Hb	Deoxyhemoglobin
HbO2	Oxyhemoglobin
HBSS	Hanks' balanced salt solution
HCL	Hydrochloric acid
HDAC3	Histone deacetylase 3
HIF1A	Hypoxia-inducible factor 1-alpha
HOXA10	Homeobox protein-A10
I-IS	Inter-implantation site
IACUC	Institutional Animal Care and Use Committees
ID4	Inhibitor of DNA binding 4
IFNG	Interferon gamma
IGFBP1	Insulin-like growth factor binding protein 1
IHC	Immunohistochemistry; immunohistochemical
IHH	Indian hedgehog
IHW	Independent hypothesis weighting
IgG	Immunoglobulin G
IL-6	Interleukin 6
IL-10	Interleukin 10

IL10RA	Interleukin 10 receptor
IL18	Interleukin 18
IL17A	Interleukin 17A
IL17RB	Interleukin 17 receptor B
IL36A	Interleukin 36 alpha
IL1A	Interleukin 1 alpha
IL1B	Interleukin 1 beta
IP	Immunoprecipitation
IPA	Ingenuity Pathway Analysis
IS	Implantation site
JAK	Janus kinase
KLF15	Kruppel-like factor 15
KLRA7	Killer cell lectin-like receptor 7
LIF	Leukemia inhibitory factor
LIFR	LIF receptor
LPM	Large peritoneal macrophages
LRP2	Low density lipoprotein-related protein 2
LTF	Lactoferrin; lactotransferrin
Ly6C	Lymphocyte antigen 6C
M	Mitotic
MAPK	Mitogen-activated protein kinase
MHCII	Major histocompatibility complex class II
MIG-6	Mitogen-inducible gene 6

MMLV	Moloney murine leukemia virus
MPA	Medroxyprogesterone acetate
mRNA	Messenger RNA
miR	microRNA
MSOT	Multispectral optoacoustic tomographic imaging
MUC1	Mucin 1
$NaBH_4$	Sodium borohydride
NAIP1	NLR family, apoptosis inhibitory protein 1
NaOH	Sodium hydroxide
NGF	Nerve growth factor
NGS	Normal goat serum
NIR	Near-infrared
NOTCH1	Notch homolog 1
OCT	Optimal cutting temperature
P4	Progesterone
PA	Photoacoustic
PBS	Phosphate buffered saline
PCA	Principal component analysis
PCR	Polymerase chain reaction
PGE2	Prostaglandin E2
PGR	Progesterone receptor
PIAS3	Protein inhibitor of activated STAT3
PI3K	Phosphoinositide 3-kinase

PLZF	Promyelocytic leukaemia zinc finger protein
PR-A	Progesterone receptor A
PR-B	Progesterone receptor B
PRKO	Progesterone receptor knockout
pSTAT3	Phosphorylated STAT3
qPCR	Quantitative PCR
RCT	Randomized controlled trial
RERG	Ras-like, estrogen-regulated, growth inhibitor
RMA	Robust multi-array average
RNA	Ribonucleic acid
RNA-seq	RNA sequencing
RPL7	Ribosomal protein L7
RT-qPCR	Quantitative reverse transcription PCR
SCARA5	Scavenger receptor class A member 5
SEM	Standard error of mean
SERM	Selective estrogen receptor modulator
SIRT1	Sirtuin 1
SLIT3	Slit guidance ligand 3
SNP	Single-nucleotide polymorphism
SO_2	Oxygen saturation
SOX17	Sex determining region Y box 17
SPINK3	Serine protease inhibitor Kazal type 3 gene
SPM	Small peritoneal macrophages

SPRM	Selective progesterone receptor modulators
SRC	Steroid receptor coactivator
SRC-1	Steroid receptor coactivator 1
SRC-2	Steroid receptor coactivator 2
SRC-3	Steroid receptor coactivator 3
STAT3	Signal transducer and activator of transcription 3
SWI/SNF	SWItch/sucrose Non-Fermentable
SYNE1	Spectrin repeat containing nuclear envelope protein 1
TEM	Transmission electron microscopy
TEOS	Tetraethyl orthosilicate
TNF	Tumor necrosis factor
TNFα	Tumor necrosis factor alpha
TNFSF13B	Tumor necrosis factor ligand superfamily member 13B
TRPV1	Transient receptor potential cation channel subfamily V member 1
uDC	Uterine dendritic cell
uNK	Uterine natural killer cell
VEGF	Vascular endothelial growth factor
Veh	Vehicle
VEZT	Vezatin
WNT4	Wnt family member 4

CHAPTER 1

INTRODUCTION

1.1 Abstract

In the healthy endometrium, progesterone and estrogen signaling coordinate in a tightly regulated, dynamic interplay to drive a normal menstrual cycle and promote an embryo-receptive state to allow implantation during the window of receptivity. It is well-established that progesterone and estrogen act primarily through their cognate receptors to set off cascades of signaling pathways and enact large-scale gene expression programs. In endometriosis, when endometrial tissue grows outside the uterine cavity, progesterone and estrogen signaling are disrupted, commonly resulting in progesterone resistance and estrogen dominance. This hormone imbalance leads to heightened inflammation and may also increase the pelvic pain of the disease and decrease endometrial receptivity to embryo implantation. This introductory chapter begins with a broad overview of the molecular mechanisms governing progesterone and estrogen signaling supporting endometrial function and how they become dysregulated in endometriosis, and it finishes with a more detailed survey of the molecular, physiological, and pathophysiological

involvement of AT-rich interaction domain 1A (ARID1A) in endometrial function and endometriosis. Understanding how these mechanisms contribute to the infertility associated with endometriosis will open new avenues of targeted medical therapies to give relief to the millions of women suffering its effects.

1.2 Introduction

The endometrium is a complex and dynamic tissue composed of epithelial cells, both luminal and glandular, surrounded by supporting stromal cells, together comprising the innermost layer of the uterus. The primary function of the uterus is supporting fertility, and the endometrium is the layer critically involved in receiving an embryo, facilitating implantation and decidualization, and supporting embryo growth and development until placentation. Successful pregnancy establishment requires an endometrium that is receptive to blastocyst invasion and ready to undergo decidualization, which is dependent upon hormonally regulated molecular processes that allow pregnancy establishment during the period of the menstrual cycle known as the window of receptivity (Cha, Sun, and Dey 2012; Vasquez and DeMayo 2013). The progesterone (P4) and estrogen (E2)-responsive signaling pathways integral for early pregnancy success are primarily induced through their cognate nuclear receptors, the progesterone receptor (PGR) and estrogen receptors (estrogen receptor 1; ESR1 and estrogen receptor 2; ESR2), respectively. These pathways are regulated in an epithelial and stromal compartment-specific manner in the endometrium (Rubel et al. 2010; Hantak, Bagchi, and Bagchi 2014; Wang, Wu, and DeMayo 2017). E2 induces epithelial proliferation to build endometrial thickness during the proliferative phase of the menstrual cycle, then P4 inhibits E2-induced proliferation and allows stromal cells to begin decidualization during the secretory phase. When the tightly regulated

balance of epithelial-stromal P4 and E2 signaling is lost, P4 resistance and E2 dominance are prone to ensue, potentially leading to uterine diseases such as endometriosis (Al-Sabbagh, Lam, and Brosens 2012; Patel et al. 2017).

Endometriosis is a common uterine disease characterized by the growth of endometrium-like tissue outside the uterine cavity (Zondervan et al. 2018; Bulun et al. 2019). Approximately 10% of reproductive-aged women suffer from this condition, which is often accompanied by chronic pain and infertility. Unfortunately, the etiology of endometriosis is not sufficiently understood to enable consistently effective treatment options. However, it is clear that functional dysregulation of the ovarian steroid hormones P4 and E2 and their downstream signaling targets plays an important role in the development and maintenance of the disease as well as its effects on the eutopic endometrium, primarily through E2-driven inflammation and P4 resistance (Patel et al. 2017; Al-Sabbagh, Lam, and Brosens 2012).

This introductory chapter will cover the known roles of P4 and E2 signaling in maintaining endometrial homeostasis and supporting pregnancy establishment before turning to focus on the mechanisms of the P4 and E2 signaling dysregulation of endometriosis, how this dysregulation impacts the clinical symptoms of endometriosis, and how hormone treatment strategies attempt to correct it. The role of ARID1A in these processes will be introduced within the broader discussions of endometrial function and endometriosis before the chapter concludes with a more focused review of ARID1A's involvement and a brief sketch of the remaining chapters.

1.3 Steroid Hormone Regulation of Endometrial Function

Studies in mice have been critical to understanding the functions of P4 and E2 in the mammalian uterus during early pregnancy (Cha, Sun, and Dey 2012; Wang and Dey 2006;

Vasquez and DeMayo 2013; Large and DeMayo 2012). Compared with the lengthy human menstrual cycle (28−30 days), mice undergo a short estrous cycle (4−5 days), but the receptive window of both species is regulated in a parallel manner by P4 and E2. In mice, a mating event, defined as gestation day (GD) 0, sets off a cascade of hormone signaling events, beginning with a preovulatory E2 surge from GD 0.5−1.5 to induce epithelial proliferation (Vasquez and DeMayo 2013). By GD 2.5, increased P4 secretions from the corpus luteum dominate, promoting stromal proliferation and inhibiting E2-induced epithelial proliferation. Next, a nidatory E2 surge on GD 3.5 acts in concert with P4 regulation to prepare the receptive endometrium on GD 4–5. The invading blastocyst then induces a decidualization reaction of the P4-primed stromal cells, where they differentiate into morphologically and functionally unique cells to surround the implanting embryo and support growth until placentation, all under critical continued P4 regulation. The primary mediators of these P4 and E2-induced events are their cognate nuclear receptors, transcriptional coregulators, and downstream signaling targets.

1.3.1 Progesterone Receptors and Progesterone Signaling

The basic endometrial function of PGR has been known for some time and recently comprehensively reviewed (Patel et al. 2015; Wetendorf and DeMayo 2014; Large and DeMayo 2012; Vasquez and DeMayo 2013; Wu, Li, and DeMayo 2018), so this discussion will briefly summarize relevant details while focusing on recent findings of functionally relevant PGR signaling regulators and downstream mediators. PGR expression is induced by E2 action through ESR1, and in turn PGR inhibits ESR1 expression, creating a fine-tuned feedback system to balance downstream effects (Patel et al. 2015). PGR is expressed as primarily two functionally distinct isoforms, PR-A and PR-B, transcribed from two promoters in the same gene, resulting in the PR-

A protein being 164 amino acids shorter than PR-B (Kastner et al. 1990). Null-mutation of both isoforms (Progesterone Receptor Knockout; PRKO) caused sterility in the female mouse due to numerous reproductive abnormalities, including severely reduced or absent ovulation, uterine hyperplasia and a lack of decidualization response, severely limited mammary gland development, and an inability to exhibit sexual behavior (Lydon et al. 1995). Specific deletion of PR-A (Mulac-Jericevic et al. 2000) or PR-B (Mulac-Jericevic et al. 2003) showed that PR-A is the primary driver of uterine PGR function and is sufficient for fertility, while PR-B is critical for mammary gland development and morphogenesis during pregnancy. PR-B also promotes uterine epithelial proliferation when not repressed by PR-A (Patel et al. 2015). Furthermore, overexpression of PR-A led to endometrial hyperproliferation and infertility (Fleisch et al. 2009; Wetendorf et al. 2017), revealing the importance of the relative PR-A/PR-B ratio to proper P4 responsiveness. Additionally, PGR has epithelial and stromal compartment-specific functions in the endometrium as revealed by ex vivo tissue-recombination experiments and in vivo epithelial-specific PGR knockout mice, while both epithelial and stromal PGR appear to be important for suppressing epithelial proliferation (Kurita et al. 2000; Franco et al. 2012).

In response to P4 binding, PGR is capable of rapid, non-genomic action though interaction with c-Src kinase to induce the pro-proliferative extracellular signal-regulated kinase/mitogen-activated protein kinase (ERK/MAPK) and Protein Kinase B (AKT) pathways, important for peri-implantation stromal proliferation (Boonyaratanakornkit et al. 2001; Vallejo et al. 2014; Patel et al. 2015). However, the canonical pathway for PGR's impact on gene expression occurs through genomic activity after P4 binding and translocation to the nucleus (Patel et al. 2015). Mechanistic studies of PGR action have been greatly aided by the identification of ligand-dependent PGR target genes in the mouse uterus through studies utilizing transcriptomic analysis of gene expression

changes after P4 exposure in PRKO mice (Jeong et al. 2005) and chromatin immunoprecipitation targeting PGR-bound gene regions (Rubel, Lanz, et al. 2012). One of the first PGR targets identified and known to be central to uterine function is the growth factor Indian hedgehog (IHH), which is induced in the epithelium and exerts paracrine effects on the stroma (Takamoto et al. 2002; Matsumoto et al. 2002). Uterine ablation of *Ihh* in the mouse resulted in uterine phenotypes very similar to PGR knockouts (Lee et al. 2006). Importantly, epithelial IHH induces stromal chicken ovalbumin upstream promoter-transcription factor II (COUP-TFII) expression (Takamoto et al. 2002; Lee et al. 2006), which both inhibits E2-induced epithelial proliferation to allow implantation and induces expression of bone morphogenetic protein 2 (BMP2) in the stroma to effect the decidualization response (Kurihara et al. 2007; Lee et al. 2010). As shown in both mouse and human cells, BMP2 is critical for decidualization through induction of Wnt family member 4 (WNT4) expression (Lee et al. 2007; Li et al. 2007), also required for successful implantation and decidualization (Franco et al. 2011). WNT4 and other Wnt family proteins canonically act through β-catenin activity (Angers and Moon 2009), and β-catenin has also been implicated in uterine development, implantation, and decidualization (Jeong, Lee, Franco, et al. 2009). In fact, a compartment-specific murine knockout of mesenchymal β-catenin showed that not only is stromal β-catenin required for decidualization, but it also indirectly opposes E2-induced epithelial proliferation (Zhang et al. 2012).

Homeobox protein-A10 (HOXA10) is another PGR target in the endometrium, and *Hoxa10* knockout mice are infertile due to uterine defects that appear to be a result of lost stromal P4 responsiveness (Benson et al. 1996; Lim et al. 1999). Interestingly, WNT4 expression is lost around the implantation site in *Hoxa10* mutant mice (Daikoku et al. 2004). Adding to the complexity, heart and neural crest derivatives expressed 2 (HAND2), a stromal-expressed PGR

target transcription factor, was also found to be required to mediate P4′s anti-proliferative action on the uterine epithelium but independently of IHH-COUP-TFII signaling (Li et al. 2011). Rather, HAND2 inhibits stromal fibroblast growth factor (FGF) signaling (Li et al. 2011), which otherwise induces epithelial proliferation through the ERK/MAPK and AKT pathways (Eswarakumar, Lax, and Schlessinger 2005). In addition, HAND2 appears to play a role in the decidualization process in both mouse and human stromal cells (Huyen and Bany 2011). Outside of these more well-described pathways, many other P4 signaling mediators involved in uterine function and fertility have been described such as insulin-like growth factor binding protein 1 (IGFBP1) (Gao et al. 1999), CCAAT enhancer binding protein beta (C/EBPβ) (Mantena et al. 2006; Wang et al. 2010), promyelocytic leukaemia zinc finger protein (PLZF) (Kommagani et al. 2016; Fahnenstich et al. 2003), mitogen-inducible gene 6 protein (MIG-6) (Jeong, Lee, Lee, et al. 2009; Yoo et al. 2015), and cysteine rich secretory protein LCCL domain containing 2 (CRISPLD2) (Yoo et al. 2014).

Though many of the important mediators and targets of uterine P4 signaling discussed above have been understood for many years, recent research, enabled by genome-wide transcriptome and cistrome analyses, has revealed new insight on P4 signaling regulators and modifiers (Wu, Li, and DeMayo 2018). Forkhead box O1 (FOXO1) was identified as a cell fate-regulating transcription factor involved in endometrial stromal decidualization partly through interaction with P4 signaling (Brosens and Gellersen 2006). Further study revealed transcriptional cross-talk and greater than 75% overlap in genome binding occupancy between FOXO1 and PGR in in vitro human endometrial stromal cell decidualization, particularly in the regulation of Wnt signaling and other factors such as IGFBP1 (Takano et al. 2007; Vasquez et al. 2015). Unexpectedly, a more recent in vivo mouse study found that rather than primarily functioning in decidualization, FOXO1 regulates epithelial integrity through regulation of PGR in vivo (Vasquez

et al. 2018). Indeed, conditional ablation of *Foxo1* in the uterus resulted in infertility primarily due to retention of epithelial integrity during the implantation window that prevented embryo invasion (Vasquez et al. 2018). Transcriptomics and expression profiling further revealed a temporally and spatially controlled mutual regulation between PGR and FOXO1 in the uterine epithelium during the window of receptivity that was validated in human endometrial samples (Vasquez et al. 2018).

FK506 binding protein prolyl isomerase 4 (FKBP52) is a P4 signaling regulator from the FK506 binding family of immunophilins that was first found to interact with and promote PGR activity in vitro (Barent et al. 1998). Targeted knockout of the *Fkbp52* gene in mice resulted in implantation failure resulting from attenuated P4-responsiveness due to a decrease in the binding of PGR by P4 (Tranguch et al. 2005). Moreover, later findings revealed a strain-specific functional importance for FKBP52 mediating P4 responsiveness, highlighting the importance of genetics in its function (Tranguch et al. 2007). This finding suggests a role for strain-specific genes or noncoding DNA regions in modifying FKBP52-PGR interactions and underlines the need to confirm findings in multiple species when making comparisons to human biology. In vitro decidualization experiments in human endometrial stromal cells confirmed a role for FKBP52 in decidualization and revealed HOXA10 as a regulator of FKBP52 in this process (Yang et al. 2012).

Signal transducer and activator of transcription 3 (STAT3) is a mediator of leukemia inhibitory factor (LIF) signaling (Cheng et al. 2001) which will be discussed in more detail hereafter. The first clue to the importance of STAT3 in uterine function resulted from mouse implantation failure after pharmacological inhibition of STAT3 activation (Catalano et al. 2005), and this result was later confirmed by the use of conditional gene knockouts that showed a decidualization defect, increased E2 signaling, and decreased P4 signaling (Sun et al. 2013; Lee, Kim, Oh, et al. 2013). More detailed analysis revealed that STAT3 directly interacts with PR-A,

indicating a direct role for STAT3-PGR crosstalk in early pregnancy establishment (Lee, Kim, Oh, et al. 2013).

GATA binding protein 2 (GATA2), a zinc finger family transcription factor, was originally identified as a PGR target in the mouse uterus via microarray analysis (Jeong et al. 2005) and later confirmed to be expressed concomitantly with PGR in the uterine epithelium at temporally and spatially critical periods during pregnancy (Rubel, Franco, et al. 2012). A follow-up study in which *Gata2* was conditionally ablated in the mouse uterus followed by genome-wide expression profiling and chromatin immunoprecipitation analysis revealed a large-scale regulatory role for GATA2 in PGR expression and downstream signaling (Rubel et al. 2016). *Gata2* uterine knockout mice were infertile due to implantation and decidualization defects, and further analysis showed that PGR protein and mRNA expression was dramatically reduced by *Gata2* attenuation (Rubel et al. 2016). Remarkably, 97% of P4-responsive genes failed to be induced without the presence of GATA2 as shown by microarray analysis (Rubel et al. 2016). Finally, cistrome analysis revealed that GATA2 both directly binds near the PGR promoter and shares occupancy with PGR at 50% of P4-responsive genes, and co-regulatory activity was confirmed with a luciferase reporter assay at *IHH* and sex determining region Y box 17 (*SOX17*) (Rubel et al. 2016). These results in the mouse were confirmed in the human by the finding of a correlation between GATA2 and PGR activity consistent with the mouse findings as well as a PGR-GATA2-SOX17 regulatory network governing female fertility (Rubel et al. 2016).

SOX17 is a transcription factor identified as a PGR target by chromatin immunoprecipitation followed by sequencing (ChIP-seq) (Rubel, Lanz, et al. 2012). It was later found to be important in implantation, gland development, and gland function in the mouse uterus through experiments utilizing a knockout of one *Sox17* allele (Hirate et al. 2016) and conditional

knockouts of *Sox17* in PGR-positive cells and uterine epithelial cells (Guimaraes-Young et al. 2016). More detailed study revealed that SOX17 controls epithelial proliferation and differentiation by regulating PGR signaling via the IHH pathway (Wang et al. 2018). Furthermore, ChIP-seq analysis showed a remarkable overlap between SOX17, PGR, and GATA2-bound regions, and SOX17 was shown to induce IHH through direct binding of an enhancer 19 kb upstream to the *Ihh* gene (Wang et al. 2018). Additionally, both the SOX17 expression pattern and a significant correlation with IHH expression were validated in human endometrial samples (Wang et al. 2018). A further interesting note from this study was the high degree of correlation between the SOX17-regulated transcriptome and the ARID1A-regulated transcriptome in the mouse uterus at GD 3.5 along with the reduction of ARID1A expression in the SOX17-deleted uterus (Wang et al. 2018). ARID1A is chromatin remodeling factor important for endometrial function that we will discuss in more detail hereafter (Kim, Yoo, Wang, et al. 2015).

1.3.2 Estrogen Receptors and Estrogen Signaling

P4 signaling in the endometrium cannot be considered on its own without also discussing the counteracting and sometimes cooperating action of E2 signaling. E2′s action in the endometrium is primarily enacted through the binding of its cognate nuclear receptors, ESR1 and ESR2, which unlike PR-A and PR-B are transcribed from separate genes (Vasquez and DeMayo 2013; Hewitt and Korach 2018; Hewitt, Winuthayanon, and Korach 2016; Hantak, Bagchi, and Bagchi 2014; Wang, Wu, and DeMayo 2017). In addition to its classical genomic activity, ESR1 can also induce rapid non-genomic signaling through the ERK/MAPK pathway (Stefkovich et al. 2018). Specifically, ESR1 has been shown to promote proliferation through this pathway in a human epithelial cell line (Migliaccio et al. 1996), and further evidence from mice indicates that

ESR1 can successfully carry out its effects on endometrial epithelial proliferation independent of classical genomic signaling (O'Brien et al. 2006), suggesting a role for non-classical ESR1 activity in epithelial proliferation. Additional research has also shown a need for the ERK/MAPK pathway in endometrial stromal decidualization (Lee, Kim, Lee, et al. 2013). Much of the current understanding of uterine ESR1 and ESR2 was learned through a variety of genetically engineered mice as well as in vitro cell culture experiments. ESR2 knockout females show no apparent uterine defect and are subfertile only due to ovulation inefficiency with no difference in uterine E2-responsiveness (Krege et al. 1998; Hewitt et al. 2003). However, there is some controversy because one study found competing evidence showing that the ESR2-null uterine epithelium is hyper-responsive to E2 treatment (Wada-Hiraike et al. 2006). The first ESR1 knockout mouse was created using gene disruption in embryonic stem cells, and the resulting females were unresponsive to E2 and infertile with an ovarian defect and hypoplastic uteri (Lubahn et al. 1993) as well as depressed PGR expression (Curtis et al. 1999). Embryo transfer experiments showed that even with a healthy embryo and proper hormonal stimulation, uteri lacking ESR1 are not competent for implantation (Curtis Hewitt et al. 2002). ESR1 is also required in the mouse for a normal decidualization response to artificial stimulation (Pawar et al. 2015) despite early reports to the contrary which likely resulted from incomplete deletion of ESR1 (Curtis et al. 1999; Curtis Hewitt et al. 2002; Hewitt and Korach 2018; Couse et al. 1995). Epithelial-specific ESR1 ablation resulted in the surprising finding that E2-induced epithelial proliferation occurs independently of epithelial ESR1, supporting previous findings from tissue recombination experiments (Winuthayanon et al. 2010; Cooke et al. 1997). It is actually stromal ESR1 that controls E2-induced epithelial proliferation through stromal-epithelial crosstalk (Cooke et al. 1997; Winuthayanon et al. 2017).

On the other hand, both epithelial and stromal ESR1 are necessary for a complete decidualization response to artificial stimulus (Pawar et al. 2015; Winuthayanon et al. 2017).

The classic role for E2 in upregulating epithelial proliferation is mediated in part by insulin-like growth factor 1 (IGF1) downstream of ESR1 in the stroma (Zhu and Pollard 2007; Adesanya et al. 1999). Mechanistically, ESR1 induces IGF1 expression by interacting with a superenhancer distal from the IGF1 transcription start site (Hewitt et al. 2019; Hewitt et al. 2012). It has been proposed that when IGF1 is expressed and secreted by the stroma, it binds its receptor IGF1R in the epithelium and induces the phosphoinositide 3-kinase (PI3K)/AKT pathway leading to proliferation (Zhu and Pollard 2007; Klotz et al. 2002; Richards et al. 1998). However, it was recently shown that disrupting E2′s induction of IGF1 is not sufficient to the impair the E2-induced uterine growth response (Hewitt et al. 2019), so other mediators must be important as well. One family of such potential paracrine mediators is the FGF family, the members of which, as we mentioned earlier in our discussion of HAND2, induce the proliferation-associated ERK/MAPK and AKT pathways (Eswarakumar, Lax, and Schlessinger 2005; Li et al. 2011). At least one FGF family member, FGF-9, is induced by E2 in the endometrial stroma (Tsai et al. 2002). In addition to its regulation by PGR in uterine stromal cells for decidualization, murine gene knockout experiments have shown that C/EBPβ is also an E2 target in both the endometrial epithelium and stroma that is critical for proliferation based on its activity regulating cyclin-dependent kinases in the Gap 2 (G2) to mitotic (M) phase cell cycle transition (Mantena et al. 2006; Wang et al. 2010). Finally, Mucin 1 (MUC1) is an E2 target in the uterine epithelium that is secreted to create a barrier to embryo attachment (Surveyor et al. 1995) until it is downregulated by P4 signaling through the IHH-COUP-TFII pathway (Lee et al. 2006; Kurihara et al. 2007; Lee et al. 2010).

In addition to its activity inducing epithelial proliferation, the other critical role for E2 in the endometrium is the induction of LIF, an interleukin-6 family cytokine, in the glandular epithelium by the nidatory E2 spike (Cha, Sun, and Dey 2012; Rosario and Stewart 2016). Maternal LIF expression is absolutely required for successful implantation and decidualization in mice (Stewart et al. 1992; Chen et al. 2000), and administration of LIF can replace the requirement of nidatory E2 for preparing a receptive uterus (Chen et al. 2000). LIF induces downstream signaling in the luminal epithelium by binding its receptor (LIFR), which associates with glycoprotein 130 (gp130) and activates STAT3 through phosphorylation by Janus kinases (JAKs) (Song and Lim 2006; Cheng et al. 2001). As discussed previously in this introduction, activated phospho-STAT3 (pSTAT3) interacts with PGR signaling to promote implantation success and decidualization (Lee, Kim, Oh, et al. 2013). In addition, LIF action on the luminal epithelium regulates several important signaling pathways, some of which have been discussed here such as IGF1 signaling, Wnt/β-catenin signaling, FGF signaling, and ERK-MAPK signaling (Rosario and Stewart 2016). One mechanism of LIF action downstream of ESR1 was recently elucidated in which LIF acts through ERK1/2 to activate the IHH-COUP-TFII pathway necessary for decidualization (Pawar et al. 2015), revealing an additional layer of complexity in E2-P4 signaling crosstalk. Furthermore, the transcription factor early growth response 1 (EGR1) has been revealed as a regulator of implantation and decidualization induced by E2 through both the LIF-STAT3 and ERK1/2 pathways (Liang et al. 2014; Kim, Kim, et al. 2014). *Egr1* knockout mouse studies and human endometrial stromal cell in vitro decidualization experiments have established EGR1 as critical for endometrial receptivity through the regulation of epithelial PGR signaling (Kim, Kim, et al. 2018), c-Kit expression (Park et al. 2018), WNT4 expression (Liang et al. 2014), and many other cell-proliferation-related targets (Szwarc et al. 2019).

1.3.3 Nuclear Receptor Coregulators in the Regulation of Progesterone and Estrogen Signaling

Before turning to a focused discussion of P4 and E2 signaling dysregulation in endometriosis, the roles of nuclear receptor coregulators in steroid hormone signaling regulation must be briefly considered. In general, nuclear receptor coregulators form large complexes to modify chromatin structure and regulate large-scale gene transcription programs (Millard et al. 2013). A family of regulatory proteins aptly named steroid receptor coactivators (SRCs), composed of SRC-1, SRC-2, and SRC-3, is critical to the regulation of PGR and ESR1 action in the female reproductive tract (Szwarc, Lydon, and O'Malley 2015). In the endometrium, SRC-1 and SRC-2 appear to be the most functionally relevant for normal functionality based on studies utilizing knockout mice (Xu et al. 1998; Mukherjee et al. 2006; Xu et al. 2000; Han et al. 2006; Jeong et al. 2007; Han et al. 2005). This is supported by the fact that SRC-1 and SRC-2 are expressed more highly than SRC-3 in the human endometrium (Gregory et al. 2002) although SRC-3 upregulation has been linked to endometrial cancer (Balmer et al. 2006; Sakaguchi et al. 2007). SRC-1 knockout mice are fertile; however, SRC-1 is necessary for full decidualization and P4-responsiveness in the uterus (Xu et al. 1998; Han et al. 2005; Han et al. 2006). Intriguingly, SRC-1 appears to downregulate PGR target genes in the endometrial epithelium but upregulate them in the stroma (Han et al. 2005). SRC-2 is even more critical for murine uterine function. Uterine ablation of *SRC-2* resulted in complete female infertility due to implantation failure and a partial loss of decidualization which was completely lost with the concomitant ablation of *SRC-1* (Mukherjee et al. 2006; Jeong et al. 2007). Microarray analysis further revealed that SRC-2 is necessary for P4 regulation of Wnt signaling, BMP2 signaling, and ESR1 signaling (Jeong et al. 2007). The requirement of SRC-2 for decidualization was also confirmed in in vitro decidualization of human endometrial stromal cells (Kommagani et al. 2013), and transcriptomic

analysis revealed that 50% of SRC-2-regulated genes are also regulated by PGR (Szwarc et al. 2018), supporting the close relationship of these factors in transcriptional regulation of the decidualization process.

ARID1A, a SWItch/sucrose Non-Fermentable (SWI/SNF) chromatin remodeling complex protein, was found to be critical for endometrial function during early pregnancy after conditional deletion in the mouse uterus resulted in infertility due to implantation and decidualization defects (Kim, Yoo, Wang, et al. 2015). *Arid1a* ablation also resulted in increased epithelial proliferation concurrent with increased epithelial E2 signaling and decreased epithelial PGR and P4 signaling (Kim, Yoo, Wang, et al. 2015). Transcriptomic analysis indicated a role for ARID1A in repressing cell cycle related genes, and further experiments revealed that ARID1A complexes with PGR, specifically PR-A, to inhibit proliferation through the upregulation of Kruppel-like factor 15 (KLF15) (Kim, Yoo, Wang, et al. 2015) and to maintain an endometrium receptive to implantation.

Recent research has highlighted the importance of other epigenetic regulators in addition to ARID1A in endometrial P4 signaling. Enhancer of zeste homolog 2 (EZH2), a polycomb-repressive complex subunit that catalyzes histone 3 lysine 27 trimethylation and leads to gene silencing, was found to be involved in the epigenetic reprogramming required for decidualization (Grimaldi et al. 2011). Results from in vitro decidualization experiments indicated a role for EZH2 downregulation in decidualizing cells in response to progestin treatment. EZH2 is also upregulated in the endometrial epithelium by E2 in conjunction with increased epithelial proliferation, whereas P4 inhibits this effect (Nanjappa et al. 2019). Moreover, uterine deletion of *Ezh2* in the mouse compromised fertility (Nanjappa et al. 2019). Another epigenetic regulator, histone deacetylase 3 (HDAC3), functions by modifying histone acetylation, and this chromatin regulator was recently shown to be critical for implantation and decidualization in the mouse uterus and in vitro

decidualization of human stromal cells (Kim et al. 2019). Furthermore, uterine *Hdac3* knockout mice exhibited decreased PGR and PGR target gene expression in the stroma, indicating a role for HDAC3 in the P4-responsiveness required for stromal decidualization (Kim et al. 2019).

1.4 Dysregulation of Progesterone and Estrogen Signaling in Endometriosis

As the work reviewed in the previous sections has demonstrated, tightly regulated signaling pathways governed by P4 and E2 in a stromal and epithelial compartment-specific manner are key to maintaining endometrial homeostasis and supporting female fertility. Dysregulation of steroid hormone signaling is common in many uterine pathologies such as endometriosis, infertility, endometrial cancer, uterine leiomyoma, and recurrent pregnancy loss (Patel et al. 2015). For the remainder of this introductory chapter, we will focus on the molecular pathophysiology and treatment of endometriosis with particular focus on recent findings that shed light on the contribution of P4 and E2 signaling dysregulation to the infertility and pelvic pain women with this disease often experience.

Endometriosis is classically defined as the presence of endometrium-like tissue located outside the uterine cavity (Zondervan et al. 2018). However, it is also important to understand this disease as a benign, heterogeneous, E2-dependent, and P4-resistant inflammatory condition that mainly affects the peritoneal cavity and ovary close to the uterus but has also been reported in distal organs such as the lungs and brain (Bulun et al. 2019). The prevalence of endometriosis is difficult to establish with certainty due to the requirement of surgical visualization of lesions for definitive diagnosis, but it is generally accepted that it occurs in about 1 in 10 women of reproductive age (Zondervan et al. 2018; Bulun et al. 2019; Parasar, Ozcan, and Terry 2017). Several theories exist attempting to explain endometriosis pathogenesis such as peritoneal

metaplasia or differentiation of circulating cells, but the most widely accepted explanation is the retrograde flow of menstrual tissue through the fallopian tubes (Zondervan et al. 2018; Bulun et al. 2019). Here, we will discuss evidence for the dysregulation of P4 (Table 1.1) and E2 (Table 1.2) signaling pathways in both endometriotic lesions and the endometriosis-affected eutopic endometrium that lead to P4 resistance and E2 dominance. These imbalances may explain the increased ability of lesions to grow outside the uterus and cause pain and the decreased ability of the uterus itself to support successful pregnancy establishment.

Table 1.1 *P4 signaling factors dysregulated in endometriotic lesions*

Molecule	Symbol	Function	Dysregulation	Reference
Progesterone Receptor	PGR	Nuclear receptor	Decreased	(Attia et al. 2000; Yin et al. 2012; Prentice et al. 1992; Colon-Caraballo et al. 2018; Mousazadeh et al. 2019; Brown et al. 2018; Wu et al. 2006; Bergqvist, Ljungberg, and Skoog 1993; Bukulmez et al. 2008; Bedaiwy et al. 2015)
Chicken ovalbumin upstream promoter-transcription factor II	COUP-TFII	Transcription factor	Decreased	(Lin et al. 2014)
Wnt family member 4	WNT4	Secreted signaling protein	Decreased	(Liang et al. 2016)
Heart and neural crest derivatives expressed 2	HAND2	Transcription factor	Decreased	(Kato et al. 2018)
Insulin-like growth factor binding protein 1	IGFBP1	Circulating growth factor binding protein	Decreased	(Klemmt et al. 2006)
Forkhead box O1	FOXO1	Transcription factor	Decreased	(Yin et al. 2012)
FK506 binding protein prolyl isomerase 4	FKBP52	Immunophilin	Decreased	(Hirota et al. 2008)
GATA binding protein 2	GATA2	Transcription factor	Decreased	(Dyson et al. 2014)

Table 1.2 *E2 signaling factors dysregulated in endometriotic lesions*

Molecule	Symbol	Function	Dysregulation	Reference
Estrogen receptor 1	ESR1	Nuclear receptor	Decreased	(Xue et al. 2007; Smuc et al. 2007; Yang et al. 2015; Dyson et al. 2014)
Estrogen receptor 2	ESR2	Nuclear receptor	Increased	(Xue et al. 2007; Smuc et al. 2007; Yang et al. 2015; Dyson et al. 2014)
Myc proto-oncogene protein	c-MYC	Transcription factor	Increased	(Pellegrini et al. 2012)
Cyclin D1	CCND1	Cell cycle regulator	Increased	(Pellegrini et al. 2012)
Growth regulating estrogen receptor binding 1	GREB1	Growth regulator	Increased	(Pellegrini et al. 2012)
Fibroblast growth factor 9	FGF-9	Secreted growth factor	Increased	(Wing et al. 2003)
Steroid receptor coactivator-1	SRC-1	Transcriptional co-activator	Increased	(Han et al. 2012)

1.4.1. Progesterone Resistance

When endometrial tissue fails to respond properly to P4 exposure, this is termed P4 resistance, and it manifests itself in endometriosis as failed induction of PGR activation, or P4 target gene transcription in the presence of bioavailable P4 (Patel et al. 2017; Al-Sabbagh, Lam, and Brosens 2012). Under this definition, P4 resistance has been well-established in both the endometriotic lesions and eutopic endometrium of women with endometriosis (Kao et al. 2003; Burney et al. 2007; Attia et al. 2000; Yin et al. 2012). Loss of P4-responsiveness can have serious consequences in both cases since P4 signaling is required to counteract E2-induced proliferation and to promote decidualization (Patel et al. 2017), which implies that P4 resistance may lead to both increased lesion growth and a non-receptive endometrium.

One potential molecular cause of P4 resistance is a loss or alteration of PGR expression, which has been documented in endometriotic lesions (Prentice et al. 1992; Attia et al. 2000; Colon-Caraballo et al. 2018; Mousazadeh et al. 2019; Brown et al. 2018; Yin et al. 2012; Wu et al. 2006; Bergqvist, Ljungberg, and Skoog 1993; Bukulmez et al. 2008; Bedaiwy et al. 2015) and eutopic endometrium from women with endometriosis (Igarashi et al. 2005; Wolfler et al. 2016; Colon-Caraballo et al. 2018; Shen et al. 2015; Bedaiwy et al. 2015; Pei et al. 2018). Further study has confirmed direct correlations between PGR loss with loss of P4-responsiveness in both lesions (Flores et al. 2018) and cells from the endometrium of women with endometriosis (Hou, Mamillapalli, and Taylor 2017). However, the contribution of PGR loss to the P4 resistance observed in endometriosis is controversial due to a few studies finding no significant difference in PGR levels in eutopic endometrium from women with endometriosis (Prentice et al. 1992; Broi et al. 2017) or lesions (Zanatta et al. 2015). These discrepancies are likely due to differences in experimental methods, lesion types and cell types analyzed, and resolution of PGR isoforms. For example, the two studies cited here finding no difference of PGR expression in the endometrium of women with endometriosis did not distinguish between PGR isoforms (Prentice et al. 1992; Broi et al. 2017), and one did not distinguish between cell compartments either (Broi et al. 2017). The study finding no difference of PGR expression in lesions looked specifically at rectosigmoid endometriosis lesions (Zanatta et al. 2015), whereas other studies found differences in PGR levels when analyzing mainly ovarian or peritoneal lesions (Prentice et al. 1992; Attia et al. 2000; Colon-Caraballo et al. 2018; Mousazadeh et al. 2019; Brown et al. 2018; Yin et al. 2012; Wu et al. 2006; Bergqvist, Ljungberg, and Skoog 1993; Bukulmez et al. 2008; Bedaiwy et al. 2015). Studies that distinguished between PR-A and PR-B tended to find a decrease of PR-B in endometriosis lesions (Attia et al. 2000; Yin et al. 2012; Mousazadeh et al. 2019; Wu et al. 2006) or endometrium

(Igarashi et al. 2005; Shen et al. 2015; Pei et al. 2018), whereas reports of PR-A were mixed (Attia et al. 2000; Yin et al. 2012; Bukulmez et al. 2008; Bedaiwy et al. 2015; Igarashi et al. 2005; Wolfler et al. 2016; Shen et al. 2015). Furthermore, there is direct evidence to support promoter hypermethylation (Wu et al. 2006; Rocha-Junior et al. 2019) and microRNA dysregulation (Pei et al. 2018; Zhou et al. 2016) as potential mechanisms for PR-B loss in endometriosis. These findings support the importance of proper PR-A/PR-B ratio in endometrial function and implicate an imbalance of PGR isoforms in the pathophysiology of endometriosis.

In addition to dysregulated PGR expression, alterations in PGR signaling mediators and regulators also contribute to P4 resistance (Al-Sabbagh, Lam, and Brosens 2012). Due to the importance of the PGR-induced IHH-COUP-TFII-WNT4 pathway in regulating epithelial proliferation and decidualization during early pregnancy as discussed above, these molecules are of great interest in the context of P4 resistance in endometriosis. In a histological comparison of IHH expression in endometrial biopsy samples from women with endometriosis and healthy controls, IHH expression was decreased in secretory phase endometrium from endometriosis patients (Smith et al. 2011). Correspondingly, later studies found COUP-TFII (Lin et al. 2014) and WNT4 (Liang et al. 2016) expression levels decreased in both endometrial samples from women with endometriosis and endometriotic lesions. These findings identified a major pathway downstream of P4 signaling that is disrupted in women with endometriosis and may lead to endometrial non-receptivity in these patients by interfering with regulation of uterine epithelial proliferation and stromal decidualization. In endometriotic lesions, the PGR target HAND2 was also found decreased along with an increase in FGF signaling, which it normally controls (Kato et al. 2018). This is another molecular consequence of P4 resistance that may lead to the increased invasiveness of endometriotic tissue (Kato et al. 2018). Further confirming the comprehensive

disruption of P4 signaling in endometriosis, HOXA10 (Taylor et al. 1999), IGFBP1 (Klemmt et al. 2006), PLZF (Burney et al. 2007), MIG-6 (Burney et al. 2007), and CRISPLD2 (Yoo et al. 2014), all PGR targets implicated in endometrial function based on mouse studies, have been shown to be dysregulated in endometriosis patients. These findings once again reinforce the idea that loss of P4 signaling in endometriosis disrupts the fine-tuned regulation of the endometrium necessary to maintain normal uterine function and fertility.

Though dysregulation of PGR target genes displays the consequences of P4 resistance in endometriosis, dysregulation of PGR signaling regulators may help explain the cause of P4 resistance. The expression of the pioneer transcription factor FOXO1 is reduced in both the endometrium (Burney et al. 2007; Su et al. 2015) and stromal cells from lesions (Yin et al. 2012) of women with endometriosis. Given the requirement of FOXO1 for proper stromal cell decidualization and regulation of endometrial epithelial integrity along with the overlapping binding regions and in vivo regulation of PGR (Takano et al. 2007; Vasquez et al. 2015; Vasquez et al. 2018), the loss of FOXO1 in endometriosis could be partially responsible for the dysregulation of both PGR expression and downstream signaling. However, since FOXO1 is also regulated by PGR, it is difficult to conclude which molecule becomes dysregulated first in endometriosis based on the current literature. Another molecule with potential implications for P4 resistance in endometriosis is Notch homolog 1 (NOTCH1). NOTCH1 and other Notch signaling molecules have been found decreased in endometrium from women and baboons with endometriosis, and silencing of NOTCH1 impaired decidualization in isolated human endometrial stromal cells potentially by downregulation of FOXO1 (Su et al. 2015), reminiscent of P4 resistance in endometriosis. Interestingly, aberrant NOTCH1 signaling has also been shown in endometriotic lesions, but in this case increased NOTCH1 activation correlated with reduced PGR

expression (Brown et al. 2018). In vitro reduction of NOTCH1 signaling restored PGR and P4-responsiveness, revealing a direct relationship between Notch signaling regulation and the maintenance of proper P4-responsiveness, both of which are disrupted in endometriosis (Brown et al. 2018).

Disruption of PGR signaling in endometriosis could also be caused by dysregulation of steroid receptor chaperone proteins like FKBP52. FKBP52 expression has been found decreased in both the endometrium and lesions of women with endometriosis (Hirota et al. 2008; Yang et al. 2012), and the endometrial FKBP52 decrease alongside PGR decrease was confirmed to be due to endometriosis pathology in a non-human primate model of endometriosis (Jackson et al. 2007). Furthermore, endometriosis model mice lose FKBP52 expression in their lesions, and conversely, deletion of *Fkbp52* increased lesion growth (Hirota et al. 2008). HOXA10 may also be involved in this process since its expression is reduced in endometriosis (Taylor et al. 1999), and in vitro experiments implicated it in the regulation of FKBP52 (Yang et al. 2012). Evidence from both baboon and human endometriosis also implicates increased microRNA (miR)-29c expression as a potential mechanistic cause for FKBP52 loss (Joshi et al. 2017).

STAT3 is another PGR regulator discussed earlier in this introduction with an important function in fertility (Lee, Kim, Oh, et al. 2013). Given its interaction with PGR during early pregnancy establishment, one might have hypothesized STAT3 activation would be reduced in endometriosis due to the context of P4 resistance, however pSTAT3 is aberrantly increased in the endometrium of both women and non-human primates with endometriosis (Kim, Yoo, Kim, et al. 2015). This is likely explained by increased levels of interleukin 6 (IL-6) (Tsudo et al. 2000), which can activate STAT3 (Zhong, Wen, and Darnell 1994). Abnormal STAT3 activity is associated with increased cell proliferation (Frank 1999) which may occur due to pSTAT3

increasing downstream signaling through hypoxia-inducible factor 1-alpha (HIF1A) in the endometrium (Kim, Yoo, Kim, et al. 2015), illustrating STAT3's pleiotropic roles. Thus, while loss of STAT3 compromises uterine function, aberrant activation is associated with endometriosis, indicating the need for tight regulation of STAT3 in conjunction with PGR signaling. One potential mechanism suggested for increased STAT3 activation in endometriosis is down-regulation of protein inhibitor of activated STAT3 (PIAS3) which has been observed in women and non-human primates with endometriosis (Yoo et al. 2016). One effect of STAT3 overexpression in endometriosis appears to be the up-regulation of the oncogenic gene repressor B cell CLL/lymphoma 6 (BCL6), a known target of STAT3 (Arguni et al. 2006) and shown to be increased in the secretory phase endometrium of women with endometriosis (Evans-Hoeker et al. 2016). Furthermore, sirtuin 1 (SIRT1), a transcriptional regulator associated with both oncogenic and tumor-suppressor roles, binds and co-localizes with BCL6 and is also up-regulated in endometrium from women and non-human primates with endometriosis, significantly correlating with BCL6 expression levels (Yoo et al. 2017). Further experiments in mice and cell culture showed that increased BCL6 and SIRT1 expression caused reduced P4 signaling through the IHH pathway, specifically by binding the gene promoter of IHH pathway protein glioma-associated oncogene homolog 1 (GLI1) to repress its transcription (Yoo et al. 2017). In turn, reduced expression of GLI1 was shown in the endometrium of women with endometriosis, confirming a mechanistic role for STAT3, BCL6, and SIRT1 overexpression in the P4 resistance of endometriosis (Yoo et al. 2017).

Earlier in this introductory chapter we discussed the importance of the large-scale gene regulatory role for GATA2 and SOX17 in P4 signaling of the endometrium. In endometriosis, there appears to be a switch from a GATA2 driven P4-responsive state to a GATA6-driven P4-

resistant state based on CpG methylation patterns (Dyson et al. 2014). Moreover, SOX17 expression is reduced in women with endometriosis, correlating with a drop in IHH expression, which SOX17 normally regulates by binding a distal *Ihh* enhancer to promote endometrial receptivity in the healthy endometrium (Wang et al. 2018). In addition, ARID1A, a chromatin remodeling complex protein potentially regulated by SOX17, is decreased in endometrium from endometriosis patients (Kim, Yoo, Wang, et al. 2015). Evidence showing direct binding of ARID1A to PR-A as well as loss of P4 signaling in mice with conditional ablation of *Arid1a* in the uterus implicates the decrease of ARID1A in endometriosis in the P4 resistance phenotype as well (Kim, Yoo, Wang, et al. 2015). Expression of HDAC3, another epigenetic regulator, was also found decreased in endometrium from women with endometriosis as well as non-human primate and mouse models of endometriosis (Kim et al. 2019). Further mechanistic study linked loss of HDAC3 to loss of P4 signaling, revealing yet another P4 signaling regulator implicated in the P4 resistance of endometriosis (Kim et al. 2019).

1.4.2. Estrogen Dominance and Inflammation

Concurrent with P4 resistance, endometriosis development and progression are driven by the upregulation of E2-induced cell proliferation and inflammation, which can both promote lesion growth and compromise endometrial receptivity (Bulun et al. 2019; Lessey and Kim 2017; Han and O'Malley 2014) (Figure 1.1). Local E2 levels are increased in endometriosis due to upregulation of E2-producing p450 aromatase expression (Noble et al. 1996) and reduction of 17β-hydroxysteroid dehydrogenase type 2 (17βHSD2), which is normally induced by P4 to convert E2 to the less potent estrone but is decreased in P4-resistant conditions (Zeitoun et al. 1998).

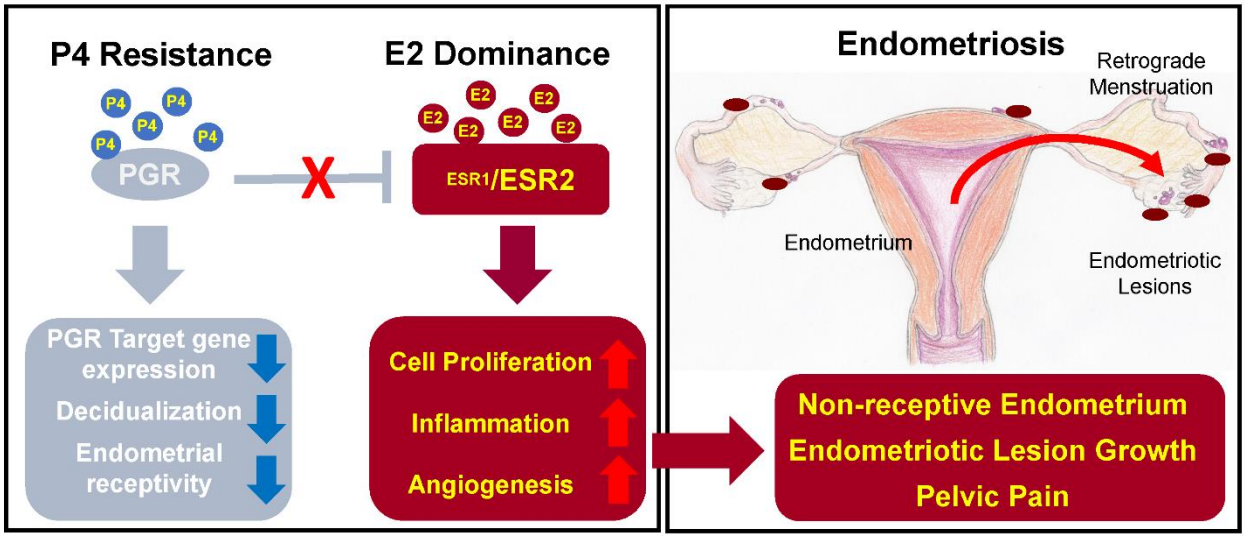

Figure 1.1 *Schematic diagram illustrating the concept of how P4 resistance and E2 dominance in endometriosis promote lesion growth and compromise endometrial receptivity.*

Since E2′s effects are primarily enacted through ESR1 and ESR2, their expression levels are important in the assessment of E2 action in endometriosis. ESR1 levels are reportedly increased in the secretory phase endometrium of women with endometriosis compared to controls (Lessey et al. 2006; Osinski et al. 2018), which may lead to increased estrogenic activity and proliferation, compromising normal uterine function. ESR2 expression is unchanged in eutopic endometrium from women with endometriosis (Osinski et al. 2018) although one study reported increased ESR2/ESR1 ratio in endometriosis-affected endometrium (Juhasz-Boss et al. 2011). The role of ESR2 in normal uterine physiology is not clear since ESR2 knockout mice have been reported to have no overt uterine defect (Krege et al. 1998; Hewitt et al. 2003); however, one study implicated ESR2 in control of proliferation through epidermal growth factor (EGF) signaling (Wada-Hiraike et al. 2006).

In contrast, the majority of the evidence indicates that endometriotic lesions upregulate ESR2 and downregulate ESR1, although reports are mixed (Xue et al. 2007; Smuc et al. 2007; Pellegrini et al. 2012; Yang et al. 2015; Dyson et al. 2014; Matsuzaki et al. 2001; Han et al. 2012).

Discrepancies are likely due to the lesion type being studied since the majority of studies analyzed only ovarian lesions (Xue et al. 2007; Smuc et al. 2007; Yang et al. 2015; Dyson et al. 2014), but those including peritoneal lesions contrastingly showed relative increases in ESR1 (Matsuzaki et al. 2001; Pellegrini et al. 2012). Mechanistically, there is evidence to support changes in promoter methylation as a cause for the increase in the ESR2/ESR1 ratio in endometriotic cells, since regions of the *ESR1* promoter become hypermethylated, leading to decreased expression (Dyson et al. 2014; Xue et al. 2007), whereas a CpG island in the *ESR2* promoter becomes hypomethylated, leading to increased expression (Xue et al. 2007). Since E2 action through ESR1 upregulates PGR expression, the loss of ESR1 in lesions has been suggested as a possible explanation for the loss of PGR (Bulun et al. 2019). These mechanistic insights support the conclusion that the ESR2/ESR1 ratio increases in endometriotic lesions.

The increase in ESR2 levels in lesions may be responsible for increased lesion survival and inflammation because E2 can act through ESR2 to induce the cyclooxygenase-II (COX-2)-prostaglandin E2 (PGE2) feedback loop (Tamura et al. 2004), which is well known to increase the inflammation and pathology of endometriosis (Wu et al. 2010). E2 also induces ESR2 to bind the Ras-like, estrogen-regulated, growth inhibitor (RERG) promoter, inducing its expression (Monsivais et al. 2014). In cooperation with PGE2, RERG was shown to translocate to the nucleus and induce cell proliferation, providing further evidence for the potential mechanism of E2-induced proliferation in endometriotic lesions (Monsivais et al. 2014). Another study identified the E2-induced, proliferation-related proteins Myc proto-oncogene protein (c-myc), cyclin D1 (CCND1), and growth-regulating estrogen receptor-binding 1 (GREB1) as increased in expression alongside ESR2 in lesions (Pellegrini et al. 2012), providing further clues to the mechanism of E2-dependent lesion growth. Additionally, FGF-9 is a cell growth-inducing factor shown to be

induced by E2 and upregulated in endometriotic lesions (Wing et al. 2003), likely in part due to the loss of P4-induced HAND2 which would normally suppress it (Li et al. 2011). ESR2 upregulation in endometriotic lesions was reproduced in a mouse model of endometriosis, where its activity was shown to drive lesion growth and be an effective target for the inhibition of lesion growth (Han et al. 2015). Mechanistically, ESR2 apparently interacts with cytoplasmic inflammatory factors to inhibit apoptosis and promote the invasiveness of lesions (Han et al. 2015). Intriguingly, there is also evidence to implicate immune cell responsiveness to E2 in endometriosis. A growing body of evidence has implicated immune system dysregulation in endometriotic lesion growth, one aspect of which is elevated macrophage populations (Symons et al. 2018). Peritoneal fluid macrophages from women with endometriosis were shown to upregulate the expression of ESR1 and ESR2, and the expression of ESRs correlated with an increase in inflammatory cytokines (Montagna et al. 2008). Further experiments in a mouse model of endometriosis showed that E2 treatment caused an increase in the macrophages present in lesions as well as the expression of macrophage migration factors (Greaves et al. 2015). In that study, ESR2 was the predominant E2 receptor expressed in macrophages from both women with endometriosis and endometriosis model mice (Greaves et al. 2015). Thus, E2 appears to directly cause an increased inflammatory response through ESR2 in addition to enhancing endometriotic cell proliferation in endometriosis.

In addition to the targets of E2 and ESRs that induce cell proliferation and inflammation in endometriosis, it is also important to consider the potential effects of SRCs on ESRs in endometriosis. Expression profiling of SRCs in endometriotic lesions identified SRC-1 as the predominant SRC in endometriosis (Kumagami et al. 2011). Although one study found that SRC-1 expression was decreased in the epithelium of proliferative phase endometriotic lesions (Suzuki

et al. 2010), additional research initiated in endometriosis model mice and validated in human endometriosis revealed that in spite of a decrease in total SRC-1, levels of a truncated form were increased (Han et al. 2012). Furthermore, this new isoform of SRC-1 was shown in vitro to decrease tumor necrosis factor alpha (TNFα)-mediated apoptosis in endometriotic cells, leading to increased cell survival and invasion and mirroring the in vivo disease pathophysiology (Han et al. 2012). Additional experiments revealed interaction between this SRC-1 isoform and ESR2 in endometriosis that may mediate a synergistic role in promoting cell survival (Han et al. 2015). Indeed, disruption of the interactions between the SRC-1 isoform and ESR2 with inhibitors suppressed endometriotic cell growth in isolated human cells and in a mouse model of endometriosis (Han et al. 2015; Cho et al. 2018). Taken together, these findings support an important role for SRC-1 isoform and ESR2 upregulation in the development and progression of endometriosis.

Although LIF expression is induced by E2 in the endometrium, and estrogenic activity is increased in endometriosis, LIF levels have been reported to be decreased in the glandular epithelium of women with this disease (Dimitriadis et al. 2006). This could be due to increased inflammatory factors in endometriosis that can suppress LIF (Arici et al. 1995). The decrease in LIF secretion from glands may also be due to intrinsic gland dysfunction in endometriosis. Specifically, the gland-specific transcription factor Forkhead box A2 (FOXA2) is required for LIF expression in mice (Kelleher et al. 2017), but it is decreased in endometrium from women with endometriosis (Yang et al. 2015; Lin et al. 2018). Thus, though increased estrogenic activity promotes harmful inflammation and cell proliferation in endometriosis, it apparently fails to properly induce LIF expression.

1.5 Pathologies Related to Steroid Hormone Signaling Dysregulation in Endometriosis

1.5.1. Infertility

One of the major clinical pathologies associated with endometriosis is infertility (Holoch and Lessey 2010; de Ziegler, Borghese, and Chapron 2010; Macer and Taylor 2012; Haydardedeoglu and Zeyneloglu 2015; Lessey and Kim 2017; Tomassetti and D'Hooghe 2018). Although up to 50% of women with endometriosis struggle with fertility problems, the causal link is unclear and controversial (Holoch and Lessey 2010). Several possible mechanisms have been proposed by which endometriosis may cause fertility defects including (1) anatomical distortions, (2) diminished ovarian reserve, (3) chronic inflammatory conditions, and (4) compromised endometrial receptivity (Haydardedeoglu and Zeyneloglu 2015; de Ziegler, Borghese, and Chapron 2010). Due to the well-studied involvement of P4 and E2 signaling in endometrial receptivity, we will focus our discussion of P4 and E2 dysregulation in endometriosis-related infertility on that topic (Figure 1.2).

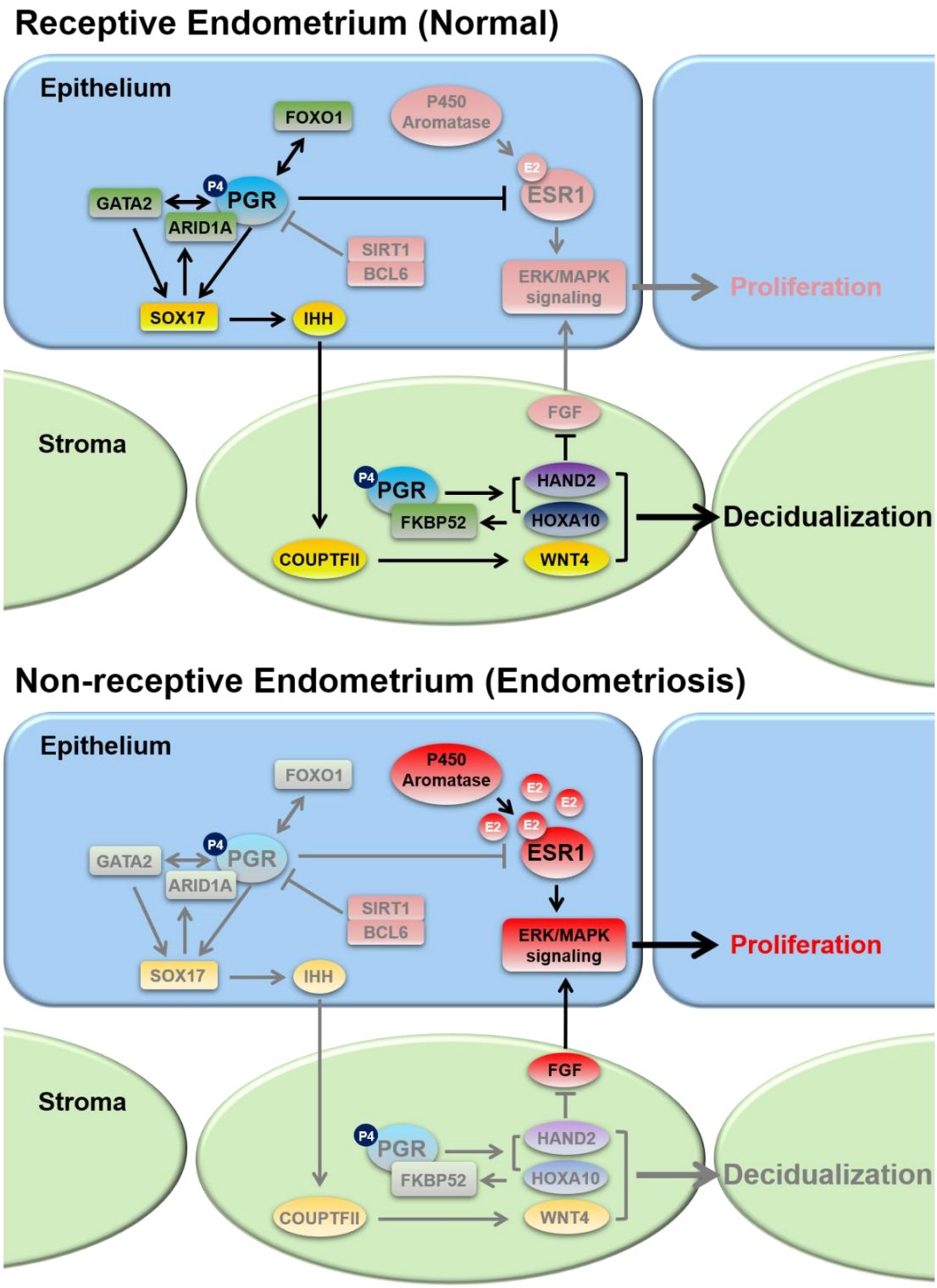

Figure 1.2 *Schematic diagram illustrating the primary known signaling pathways and transcriptional regulators involved in P4 and E2 governance of endometrial epithelial-stromal crosstalk that are dysregulated in endometriosis.* P4 resistance and E2 dominance in endometriosis results in epithelial proliferation and defective decidualization that can compromise endometrial function.

Because of the integral involvement of P4 and E2 signaling pathways in early pregnancy establishment and their dysregulation in the endometriosis-affected endometrium that we have described above, it is intuitive to draw a conceptual link between the P4 resistance and E2 dominance of endometriosis and the endometrial non-receptivity associated with this disease. In addition to the broad conceptual link, several specific molecular pathways we have discussed are implicated in both female infertility and endometriosis. For example, total endometrial PGR expression and PR-A/PR-B expression ratio are critical for successful mammalian pregnancy as shown primarily in mice (Lydon et al. 1995; Mulac-Jericevic et al. 2000; Mulac-Jericevic et al. 2003; Fleisch et al. 2009; Wetendorf et al. 2017), but either PGR total expression or PR-A/PR-B ratios are dysregulated in the endometrium of many women with endometriosis (Igarashi et al. 2005; Wolfler et al. 2016; Colon-Caraballo et al. 2018; Shen et al. 2015; Bedaiwy et al. 2015; Pei et al. 2018). In fact, a recent translational study showed that in women diagnosed and treated for endometriosis, PGR expression levels were higher in women with subsequent spontaneous pregnancies within one year versus those who did not successfully achieve pregnancy (Moberg et al. 2015). Additionally, the inhibitory action of PGR on ESR1 normally prevails in the endometrium during the window of receptivity, but women with endometriosis exhibit increased ESR1 through the mid-secretory phase, which contains the implantation window in women (Lessey et al. 2006; Osinski et al. 2018).

The rise in ESR1 in endometriosis corresponds to a decrease in αv/β3 integrin (Lessey et al. 1994), which is an adhesion molecule normally expressed in the endometrium during the receptive window and putatively involved in successful implantation (Lessey et al. 2006). HOXA10, a P4 target decreased in the endometrium of women with endometriosis (Taylor et al. 1999) and required for fertility in mice (Benson et al. 1996; Lim et al. 1999), was also identified

as a direct regulator of αv/β3 integrin expression (Daftary et al. 2002). Furthermore, non-human primates induced with endometriosis exhibit reduced HOXA10 and αv/β3 integrin expression (Kim et al. 2007). In addition to regulating αv/β3 integrin, HOXA10 regulates FKBP52, a PGR regulator required for implantation and decidualization (Yang et al. 2012; Tranguch et al. 2005) and reduced in the endometrium of women and non-human primates with endometriosis (Hirota et al. 2008; Yang et al. 2012; Jackson et al. 2007).

Several other steroid hormone-regulated pathways we have discussed are both implicated in endometriosis and closely involved in pregnancy establishment. Proteins involved in regulation and mediation of the P4-responsive IHH pathway including GATA2, SOX17, IHH, COUP-TFII, and WNT4 are required for successful implantation in mice (Rubel et al. 2016; Guimaraes-Young et al. 2016; Lee et al. 2006; Kurihara et al. 2007; Franco et al. 2011) but are reduced in the endometrium of women with endometriosis (Liang et al. 2016; Lin et al. 2014; Smith et al. 2011; Wang et al. 2018; Dyson et al. 2014), revealing a potential large-scale molecular connection between P4 resistance and fertility problems in endometriosis. The transcriptional regulators FOXO1, ARID1A, and HDAC3 are three additional factors associated with P4 signaling that are required for uterine receptivity in mice and down-regulated in the endometrium of women with endometriosis, further corroborating the association between the P4 resistance of endometriosis with infertility (Vasquez et al. 2018; Kim, Yoo, Wang, et al. 2015; Kim et al. 2019; Burney et al. 2007; Su et al. 2015). Finally, the E2-responsive cytokine LIF, required for fertility in mice and women (Chen et al. 2000; Stewart et al. 1992), is both decreased generally in endometrium from women with endometriosis (Dimitriadis et al. 2006) and specifically correlated with failure to achieve pregnancy in women with the disease (Moberg et al. 2015). Taken together, the evidence of dysregulation in these pregnancy-associated pathways and molecules in endometriosis is a

strong indicator of a causative relationship between endometriosis and endometrial non-receptivity related to P4 and E2 signaling dysregulation.

1.5.2. Pelvic Pain

In addition to infertility, it is commonly known that many women with endometriosis experience pelvic pain. Indeed, one study found 80% of women diagnosed with chronic pelvic pain to have endometriosis, firmly establishing the association (Carter 1994). Several mechanisms have been proposed for the pain of endometriosis including invasion of lesions into highly innervated regions, increased endometrial nerve density, increased neuroangiogenesis, neuroinflammation, and central and peripheral sensitization (Morotti, Vincent, and Becker 2017; Berkley, Rapkin, and Papka 2005; Morotti et al. 2014). A comprehensive discussion of endometriosis pain is not our purpose here, but we will briefly mention several links that have been discovered between E2 signaling and the pain mechanisms of endometriosis. First, several factors involved in nerve growth and found upregulated in women with endometriosis (Zondervan et al. 2018) have been found to be regulated by E2, including nerve growth factor (NGF) (Bjorling et al. 2002), vascular endothelial growth factor (VEGF) (McLaren et al. 1996), and brain-derived neurotrophic factor (BDNF) (Krizsan-Agbas et al. 2003). Additionally, hormonal therapies designed to combat the E2 dominance of endometriosis have been shown to decrease endometrial nerve fiber density in women with endometriosis, implying a role for E2 in increased innervation (Tokushige et al. 2008). E2 has also been implicated in the neuroinflammation of endometriosis by increasing macrophage-nerve interactions in endometriotic lesions (Greaves et al. 2015). Furthermore, a recent study revealed a role for E2 in regulating the axonal guidance protein slit guidance ligand 3 (SLIT3) in the process of neuroangiogenesis in endometriotic lesions (Greaves,

Collins, et al. 2014). Finally, nociceptors are sensory nerve endings that transmit noxious stimuli to the central nervous system in the presence of potential damage, and transient receptor potential cation channel subfamily V member 1 (TRPV1), an ion channel protein associated with these neurons, has been found to be increased in endometriotic lesions of women with chronic pelvic pain (Rocha et al. 2011) and to be responsive to E2 (Greaves, Grieve, et al. 2014). These mechanisms, among others, are potential avenues by which E2 elevation in endometriosis may worsen the pain associated with the disease.

1.6 Hormone Therapies for Endometriosis

Treatments for endometriosis that aim to alter E2 and P4 signaling are currently in use, such as combined oral contraceptives (COCs), progestins, gonadotropin-releasing hormone (GnRH) agonists, and aromatase inhibitors, and others are still under development, such as GnRH antagonists, selective estrogen receptor modulators (SERMs), and selective progesterone receptor modulators (SPRMs) (Vercellini et al. 2018; Tosti et al. 2017; Ferrero, Evangelisti, and Barra 2018) (Table 1.3).

Table 1.3 *Hormone therapies for endometriosis*

	Treatment Type	Molecular Action	Therapeutic Effect	Reference
Estrogen (E2) Signaling Modifiers	Gonadotropin-releasing hormone (GnRH) agonists	Decrease E2 production through negative feedback	Reduce endometriosis-related pain	(Ferrero, Evangelisti, and Barra 2018; Brown, Pan, and Hart 2010)
	GnRH antagonists	Decrease E2 production by competing for GnRH receptors	Reduce endometriosis-related pain	(Cetel et al. 1983; Taylor et al. 2017)
	Aromatase inhibitors	Decrease E2 production by inhibiting conversion of androgens to E2	Reduce endometriosis-related pain and lesion size	(Dunselman et al. 2014; Bilotas et al. 2010; Verma and Konje 2009)
	Selective estrogen receptor modulators (SERMs)	Decrease estrogen receptor 1 (ESR1) action through direct inhibition	Reduce endometriotic lesions	(Ferrero, Evangelisti, and Barra 2018; Kulak et al. 2011; Yao et al. 2005; Stratton et al. 2008)
Progesterone (P4) Signaling Modifiers	Combined oral contraceptives (COCs)	Suppress ovarian steroid production and supplement P4 levels	Reduce endometriosis-related pain and recurrence after surgery	(Dunselman et al. 2014; Vercellini et al. 2008; Harada et al. 2008; Harada et al. 2017)
	Progestins	Supplement P4 levels	Reduce endometriosis-related pain and lesions	(Dunselman et al. 2014; Tosti et al. 2017; Muneyyirci-Delale and Karacan 1998; Crosignani et al. 2006; Lockhat, Emembolu, and Konje 2005; Sroyraya et al. 2018; Selak et al. 2007; Strowitzki et al. 2010; Harada et al. 2009; Fu et al. 2008; Hayashi et al. 2012; Shimizu et al. 2011)
	Selective progesterone receptor modulators (SPRMs)	Interact with progesterone receptor (PGR) to enhance downstream effects	Reduce endometriosis-related pain and lesions	(Tosti et al. 2017; Kettel et al. 1994; Kettel et al. 1996)

These treatments generally aim to treat the lesion growth itself and/or the pelvic pain of the disease. Currently, no medical treatments are available to treat the infertility associated with endometriosis because hormone therapies interfere with ovarian function (Tomassetti and D'Hooghe 2018), although some evidence indicates a possible benefit to timed treatments combined with surgery or assisted reproductive technologies (Lessey and Kim 2017).

Several medical treatments for endometriosis directly aim to reduce E2 production or action in order to mitigate E2 dominant conditions. GnRH agonists are normally second-line treatments that decrease hormone levels by downregulating the pituitary through negative feedback mechanisms (Ferrero, Evangelisti, and Barra 2018). In randomized controlled trials (RCTs), GnRH agonists have been shown to be effective in reducing endometriosis-related pain (Brown, Pan, and Hart 2010), but they may also have adverse effects such as bone mineral density loss due to a hypoestrogenic state, requiring hormone "add-back" for long term use (Ferrero, Evangelisti, and Barra 2018). GnRH antagonists are also currently under investigation for endometriosis treatment. Like GnRH agonists, they downregulate gonadotropins, but they do not cause flare-ups like GnRH agonists because they rapidly and directly compete for GnRH receptors (Cetel et al. 1983). A recent RCT showed one GnRH antagonist to be effective at reducing endometriosis pain but to have similar hypoestrogenic adverse effects as GnRH agonists (Taylor et al. 2017). Aromatase inhibitors such as anastrazole or letrozole are also in use for some endometriosis patients, although they are recommended only for women who do not respond to other available treatments due to severe side effects (Dunselman et al. 2014). In a mouse model of endometriosis, aromatase inhibitors decreased lesion size by increasing apoptosis and diminishing VEGF and PGE2 levels (Bilotas et al. 2010). Clinical trials have shown some success for aromatase inhibitors in reducing chronic pelvic pain, but significant adverse effects such as

irregular bleeding and joint pain have been reported (Verma and Konje 2009). There is also a relatively new category of drugs under investigation aimed at targeted downregulation of E2 signaling termed SERMs, and these bind directly to ESRs in a tissue-specific manner (Ferrero, Evangelisti, and Barra 2018). These have been shown to reduce lesions through downregulation of ESR1 and cell proliferation in rat models of endometriosis (Kulak et al. 2011; Yao et al. 2005), but a clinical trial in which treatment group endometriosis pain returned more quickly after surgery tempers enthusiasm presently and points to the need for further study before SERMs can be broadly used (Stratton et al. 2008).

Other medical treatments for endometriosis primarily center on treating the dysregulation of P4 signaling in endometriosis. COCs consisting of a formulation of E2 and progestins that suppress ovarian steroid production are often used as a first-line therapy for chronic treatment of endometriosis pain due to their practical benefits and safety over long-term use (Dunselman et al. 2014). COCs have shown efficacy in preventing endometriosis recurrence after surgical removal of lesions (Vercellini et al. 2008) as well as pain associated with the disease (Harada et al. 2008; Harada et al. 2017). It has been suggested that progestin-only therapies may be a better choice since the inclusion of E2 could exacerbate estrogenic conditions in the context of P4 resistance (Casper 2017). Progestin-based therapies such as norethisterone acetate, levonorgestrel, and medroxyprogesterone acetate (MPA) are another first-line treatment choice for endometriosis pain (Dunselman et al. 2014). These compounds cause decidualization and atrophy of both the eutopic endometrium and endometriotic tissue (Tosti et al. 2017) and have proven to be effective at reducing endometriosis-related pain in clinical trials (Muneyyirci-Delale and Karacan 1998; Crosignani et al. 2006; Lockhat, Emembolu, and Konje 2005). MPA was specifically shown to have equivalent efficacy to a GnRH agonist at reducing pain but without the adverse

hypoestrogenic effects on bone density (Crosignani et al. 2006). In fact, one study revealed that MPA can decrease ESR1 and ESR2 while increasing PR-A and PR-B in the endometrium women with endometriosis (Sroyraya et al. 2018). Another drug in this category, danazol, works by promoting a high androgen, low E2 environment (Selak et al. 2007). Danazol has demonstrated efficacy in treating pain and reducing lesions in endometriosis, but significant androgenic side-effects occur (Selak et al. 2007). A more recently developed progestin, dienogest (DNG), shows much promise. DNG has been shown to successfully reduce endometriosis-associated pelvic pain with limited adverse effects such as minor irregular bleeding (Strowitzki et al. 2010; Harada et al. 2009). Furthermore, DNG inhibits endometriotic stromal cell proliferation (Fu et al. 2008), increases the PR-B/PR-A ratio and decreases the ESR2/ESR1 ratio (Hayashi et al. 2012), and inhibits E2 production and aromatase expression (Shimizu et al. 2011).

While progestins are an effective treatment option for many women with endometriosis, P4 resistance renders many others unresponsive to progestin treatment (Vercellini, Cortesi, and Crosignani 1997). This dilemma serves as a call for new treatment strategies, one of which may be SPRMs currently under investigation. These drugs interact directly with PGR to alter its downstream effects for the purpose of reducing proliferation and prostaglandin production (Tosti et al. 2017). Mifepristone trials have indicated its efficacy in endometriosis pain improvement and lesion reduction, although results are mixed (Kettel et al. 1994; Kettel et al. 1996). One early report indicated asoprisnil, which has mixed P4 agonist/antagonist activity and endometrial selectivity, also succeeded in lowering endometriosis-related pain, but this trial was apparently cut short due to some women developing endometrial hyperplasia (Tosti et al. 2017). Clearly, further investigation must be carried out to assess the safety and efficacy of this class of molecules, but it represents a potential new avenue for women who do not respond to currently available therapies.

1.7 ARID1A in Endometrial Function and Pathophysiology

Having broadly reviewed the primary known physiological processes and molecular pathways that govern endometrial homeostasis in the context of pregnancy and how they are dysregulated in endometriosis, we can now turn to focus on ARID1A, already introduced as a chromatin remodeling complex subunit important in the uterus for the establishment of pregnancy and associated with endometriosis when its gene is mutated and/or underexpressed. ARID1A is a 250 kDa subunit of the mammalian SWI/SNF BRG1-associated factors (BAF) complex which together binds at many loci in the genome to maintain chromatin accessibility or remodel nucleosome structure (Centore et al. 2020). As a result, these changes in structure affect the ability of transcription factors to access particular regions of the genome to facilitate expression of the genes therein. ARID1A's biochemical function is to provide rigidity of structure to the complex, non-specifically bind DNA, and facilitate the BAF complex's ability to slide along DNA (Mathur 2018; He et al. 2020).

ARID1A is essential for embryonic development, as *Arid1a*-null mouse embryos fail to gastrulate (Gao et al. 2008). It is also necessary for maintenance of pluripotency in embryonic stem cells, and it suppresses cell proliferation and tissue regeneration (Gao et al. 2008; Sun et al. 2016). Of all the SWI/SNF subunits, *ARID1A* is the most frequently mutated in cancers, with substantial percentages of ovarian, gastric, bladder, endometrial, and lung tumors, to name a few, harboring inactivating mutations that cause loss of ARID1A protein expression (Mathur 2018). Gynecological cancers including clear cell ovarian carcinoma and endometrioid ovarian carcinoma, which are strongly associated with endometriosis, are some of the most common cancer types to display *ARID1A* mutations (Wang et al. 2020). *ARID1A* inactivation is not, on its own, enough to drive malignant transformation; rather, *ARID1A* mutations appear to typically be later

events that contribute to the progression rather than initial development of tumors, particularly in the case of endometrial cancers (Wang et al. 2020).

Not all *ARID1A* mutations are associated with cancer. Inactivating mutations that cause expression loss have been identified in non-malignant deeply infiltrating endometriotic lesions (Anglesio et al. 2017) and ovarian endometriomas (Suda et al. 2018) without concurrent cancer, and mutations in normal, apparently healthy endometrial tissue have also been reported (Lac et al. 2019). Furthermore, the ARID1A protein expression level is reduced in endometrial samples from women with endometriosis (Kim, Yoo, Wang, et al. 2015). Since *ARID1A* mutations in benign endometrial tissue are very rare (Suda et al. 2018; Lac et al. 2019), the decrease in ARID1A expression in the endometrium of women with endometriosis likely stems from dysfunction at the epigenetic, transcriptional, or post-transcriptional level rather than from genetic mutations.

This conclusion fits well with what is currently known about the genetics of endometriosis. Though having a family member with endometriosis increases a woman's chances of developing it as well, familial candidate gene studies and genetic association studies have not yielded meaningful results (Bulun et al. 2019). Numerous genome-wide association studies (GWASs) have searched for single-nucleotide polymorphisms (SNPs) significantly associated with endometriosis in thousands of cases and controls (Bulun et al. 2019). Meta-analyses of these studies have identified several loci of interest including sites near *WNT4*, *GREB1*, *VEZT* (vezatin), *CDKN2B-AS1* (LncRNA cyclin-dependent kinase inhibitor 2B antisense RNA 1), *ID4* (Inhibitor of DNA binding 4), *FN1* (Fibronectin 1), *CCDC170* (Coiled-coil domain containing 170), *ESR1*, *SYNE1* (Spectrin repeat containing nuclear envelope protein 1), and *FSHB* (Follicle stimulating hormone subunit beta), many of which play roles in steroid hormone signaling and function (Nyholt et al. 2012; Rahmioglu et al. 2014; Sapkota et al. 2017). However, no endometriosis-associated SNPs

have been reported in the *ARID1A* gene despite one group specifically looking for them (Falconer et al. 2012). Therefore, while somatic *ARID1A* mutations may contribute to endometriotic lesion progression in some cases, there is currently no evidence for a genetic basis of *ARID1A*-related endometrial dysfunction in endometriosis.

At the molecular level, focused mechanistic study of ARID1A's function in endometriotic epithelial cells has shown that in this cell context, ARID1A promotes chromatin accessibility and maintenance of epithelial cell identity, whereas ARID1A loss leads to the accessibility and expression of epithelial to mesenchymal transition-related genes (Wilson et al. 2019). Furthermore, ARID1A bound regions of the genome in sorted mouse endometrial epithelial cells are associated with accessible chromatin near promoters of genes related to inflammation and apoptosis (Reske et al. 2021).

As demonstrated in mice, ARID1A is required for normal physiological female reproductive function through enabling embryo implantation and uterine stromal decidualization (Kim, Yoo, Wang, et al. 2015). To maintain uterine receptivity during early pregnancy, uterine ARID1A must be present to maintain epithelial PGR signaling and suppress E2-induced epithelial proliferation (Kim, Yoo, Wang, et al. 2015). Moreover, ARID1A expression is decreased in endometrial samples from infertile women with endometriosis, ARID1A colocalizes with PGR in both the human and mouse endometrium, and ARID1A levels correlate with PGR in endometrium affected by endometriosis (Kim, Kim, et al. 2021; Kim, Yoo, Wang, et al. 2015).

This dissertation aims to further determine the physiological function of ARID1A in the endometrium and elucidate the impact of ARID1A loss in endometriosis-related infertility. We hypothesized that ARID1A loss connects endometriosis and infertility by causing increased lesion development and a non-receptive endometrium. After this introductory Chapter 1, Chapter 2

describes a critical role of ARID1A in endometrial gland development and pregnancy function that is dysregulated in endometriosis using a multi-model approach involving endometrial epithelial-specific *Arid1a* knockout mice, non-human primates with experimentally induced endometriosis, and clinical human endometrial biopsy samples from women with endometriosis. Chapter 3 provides evidence that endometrial epithelial ARID1A is required in vivo to suppress inflammation and regulate uterine immune homeostasis during early pregnancy. In Chapter 4, the pathophysiological relationship between ARID1A loss, endometriosis lesion development, and endometriosis-related infertility is explored using mouse models of endometriosis. Chapter 5 presents a new experimental method for in vivo imaging of endometriosis lesion development and pregnancy progression in mice using nanoparticle labeling and photoacoustic imaging. The concluding Chapter 6 serves to summarize and discuss the overall findings of this dissertation and present directions for future studies.

1.8 Acknowledgements

Work reported in this chapter was supported in part by the Eunice Kennedy Shriver National Institute of Child Health and Human Development of the National Institutes of Health under Award Numbers R01HD084478 and T32HD087166 as well as MSU AgBio Research and Michigan State University. The content is solely the responsibility of the authors and does not necessarily represent the official views of the National Institutes of Health. We thank Olivia Jeong for illustration.

CHAPTER 2

ENDOMETRIAL EPITHELIAL ARID1A IS CRITICAL FOR UTERINE GLAND FUNCTION IN EARLY PREGNANCY

Content in this chapter is a modified version of a previously published work (Marquardt et al. 2021): Ryan M. Marquardt, Tae Hoon Kim, Jung-Yoon Yoo, Hanna E. Teasley, Asgerally T. Fazleabas, Steven L. Young, Bruce A. Lessey, Ripla Arora, and Jae-Wook Jeong (2021). Endometrial epithelial ARID1A is critical for uterine gland function in early pregnancy establishment. *FASEB J*; 35:e21209.

2.1 Abstract

Though endometriosis and infertility are clearly associated, the pathophysiological mechanism remains unclear. Previous work has linked endometrial ARID1A loss to endometriosis-related endometrial non-receptivity. In this chapter, we show in mice that ARID1A regulates transcription of the *Foxa2* gene required for endometrial gland function. Uterine specific deletion of *Arid1a* compromises gland development and diminishes *Foxa2* and *Lif* expression. Deletion of *Arid1a* with lactoferrin (*Ltf*)-*iCre* in the adult mouse endometrial epithelium preserves gland development while still compromising gland function. Mice lacking endometrial epithelial *Arid1a* are severely sub-fertile due to defects in implantation, decidualization, and endometrial receptivity from disruption of the LIF-STAT3-EGR1 pathway. FOXA2 is also reduced in the endometrium of women with endometriosis in correlation with diminished ARID1A, and both ARID1A and FOXA2 are reduced in non-human primates induced with endometriosis. Our

findings describe a role for ARID1A in the endometrial epithelium supporting early pregnancy establishment through the maintenance of gland function.

2.2 Introduction

A primary function of the uterus is to support fertility by protecting and nourishing an embryo as it develops into a fetus and matures until birth. The inner layer of the uterus, the endometrium, is composed of a luminal epithelial cell layer surrounded by a supportive stromal cell layer containing epithelial gland structures. In the presence of an embryo, these distinct cell types coordinate through complex epithelial-stromal crosstalk to facilitate implantation and the establishment of a healthy pregnancy (Hantak, Bagchi, and Bagchi 2014).

The ovarian steroid hormones P4 and E2 govern the human menstrual cycle in a 28-30 day process where E2-driven proliferation builds endometrial thickness in the proliferative phase before giving way to the P4-dominated secretory phase, which contains the transient window of embryo receptivity that depends on the length of P4 exposure (Wilcox, Baird, and Weinberg 1999). In order for successful pregnancy establishment to take place, endometrial epithelial cells must cease proliferation to allow embryo invasion, and stromal cells must be ready to differentiate into epithelioid secretory cells in a process called decidualization (Cha, Sun, and Dey 2012). In mice a parallel process occurs, but instead of a menstrual cycle, mice undergo a 4-5 day estrous cycle, in which the implantation window opens with a nidatory E2 surge (Cha, Sun, and Dey 2012; Wetendorf and DeMayo 2014).

P4 and E2 maintain a tightly regulated, dynamic balance in the endometrium as they enact downstream signaling pathways, primarily through their cognate receptors, the PGR isoforms PR-A and PR-B, and the estrogen receptors (ESR1 and ESR2) (Cha, Sun, and Dey 2012; Wetendorf

and DeMayo 2014; Kumar et al. 2011). However, as reviewed in Chapter 1, dysregulation of P4 and E2 signaling is common in uterine diseases such as endometriosis (Marquardt et al. 2019; Kumar et al. 2014). Endometriosis occurs when endometrium-like tissue grows outside the uterus. Affecting about 1 in 10 women of reproductive age, this common disease frequently causes dysmenorrhea, chronic pelvic pain, and loss of fertility (Zondervan et al. 2018). Severe endometriosis can compromise fertility by directly diminishing ovarian reserve through endometriomas or by the distorting of pelvic anatomy, but these mechanisms do not explain the fertility defects observed in mild cases of endometriosis when endometrial receptivity is apparently affected (Holoch and Lessey 2010; de Ziegler, Borghese, and Chapron 2010).

The nidatory E2 surge in the mouse induces secretion of LIF, a cytokine necessary for implantation and decidualization, from endometrial glands (Cha, Sun, and Dey 2012). Abundant evidence in several mammalian species supports the essential role of uterine glands and secretion of LIF in processes necessary for pregnancy success including implantation, decidualization, and placentation (Kelleher, DeMayo, and Spencer 2019; Kelleher et al. 2017). LIF expression is reportedly decreased in the glandular epithelium of women with endometriosis (Dimitriadis et al. 2006), which may reflect more general gland dysfunction. FOXA2, one of three FoxA family transcription factors involved in the development and function of many organs (Golson and Kaestner 2016), is necessary for endometrial gland development, LIF expression, and pregnancy establishment in mice (Jeong et al. 2010; Kelleher et al. 2017). Being the only FoxA family member expressed in the mouse and human uterus, FOXA2 is specific to the glandular epithelium, and its mutation or loss of expression has been reported in uterine diseases such as endometrial cancers (Neff et al. 2018) and endometriosis (Yang et al. 2015; Lin et al. 2018; Hawkins et al. 2011). Though its physiological function in the human endometrium is not well characterized,

recent evidence indicates that FOXA2 coordinates with other factors and pathways critically involved in uterine receptivity, implantation, and decidualization (Kelleher et al. 2019).

ARID1A, a 250 kDa SWI/SNF chromatin remodeling complex subunit with known tumor suppressor function, has been linked to both endometriosis and regulation of endometrial receptivity (Mathur 2018; Kim, Yoo, Wang, et al. 2015; Anglesio et al. 2017). Though it is commonly mutated in endometriosis-associated ovarian cancers (Wiegand et al. 2010), the role of ARID1A in normal uterine physiology and in benign diseases such as endometriosis is not well understood. In normal conditions, ARID1A maintains strong nuclear expression in all uterine compartments throughout the menstrual cycle in women and throughout early pregnancy in mice (Kim, Yoo, Wang, et al. 2015). However, inactivating mutations in the *ARID1A* gene have been identified in deeply infiltrating endometriotic lesions (Anglesio et al. 2017) and ovarian endometriomas (Suda et al. 2018), and ARID1A expression is reduced in eutopic endometrial epithelium and stroma from women with endometriosis (Kim, Yoo, Wang, et al. 2015). Though other cancer-associated genes are frequently mutated in the normal eutopic endometrium and in that of women of endometriosis, *ARID1A* mutations are very rare (Suda et al. 2018; Lac et al. 2019), implying that the decrease in ARID1A expression in the endometrium of women with endometriosis likely takes place at the epigenetic, transcriptional, or post-transcriptional level. We previously reported that deletion of uterine *Arid1a* in mice ($Pgr^{cre/+}Arid1a^{f/f}$) causes infertility due to implantation and decidualization defects, increased E2-induced epithelial proliferation, and decreased epithelial P4 signaling at pre-implantation (Kim, Yoo, Wang, et al. 2015). Based on these findings, we hypothesized that endometrial epithelial ARID1A is critical to regulate gene expression programs necessary for early pregnancy.

In this chapter, we used a multi-model approach to determine the role of endometrial epithelial ARID1A in endometrial gland function and early pregnancy establishment with regard to endometriosis-related infertility. Continuing our study of *Pgr*$^{cre/+}$*Arid1a*$^{f/f}$ mice, we report the additional finding that deletion of *Arid1a* in the mouse uterus caused an endometrial gland defect, another potential cause of infertility, starting during prepubertal development and affecting early pregnancy. ChIP analysis revealed that ARID1A directly binds at the *Foxa2* promoter at this stage. Targeting deletion of *Arid1a* to the endometrial epithelium of adult mice (*Ltf*$^{iCre/+}$*Arid1a*$^{f/f}$) resulted in defects of implantation, decidualization, endometrial receptivity, gland function, and critical signaling downstream of FOXA2 and LIF during early pregnancy. Furthermore, endometrial biopsy samples from women with endometriosis exhibited a decrease of FOXA2 that correlates with ARID1A levels. Decreases in both ARID1A and FOXA2 expression in the endometrium of non-human primates with induced endometriosis confirmed that this effect is endometriosis-specific.

2.3 Results

2.3.1 Uterine ARID1A is Critical for Endometrial Gland Development and Function and Binds the Foxa2 Promoter in Pregnant Mice

Because of the importance of FOXA2 and endometrial glands in the implantation process (Jeong et al. 2010; Kelleher et al. 2017; Kelleher et al. 2018), we analyzed gland formation and function in uterine-specific *Arid1a* knockout mice (*Pgr*$^{cre/+}$*Arid1a*$^{f/f}$) (Kim, Yoo, Wang, et al. 2015). *Pgr*$^{cre/+}$*Arid1a*$^{f/f}$ mice had significantly fewer endometrial glands compared to controls at gestation day (GD) 3.5, which marks the pre-implantation stage (Cha, Sun, and Dey 2012) (-2.20 fold, p=0.0165; Figure 2.1A). IHC analysis revealed a lack of FOXA2 in *Pgr*$^{cre/+}$*Arid1a*$^{f/f}$ glands

(Figure 2.1B). Due to the limitations of analyzing thin tissue sections, we utilized a whole-mount immunofluorescence approach combined with confocal imaging and quantitative image analysis to visualize the uterine structure in three dimensions (Arora et al. 2016). Three-dimensional imaging during early pregnancy revealed that in contrast to the abundance of uniformly oriented FOXA2-positive glands in control mice, *c* mice exhibited very few randomly scattered FOXA2-positive glands (Figure 2.1C). In order to more clearly understand the molecular dysregulation, we utilized our previously published transcriptomic data from GD 3.5 $Pgr^{cre/+}Arid1a^{f/f}$ mouse uteri (Kim, Yoo, Wang, et al. 2015) to compare the dysregulated genes to those dysregulated in $Pgr^{cre/+}Foxa2^{f/f}$ uteri at GD 3.5 (Filant, Lydon, and Spencer 2014). Out of a total of 2,075 genes differentially expressed due to *Arid1a* loss (2,556 probes >1.5 fold change, duplicate genes removed), 316 (15.23%) were also differentially expressed in $Pgr^{cre/+}Foxa2^{f/f}$ mice (out of 915 probes >1.5 fold change, duplicate genes removed; Figure 2.1D, Table A.1). Due to the importance of LIF in implantation (Stewart et al. 1992) and its diminished expression in the GD 3.5 $Pgr^{cre/+}Foxa2^{f/f}$ mouse uterus (Jeong et al. 2010; Kelleher et al. 2017), we analyzed *Lif* expression in the GD 3.5 $Pgr^{cre/+}Arid1a^{f/f}$ mouse uterus with quantitative reverse transcription polymerase chain reaction (RT-qPCR) and found it to be significantly reduced (-8.44 fold, p=0.0357; Figure 2.1E). We also confirmed that *Foxa2* mRNA transcripts were decreased in the $Pgr^{cre/+}Arid1a^{f/f}$ mouse uterus along with serine protease inhibitor Kazal type 3 gene (*Spink3*) and Chemokine (C-X-C motif) ligand 15 (*Cxcl15*), previously recognized gland-specific genes (Filant, Lydon, and Spencer 2014; Kelleher et al. 2017; Kelleher et al. 2018) (-8.83 fold, p=0.0159; -71.86 fold, p=0.0159; -5.66 fold, p=0.0002; respectively; Figure 2.1E). Together, these findings reveal a major defect of endometrial gland structure and function in $Pgr^{cre/+}Arid1a^{f/f}$ mice during early pregnancy.

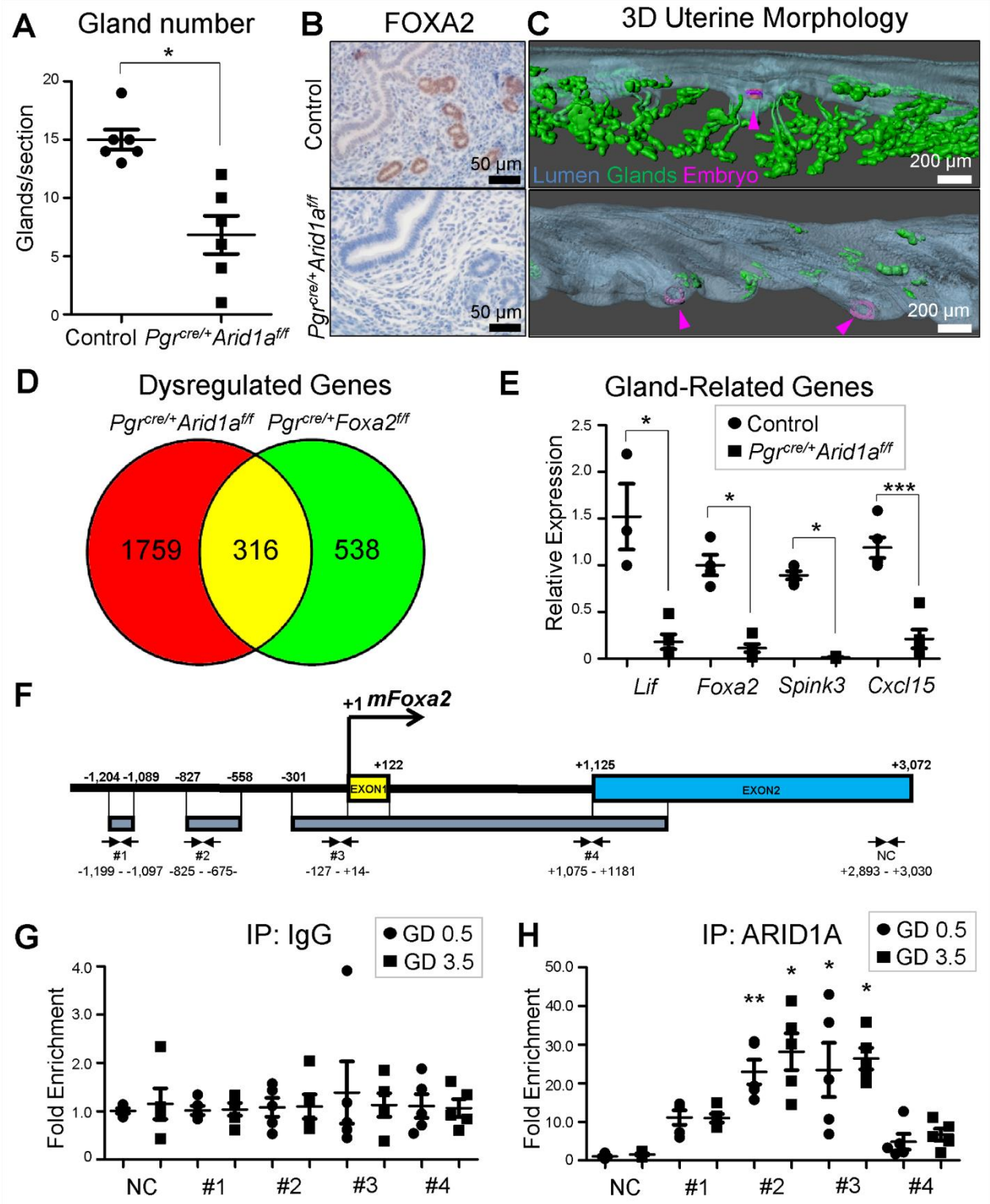

Figure 2.1 *Uterine ARID1A is critical for endometrial gland development and function and binds the Foxa2 promoter in pregnant mice.* **(A)** Endometrial gland counts in control and *Pgr*$^{cre/+}$*Arid1a*$^{f/f}$ mice at GD 3.5. The graph represents the mean ± standard error of mean (SEM) of the number of glands per uterine tissue section (n=6; *, p<0.05). **(B)** Representative images of FOXA2 IHC in control and *Pgr*$^{cre/+}$*Arid1a*$^{f/f}$ mouse uterine sections at GD 3.5 (n=4). **(C)** Three-dimensional

Figure 2.1 (cont'd)
uterine morphology of control and *Pgr*$^{cre/+}$*Arid1a*$^{f/f}$ uterine horns during early pregnancy based on whole-mount immunofluorescence for E-cadherin and FOXA2, where the 3D luminal structure (blue) is constructed by subtracting the FOXA2 (green) from the E-cadherin signal (n=4). Arrowheads indicate embryos within the uterine horns. **(D)** Overlapping genes dysregulated at GD 3.5 in the uterus by deletion of *Arid1a* or *Foxa2*. **(E)** Relative expression of endometrial gland-related gene mRNA normalized to *Gapdh* (*Lif*, *Foxa2*) or *Rpl7* (*Spink 3*, *Cxcl15*) in whole uterine tissue preparations at GD 3.5. The graphs represent the mean ± SEM (Control, n=3-5; *Pgr*$^{cre/+}$*Arid1a*$^{f/f}$, n=5); *, $p<0.05$; ***, $p<0.001$). **(F)** The schematic shows putative ARID1A binding sites near the *Foxa2* gene (#1, 2, 3, 4). **(G)** Fold enrichment based on RT-qPCR targeting putative ARID1A binding sites in GD 0.5 and GD 3.5 mouse uteri after ChIP using IgG control. The graph shows the mean ± SEM (n=5). **(H)** Fold enrichment based on RT-qPCR targeting putative ARID1A binding sites in GD 0.5 and GD 3.5 mouse uteri after ChIP using anti-ARID1A antibody. The graph shows the mean ± SEM (n=5; *, $p<0.05$; **, $p<0.01$).

Because deletion of *Foxa2* during early postnatal development causes drastic loss of gland formation (Jeong et al. 2010; Filant, Lydon, and Spencer 2014), we analyzed the 3-4-week-old *Pgr*$^{cre/+}$*Arid1a*$^{f/f}$ mouse uterus to determine if the gland defect found during early pregnancy was also present before maturity. Indeed, 4-week-old *Pgr*$^{cre/+}$*Arid1a*$^{f/f}$ mice exhibited a significantly decreased endometrial gland number and loss of FOXA2 expression, and 3-week-old *Pgr*$^{cre/+}$*Arid1a*$^{f/f}$ mice showed a lack of FOXA2-positive gland elongation compared to controls based on 3D image reconstruction (Figure A.1A-C). These findings indicate that the structural and functional gland defect in *Pgr*$^{cre/+}$*Arid1a*$^{f/f}$ mice is not specific to early pregnancy but starts during prepubertal development.

Analysis of publicly available ARID1A ChIP-seq data from HepG2 cells (Raab, Resnick, and Magnuson 2015) identified putative binding sites for ARID1A near the *Foxa2* gene (Figure 2.1F). To determine whether ARID1A binds these sites in the mouse uterus during early pregnancy, we performed ChIP-qPCR on whole uterine tissue lysates from wildtype mice at GD 0.5 and GD 3.5 with primers designed to target the putative binding regions. As expected, immunoprecipitation (IP) with nonspecific Immunoglobulin G (IgG) showed no region of

significant enrichment compared to the negative control; however, IP with an ARID1A antibody followed by qPCR revealed significant enrichment of putative binding sites #2 (GD 0.5, 22.95 fold, $p<0.01$; GD 3.5, 18.73 fold, $p<0.05$) and #3 (GD 0.5, 23.47 fold, $p<0.05$; GD 3.5, 17.53 fold, $p<0.05$) over the negative control region (Figure 2.1G, H). This finding indicates that ARID1A directly binds the *Foxa2* promoter region in vivo.

2.3.2 Endometrial Epithelial-Specific Arid1a Loss Causes Severe Sub-Fertility and Compromises Gland Function in Mice

To further dissect the relationship between ARID1A and FOXA2 in the endometrium during early pregnancy, we conditionally ablated *Arid1a* in the adult mouse endometrial epithelium by crossing $Ltf^{iCre/+}$ (Daikoku et al. 2014) and $Arid1a^{f/f}$ (Gao et al. 2008) mice. When crossed with $Arid1a^{f/f}$ mice, this model causes *Arid1a* deletion in the luminal and glandular epithelium, while retaining *Arid1a* expression in the stroma in contrast to $Pgr^{cre/+}Arid1a^{f/f}$ mice which delete *Arid1a* in both epithelial and stromal compartments (Figure 2.2A, B). Additionally, this approach circumvents any developmental defects by restricting iCre expression to adulthood. To assess overall fecundity, $Ltf^{iCre/+}Arid1a^{f/f}$ and control females were housed with wildtype male mice in a six month fertility trial. Both groups of mice engaged in normal mating activity resulting in the observation of copulatory plugs, and control mice had expected numbers of litters and pups/litter. However, $Ltf^{iCre/+}Arid1a^{f/f}$ females were found to be severely sub-fertile, and the only three pups found were dead upon discovery (n=6; Figure A.2A). To determine if an ovarian defect was responsible for the severe sub-fertility of $Ltf^{iCre/+}Arid1a^{f/f}$ females, we examined ovarian histology, finding no anatomical abnormalities and normal development of corpora lutea (Figure A.2B). Furthermore, analysis of serum ovarian steroid hormone levels at GD 3.5 revealed no

differences between *Ltf*$^{iCre/+}$*Arid1a*$^{f/f}$ mice and controls in total E2 or P4 (Figure A.2C). These analyses indicate that the severe sub-fertility phenotype of *Ltf*$^{iCre/+}$*Arid1a*$^{f/f}$ mice is not due to a defect of ovarian function.

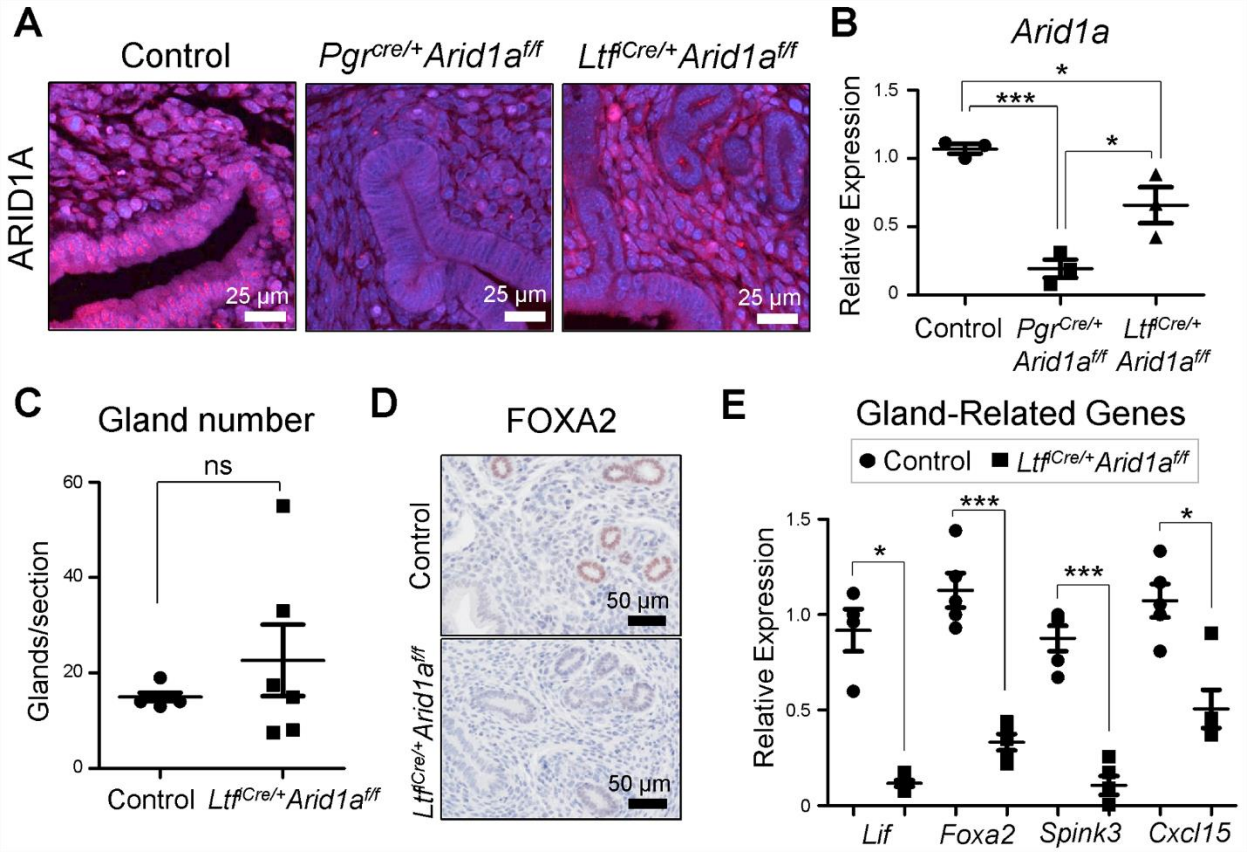

Figure 2.2 *Endometrial epithelial-specific Arid1a loss compromises gland function*. **(A)** Representative images show immunofluorescence staining of ARID1A (Texas Red) and DAPI (Blue) demonstrating strong ARID1A expression in the endometrial epithelium and stroma of control mice, loss of ARID1A expression in both epithelium and stroma of *Pgr*$^{cre/+}$*Arid1a*$^{f/f}$ mice, and loss of ARID1A in the epithelium but not stroma of *Ltf*$^{iCre/+}$*Arid1a*$^{f/f}$ mice at GD 3.5 (n=3/genotype). **(B)** Relative expression of *Arid1a* mRNA normalized to *Rpl7* in RT-qPCR using whole uterine tissue preparations. The graph displays the mean ± SEM (n=3/genotype; *, $p<0.05$; ***, $p<0.001$). **(C)** Endometrial gland counts in control and *Ltf*$^{iCre/+}$*Arid1a*$^{f/f}$ mice at GD 3.5. The graph represents the mean ± SEM of the number of glands per uterine tissue section (n=6; ns, $p>0.05$). **(D)** Representative images of FOXA2 IHC in control and *Ltf*$^{iCre/+}$*Arid1a*$^{f/f}$ mouse uterine sections (n=4). **(E)** Relative expression of endometrial gland-related gene mRNA normalized to *Rpl7* in whole uterine tissue preparations determined with RT-qPCR. The graphs represent the mean ± SEM (Control, n=4-5; *Ltf*$^{iCre/+}$*Arid1a*$^{f/f}$, n=5; *, $p<0.05$; ***, $p<0.001$).

To determine if endometrial epithelial *Arid1a* loss in adult mice compromises gland structure or function, we examined *Ltf*$^{iCre/+}$*Arid1a*$^{f/f}$ endometrial glands at GD 3.5. Gland counts from transverse uterine tissue sections revealed no difference in gland number between *Ltf*$^{iCre/+}$*Arid1a*$^{f/f}$ mice and controls (Figure 2.2C). Though the quantity of glands was unchanged, *Ltf*$^{iCre/+}$*Arid1a*$^{f/f}$ mice exhibited a defect of gland function at GD 3.5 indicated by decreased FOXA2 expression and significant decreases in uterine *Lif* (-7.89 fold, p=0.0159), *Foxa2* (-3.38 fold, p<0.0001), *Spink3* (-8.26 fold, p<0.0001), and *Cxcl15* (-3.12 fold, p=0.0159) mRNA levels (Figure 2.2D, E).

2.3.3 Ltf$^{iCre/+}$*Arid1a*$^{f/f}$ *Mice Exhibit Implantation and Decidualization Defects*

On the morning of GD 4.5, implantation sites were visible in control mouse uteri but not in *Ltf*$^{iCre/+}$*Arid1a*$^{f/f}$ uteri (Figure 2.3A). Hematoxylin and eosin (H&E) staining of transverse tissue sections revealed that though luminal closure and embryo apposition had occurred in *Ltf*$^{iCre/+}$*Arid1a*$^{f/f}$ mice, the decidualization response of stromal cells surrounding the embryo did not occur as in controls (Figure 2.3B). COX-2, a marker of decidualization (Kelleher et al. 2017), was present in stromal cells surrounding the embryo in controls but was limited to the epithelium in *Ltf*$^{iCre/+}$*Arid1a*$^{f/f}$ mice, providing molecular evidence of early decidualization response failure (Figure 2.3C).

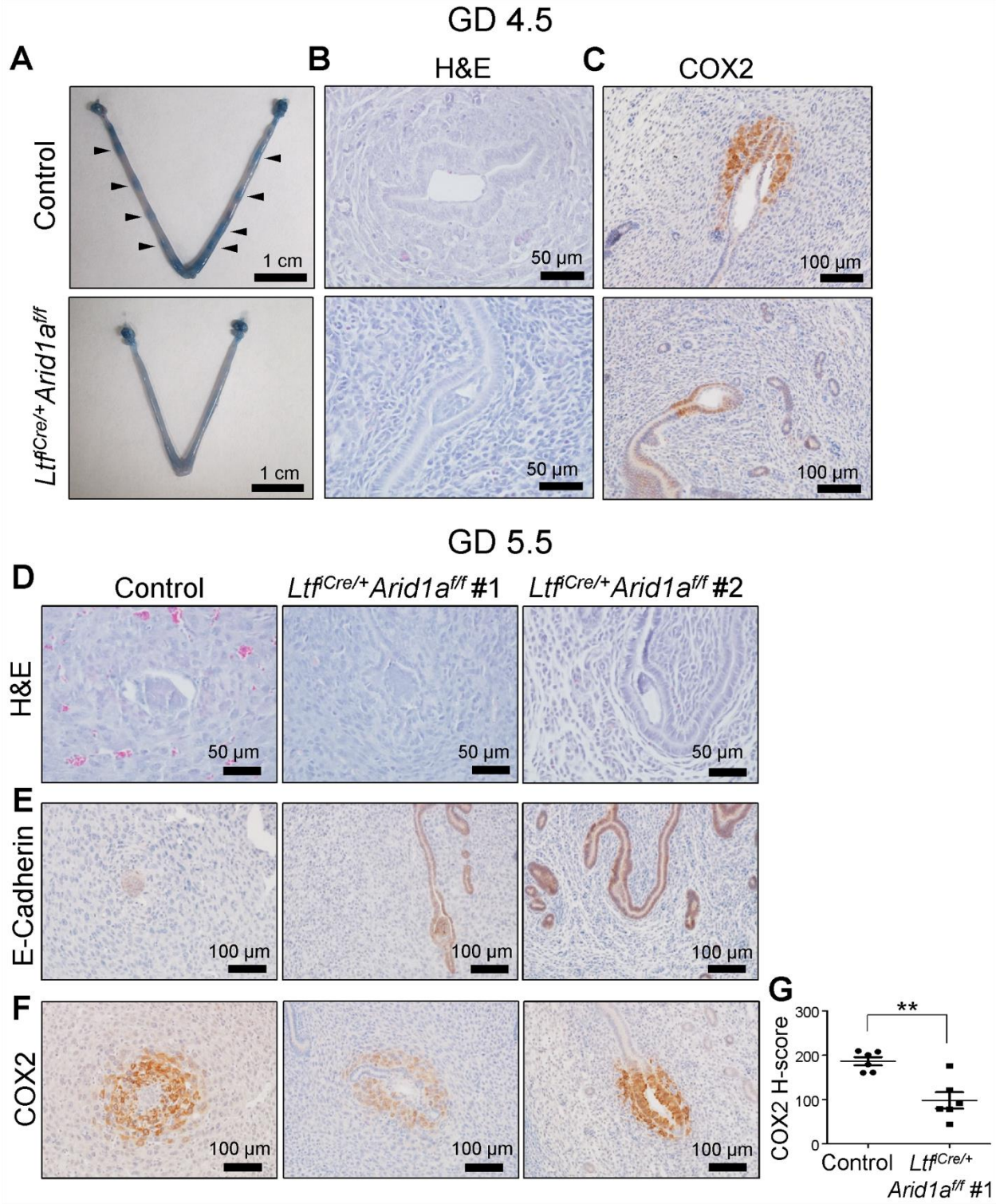

Figure 2.3 *Ltf*$^{iCre/+}$*Arid1a*$^{f/f}$ *mice exhibit an implantation defect*. **(A)** Implantation sites were grossly visible in control but not *Ltf*$^{iCre/+}$*Arid1a*$^{f/f}$ uteri at GD 4.5 after intravenous injection of Chicago Sky Blue 6B dye. Arrowheads indicate clear implantation sites (n=3). **(B)** Representative images of H&E staining showing decidualization of stromal cells around an implanting embryo in control but not *Ltf*$^{iCre/+}$*Arid1a*$^{f/f}$ uterine sections at GD 4.5 (n=11 IS). **(C)** Representative images

Figure 2.3 (cont'd)
of COX-2 IHC in control and *Ltf*$^{iCre/+}$*Arid1a*$^{f/f}$ mouse uteri at GD 4.5 (n=6 IS). **(D)** Representative images of H&E staining in control and *Ltf*$^{iCre/+}$*Arid1a*$^{f/f}$ uterine sections at GD 5.5 (n=5). In contrast to the control, the *Ltf*$^{iCre/+}$*Arid1a*$^{f/f}$ mouse luminal epithelium remained intact surrounding the embryos. Most *Ltf*$^{iCre/+}$*Arid1a*$^{f/f}$ implantation sites (18/21, 86%) exhibited some decidualizing stromal cells based on morphology (*Ltf*$^{iCre/+}$*Arid1a*$^{f/f}$ #1), though not to the same degree as controls. Some *Ltf*$^{iCre/+}$*Arid1a*$^{f/f}$ IS (3/21, 14%), however, underwent little to no decidualization (*Ltf*$^{iCre/+}$*Arid1a*$^{f/f}$ #2). **(E)** Representative images of E-cadherin IHC in control and *Ltf*$^{iCre/+}$*Arid1a*$^{f/f}$ mouse uteri at GD 5.5 (control and *Ltf*$^{iCre/+}$*Arid1a*$^{f/f}$ #1, n=6 IS; *Ltf*$^{iCre/+}$*Arid1a*$^{f/f}$ #2, n=3 IS). **(F)** Representative images of COX-2 IHC in control and *Ltf*$^{iCre/+}$*Arid1a*$^{f/f}$ mouse uteri at GD 5.5 (control and *Ltf*$^{iCre/+}$*Arid1a*$^{f/f}$ #1, n=6 IS; *Ltf*$^{iCre/+}$*Arid1a*$^{f/f}$ #2, n=3 IS). **(G)** Semi-quantitative H-score of COX-2 staining strength in uterine sections of control versus *Ltf*$^{iCre/+}$*Arid1a*$^{f/f}$ #1 phenotype group mice at GD 5.5. The graph represents the mean ± SEM (n=6 IS; **, $p<0.01$).

At post-implantation (GD 5.5), H&E analysis and IHC for E-cadherin, an epithelial tight junction protein, showed that the luminal epithelium remained intact around the embryo in all *Ltf*$^{iCre/+}$*Arid1a*$^{f/f}$ mice analyzed, whereas no luminal epithelium remained in controls due to successful embryo implantation (Figure 2.3D, E). H&E and COX-2 IHC revealed two subsets of decidual cell phenotypes in *Ltf*$^{iCre/+}$*Arid1a*$^{f/f}$ mice at GD 5.5. In 85.71% (18/21) of implantation sites observed (*Ltf*$^{iCre/+}$*Arid1a*$^{f/f}$ #1), some decidualization occurred, but not to the degree of controls as evidenced by less apparent decidual cell morphology and a significant reduction in COX-2 expression as indicated by H-score (-1.90 fold, p=0.0017; Figure 2.3D-F, center panel; G). In the remaining 14.29% of implantation sites (*Ltf*$^{iCre/+}$*Arid1a*$^{f/f}$ #2), little to no decidualization was apparent in the stroma (Figure 2.3D-F, right panel). In spite of defective implantation, embryos in *Ltf*$^{iCre/+}$*Arid1a*$^{f/f}$ uteri were firmly attached and could not be flushed (n=3).

To confirm the decidualization defect of *Ltf*$^{iCre/+}$*Arid1a*$^{f/f}$ mice, we performed hormonally and physically stimulated artificial decidualization induction to mimic an invading embryo (Kim, Yoo, Wang, et al. 2015). Though the stimulated horn of control mice underwent a robust decidualization reaction by decidualization day 5, very little decidualization occurred in the stimulated horn of *Ltf*$^{iCre/+}$*Arid1a*$^{f/f}$ mice as evidenced by gross morphology, significantly

decreased uterine horn weight ratio (-4.80 fold, p=0.0022), and cell morphology (Figure 2.4). This result clearly confirmed that the lack of a proper decidualization response in *Ltf*$^{iCre/+}$*Arid1a*$^{f/f}$ endometrial stromal cells was not merely a result of a lack of stimulation by the embryo. Together, these data display an implantation defect in *Ltf*$^{iCre/+}$*Arid1a*$^{f/f}$ mice resulting primarily from a failure of decidualization response.

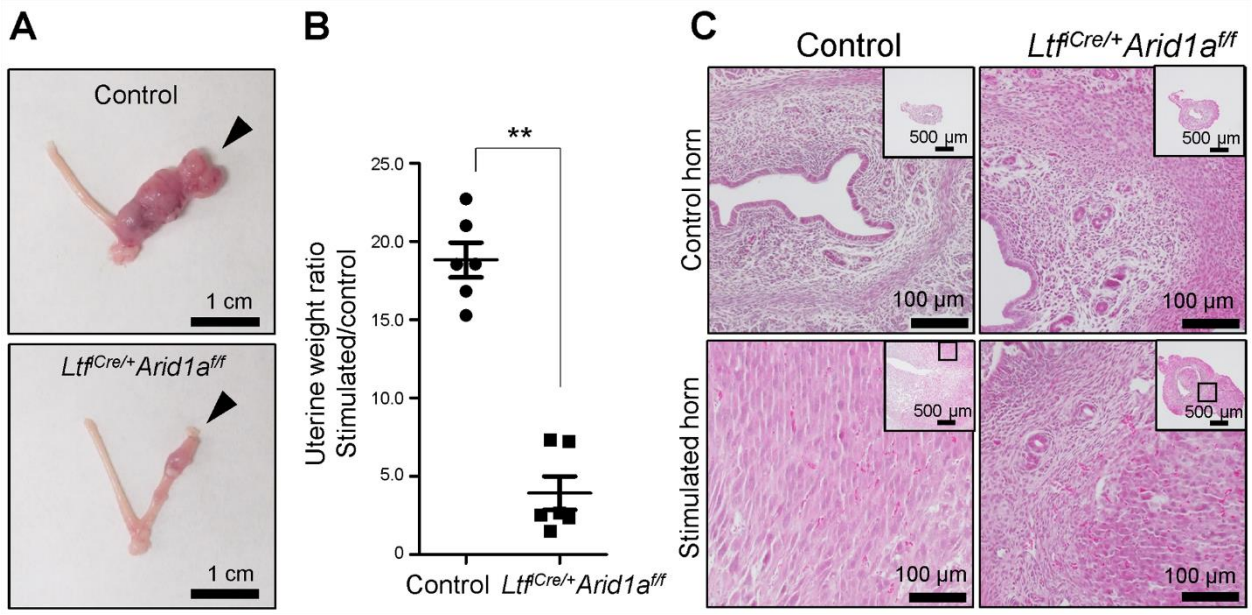

Figure 2.4. *Ltf*$^{iCre/+}$*Arid1a*$^{f/f}$ *mice exhibit a decidualization defect*. **(A)** Gross morphology of decidualization day 5 control and *Ltf*$^{iCre/+}$*Arid1a*$^{f/f}$ uteri, arrowheads indicating the stimulated uterine horn (n=6). **(B)** Stimulated/control horn weight ratio in control and *Ltf*$^{iCre/+}$*Arid1a*$^{f/f}$ mice. The graph represents the mean ± SEM (n=6; **, p<0.01). **(C)** Representative images of H&E staining show the decidual cell morphology in the stimulated horn of controls but defective decidualization in *Ltf*$^{iCre/+}$*Arid1a*$^{f/f}$ mice (n=6).

2.3.4 Ltf$^{iCre/+}$*Arid1a*$^{f/f}$ *Mice Exhibit a Non-Receptive Endometrium*

To assess the receptivity of the luminal epithelium in *Ltf*$^{iCre/+}$*Arid1a*$^{f/f}$ mice, we analyzed cell proliferation at pre-implantation (GD 3.5) using IHC for Ki67 and found that epithelial cell proliferation was significantly increased (16.44 fold, p<0.001) and stromal cell proliferation was significantly decreased (-4.71 fold, p<0.001) in *Ltf*$^{iCre/+}$*Arid1a*$^{f/f}$ uteri compared to controls (Figure 2.5). A highly proliferative epithelium at this stage indicates a non-receptivity to embryo

implantation (Kim, Yoo, Wang, et al. 2015), while an under-proliferative stroma could indicate a failure to properly prepare for decidualization (Hantak, Bagchi, and Bagchi 2014; Cha, Sun, and Dey 2012).

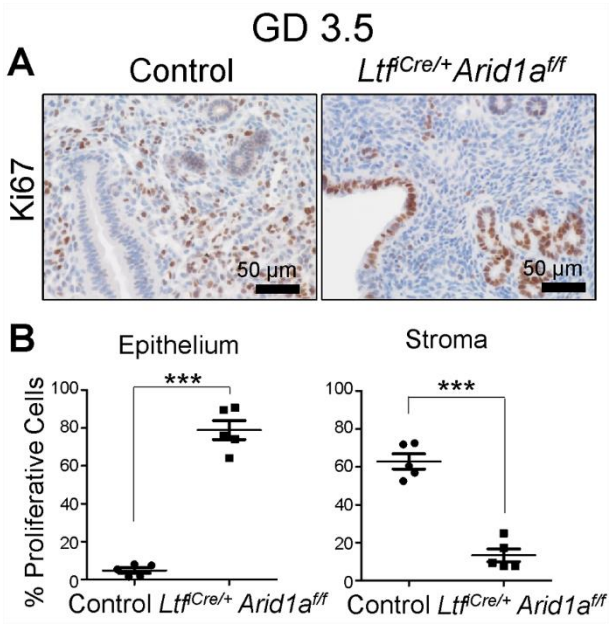

Figure 2.5 *Ltf*$^{iCre/+}$*Arid1a*$^{f/f}$ *mice exhibit a non-receptive endometrium*. **(A)** Representative images of Ki67 IHC in control and *Ltf*$^{iCre/+}$*Arid1a*$^{f/f}$ mouse uteri (n=3). **(B)** Percentage of proliferative cells in epithelial and stromal compartments of mouse endometrial tissue sections. The graphs represent the mean percentage of proliferative cells ± SEM (n=3, 5 tissue regions; ***, p<0.001).

A loss of PGR as previously shown in *Pgr*$^{cre/+}$*Arid1a*$^{f/f}$ mice (Kim, Yoo, Wang, et al. 2015) could explain the finding of a highly proliferative epithelium. However, the *Ltf*$^{iCre/+}$*Arid1a*$^{f/f}$ epithelium largely retained PGR expression at GD 3.5, and the PGR signal strength was not significantly different from controls based on H-score in the epithelium or the stroma, although there were patches of epithelial cells negative for PGR (Figure A.3A, B). Western blotting confirmed that total levels of the PGR isoforms PR-A and PR-B were not changed in *Ltf*$^{iCre/+}$*Arid1a*$^{f/f}$ uteri (Figure A.3C, D). Correspondingly, IHC revealed no changes in total ESR1 or pESR1 levels at this stage in *Ltf*$^{iCre/+}$*Arid1a*$^{f/f}$ uterine sections (Figure. A.3E, F). RT-qPCR analysis of P4 and E2 target gene expression in GD 3.5 *Ltf*$^{iCre/+}$*Arid1a*$^{f/f}$ uteri revealed that though

the majority of genes tested were not different than controls to the level of statistical significance, the P4 targets amphiregulin (*Areg*) and low density lipoprotein-related protein 2 (*Lrp2*) (Jeong et al. 2005) were significantly decreased, and the E2 targets chloride channel accessory 3 (*Clca3*), *Ltf*, and complement component 3 (*C3*) were significantly increased (Figure A3G, H). Taken together, these results indicate that PGR loss in patches of epithelial cells likely contributes to increased E2-induced epithelial proliferation in $Ltf^{iCre/+}Arid1a^{f/f}$ mice, though not to the degree previously noted in $Pgr^{cre/+}Arid1a^{f/f}$ mice (Kim, Yoo, Wang, et al. 2015).

FOXO1 is a transcription factor with known roles in regulating epithelial integrity (Vasquez et al. 2018) and decidualization (Takano et al. 2007) during implantation, and its expression is reciprocal to PGR (Vasquez et al. 2018). We profiled FOXO1 and PGR expression in $Ltf^{iCre/+}Arid1a^{f/f}$ mice during early pregnancy using IHC. At GD 3.5, we found that in patches of the luminal epithelium negative for PGR expression, nuclear FOXO1 expression was increased (Figure A.4A). Observation of the epithelium around implantation sites (IS) at GD 4.5 and at GD 5.5 inter-implantation sites (I-IS) revealed no marked changes in FOXO1 or PGR expression between $Ltf^{iCre/+}Arid1a^{f/f}$ mice and controls, implying that the non-receptive endometrium of $Ltf^{iCre/+}Arid1a^{f/f}$ mice is not due to dysregulation of FOXO1 (Figure A.4B, C).

2.3.5 The pSTAT3-EGR1 Pathway is Dysregulated during Early Pregnancy in $Ltf^{iCre/+}Arid1a^{f/f}$ Mice

Since $Ltf^{iCre/+}Arid1a^{f/f}$ mice exhibited decreased *Lif* expression at the pre-implantation stage, we examined the downstream effects of the decrease in *Lif* as another potential explanation for the defects in implantation, decidualization, and endometrial receptivity. For successful implantation to take place, STAT3 must be activated by phosphorylation downstream of LIF after

the GD 3.5 E2 surge, whereupon it induces EGR1 expression in the stroma (Lee, Kim, Oh, et al. 2013; Liang et al. 2014; Kim, Kim, et al. 2018). At GD 3.5, pSTAT3 is normally expressed robustly in endometrial epithelial cells (Lee, Kim, Oh, et al. 2013), but IHC analysis revealed that *Ltf*$^{iCre/+}$*Arid1a*$^{f/f}$ mice exhibit significantly decreased pSTAT3 (-8.96 fold, p=0.0079; Figure 2.6A, B). The further dysregulation of this pathway was evident in that EGR1 expression was significantly reduced in the GD 3.5 *Ltf*$^{iCre/+}$*Arid1a*$^{f/f}$ endometrial stroma based on IHC H-score (-2.09 fold, p=0.0242; Figure 2.6C, D).

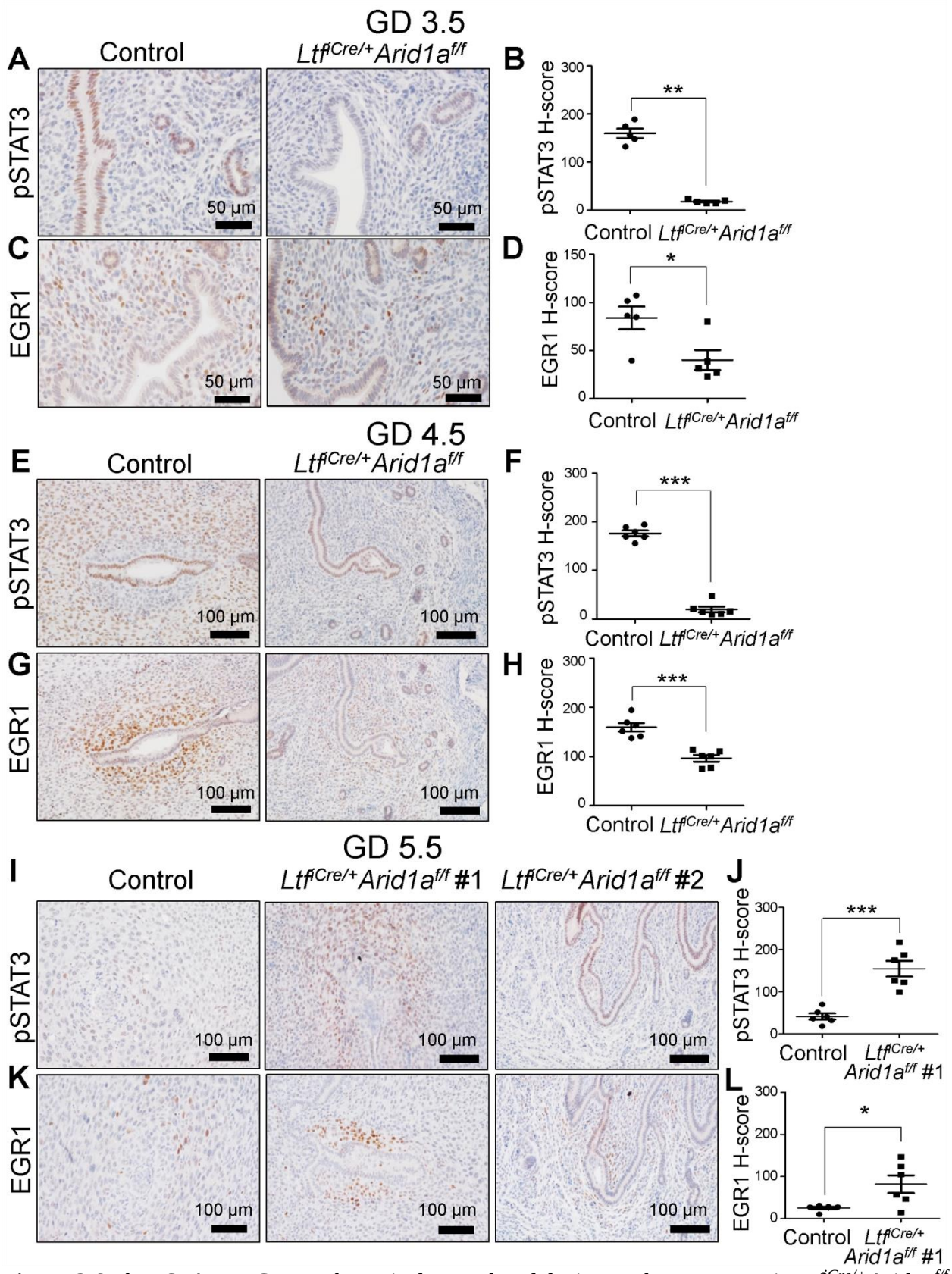

Figure 2.6 *The pSTAT3-EGR1 pathway is dysregulated during early pregnancy in Ltf*$^{iCre/+}$*Arid1a*$^{f/f}$

Figure 2.6 (cont'd)
mice. **(A)** Representative images of pSTAT3 IHC in control and *Ltf*$^{iCre/+}$*Arid1a*$^{f/f}$ mouse uterine tissue sections at GD 3.5 (n=3). **(B)** Semi-quantitative H-score of epithelial pSTAT3 staining strength at GD 3.5. The graph represents the mean ± SEM (n=3, 5 tissue regions; **, p<0.01). **(C)** Representative images of EGR1 IHC in control and *Ltf*$^{iCre/+}$*Arid1a*$^{f/f}$ mouse uterine tissue sections at GD 3.5 (n=3). **(D)** Semi-quantitative H-score of stromal EGR1 staining strength. The graph represents the mean ± SEM (n=3, 5 tissue regions; *, p<0.05). **(E)** Representative images of pSTAT3 IHC in control and *Ltf*$^{iCre/+}$*Arid1a*$^{f/f}$ mouse uterine tissue sections at GD 4.5 (n=6 IS). **(F)** Semi-quantitative H-score of stromal pSTAT3 staining strength. The graph shows the mean ± SEM (n= 6 IS; ***, p<0.001). **(G)** Representative images of EGR1 IHC in control and *Ltf*$^{iCre/+}$*Arid1a*$^{f/f}$ mouse uterine tissue sections at GD 4.5 (n=6 IS). **(H)** Semi-quantitative H-score of stromal EGR1 staining strength. The graph shows the mean ± SEM (n=6 IS; ***, p<0.001). **(I)** Representative images of pSTAT3 IHC in control and *Ltf*$^{iCre/+}$*Arid1a*$^{f/f}$ mouse uterine tissue sections at GD 5.5 (control and *Ltf*$^{iCre/+}$*Arid1a*$^{f/f}$ #1, n=6 IS; *Ltf*$^{iCre/+}$*Arid1a*$^{f/f}$ #2, n= 3 IS). **(J)** Semi-quantitative H-score of stromal pSTAT3 staining strength in control versus *Ltf*$^{iCre/+}$*Arid1a*$^{f/f}$ #1. The graph shows the mean ± SEM (n=6 IS; ***, p<0.001). **(K)** Representative images of EGR1 IHC in control and *Ltf*$^{iCre/+}$*Arid1a*$^{f/f}$ mouse uterine tissue sections at GD 5.5 (control and *Ltf*$^{iCre/+}$*Arid1a*$^{f/f}$ #1, n=6 IS; *Ltf*$^{iCre/+}$*Arid1a*$^{f/f}$ #2, n=3 IS). **(L)** Semi-quantitative H-score of stromal EGR1 staining strength in control versus *Ltf*$^{iCre/+}$*Arid1a*$^{f/f}$ #1. The graph shows the mean ± SEM (n=6 IS; *, p<0.05).

To determine if pSTAT3-EGR1 pathway dysregulation contributes to the implantation and decidualization defects of *Ltf*$^{iCre/+}$*Arid1a*$^{f/f}$ mice, we continued IHC analysis through the implantation window. While pSTAT3 and EGR1 were strongly expressed in decidualizing cells of control mice at GD 4.5, these proteins were significantly reduced in *Ltf*$^{iCre/+}$*Arid1a*$^{f/f}$ mice in the stroma surrounding embryos (-8.86 fold, p<0.0001; -1.66 fold, p=0.0002; respectively; Figure 2.6E-H). This finding combined with the known importance of pSTAT3 and EGR1 in decidualization (Lee, Kim, Oh, et al. 2013; Kim, Kim, et al. 2018) implicates dysregulation of the pSTAT3-EGR1 pathway in the decidualization defect of *Ltf*$^{iCre/+}$*Arid1a*$^{f/f}$ mice at GD 4.5. At GD 5.5, pSTAT3 and EGR1 expression normally decrease in the decidua (Liang et al. 2014; Lee, Kim, Oh, et al. 2013). In *Ltf*$^{iCre/+}$*Arid1a*$^{f/f}$ uterine sections, the implantation sites matching the major phenotype previously identified by histology (*Ltf*$^{iCre/+}$*Arid1a*$^{f/f}$ #1) exhibited significantly increased pSTAT3 and EGR1 expression in the stroma compared to controls (3.72 fold, p=0.0002; 3.24 fold, p=0.0411; respectively), whereas the minority phenotype (*Ltf*$^{iCre/+}$*Arid1a*$^{f/f}$ #2) was

apparently unchanged (Figure 2.6I-L). These findings reveal that the endometrial pSTAT3 and EGR1 activity critical for successful implantation is spatiotemporally dysregulated throughout early pregnancy as a result of epithelial *Arid1a* deletion.

Implantation and decidualization failure in $Pgr^{cre/+}Foxa2^{f/f}$ mice can be rescued by LIF repletion (Jeong et al. 2010; Kelleher et al. 2017; Kelleher et al. 2018). To determine if the implantation defect in $Ltf^{cre/+}Arid1a^{f/f}$ mice was due primarily to decreased LIF expression at preimplantation and failure to activate the pSTAT3-EGR1 pathway, we administered recombinant LIF or vehicle (saline) at GD 3.5 and analyzed the uteri at GD 5.5. In both the vehicle and LIF-treated $Ltf^{cre/+}Arid1a^{f/f}$ mice, no successful implantation sites were evident morphologically or histologically (Figure A.5A, B). Additionally, IHC revealed strong pSTAT3 and EGR1 expression around the embryos matching the majority phenotype based on histology ($Ltf^{cre/+}Arid1a^{f/f}$ #1) in both groups, consistent with our findings in untreated $Ltf^{cre/+}Arid1a^{f/f}$ mice and contrasting with control mice at this stage (Figure A.5C, D; Figure 2.6I, K).

2.3.6 FOXA2 and ARID1A are Attenuated in Tandem in Women and Non-Human Primates with Endometriosis

To determine if ARID1A attenuation in women with endometriosis compromises endometrial gland function as found in mice, we examined FOXA2 expression in eutopic endometrial samples from women with and without endometriosis using IHC. Consistent with previous findings (Kelleher et al. 2019; Yang et al. 2015), FOXA2 expression was strong across the secretory and proliferative phases of the menstrual cycle in the endometrial glands of control women and women with endometriosis (Figure 2.7A, B). However, FOXA2 was decreased in women with endometriosis, and this decrease reached a level of statistical significance in secretory

phase endometrium based on IHC H-score of staining strength in endometrial glands (-1.97 fold, $p<0.01$; Figure 2.7A, B). Moreover, correlation analysis of FOXA2 and ARID1A gland-specific H-scores in serial secretory phase endometrial sections from women with endometriosis revealed a significant correlation between FOXA2 and ARID1A expression (Spearman correlation coefficient $r=0.5982$, $p=0.0308$; Figure 2.7C, D). This finding supports the translational relevance of ARID1A's role in endometrial gland function to human endometriosis.

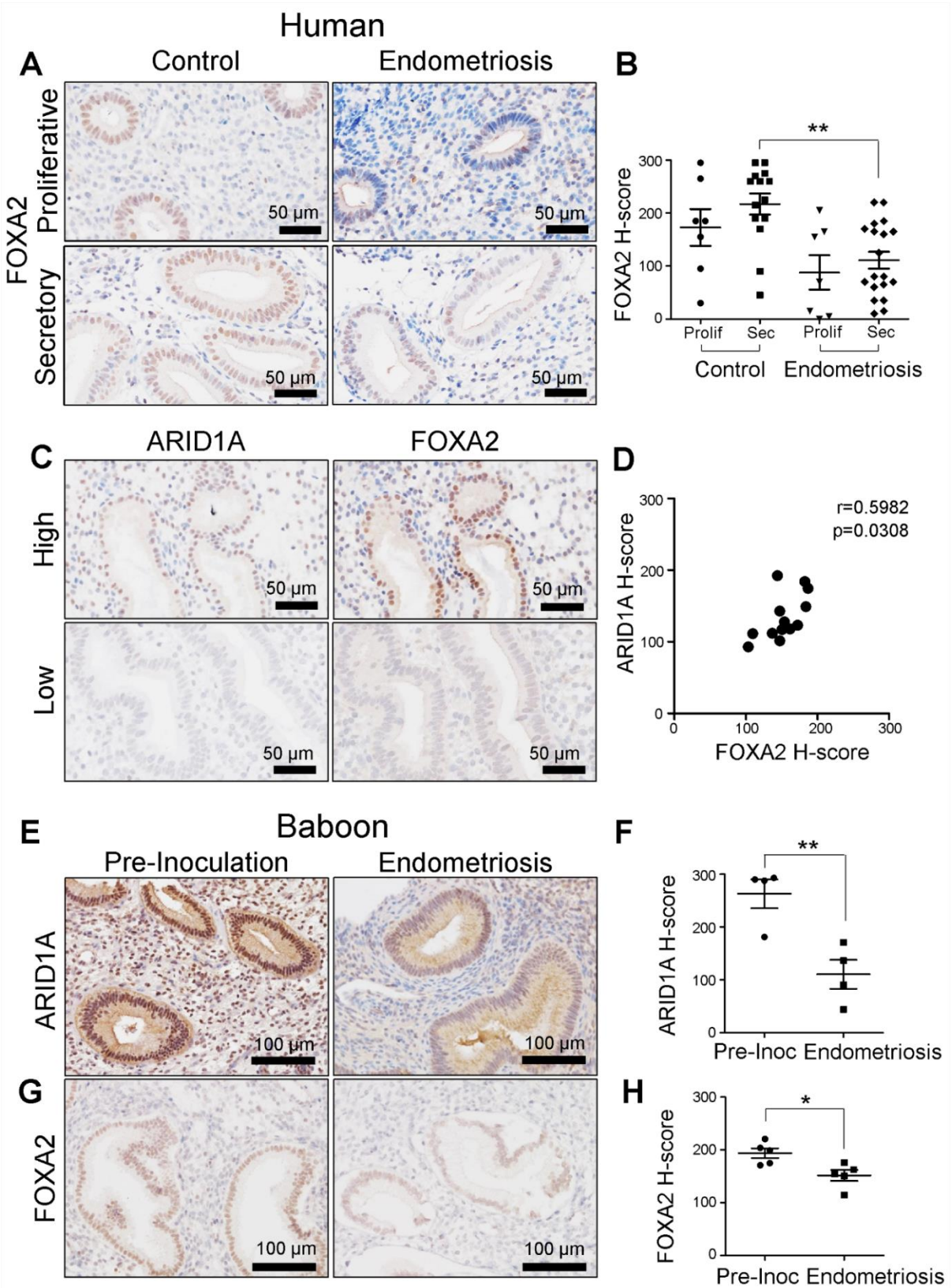

Figure 2.7 *FOXA2 and ARID1A are attenuated in tandem in women and non-human primates with*

Figure 2.7 (cont'd)
endometriosis. **(A)** Representative images of FOXA2 IHC in endometrial biopsy samples from control women without endometriosis and women with confirmed endometriosis from the proliferative (n=7) and secretory (control n=14, endometriosis n=19) phases of the menstrual cycle. **(B)** Semi-quantitative H-score of FOXA2 staining strength in endometrial glands for the sample set pictured representatively in part (A). The graph shows the mean ± SEM (**, $p<0.01$). **(C)** Representative images of strong and weak ARID1A and FOXA2 IHC in serial endometrial biopsy sections from women with endometriosis (n=13). **(D)** Correlation analysis of H-scores of FOXA2 staining strength and ARID1A staining strength in endometrial glands from IHC analysis of serial endometrial sections from women with endometriosis (n=13; $p=0.0308$). **(E)** Representative images of ARID1A IHC in paired endometrial biopsy samples from baboons before induction of endometriosis and after 15-16 months of endometriosis development (n=4). **(F)** Semi-quantitative H-score of ARID1A staining strength in endometrial glands for the sample set pictured representatively in part (E). The graph shows the mean ± SEM (n=4; **, $p<0.01$). **(G)** Representative images of FOXA2 IHC in paired endometrial biopsy samples from baboons before induction of endometriosis and after 15-16 months of endometriosis development (n=5). **(H)** Semi-quantitative H-score of FOXA2 staining strength in endometrial glands for the sample set pictured representatively in part (G). The graph shows the mean ± SEM (n=5; *, $p<0.05$).

To determine if endometriosis development alone is sufficient to cause reduction of ARID1A and FOXA2 in the eutopic endometrium, we utilized endometrial samples from a non-human primate model of endometriosis where menstrual effluent is inoculated into the peritoneal cavity to establish endometriotic lesions (Fazleabas 2006). Paired IHC analysis of samples taken before induction of endometriosis and 15-16 months after induction revealed significant decreases in both ARID1A (-2.38 fold, $p=0.0034$) and FOXA2 (-1.28 fold, $p=0.0147$) in baboon eutopic endometrial glands (Figure 2.7E-H). These findings show that simply inducing development of endometriotic lesions is sufficient to reduce both ARID1A and FOXA2 levels in baboon eutopic endometrial glands.

2.4 Discussion

ARID1A is primarily known for its roles in embryonic development (Gao et al. 2008) and as a tumor suppressor in many cancers, particularly endometriosis-related cancers of the female

reproductive tract (Mathur 2018; Wiegand et al. 2010; Chene et al. 2015). However, recent findings from our group and others have established a role for ARID1A in normal uterine function and in cases of endometriosis without cancer (Kim, Yoo, Wang, et al. 2015; Wang et al. 2016; Anglesio et al. 2017; Chene et al. 2015). In this chapter, we found that ARID1A plays an important role in endometrial gland development and function. We utilized three distinct mammalian systems to examine the importance and mechanism of ARID1A function in the endometrium: 1) conditional knockout mice revealed the temporal and compartment-specific physiological and molecular effects of *Arid1a* deletion in uterus; 2) endometrial biopsy samples from women with endometriosis confirmed the association between human endometriosis pathophysiology, decreased ARID1A expression, and endometrial gland dysfunction; and 3) a baboon model of endometriosis established a direct cause-effect relationship between endometriosis progression, ARID1A attenuation, and endometrial gland dysfunction.

Deletion of uterine *Arid1a* in mice ($Pgr^{cre/+}Arid1a^{f/f}$) compromised the ability of the endometrial epithelium to form typical numbers of glands by abrogating the expression of FOXA2, and our comparative analysis of transcriptomic data (Filant, Lydon, and Spencer 2014; Kim, Yoo, Wang, et al. 2015) confirmed the molecular impact of uterine *Arid1a* loss on FOXA2-regulated genes. In particular, we found *Lif* expression diminished in the preimplantation $Pgr^{cre/+}Arid1a^{f/f}$ uterus, which is the key molecular dysfunction caused by *Foxa2* deletion resulting in implantation and decidualization defects (Jeong et al. 2010; Kelleher et al. 2017; Kelleher et al. 2018). Though IHC results indicated $Pgr^{cre/+}Arid1a^{f/f}$ glands were FOXA2-negative, our method of analyzing uterine structure in 3D overcame the limitations of analyzing thin tissue sections to more holistically demonstrate a generalized failure of $Pgr^{cre/+}Arid1a^{f/f}$ uteri to develop the FOXA2-positive gland structures necessary to support early pregnancy establishment, in spite of a few

scattered FOXA2-positive regions (Kelleher, DeMayo, and Spencer 2019). Our ChIP-qPCR data from wildtype mice further revealed that uterine ARID1A regulation of FOXA2 expression during early pregnancy occurs in conjunction with direct binding of ARID1A at the *Foxa2* promoter.

Because of the defect of gland development resulting from early postnatal deletion of *Arid1a* in $Pgr^{cre/+}Arid1a^{f/f}$ mice, these mice are limited as a model of the ARID1A and FOXA2 downregulation in endometria of women with endometriosis that still appear to retain normal numbers of glands. Additionally, *Arid1a* is deleted in all uterine compartments of $Pgr^{cre/+}Arid1a^{f/f}$ mice (Soyal et al. 2005; Kim, Yoo, Wang, et al. 2015), which does not allow distinction between the epithelial and stromal functions of ARID1A. To overcome these limitations, we utilized $Ltf^{iCre/+}Arid1a^{f/f}$ mice to determine the effect of *Arid1a* deletion in the adult endometrial epithelium on reproductive function. $Ltf^{iCre/+}$ mice do not express iCre until sexual maturity, and uterine expression is limited to the luminal and glandular epithethelium (Daikoku et al. 2014). However, $Ltf^{iCre/+}$ mice also express iCre in some myeloid lineage immune cells (Daikoku et al. 2014; Kovacic et al. 2014), so we cannot rule out the possibility of phenotypic effects resulting from *Arid1a* deletion in these cell types.

Our comprehensive characterization of the early pregnancy stage phenotypes of $Ltf^{iCre/+}Arid1a^{f/f}$ mice lends understanding of the epithelial-specific role of ARID1A in the endometrium, particularly in comparison with $Pgr^{cre/+}Arid1a^{f/f}$ mice (Table 2.1). Our data show that $Ltf^{iCre/+}Arid1a^{f/f}$ mice are severely sub-fertile due to uterine defects similar to those of $Pgr^{cre/+}Arid1a^{f/f}$ mice. However, though $Pgr^{cre/+}Arid1a^{f/f}$ mice exhibit major dysregulation of epithelial PGR signaling during early pregnancy (Kim, Yoo, Wang, et al. 2015), we found that this was not a major phenotype of $Ltf^{iCre/+}Arid1a^{f/f}$ mice, implying an important role for stromal ARID1A in coordinating epithelial PGR signaling. On the other hand, both conditional knockout

models led to increased preimplantation epithelial proliferation, implying that suppression of this phenotype may be mediated in an epithelial cell-autonomous manner by ARID1A rather than through effects on stromal-epithelial juxtacrine signaling. Unlike *Pgr*$^{cre/+}$*Arid1a*$^{f/f}$ mice, *Ltf*$^{iCre/+}$*Arid1a*$^{f/f}$ mice had normal numbers of endometrial glands during early pregnancy, but *Ltf*$^{iCre/+}$*Arid1a*$^{f/f}$ mice still exhibited reductions of uterine *Foxa2* and *Lif* expression, which demonstrates normal gland structure formation but compromised gland function.

Table 2.1 *Phenotype comparison of Pgr*$^{cre/+}$*Arid1a*$^{f/f}$ *and Ltf*$^{iCre/+}$*Arid1a*$^{f/f}$ *mice*

Phenotype	***Pgr*$^{Cre/+}$*Arid1a*$^{f/f}$**	***Ltf*$^{iCre/+}$*Arid1a*$^{f/f}$**
Fertility	Infertile (Kim, Yoo, Wang, et al. 2015)	Severely sub-fertile
Ovarian Function	Normal (Kim, Yoo, Wang, et al. 2015)	Normal
Implantation	Defect (open lumen) (Kim, Yoo, Wang, et al. 2015)	Defect (closed lumen)
Decidualization	Defect (Kim, Yoo, Wang, et al. 2015)	Defect
Uterine Receptivity	Non-receptive (Kim, Yoo, Wang, et al. 2015)	Non-receptive
Uterine Epithelial PGR Expression	Major decrease (Kim, Yoo, Wang, et al. 2015)	Minor decrease
Uterine Epithelial pESR1 Expression	Increased (Kim, Yoo, Wang, et al. 2015)	Normal
Endometrial Gland Number	Decreased	Normal
Uterine FOXA2 Expression	Decreased	Decreased
Uterine *Lif* Expression	Decreased	Decreased

After LIF is secreted from endometrial glands at GD 3.5 and localizes to the glandular epithelium and sub-luminal stroma around the implanting embryo by GD 4.5 (Song et al. 2000), it binds its transmembrane receptor and activates STAT3 via phosphorylation, then pSTAT3 translocates to the nucleus to induce EGR1 expression, which is rapid and transient in the sub-luminal stroma around the implanting embryo at this stage (Liang et al. 2014). Each step in this pathway is critical for implantation and decidualization success (Kim, Kim, et al. 2018; Lee, Kim, Oh, et al. 2013; Stewart et al. 1992). Here, we show that *Ltf*$^{iCre/+}$*Arid1a*$^{f/f}$ mice fail to express normal amounts of *Lif* at GD 3.5 and experience disrupted pSTAT3 and EGR1 expression before, during, and after the implantation period. Notably, *Egr1* knockout mice exhibit increased epithelial proliferation, decreased stromal proliferation, and compromised decidualization (Kim, Kim, et al. 2018), matching our finding in *Ltf*$^{iCre/+}$*Arid1a*$^{f/f}$ mice and providing a potential molecular explanation for the non-receptive endometrium phenotype. A failure to secrete sufficient amounts of LIF from ARID1A-deficient glands to activate STAT3 signaling in the stroma could thus explain how an epithelial cell defect of ARID1A compromises decidualization, a stromal cell process.

The varying phenotypes found in *Ltf*$^{iCre/+}$*Arid1a*$^{f/f}$ mice at GD 5.5 appear to represent a failure of the decidualization process at two different stages: one at the stage characteristic of the normal GD 4.5 expression patterns of pSTAT3 and EGR1 (*Ltf*$^{iCre/+}$*Arid1a*$^{f/f}$ #1), and one matching the normal GD 3.5 patterns *Ltf*$^{iCre/+}$*Arid1a*$^{f/f}$ #2). The source of the variation in these results is unclear, but it could possibly have resulted from slightly different timing from mating event to sample collection between mice or from localized variation in iCre activity.

Overall, our data from *Ltf*$^{iCre/+}$*Arid1a*$^{f/f}$ mice support the hypothesis that epithelial ARID1A is necessary to potentiate the FOXA2 expression and tightly regulated LIF-STAT3-EGR1 pathway

signaling required in the uterus to support implantation and decidualization. However, restoring LIF levels alone did not reverse the implantation failure that resulted from loss of epithelial ARID1A, which implies that deletion of *Arid1a* in the adult endometrial epithelium must cause other molecular defects besides reduction of FOXA2 expression that preclude early pregnancy establishment.

Genetically engineered mice are powerful tools to study the molecular regulation of early pregnancy due to the similarity between mouse and human reproduction (Cha, Sun, and Dey 2012); however, studies in higher primates and directly in women are necessary to draw stronger conclusions about the relevance of any findings to human pathophysiology. We previously found a reduction of ARID1A expression in the endometrium of infertile women with endometriosis (Kim, Yoo, Wang, et al. 2015). Here, our findings were consistent with reports that FOXA2 expression is markedly reduced in endometrium from women with endometriosis (Lin et al. 2018; Yang et al. 2015), and we demonstrated a correlation between endometrial ARID1A and FOXA2 expression among women with endometriosis. This finding supports the idea that ARID1A regulates FOXA2 and gland function in women as well as in mice and that this function is compromised by endometriosis. However, no direct cause-effect relationship between endometriosis and ARID1A-FOXA2 expression can be established with this type of associational study: it is not clear whether endometriosis causes this particular molecular dysfunction or if it is a risk factor for endometriosis development. The use of a non-human primate model of induced endometriosis allows paired sample analysis before and after disease development in a menstruating species biologically similar to humans (Fazleabas 2006). In this way, our study in baboons establishes that the presence of endometriotic lesions precipitates the parallel downregulation of ARID1A and FOXA2 in the eutopic endometrium, indicating that

endometriosis pathophysiology causes disruption of ARID1A's regulation of endometrial gland function.

Worthy of note, a recent report showed that endometrial epithelial expression of the transcription factor SOX17 is critical for successful implantation and decidualization in mice and is reduced in the endometrial glands of women with endometriosis (Wang et al. 2018). Interestingly, transcriptomic analysis of endometrial epithelial specific SOX17 knockout mice revealed that SOX17-regulated gene expression patterns remarkably overlapped with ARID1A-regulated genes and FOXA2-regulated genes (Wang et al. 2018). Furthermore, ablation of SOX17 diminished the protein levels of ARID1A and FOXA2 in the endometrium, which when taken together with our data, indicates a possible hierarchical relationship between these three proteins in the endometrium, with SOX17 positively regulating ARID1A which in turn promotes FOXA2 expression and gland function (Wang et al. 2018).

Our complementary experimental methods utilizing samples from mice, women, and non-human primates coordinate to reveal the critical function of epithelial ARID1A in the endometrium that is compromised in cases affected by endometriosis. As more is determined about the connection between endometriosis and infertility, ARID1A will continue to be a crucial molecular factor to consider when developing potential therapies to combat the effects of these common and devastating conditions.

2.5 Materials and Methods

2.5.1 Mouse Models

All mouse procedures were approved by the Institutional Animal Care and Use Committee of Michigan State University. All mice were housed and bred in a designated animal care facility

at Michigan State University under controlled humidity and temperature conditions and a 12 hour light/dark cycle at 5 mice/cage maximum. Access to water and food (Envigo 8640 rodent diet) was ad libitum. ChIP assays were conducted in C57BL/6 mice. *Arid1a* conditional knockout mice were generated by crossing $Pgr^{cre/+}$(Soyal et al. 2005) or $Ltf^{iCre/+}$ (Daikoku et al. 2014) (The Jackson Laboratory Stock No: 026030) males with $Arid1a^{f/f}$ (Gao et al. 2008) (generously provided by Dr. Zhong Wang, University of Michigan) females. All experiments using adult mice were performed in 8-12-week-old mice. Experiments involving $Ltf^{iCre/+}Arid1a^{f/f}$ mice were carried out using 12-week-old mice to ensure sufficient iCre activation. For breeding, one male mouse was normally placed into a cage with one female mouse. Occasionally, one male mouse was housed with two female mice to increase breeding success, and females were separated with their pups until weaning. After weaning at P21-P28, male and female littermates were housed separately until use in breeding or experiments. Mice of appropriate genotypes were randomly allocated to experimental groups, using littermates for comparisons when possible.

2.5.2 Mouse Procedures and Tissue Collection

Uterine samples from specific times of pregnancy were obtained by mating control or conditional *Arid1a* knockout female mice with wildtype male mice with the morning of identification of a vaginal plug defining GD 0.5. Uteri were collected at GD 3.5, 4.5, and 5.5, and implantation sites were visualized on GD 4.5 by intravenous injection of 1% Chicago Sky Blue 6B dye (Sigma-Aldrich, St. Louis, MO) before necropsy and on GD 5.5 by gross morphology with histological confirmation. At time of dissection, isolated uterine tissue was either snap-frozen and stored at -80°C for RNA/protein extraction or fixed with 4% (vol/vol) paraformaldehyde for histological analysis. Ovaries were collected on GD 3.5 and fixed with 4% (vol/vol)

paraformaldehyde for histological analysis. The serum P4 and E2 levels were analyzed by the University of Virginia Center for Research in Reproduction Ligand Assay and Analysis Core using samples taken at GD 3.5. For the fertility trial, adult female control or *Ltf*$^{iCre/+}$*Arid1a*$^{f/f}$ female mice were housed with wildtype male mice for 6 months, and the number of litters and pups born during that period was recorded. To quantify the number of glands, gland structures were counted based on histology in transverse tissue sections. To artificially induce decidualization, we mechanically stimulated one horn following hormonal preparation as previously described (Kim, Yoo, Wang, et al. 2015).

2.5.3 Human Endometrial Tissue Samples

This study has been approved by Institutional Review Boards of Michigan State University, Greenville Health System and University of North Carolina. All methods were carried out in accordance with relevant guidelines and regulations, and written informed consent was obtained from all participants. The human endometrial samples were obtained from Michigan State University's Center for Women's Health Research Female Reproductive Tract Biorepository (Grand Rapids, MI), the Greenville Hospital System (Greenville, SC), and the University of North Carolina (Chapel Hill, NC). Subject selection and sample collection were performed as previously reported (Kim, Yoo, Wang, et al. 2015). Briefly, endometrial biopsies were obtained at the time of surgery from regularly cycling women between the ages of 18 and 45. Use of an intrauterine device (IUD) or hormonal therapies in the 3 months preceding surgery was exclusionary for this study. Histologic dating of endometrial samples was done based on the criteria of Noyes (Noyes, Hertig, and Rock 1975). For comparison of endometrium from women with endometriosis and women without endometriosis, we used eutopic endometrium derived from women with

laparoscopically confirmed endometriosis and compared it to control endometrium from women laparoscopically negative for endometriosis. Control samples from 21 women were collected from the proliferative (n=7) and secretory phases (n =14). Endometriosis-affected eutopic endometrium samples from 37 women were collected from the proliferative (n=7) and secretory phases (n=30).

2.5.4 Baboon Endometrium Samples

Use of the baboon endometriosis animal model was reviewed and approved by the Institutional Animal Care and Use Committees (IACUCs) of the University of Illinois at Chicago and Michigan State University. Endometriosis was induced by laparoscopically guided intraperitoneal inoculation of menstrual effluent on two consecutive cycles with a pipelle after confirmation of no pre-existing lesions as previously described (Fazleabas 2006). Eutopic endometrial tissues were collected from nine early secretory phase baboons once at pre-inoculation and again at 15-16 months post-inoculation.

2.5.5 Histology and Immunostaining

Fixed, paraffin-embedded tissues were cut at 5 μm, mounted on slides, deparaffinized, and rehydrated in a graded alcohol series. For H&E, slides were sequentially submerged in hematoxylin, 0.25% hydrochloric acid (HCL), 1% lithium carbonate, and eosin, followed by dehydration and mounting. Immunostaining was performed as previously described (Kim, Yoo, Wang, et al. 2015) with specific commercially available primary antibodies (Table A.2). For IHC, biotinylated secondary antibodies (Vector Laboratories, Burlingame, CA) were used, followed by incubation with horseradish peroxidase (Thermo Fisher Scientific, Waltham, MA) and developing using the Vectastain Elite diaminobenzidine (DAB) kit (Vector Laboratories). For

immunofluorescence, appropriate species-specific fluorescently tagged secondary antibodies (Invitrogen, Carlsbad, CA) were used before mounting with DAPI (Vector Laboratories) for imaging. To compare the IHC staining intensities, a semiquantitative grade (H-score) was calculated by adding the percentage of strongly stained nuclei (3x), the percentage of moderately stained nuclei (2x), and the percentage of weakly stained nuclei (1x) in a region of approximately 100 cells, giving a possible range of 0–300. The percentage of Ki67-positive cells was counted in representative fields of approximately 150 epithelial cells and 150 stromal cells.

2.5.6 Whole Mount Immunofluorescence and Imaging

Three-dimensional imaging of mouse uteri was performed as previously described (Arora et al. 2016). Briefly, samples were fixed with a 4:1 ratio of Methanol:DMSO and stained using whole-mount immunofluorescence. Primary antibodies (Table A.2) for mouse CDH1 (E-cadherin) and FOXA2 were utilized to identify total epithelium and glandular epithelium, respectively, followed by fluorescently conjugated Alexa Fluor IgG (Invitrogen) secondary antibodies. Embryos were identified using a combination of Hoechst and CDH1. Uteri were imaged using a Leica SP8 TCS confocal microscope with white-light laser, using a 10× air objective with *z* stacks that were 7 µm apart. Full uterine horns were imaged using 18×2 tile scans and tiles were merged using the mosaic merge function of the Leica software. Leica Image format files were analyzed using Imaris v9.1 (Bitplane, Zürich, Switzerland). Using the channel arithmetic function, the glandular FOXA2+ signal was removed from the E-CAD+ signal to create lumen-only signal. Surfaces were created in surpass 3D mode for the lumen-only signal and the FOXA2+ glandular signal.

2.5.7 RNA Isolation and RT-qPCR

As previously described (Kim, Yoo, Wang, et al. 2015), RNA was extracted from the uterine tissues using the RNeasy total RNA isolation kit (Qiagen, Valencia, CA). mRNA expression levels were measured by real-time PCR TaqMan or SYBR green analysis using an Applied Biosystems StepOnePlus system according to the manufacturer's instructions (Applied Biosystems, Foster City, CA) using pre-validated primers (Table A.3), probes (Table A.4), and either PowerUp SYBR Green Master Mix or TaqMan Gene Expression Master Mix (Applied Biosystems). The amplification conditions for TaqMan probes were 2 minutes at 50˚C, 10 minutes at 95˚C, then 40 cycles of 15 seconds at 95˚C followed by 1 minute at 60˚C. The amplification conditions for SYBR Green primers were 10 minutes at 95˚C, 40 cycles of 15 seconds at 95˚C followed by 1 minute at 60˚C, then a melt curve phase consisting of 15 seconds at 95˚C, 1 minute at 60˚C, and 15 seconds at 95˚C. Template complementary DNA (cDNA) was produced from 3 μg of total RNA using random hexamers and Moloney murine leukemia virus (MMLV) reverse transcriptase (Invitrogen). The mRNA quantities were normalized against the ribosomal protein L7 (*Rpl7*) mRNA for SYBR green primers or the glyceraldehyde-3-phosphate dehydrogenase (*Gapdh*) mRNA for TaqMan probes.

2.5.8 Chromatin Immunoprecipitation

ChIP assays were conducted by Thermo Scientific (Pittsburgh, PA, USA) using uteri of C57BL/6 mice at day 0.5 and 3.5 of gestation (GD 0.5 and 3.5). ChIP assays were performed as previously described (Kim, Yoo, Wang, et al. 2015). Briefly, for each ChIP reaction, 100 μg of chromatin was immunoprecipitated by 4 μg of antibodies against ARID1A (Table A1). Eluted

DNA was amplified with specific primers (Table A.3) using SYBR Green Master (Roche, Basel, Switzerland), and the resulting signals were normalized to input activity.

2.5.9 Comparative Transcriptomic Analysis

Comparisons of GD 3.5 $Pgr^{cre/+}Arid1a^{f/f}$ to GD 3.5 $Pgr^{cre/+}Foxa2^{f/f}$ uterine dysregulated genes were performed by comparing differentially expressed genes determined in our previously reported, publicly available $Pgr^{cre/+}Arid1a^{f/f}$ transcriptomics analysis (GSE72200) (Kim, Yoo, Wang, et al. 2015) with differentially expressed genes determined by previously reported transcriptomics analysis of $Pgr^{cre/+}Foxa2^{f/f}$ mice publicly available from the Gene Expression Omnibus (GEO) database (GSE48339) (Filant, Lydon, and Spencer 2014). The differentially expressed gene lists used for comparative transcriptomics were prepared by the original authors of the studies according to their published methods of analysis (Kim, Yoo, Wang, et al. 2015; Filant, Lydon, and Spencer 2014). Briefly, for the $Pgr^{cre/+}Arid1a^{f/f}$ microarray, hybridization was performed using a GeneChip Mouse Genome Array, whereas the $Pgr^{cre/+}Foxa2^{f/f}$ microarray utilized a Mouse Gene 1.0 ST microarray. In both cases, the Affymetrix Fluidics Station 450 was utilized for washing and staining. Both arrays were scanned with a GeneChip Scanner 3000 (Affymetrix, Santa Clara, CA), and GeneSpring software (Agilent Technologies, Santa Clara, CA) was used to analyze the data. In both cases, normalization of the array data was done using the robust multi-array average (RMA) method (Irizarry et al. 2003). For the $Pgr^{cre/+}Arid1a^{f/f}$ microarray, filtering was based on the requirement that genes be upregulated by at least 150% of controls or downregulated to 66% or less than controls (Kim, Yoo, Wang, et al. 2015), whereas the $Pgr^{cre/+}Foxa2^{f/f}$ microarray analysis filtered using analysis of variance (ANOVA) ($p=0.05$) with a Benjamini and Hochberg false discovery rate (FDR) multiple test correction (Filant, Lydon,

and Spencer 2014). Before calculating overlap, duplicate genes present in the gene lists (due to the presence of multiple array probes for some genes) were removed based on GeneBank ID or gene symbol.

2.5.10 Statistical Analysis

To assess statistical significance of parametric data, we used student's t-test for comparison of two groups or one-way ANOVA followed by Tukey's post-hoc test for multiple comparisons. For non-parametric data, we used the Mann-Whitney U test for comparison of two groups or Kruskal-Wallis rank test followed by Dunn's test for multiple comparisons. Pearson's Correlation Coefficient was used to assess correlation. All statistical tests were two-tailed when applicable, and a value of $p<0.05$ was considered statistically significant. Statistical analyses were performed using either the Instat or Prism package from GraphPad (San Diego, CA). Statistical test results (p-values) are presented with the results in the text and symbolically in the figures, with explanations in figure legends. The value of n for each experiment, representing number of animals unless noted as number of implantation sites, is reported in the appropriate figure legend.

2.6 Data Availability

The data that support the findings of this study are available within the chapter and Appendix A.

2.7 Acknowledgments

Research reported in this chapter was supported in part by the Eunice Kennedy Shriver National Institute of Child Health & Human Development of the National Institutes of Health

under Award Number R01HD084478 to J.W.J., F31HD101207 and T32HD087166 to R.M.M., and P50HD28934 (National Center for Translational Research in Reproduction and Infertility) to The University of Virginia Center for Research in Reproduction Ligand Assay and Analysis Core; MSU AgBio Research, and Michigan State University. The content is solely the responsibility of the authors and does not necessarily represent the official views of the National Institutes of Health. We are grateful for the generous donation of *Arid1a*$^{f/f}$ mice by Dr. Zhong Wang, University of Michigan. We would like to thank Erin Vegter and Samantha Hrbek for technical support.

CHAPTER 3

ENDOMETRIAL EPITHELIAL ARID1A IS REQUIRED FOR UTERINE IMMUNE HOMEOSTASIS DURING EARLY PREGNANCY

This chapter is not published at the time of dissertation submission. The following study is in collaboration with Soo Huyn Ahn and Margaret G. Petroff at the Department of Pathobiology and Diagnostic Investigation in the Michigan State University College of Veterinary Medicine and Jake J. Reske, Ronald L. Chandler, Tae Hoon Kim, and Jae-Wook Jeong at the Department of Obstetrics, Gynecology & Reproductive Biology in the Michigan State University College of Human Medicine.

3.1 Abstract

A growing body of work suggests epigenetic dysregulation contributes to endometriosis pathophysiology and female infertility. The chromatin remodeling complex subunit ARID1A must be properly expressed to maintain normal uterine function. Endometrial epithelial ARID1A is indispensable for pregnancy establishment in mice through regulation of endometrial gland function; however, ARID1A expression is decreased in infertile women with endometriosis. We hypothesized that ARID1A performs critical operations in the endometrial epithelium necessary for fertility besides maintaining gland function. To identify alterations in uterine gene expression resulting from loss of epithelial ARID1A, we performed RNA-sequencing analysis on pre-implantation pregnant uteri from $Ltf^{iCre/+}Arid1a^{f/f}$ and control mice. Differential expression analysis identified 4,181 differentially expressed genes enriched for immune-related Ingenuity Canonical Pathways including Agranulocyte Adhesion and Diapedesis and Natural Killer Cell Signaling. RT-qPCR confirmed an increase in pro-inflammatory cytokine and macrophage-related

gene expression but a decrease in natural killer cell signaling. Immunostaining confirmed a uterus-specific increase in macrophage infiltration. Flow cytometry delineated an increase of inflammatory macrophages and a decrease of uterine dendritic cells in *Ltf*$^{iCre/+}$*Arid1a*$^{f/f}$ uteri. These findings demonstrate a role for endometrial epithelial ARID1A in suppressing inflammation and maintaining uterine immune homeostasis, which are required for successful pregnancy and gynecological health.

3.2 Introduction

The endometrium, the inner lining of the uterus, is a highly dynamic and interconnected group of cells consisting of luminal epithelium, glandular epithelium, and stroma. Luminal epithelial cells face the uterine lumen and are the first uterine cells to interact with an embryo in the context of pregnancy. Glandular epithelial cells form gland structures apart from the uterine lumen and perform critical functions for pregnancy through their secretions, which contact the contents of the lumen, the luminal epithelium, and the surrounding stroma (Kelleher, DeMayo, and Spencer 2019). The stroma plays a supportive role from its position surrounding the epithelial cells and consists of a mixture of stromal fibroblasts, endothelial cells, and immune cells.

Together, these endometrial compartments maintain a dynamic homeostasis through tight regulation by the ovarian steroid hormones E2 and P4. Signaling primarily through their nuclear receptors, E2 and P4 function in a complex epithelial-stromal crosstalk that governs the menstrual cycle in humans, the estrous cycle in mice, and the window of implantation in both species (Wu, Li, and DeMayo 2018; Li et al. 2021). Additionally, the differentiation of uterine stromal fibroblasts into specialized, secretory decidual cells is essential for pregnancy progression and is a progesterone-dependent cyclical process in humans, whereas it relies on the presence of an

embryo and nidatory E2 to induce LIF secretion from glands in rodents (Gellersen and Brosens 2014; Cha, Sun, and Dey 2012). Proper embryo implantation and complete decidualization are required not only for the establishment of pregnancy but also for the healthy progression of pregnancy to placentation and on-time delivery (Ticconi et al. 2021).

To facilitate proper vascularization and tissue remodeling in the formation of the decidua, which goes on to act as a physical scaffold and provide essential nutritional support and immune tolerance for the developing embryo until placentation, at least three specific immune cell types must maintain an appropriate spaciotemporal balance (Mori et al. 2016). Uterine natural killer cells (uNKs), an innate lymphoid cell type, constitute the majority of all human decidual lymphocytes and contribute to angiogenesis, vascular remodeling, and proper placentation (Mori et al. 2016; Koopman et al. 2003). More recently, a critical role for uNKs has been described in clearing senescent decidual cells (Brighton et al. 2017; Lucas et al. 2020). In mice, uNKs appear by gestation day (GD) 6.5, just after implantation, peak at GD 12.5 after the placenta is fully formed, and play a role in decidual integrity (Croy et al. 2010).

Macrophages, a class of innate myeloid immune cells, are another common cell type in the uterus, and they can originate from circulating monocytes or be resident to the tissue (Mori et al. 2016). These cells are key sensors of infection and regulators of the inflammatory response, and subtypes of macrophages can be either proinflammatory or anti-inflammatory depending on the cytokines they secrete. Homeostatic uterine macrophages are thought to be primarily anti-inflammatory outside of transient inflammation in preparation for pregnancy, but an abundance of proinflammatory macrophage activity in the uterus is associated with pathologies (Chambers et al. 2020).

Dendritic cells in general are myeloid antigen-presenting cells that link innate immunity to the adaptive immune system. Uterine dendritic cells (uDCs) are normally rare, but increasing numbers are recruited to the decidua and appear to function there in tissue remodeling and angiogenesis (Mori et al. 2016; Plaks et al. 2008; Collins, Tay, and Erlebacher 2009). Numbers of uNKs, uterine macrophages, and uDCs have all been reported to fluctuate during endometrial cycling and peak at the secretory phase, implying either direct or indirect regulation by steroid hormones, but the mechanism has not been well characterized (Vallve-Juanico, Houshdaran, and Giudice 2019).

When the normal hormone and immune-regulated homeostatic balance of the endometrium is lost, gynecological pathologies can develop including recurrent implantation failure, recurrent pregnancy loss, endometrial cancer, and endometriosis, as we saw in Chapter 1 (Marquardt et al. 2019). Endometriosis occurs when endometrium-like glands and stroma form ectopic lesions outside the uterus, and along with a high prevalence of chronic pain, it is often accompanied by infertility or subfertility (Saunders and Horne 2021). The prevalence of this E2-driven, P4-resistant inflammatory disorder is estimated at 10% of reproductive-age women, but the heterogeneity of its clinical presentation contributes to a high frequency of delayed diagnosis, making true prevalence estimates and systematic study difficult (Zondervan, Becker, and Missmer 2020). Surgical resection of lesions and hormone suppression are the standard treatment options for endometriosis-related pain, but suppression of ovulation precludes fertility, and surgical treatments have mixed results on fertility outcomes, leaving in vitro fertilization as the typical option for women affected by endometriosis-related infertility (Bulun et al. 2019). While its pathogenesis is not thoroughly understood and is almost certainly multifactorial, perturbations in local and systemic immune cell populations have been clearly implicated in both endometriotic lesion

establishment and dysregulation of the endometrial environment (Vallve-Juanico, Houshdaran, and Giudice 2019).

Substantial work from our group and others has also identified a wide array of epigenetic factors dysregulated in the endometrium of women with endometriosis including histone-modifying enzymes, DNA modifiers, and chromatin architecture modifiers (Kim, Young, et al. 2021; Yoo et al. 2017; Mai et al. 2021; Kim et al. 2019; Kim, Yoo, Wang, et al. 2015; Zhang et al. 2017). The SWI/SNF chromatin remodeling complex subunit ARID1A is commonly known for its tumor suppressor role and its prevalent inactivating mutations in endometriosis-associated ovarian carcinomas, but it is also mutated in non-cancerous endometriotic lesions and underexpressed in the endometrium of infertile women with endometriosis (Maeda and Shih Ie 2013; Kim, Yoo, Wang, et al. 2015; Anglesio et al. 2017). Furthermore, studies using mouse models have shown that deletion of uterine *Arid1a* drives increased endometriosis-like lesion establishment and causes endometrial-factor infertility related to disrupted P4 and E2 signaling (Kim, Kim, et al. 2021; Kim, Yoo, Wang, et al. 2015; Mai et al. 2021). Focused study on the role of ARID1A in the endometrial epithelium has revealed its critical cell-type-specific roles of maintaining epithelial identity (Wilson et al. 2019; Reske et al. 2021) and enabling gland development and function in pregnancy, as shown in Chapter 2 (Marquardt et al. 2021). Deletion of *Arid1a* in the adult mouse endometrial epithelium led to early pregnancy defects through attenuation of FOXA2 expression and LIF secretion from uterine glands. However, disruption of this pathway does not appear to fully explain the pregnancy-related uterine defects resulting from epithelial *Arid1a* deletion, which led us to hypothesize that endometrial epithelial ARID1A performs other critical functions in the endometrial epithelium necessary for fertility.

In this chapter, we utilized RNA-sequencing analysis of endometrial epithelium-specific *Arid1a* knockout mice driven by *Ltf-iCre* (*Ltf*$^{iCre/+}$*Arid1a*$^{f/f}$) to explore the in vivo uterine transcriptome dysregulation in early pregnancy that results from loss of epithelial ARID1A. Our analysis revealed large scale disruption of immune-related pathways, most notably an increase in proinflammatory cytokine gene expression and a decrease in uNK cell markers. Further functional study demonstrated a marked increase in uterine infiltration by proinflammatory macrophages with correspondent decreases in uNKs and uDCs, revealing a critical role for endometrial epithelial ARID1A in maintaining uterine immune homeostasis during early pregnancy.

3.3 Results

3.3.1 Deletion of Endometrial Epithelial Arid1a in Mice Causes Diminished Implantation Site Size and uNK Cell Numbers at GD 7.5

As we saw in Chapter 2, *Ltf*$^{iCre/+}$*Arid1a*$^{f/f}$ mice are severely subfertile and exhibit implantation and decidualization defects at the peri-implantation and early post-implantation stages (GD 4.5-5.5), but the effects of endometrial epithelial *Arid1a* deletion on subsequent stages of pregnancy have not been previously reported (Marquardt et al. 2021). We collected uterine samples at GD 7.5 and found that although the number of implantation sites was not different from controls (Control=4.88±1.47, *Ltf*$^{iCre/+}$*Arid1a*$^{f/f}$=5.00±1.13, p=0.8578), *Ltf*$^{iCre/+}$*Arid1a*$^{f/f}$ implantation sites were significantly decreased in diameter (Control=3.80±0.05mm, *Ltf*$^{iCre/+}$*Arid1a*$^{f/f}$=2.89±0.13mm, p=0.0002) and weight (Control=0.0092±0.0006g, *Ltf*$^{iCre/+}$*Arid1a*$^{f/f}$=0.0060±0.0004g, p=0.0092; Figure 3.1).

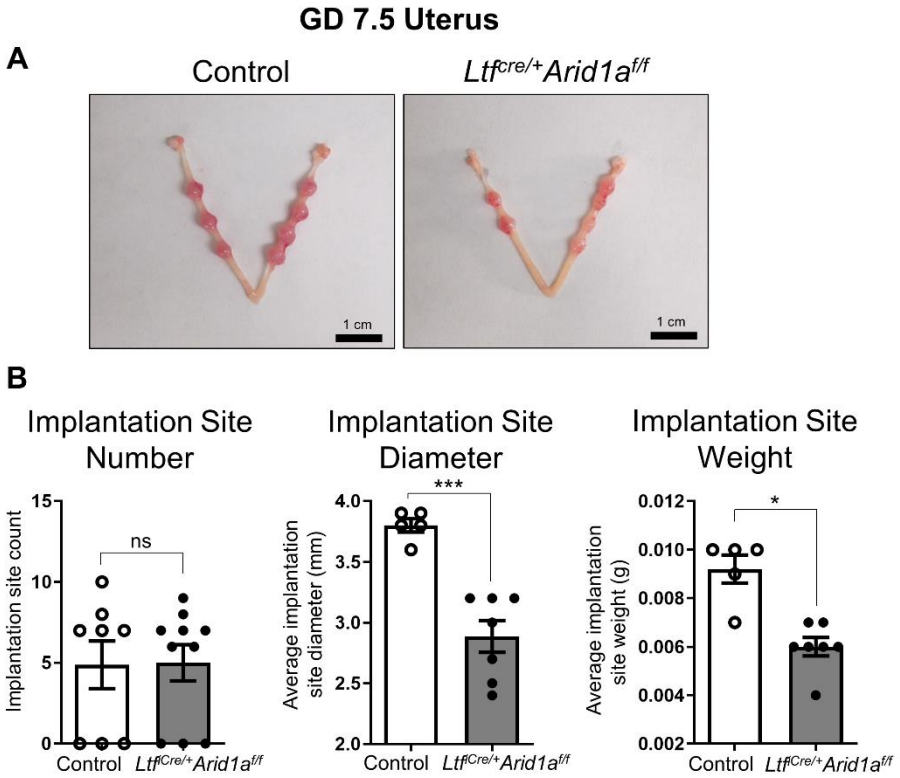

Figure 3.1 *Deletion of endometrial epithelial Arid1a in mice causes diminished implantation site size and uNK cell numbers at GD 7.5*. **(A)** Implantation sites were grossly visible in both control (n=8) and *Ltf*$^{iCre/+}$*Arid1a*$^{f/f}$ (n=10) uteri at GD 7.5, appearing smaller in *Ltf*$^{iCre/+}$*Arid1a*$^{f/f}$ uteri. **(B)** Implantation site number (left) as counted based on gross morphology was similar between control (n=8, empty bar) and *Ltf*$^{iCre/+}$*Arid1a*$^{f/f}$ (n=10, grey bar) uteri at GD 7.5, but the average implantation site diameter (middle) and weight (right) were significantly decreased in *Ltf*$^{iCre/+}$*Arid1a*$^{f/f}$ (n=7, grey bar) uteri compared to controls (n=5, empty bar). The graphs represent the mean ± SEM. *, $p<0.05$; ***, $p<0.001$; ns, $p>0.05$.

Immunohistochemical staining of implantation site cross sections for the decidualization marker COX-2 revealed a substantially diminished decidual area (Figure 3.2A). Concurrent with the development of the decidua, uNK cells normally proliferate in a healthy implantation site and function in angiogenesis and vascular remodeling (Croy et al. 2010; Mori et al. 2016). However, *Ltf*$^{iCre/+}$*Arid1a*$^{f/f}$ mice exhibit significantly decreased numbers of uNK cells at GD 7.5 counted based on *Dolichos biflorus* (DBA) lectin staining (Control=390.00±90.63, *Ltf*$^{iCre/+}$*Arid1a*$^{f/f}$=13.40±5.92, p=0.0079; Figure 3.2B, C).

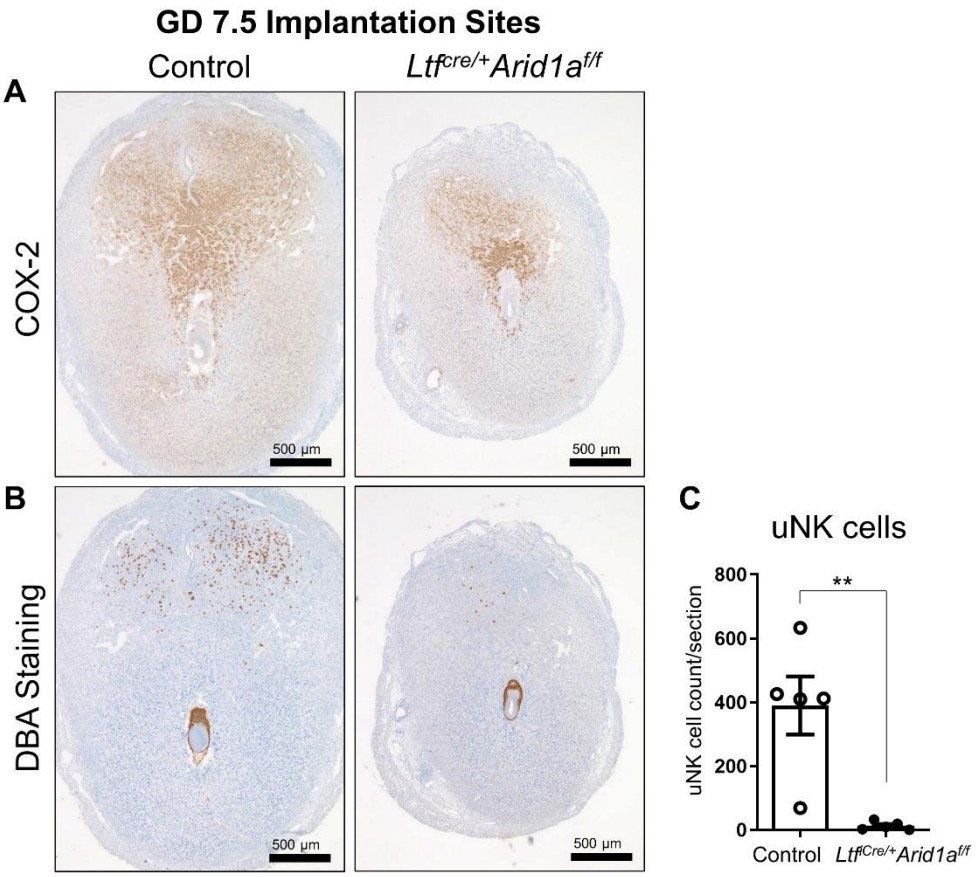

Figure 3.2 *Deletion of endometrial epithelial Arid1a in mice causes diminished uNK cell numbers in GD 7.5 decidua*. **(A)** Representative images of COX2 IHC in control and *Ltf*$^{iCre/+}$*Arid1a*$^{f/f}$ mouse uteri at GD 7.5 (n=5 IS/genotype). **(B)** Representative images of DBA lectin staining for uNK cells in control and *Ltf*$^{iCre/+}$*Arid1a*$^{f/f}$ mouse uteri at GD 7.5 (n=5 IS/genotype). **(C)** Quantification of the average number of DBA-stained uNK cells counted per tissue section in control (n=5 IS, empty bar) and *Ltf*$^{iCre/+}$*Arid1a*$^{f/f}$ (n=5 IS, grey bar) uteri. The graph represents the mean ± SEM. **, $p<0.01$.

3.3.2 RNA-Sequencing Analysis of Ltf$^{iCre/+}$*Arid1a*$^{f/f}$ *Uteri at GD 3.5 Reveals Altered Immune Pathways*

Seeking to discover gene expression changes earlier in pregnancy that could explain compromised decidualization and deficiency of uNK cells due to *Arid1a* deletion, we performed RNA-sequencing analysis on *Ltf*$^{iCre/+}$*Arid1a*$^{f/f}$ uteri collected at GD 3.5, when the uterus is preparing to receive an implanting embryo and just before the onset of decidualization. Principal component analysis (PCA) of filtered, normalized log-transformed gene counts showed that the

five *Ltf*$^{iCre/+}$*Arid1a*$^{f/f}$ and five control *Arid1a*$^{f/f}$ samples segregated from one another based on overall gene expression (Figure 3.3A). Differential expression analysis revealed that 4,181 uterine genes (2,174 increased, 2,007 decreased) were significantly dysregulated due to deletion of endometrial epithelial *Arid1a*, which is visualized by hierarchical clustering heatmap (FDR<0.05; Figure 3.3B). Ingenuity Pathway Analysis (IPA) of this gene set identified the most statistically significant overlaps with Canonical Pathways related to lipid biosynthesis, cell cycle regulation, and immune function and with Upstream Regulators including steroid hormones, cytokines, and other immune modulators (Figure 3.3C, D).

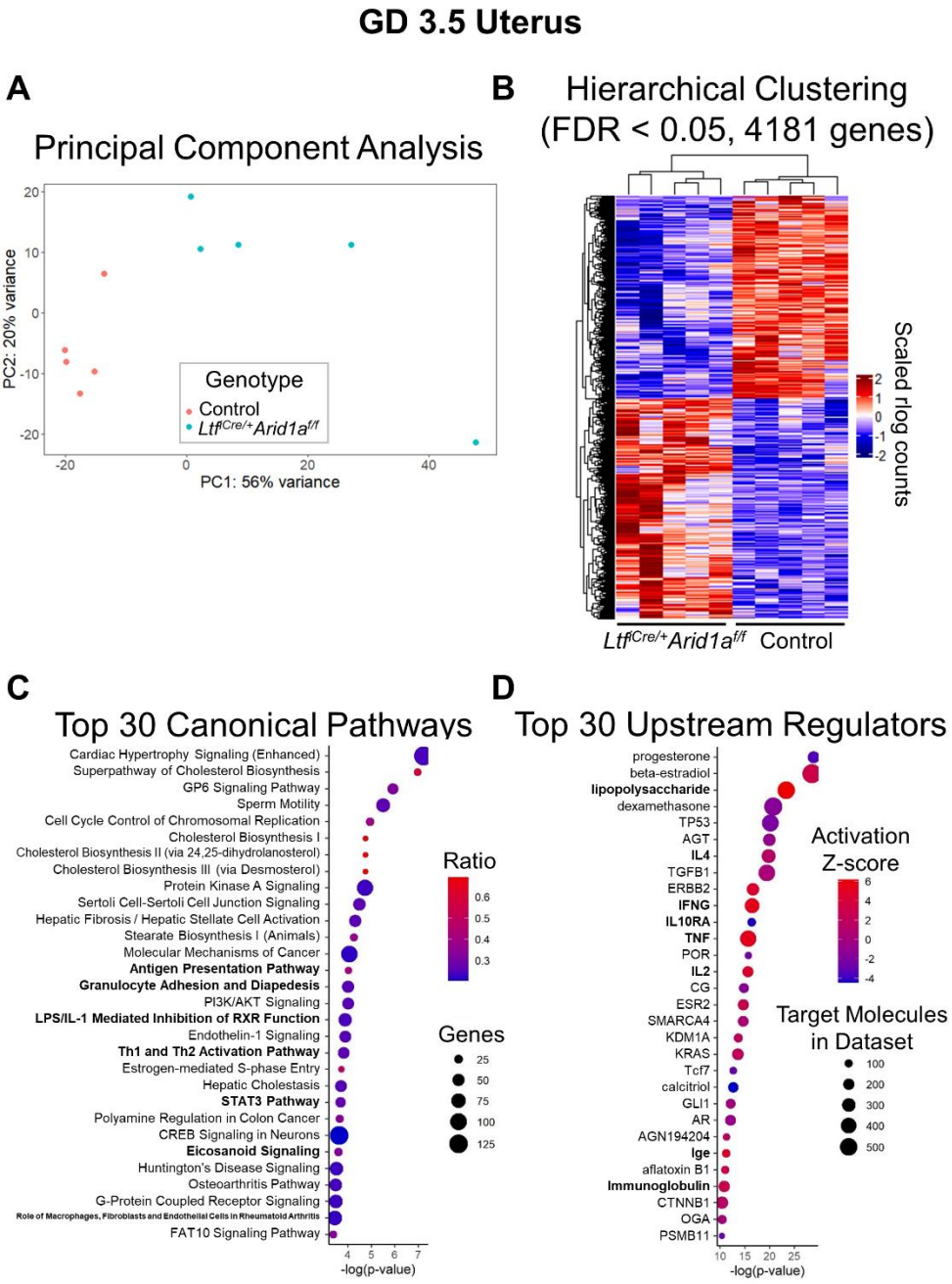

Figure 3.3 *RNA-sequencing analysis of Ltf$^{iCre/+}$Arid1a$^{f/f}$ uteri at GD 3.5 reveals large scale transcriptome dysregulation*. **(A)** RNA-sequencing was performed on GD 3.5 control and *Ltf$^{iCre/+}$Arid1a$^{f/f}$* uterine RNA samples (n=5/genotype). The PCA plot graphically shows that the overall gene expression patterns are distinct between groups. The plot was created using DESeq2 and ggplot2 in Rstudio. **(B)** Differential expression analysis with DESeq2 identified 4,181 (2,007 decreased, 2,174 increased) significantly differentially expressed genes (DEGs) meeting the threshold of FDR<0.05, corrected for multiple testing by independent hypothesis weighting. Hierarchical cluster analysis clearly distinguished the two groups based on gene expression patterns. The plot was created using ComplexHeatmap in Rstudio. **(C)** Ingenuity Pathway Analysis of the 4,181 genes differentially expressed between control and *Ltf$^{iCre/+}$Arid1a$^{f/f}$* uteri (FDR<0.05)

Figure 3.3 (cont'd)
identified 194 significantly enriched Canonical Pathways ($p<0.05$). The plot shows the top 30 pathways from this list based on their corresponding p-values and also displays Ratios (genes in current set/total genes in pathway) and number of genes from each pathway dysregulated in *Ltf*$^{iCre/+}$*Arid1a*$^{f/f}$ uteri. **(D)** Ingenuity Pathway Analysis of the 4,181 genes differentially expressed between control and *Ltf*$^{iCre/+}$*Arid1a*$^{f/f}$ uteri (FDR<0.05) identified 1,526 significantly enriched Upstream Regulators ($p<0.05$). The plot shows the top 30 Upstream Regulators from this list based on their corresponding p-values and also displays activation z-score and number of target molecules in the dataset. The plots were created with ggplot2 in Rstudio.

Because of the large number and broad spectrum of immune-related pathways in the dataset and the known change in uNK cells in *Ltf*$^{iCre/+}$*Arid1a*$^{f/f}$ uteri, we examined the immune-related changes more closely. Altered immune-related canonical pathways involved both the innate and adaptive immune response and both lymphoid and myeloid immune cells (Figure 3.4A). Upstream regulator analysis revealed activation of inflammatory factor targets, notably interferon gamma (IFNG), tumor necrosis factor (TNF), and interleukin 1 beta (IL1B) and deactivation of target molecules for the anti-inflammatory interleukin 10 (IL-10) receptor (IL10RA; Figure 3.4B).

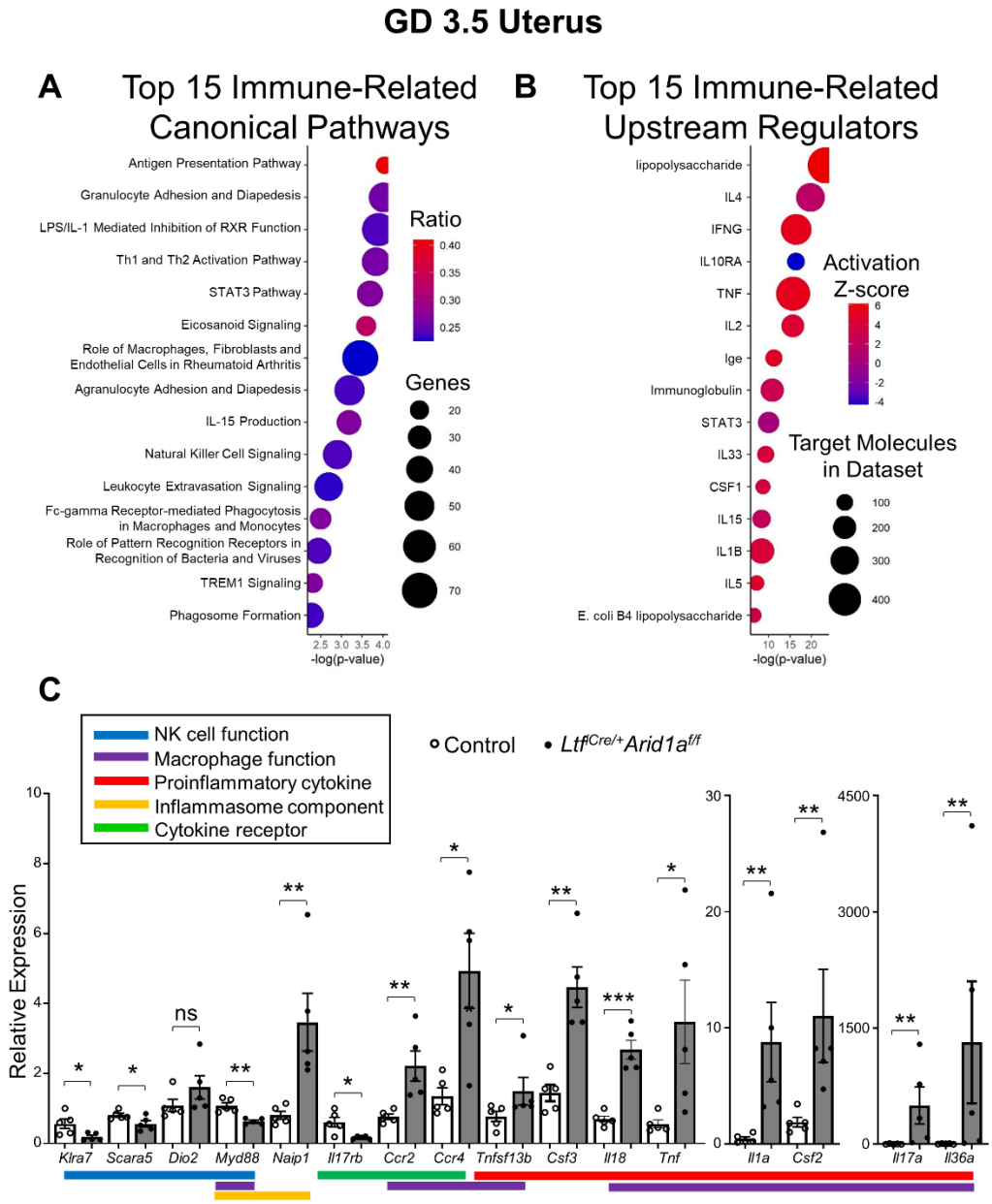

Figure 3.4 *Ltf*$^{iCre/+}$*Arid1a*$^{f/f}$ *uteri exhibit immune-related gene expression changes at GD 3.5*. **(A)** Ingenuity Pathway Analysis of the 4,181 genes differentially expressed between *Arid1a*$^{f/f}$ and *Ltf*$^{iCre/+}$*Arid1a*$^{f/f}$ uteri (FDR<0.05) identified 194 significantly enriched Canonical Pathways (p<0.05). The plot shows the top 15 immune-related pathways from this list based on their corresponding p-values and also displays Ratios (genes in current set/total genes in pathway) and number of genes from each pathway dysregulated in *Ltf*$^{iCre/+}$*Arid1a*$^{f/f}$ uteri. **(B)** Ingenuity Pathway Analysis of the 4,181 genes differentially expressed between *Arid1a*$^{f/f}$ and *Ltf*$^{iCre/+}$*Arid1a*$^{f/f}$ uteri (FDR<0.05) identified 1,526 significantly enriched Upstream Regulators (p<0.05). The plot shows the top 15 immune-related Upstream Regulators from this list based on their corresponding p-values and also displays activation z-score and number of target molecules in the dataset. The plots were created with ggplot2 in Rstudio. **(C)** Relative expression levels of the mRNA from each gene were normalized to *Rpl7* in whole uterine RNA preparations from control (n=5, empty bar and

Figure 3.4 (cont'd)
empty dot) and *Ltf*$^{iCre/+}$*Arid1a*$^{f/f}$ (n=5, grey bar and filled dot) uteri at GD3.5 determined with RT-qPCR. The graphs represent the mean ± SEM. *, p<0.05; **, p<0.01; ***, p<0.001; ns, p>0.05.

RT-qPCR validation of individual differentially expressed genes from the RNA-seq data confirmed that several genes coding for proinflammatory cytokines (interleukin 36 alpha, *Il36a*; interleukin 17A, *Il17a*; colony-stimulating factor 2, *Csf2*; interleukin 1 alpha, *Il1a*; *Tnf*; interleukin-18, *Il18*; colony-stimulating factor 3, *Csf3*; tumor necrosis factor ligand superfamily member 13B, *Tnfsf13b*) and cytokine receptors (C-C motif chemokine receptor 2, *Ccr2*; C-C motif chemokine receptor 4, *Ccr4*) were highly upregulated in the *Ltf*$^{iCre/+}$*Arid1a*$^{f/f}$ uterus (p=0.0079, 0.0079, 0.0079, 0.0079, 0.0159, 0.0001, 0.0013, 0.0469, 0.0079, 0.0317, respectively; Figure 3.4C). One receptor component (interleukin-17 receptor B, *Il17rb*) was decreased, possibly a compensatory effect due to the incredibly high levels of *Il17a* (p=0.0317; Figure 3.4C). Genes related to innate immunity were also modulated, with one inflammasome-related gene (NLR family, apoptosis inhibitory protein 1, *Naip1*) increased and another (myeloid differentiation primary response 88, *Myd88*) decreased (p=0.0079, 0.0013, respectively; Figure 3.4C).

The NK cell receptor gene (killer cell lectin-like receptor 7, *Klra7*) was downregulated, consistent with the finding of diminished uNK cells at GD 7.5 (p=0.0316; Figure 3.4C). Scavenger Receptor Class A Member 5 (*SCARA5*) and iodothyronine deiodinase 2 (*DIO2*) have been identified as marker genes for a diverging decidual response in vivo (Lucas et al. 2020). A shift toward dominance of senescent decidual cells, indicated by decreased *SCARA5* and increased *DIO2*, is associated uNK cell-deficient pre-pregnancy endometrium in humans (Lucas et al. 2020). Along with decreased uNK cell signaling and cell proliferation, *Ltf*$^{iCre/+}$*Arid1a*$^{f/f}$ uteri exhibited significantly decreased *Scara5* and increased *Dio2* expression, though not quite to a level of statistical significance (p=0.0480, 0.0952, respectively; Figure 3.4C). Together, these results

indicate that a highly proinflammatory uterine environment results from deletion of endometrial epithelial *Arid1a* concomitant with a decrease in normal uNK cell regulation of the endometrium.

3.3.3 Uterine Macrophage Numbers are Elevated in Ltf$^{iCre/+}$Arid1a$^{f/f}$ Mice at GD 3.5

Next, we asked if the pro-inflammatory gene expression in the *Ltf*$^{iCre/+}$*Arid1a*$^{f/f}$ uterus at GD 3.5 was intrinsic to the endometrial stromal and epithelial cells or if it coincided with altered immune cell populations. Since macrophages are one of the major cell types that produce proinflammatory cytokines such as TNF and IL-1A, and CSF2 and CCR2 are involved in the proliferation and homing of monocytes and macrophages, we assessed uterine macrophages in *Ltf*$^{iCre/+}$*Arid1a*$^{f/f}$ mice by immunostaining for EGF-like module-containing mucin-like hormone receptor-like 1 (F4/80), a cell surface marker for macrophages and, to a lesser extent, monocytes (Hamilton 2019; Zhao et al. 2015). While F4/80 positive cells were common in the control uterus, comprising approximately 30% of the stromal compartment, the percent of F4/80 positive cells was significantly increased, nearly doubling, in *Ltf*$^{iCre/+}$*Arid1a*$^{f/f}$ uteri (Control=27.86±5.03, *Ltf*$^{iCre/+}$*Arid1a*$^{f/f}$=57.30±5.49, p=0.0042; Figure 3.5). To determine if the changes in macrophage numbers were systemic or specific to the uterus, we stained control and *Ltf*$^{iCre/+}$*Arid1a*$^{f/f}$ spleen tissue for F4/80, finding no difference in macrophage appearance or number (Control=93.73±1.43, *Ltf*$^{iCre/+}$*Arid1a*$^{f/f}$=93.55±1.80, p>0.9999, Figure B.1).

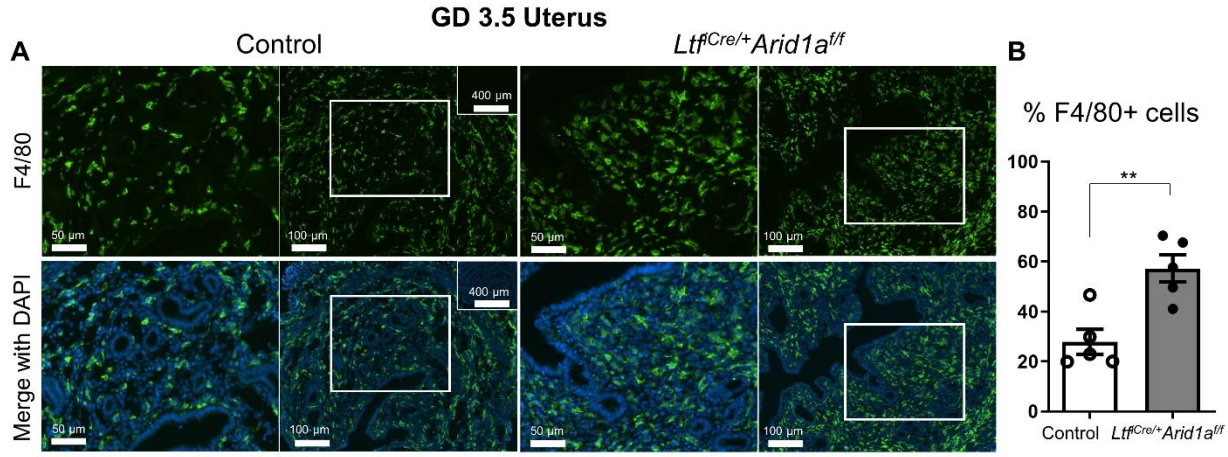

Figure 3.5 *Uterine F4/80+ macrophage numbers are elevated in Ltf$^{iCre/+}$Arid1a$^{f/f}$ mice at GD 3.5.* **(A)** Representative images of F4/80 immunofluorescence (green) counterstained with DAPI (blue) in control (left) and *Ltf$^{iCre/+}$Arid1a$^{f/f}$* (right) mouse uterine sections at GD 3.5 (n=5/genotype) For each group, the left image is higher magnification (scale bar=50 µm) and the right image is a lower magnification region containing the zoomed region (indicated by large white rectangle; scale bar=100 µm). The small insets in the upper right corner of the control images show no primary antibody negative controls (scale bar=400 µm). **(B)** The percentage of F4/80-positive uterine cells was counted in representative stromal fields of approximately 350 cells per sample of control (n=5, empty bar) and *Ltf$^{iCre/+}$Arid1a$^{f/f}$* (n=5, grey bar) uteri at GD3.5. The graph represents the mean ± SEM. **, p<0.01.

To better characterize and more comprehensively assess the myeloid immune cell population in the *Ltf$^{iCre/+}$Arid1a$^{f/f}$* GD 3.5 uterus, we performed flow cytometry analysis, selecting among live, singlet leukocytes for cluster of differentiation molecule 11B (CD11b)+ major histocompatibility complex class II (MHCII)+ cells, which were not different between genotypes (p=0.5396, Figure 3.6A, Figure B.2). Within this myeloid population, F4/80- cluster of differentiation 64 (CD64)- lymphocyte antigen 6C (Ly6C)+ cells were unchanged, F4/80+ CD64+ Ly6C+ cells were significantly increased, and F4/80+ CD64+ Ly6C- cells were significantly decreased (p=0.8154, 0.0050, 0.0029, respectively; Figure 3.6A, B; Figure B.2). Since CD64 is expressed primarily on macrophages, and Ly6C is thought to be specific to circulation-derived inflammatory monocytes and macrophages, the increase of F4/80+ macrophages in *Ltf$^{iCre/+}$Arid1a$^{f/f}$* uteri appears to be driven by infiltration of circulating Ly6C+ inflammatory cells

rather than new growth of resident macrophages (Akinrinmade et al. 2017; Yang et al. 2019; Groves et al. 2018; Zhao et al. 2015; Krishnarajah et al. 2022; Yu et al. 2016). Further myeloid immune cell analysis revealed that Ly6G+ neutrophil numbers were consistent between genotypes, but CD64- cluster of differentiation 24 (CD24)+ uDCs, important for proper decidua formation, were significantly decreased in *Ltf*$^{iCre/+}$*Arid1a*$^{f/f}$ mice (Plaks et al. 2008; Yu et al. 2016) (p=0.7818, 0.0016, respectively; Figure 3.6C, D; Figure B.2).

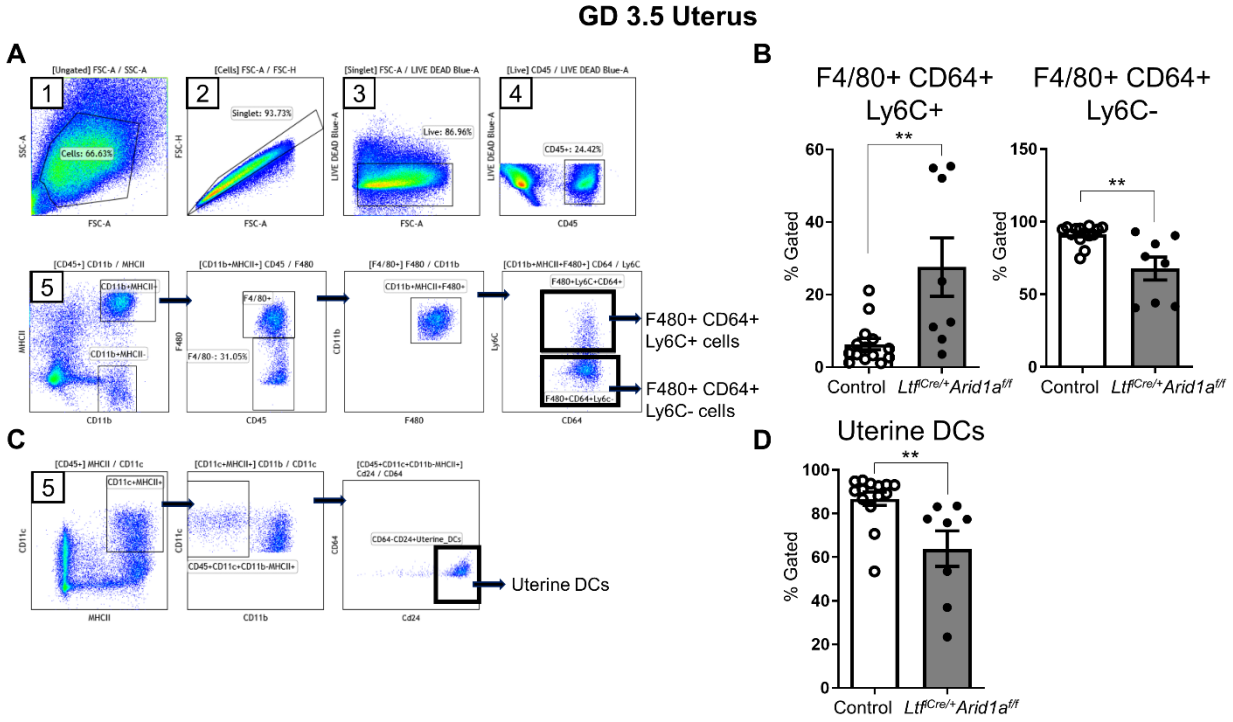

Figure 3.6 *F4/80+ CD64+ Ly6C+ cells are increased while uDCs are decreased in Ltf*$^{iCre/+}$*Arid1a*$^{f/f}$ *uteri at GD 3.5*. **(A)** The flow gating strategy to identify F4/80+ CD64+ Ly6C+ and F4/80+ CD64+ Ly6C- cells in the mouse uterus is shown. **(B)** The % Gated proportion of F4/80+ CD64+ Ly6C+ cells (left) and F4/80+ CD64+ Ly6C- (right) cells in control (n=14, empty bar) and *Ltf*$^{iCre/+}$*Arid1a*$^{f/f}$ (n=8, grey bar) uteri at GD3.5 is shown. **(C)** The flow gating strategy to identify uDCs in the uterus is shown. **(D)** % Gated proportion of uDCs in control (n=14, empty bar) and *Ltf*$^{iCre/+}$*Arid1a*$^{f/f}$ (n=8, grey bar) uteri at GD3.5. The graphs represent the mean ± SEM. **, p<0.01.

To assess the extrauterine peritoneal myeloid immune environment, we quantified monocytes, CD11b+ cells, large peritoneal macrophages, and small peritoneal macrophages in

matched peritoneal fluid (Hogg et al. 2021). This analysis yielded no significantly altered peritoneal immune cell populations, suggesting again that the changes observed in myeloid immune cell composition in GD 3.5 *Ltf*$^{iCre/+}$*Arid1a*$^{f/f}$ mice are specific to the uterus (p=0.3214, 0.5941, 0.6783, 0.7649, respectively; Figure B.3). Together, these data demonstrate that deletion of endometrial epithelial *Arid1a* causes uterine-specific infiltration of circulating inflammatory myeloid cells during early pregnancy, resulting in elevated numbers of inflammatory macrophages alongside decreased uDCs and altered uNK cell signaling in the uterus.

3.4 Discussion

In gynecological pathologies such as endometriosis and infertility, the normally tightly regulated epigenetic landscape and immune environment of the endometrium are thrown off balance (Zondervan et al. 2018). We previously showed that endometrial ARID1A levels are diminished in women with endometriosis and that abolishing endometrial epithelial ARID1A expression drives a loss of endometrial receptivity and failure of pregnancy establishment and maintenance (See Chapter 2) (Kim, Yoo, Wang, et al. 2015; Marquardt et al. 2021). Past research has also demonstrated that the endometrium of women with endometriosis experiences an increase of proinflammatory macrophages and alterations in uNK cell and uDC activity (Vallve-Juanico, Houshdaran, and Giudice 2019). In this study, we describe a possible mechanism for a connection between these phenomena.

When we deleted *Arid1a* the endometrial epithelium using *Ltf*$^{iCre/+}$*Arid1a*$^{f/f}$ mice, massive changes immune-related gene expression patterns resulted in the pre-implantation (GD 3.5) uterus. Uterine expression of the proinflammatory cytokine genes *Il36a*, *Il17a*, *Csf2*, *Il1a*, *Tnf*, *Il18*, *Csf3*, and *Tfnfs13b* spiked alongside increased uterus-specific infiltration of F4/80+ CD64+ Ly6C+

inflammatory macrophages. At the same time, uDC numbers were diminished and pro-decidual uNK markers decreased. These disruptions were followed by reduced implantation site size, compromised decidua formation, and dramatic diminution of uNK cell presence post-implantation (GD 7.5). Interestingly, increases *IL-17A*, *IL18*, *TNFSF13B*, and TNF signaling have all been previously identified in endometriosis conditions (Ahn et al. 2016; Ahn et al. 2015; Richter et al. 2005). Increased IL-18 has been linked to failed embryo transfer and recurrent miscarriage (Ledee-Bataille et al. 2004; Wilson et al. 2004). Furthermore, TNF can inhibit trophoblast invasion, and one report showed that inhibiting its activity may improve live birth rates in women with recurrent spontaneous abortion (Haider and Knofler 2009; Winger and Reed 2008). Finally, high levels of uterine IL-36A were shown to correlate with an increased rate of fetal loss in mice (Murrieta-Coxca et al. 2016).

Whether uNK cell numbers are altered in women with endometriosis is controversial; however, they do appear to be phenotypically altered with increased cytotoxicity (Vallve-Juanico, Houshdaran, and Giudice 2019). In human pregnancy, the literature is clear regarding the importance of uNK cells for vasculature remodeling in the formation of the decidua and later on the placenta (Dosiou and Giudice 2005). Moreover, a role for uNK cells in clearing senescent decidual cells has recently been described as important for maintaining uterine homeostasis and implantation (Brighton et al. 2017). An appropriate spaciotemporal balance between *SCARA5*+ decidual cells and *DIO2*+ senescent decidual cells must be maintained to allow implantation and prevent pregnancy loss, and low *SCARA5*, high *DIO2*, and low uNK populations are associated with recurrent pregnancy loss (Lucas et al. 2020). Our data from early pregnancy in $Ltf^{iCre/+}Arid1a^{f/f}$ mice suggests that a lack of epithelial ARID1A leads to an early skew toward a pro-senescent decidual state that corresponds to the lack of sufficient uNK cells in the decidual

post-implantation. Though uNK cells regulate the structure of the decidua and development of the placenta, they are not necessary in rodents for the delivery of normal numbers of pups (Renaud et al. 2017; Ashkar et al. 2003; Ratsep et al. 2015). Therefore, it is not clear if the diminished uNK cell population in *Ltf*$^{iCre/+}$*Arid1a*$^{f/f}$ mice contributes to pregnancy failure or is simply a byproduct of the compromised early decidualization response. It also remains to be seen whether this phenomenon is a factor in endometriosis-related infertility in the human case.

The density of mature uDCs has been shown to be reduced in the endometrium of women with endometriosis potentially altering coordination of adaptive immunity and angiogenesis, though the functional outcome has not been thoroughly studied (Schulke et al. 2009; Maridas et al. 2014; Vallve-Juanico, Houshdaran, and Giudice 2019). In mice, depletion of uDCs during pregnancy resulted in defective implantation, improper decidua formation, and embryo resorption (Plaks et al. 2008). Therefore, the reduction of uDCs following deletion of endometrial epithelial *Arid1a* in *Ltf*$^{iCre/+}$*Arid1a*$^{f/f}$ mice may contribute to their compromised implantation and decidualization.

In endometriosis conditions, research to date has indicated that a decrease of anti-inflammatory macrophages and an increase of total macrophages accompanies upregulated proinflammatory cytokine signaling (Vallve-Juanico, Houshdaran, and Giudice 2019). Similarly, our RNA-seq differentially expressed gene upstream regulator analysis identified deactivation of anti-inflammatory IL10RA target molecules but strong activation of proinflammatory TNF signaling targets in *Ltf*$^{iCre/+}$*Arid1a*$^{f/f}$ uteri. TNF is considered a “master-regulator” of inflammatory cytokine production, and it can both be produced by and activate macrophages (Parameswaran and Patial 2010).

To analyze the relationship between increased inflammatory gene expression and macrophage cell presence in *Ltf*$^{iCre/+}$*Arid1a*$^{f/f}$ uteri, we quantified macrophages with immunostaining and flow cytometry. Immunostaining identified a uterus-specific increase in total F4/80+ macrophages when endometrial epithelial *Arid1a* was deleted, but this analysis could not determine the source or characteristics of the cells since F4/80 marks tissue-resident macrophages as well as macrophages derived from circulating monocytes (Yu et al. 2016). In our flow cytometry analysis, we were able to discriminate among F4/80+ CD64+ macrophages utilizing the monocyte and monocyte-derived cell marker Ly6C (Krishnarajah et al. 2022; Zhao et al. 2015; Yu et al. 2016; Yang et al. 2019). Since the Ly6C+ population increased in *Ltf*$^{iCre/+}$*Arid1a*$^{f/f}$ uteri and the Ly6C- population decreased, we conclude that the increased F4/80+ macrophages in the uterus were derived from circulating inflammatory monocytes (Krishnarajah et al. 2022; Zhao et al. 2015; Yu et al. 2016; Yang et al. 2019). Since the F4/80- CD64- Ly6C+ cell populations were not different between genotypes, it appears that the altered cell type should be defined as an inflammatory monocyte-derived macrophage population rather than a classical monocyte population. However, we cannot conclude this with certainty since some monocytes also express F4/80 and CD64, and there is disagreement over whether Ly6C+ cells should be labeled as macrophages (Krishnarajah et al. 2022; Zhao et al. 2015; Yu et al. 2016; Yang et al. 2019).

The observations of increased uterine proinflammatory cytokine gene expression and increased inflammatory macrophage infiltration in *Ltf*$^{iCre/+}$*Arid1a*$^{f/f}$ mice raise the question of what factor first initiates the inflammatory conditions after epithelial deletion of *Arid1a*. Some level of inflammation is normal and required to facilitate implantation, but the inflammatory conditions we observed in *Ltf*$^{iCre/+}$*Arid1a*$^{f/f}$ uteri were far beyond normal control levels. E2 signaling is generally considered to be proinflammatory although this is a generalizations of highly complex

and context-dependent realities (Straub 2007). We reported a skew toward E2 signaling dominance in *Ltf*$^{iCre/+}$*Arid1a*$^{f/f}$ uterine gene expression in Chapter 2, which could contribute to the inflammatory environment, but serum E2 and P4 levels were not significantly altered (Marquardt et al. 2021). We also demonstrated a defect of uterine gland function in *Ltf*$^{iCre/+}$*Arid1a*$^{f/f}$ mice in Chapter 2 which resulted in diminished *Lif* expression (Marquardt et al. 2021). LIF regulates uterine immune cell composition in mice; however, *Lif* knockouts have half the normal numbers of uterine macrophages and double the uNKs, which is opposite from our findings here (Schofield and Kimber 2005).

A more plausible mechanism for the triggering of extraordinary inflammation in *Ltf*$^{iCre/+}$*Arid1a*$^{f/f}$ pregnant uteri is suggested by the fact that epithelial cells in the uterus as well as in other tissue types are known to produce TNF, CSF2, and other proinflammatory cytokines in certain circumstances (Laird et al. 1996; Roulis et al. 2011; Ahn et al. 2015; Robertson, Mayrhofer, and Seamark 1992; Zhao and Chegini 1999). In fact, ARID1A has been shown to directly bind near the promoter regions of *Il36a, Tnfsf13*, and other TNF-signaling related genes in the murine endometrial epithelium (Reske et al. 2021). Furthermore, in 12Z endometriotic epithelial cells, genes bound by ARID1A and upregulated by knockdown of *ARID1A* expression include TNF signaling-related and inflammatory response pathway genes (Wilson et al. 2019). One gene from this ARID1A-bound and regulated group is *CCL2*, the gene for monocyte chemoattractant protein-1 (MCP-1), a major chemoattractant that regulates the migration of monocytes and macrophages by binding its receptor CCR2 (Deshmane et al. 2009). Expression of both genes increases in endometriosis conditions (Jolicoeur et al. 1998; Ahn et al. 2016). Interestingly, we also found *Ccr2* gene expression increased in *Ltf*$^{iCre/+}$*Arid1a*$^{f/f}$ uteri. Together, these data suggest a mechanism where loss of endometrial epithelial ARID1A leads to cell-autonomous secretion of CCL2, TNF,

CSF2, and other inflammatory factors, which leads to recruitment of inflammatory macrophages into the uterus, further exacerbating the inflammatory environment (Figure 3.7). Such a strong inflammatory response in the uterus can then result in decreased uDCs and uNKs like we observed in *Ltf*$^{iCre/+}$*Arid1a*$^{f/f}$ uteri as well as generally hostile, non-receptive conditions (Zhao et al. 2015).

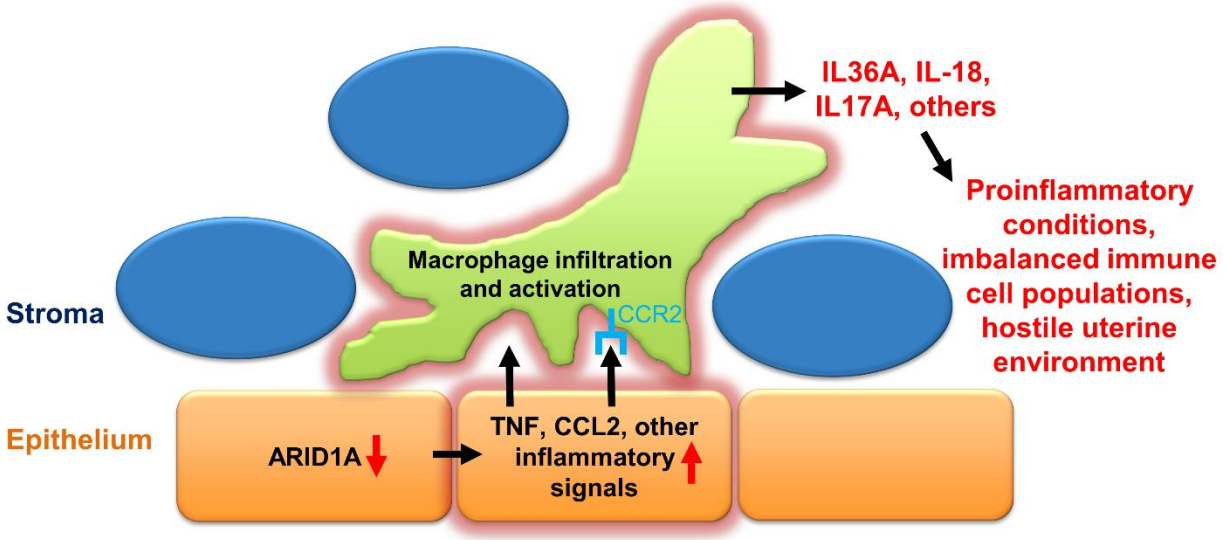

Figure 3.7 *Proposed Mechanism: Endometrial epithelial ARID1A loss leads to increased proinflammatory cytokine expression and macrophage-driven uterine inflammation during early pregnancy.*

One limitation of our study is that all our gene expression analyses were performed on whole uterine tissue, which did not allow us to distinguish between gene expression in endometrial epithelial, stromal, and immune cells. Therefore, we cannot be certain whether the increased expression of proinflammatory cytokine genes we observed in *Ltf*$^{iCre/+}$*Arid1a*$^{f/f}$ uteri was driven by direct changes in the epithelial cells or indirect changes in stromal or immune cells. Additionally, *Ltf-iCre* can reportedly be expressed in neutrophils and other myeloid lineage immune cells (Daikoku et al. 2014; Kovacic et al. 2014). Although we did not observe changes in the number of uterine neutrophils, and systemic myeloid immune cell alterations were not evident as assessed in the spleen or peritoneal fluid, we cannot rule out the possible contribution of *Arid1a* deletion in

Ltf$^{iCre/+}$*Arid1a*$^{f/f}$ myeloid immune cells themselves. Furthermore, we did not assess whether changes occurred in uterine adaptive immune cell populations or in the uterine immune environment of non-pregnant mice, both of which are areas of interest for future study.

In summary, we have shown that deletion of endometrial epithelial *Arid1a* in mice causes large scale uterine transcriptome dysregulation during early pregnancy, including many genes related to immune function. Most notably, we found increases in proinflammatory cytokine expression and alterations in uNK cell signaling. At the cell level, increased proinflammatory cytokine transcription accompanied a uterine-specific influx of proinflammatory macrophages, a decrease in uDCs, and, after implantation, a diminished uNK cell population at implantation sites. Many of the immune-related changes we observed parallel observations from the dysregulated endometrial immune environment present in women with endometriosis, suggesting that diminished endometrial epithelial ARID1A in endometriosis conditions may contribute to the proinflammatory environment and negatively impact receptivity of the endometriosis-affected endometrium to pregnancy.

3.5 Materials and Methods

3.5.1 Mouse Models

All mouse procedures were approved by the Institutional Animal Care and Use Committee of Michigan State University. All mice were housed and bred in a designated animal care facility at Michigan State University under controlled humidity and temperature conditions and a 12 hour light/dark cycle at 5 mice/cage maximum. Access to water and food (Envigo 8640 rodent diet) was ad libitum. Endometrial epithelial conditional *Arid1a* knockout mice were generated in mixed background C57BL/6, 129S6/SvEvTac, 129P2/OlaHsd, 129S1/SvImJ strain mice by initially

crossing *Ltf*$^{iCre/+}$ (Daikoku et al. 2014) (Jackson Laboratory Stock No: 026030) males with *Arid1a*$^{f/f}$ (Gao et al. 2008) (Jackson Laboratory Stock No: 027717) females and then selecting *Ltf*$^{iCre/+}$*Arid1a*$^{f/f}$ males and *Arid1a*$^{f/f}$ females from the F2 generation for continuous breeding. All experiments were performed in 12-15-week-old mature adult mice to ensure sufficient *Ltf*$^{iCre/+}$ activation. For breeding, one male mouse was normally placed into a cage with one female mouse. Occasionally, one male mouse was housed with two female mice to increase breeding success, and females were separated with their pups until weaning. After weaning at P21-P28, male and female littermates were separated and housed in groups at 5 mice/cage maximum until use in breeding or experiments. Mice of appropriate genotypes were randomly allocated to experimental groups, using littermates for comparisons when possible.

3.5.2 Mouse Procedures and Tissue Collection

Uterine samples from specific times of pregnancy were obtained by mating control or conditional *Arid1a* knockout female mice with proven wildtype male breeder mice defining morning of identification of a vaginal plug as GD 0.5. Part of each uterine sample isolated at GD 3.5 was snap-frozen and stored at -80°C for RNA extraction. The remaining uterine tissues and paired spleen tissues were prepared for histological analysis by fixing for 6 hours in 4% (vol/vol) paraformaldehyde (Fisher Scientific, Hampton, NH, Cat. #04042-500), cryopreserving in a series of sucrose solutions increasing from 10% to 15% to 20% sucrose in Hanks' Balanced Salt Solution (HBSS; Gibco, Grand Island, NY, Cat. #14170-112), and deep freezing in Tissue-Tek optimal cutting temperature (OCT) compound (Sakura Finetek USA, Torrance, CA, Cat. # 4583) at -80°C. Whole uterine samples collected at GD 7.5 were photographed and weighed before fixing with 4% (vol/vol) paraformaldehyde and processing in a graded alcohol series for paraffin embedding.

Implantation sites were identified and measured based on gross morphology with subsequent histological confirmation. Individual implantation sites were weighed after tissue processing but before embedding.

3.5.3 Histology and Immunostaining

For IHC and DBA lectin staining, fixed, paraffin-embedded tissues were cut at 5 μm, mounted on slides, deparaffinized, and rehydrated in a graded alcohol series. Immunostaining was performed by incubating overnight at 4°C with a COX-2-specific primary antibody (Cayman Chemical, Ann Arbor, MI, Cat. #160106, 1:1000) after citrate-based antigen unmasking, quenching of exogenous peroxidases with 3% hydrogen peroxide in methanol, and blocking with 10% normal goat serum (NGS; Vector Laboratories, Cat. #S-1000) in pH 7.5 phosphate buffered saline (PBS). A biotinylated anti-rabbit secondary antibody (Vector Laboratories, Burlingame, CA, Cat. #BA-1000) was applied, followed by incubation with horseradish peroxidase (Thermo Fisher Scientific, Waltham, MA, Cat. #434323) and developing using the Vectastain Elite DAB kit (Vector Laboratories, Cat. #SK-4100).

DBA staining was performed largely as previously described (Croy et al. 2010) by incubation with biotinylated *Dolichos biflorus* lectin (Vector Laboratories, B-1035-5, 1:250) overnight at 4°C after treatment with 1% hydrogen peroxide in pH 7.5 PBS and blocking with 10% NGS (Vector Laboratories, Cat. #S-1000) in pH 7.5 PBS. Horseradish peroxidase (Thermo Fisher Scientific, Cat. #434323) was applied followed by developing using the Vectastain Elite DAB kit (Vector Laboratories, Cat. #SK-4100).

For immunofluorescence, frozen, OCT-embedded tissues were cut at 10 μm, mounted on slides, fixed in 4% (vol/vol) paraformaldehyde (Fisher Scientific, Cat. #04042-500), immersed in

0.3% hydrogen peroxide in methanol, and washed in 1/40 Triton-X 100 (Fisher Scientific, Cat. #BP151-500) before blocking with 10% NGS (Vector Laboratories, Cat. #S-1000) in pH 7.5 PBS and incubating with an F4/80 primary antibody (BioLegend, San Diego, CA, Cat. #123101) diluted in 10% NGS in PBS overnight at 4°C. An anti-Rat Alexa Fluor 488 secondary antibody (Thermo Fisher Scientific, A-21208) was used before mounting with VECTASHIELD® Antifade Mounting Medium with DAPI (Vector Laboratories, Cat. #H-1200). Imaging was performed with a Nikon epi-fluorescence microscope and NIS-Elements imaging software (Nikon Instruments, Melville, NY). The percentage of F4/80-positive uterine cells was counted in representative stromal fields of approximately 350 cells per sample. The percentage of F4/80-positive spleen cells was counted in representative red pulp fields of approximately 500 cells per sample.

3.5.4 RNA Isolation and RT-qPCR

As previously described (Kim, Yoo, Wang, et al. 2015), total RNA was extracted from uterine tissues using the RNeasy Mini Kit for total RNA isolation (Qiagen, Valencia, CA, Cat. #74106). Template cDNA was produced from 3 μg of total RNA using random hexamers and MMLV Reverse transcriptase (Thermo Fisher Scientific, Cat. # 28025013). cDNA levels were measured by real-time PCR SYBR green analysis using an Applied Biosystems StepOnePlus system according to the manufacturer's instructions (Applied Biosystems, Foster City, CA,) using pre-validated primers (Table B.1) and PowerUp SYBR Green Master Mix (Thermo Fisher Scientific, Cat. #A25742). The amplification conditions were 10 minutes at 95˚C, 40 cycles of 15 seconds at 95˚C followed by 1 minute at 60˚C, then a melt curve phase consisting of 15 seconds at 95˚C, 1 minute at 60˚C, and 15 seconds at 95˚C. Expression levels were normalized against *Rpl7*.

3.5.5 RNA-Sequencing

Libraries were prepared by the Van Andel Genomics Core from 500 ng of total RNA using the KAPA mRNA Hyperprep kit (v4.17) (Kapa Biosystems, Wilmington, MA USA). RNA was sheared to 300-400 bp. Prior to PCR amplification, cDNA fragments were ligated to IDT Illumina UDI dual Indexed adapters (Illumina Inc, San Diego CA, USA). Quality and quantity of the finished libraries were assessed using a combination of Agilent DNF-474 HS fragment kit (Agilent Technologies, Inc.) using a Fragment Analyzer (Agilent Technologies, Inc.), and QuantiFluor® dsDNA System (Promega Corp., Madison, WI, USA). Individually indexed libraries were pooled and 50 bp, paired end sequencing was performed on an Illumina NovaSeq6000 sequencer using an S2, 100 bp sequencing kit (Illumina Inc., San Diego, CA, USA) to an average depth of 50M reads per sample. Base calling was done by Illumina RTA3 and output of NCS was demultiplexed and converted to FastQ format with Illumina Bcl2fastq v1.9.0.

3.5.6 RNA-Sequencing Analysis

Based on previously described methods (Wilson et al. 2019), raw reads were trimmed with cutadapt (Martin 2011) v1.18 and Trim Galore! (http://www.bioinformatics.babraham.ac.uk/projects/trim_galore/) v0.6.4_dev. Quality control analysis was performed using FastQC (https://www.bioinformatics.babraham.ac.uk/projects/fastqc/) v0.11.9. Trimmed reads were aligned to the GRCm38 genome assembly using STAR (Dobin et al. 2013) v2.7.3a, and feature counting was performed using the command '--quantMode GeneCounts'. Output gene count files were constructed into an experimental read count matrix in R. Low count genes were filtered (1 count per sample on average) prior to DESeq2 (Love, Huber, and Anders 2014; Love et al. 2015)

v1.30.1 count normalization and subsequent differential expression analysis. Calculated differential expression probabilities were corrected for multiple testing by independent hypothesis weighting (IHW (Ignatiadis et al. 2016) v 1.18.0) for downstream analysis, referred to as false discovery rate (FDR) for simplicity. Differentially expressed gene thresholds were set at FDR < 0.05. All reported instances of log2(fold-change) data from RNA-seq were adjusted by apeglm v1.12.0 for LFC shrinkage (Zhu, Ibrahim, and Love 2019). Principal component analysis was calculated based on the top 500 genes by variance using DESeq2 and plotted with ggplot2 (Wickham 2016) v3.3.3. The RNA-seq heatmap was generated with ComplexHeatmap v2.6.2 (Gu, Eils, and Schlesner 2016) and circlize v0.4.12 (Gu et al. 2014) using scaled regularized-logarithm (rlog) counts for visualization. Differentially expressed genes were classified using QIAGEN IPA with results plotted with ggplot2.

3.5.7 Flow Cytometry

Uterine horns from GD3.5 mice were excised, spliced open longitudinally, and finely chopped using spring scissors. To prepare single cell suspensions, uterine tissue fragments were continuously digested in Enzyme buffer (Liberase™ TH Research Grade (0.09625mg/mL, Millipore Sigma, Burlington, MA, Cat. #LIBTH-RO), 100U of DNaseI (Millipore Sigma, Cat. #AMPD1) in RPMI 1640 (Gibco, Grand Island, NY, Cat. #11835-030) at 37°C. To aid dissociation, samples were taken out every 20 minutes and pushed through 18 and 23 gauge needles. Once fragments were dissociated (after 60 to 90 minutes), samples were filtered through 70 um mesh, centrifuged at 400 x g for 5 minutes, then resuspended in flow staining buffer (5% fetal bovine serum in PBS) to neutralize the Liberase™ TH enzyme. Red blood cells were lysed by resuspending the cell pellet in 1 mL of ACK (Ammonium-Chloride-Potassium) lysis buffer. To

collect peritoneal fluid samples, 2-3 mL PBS was injected into the peritoneal cavity, the mouse was gently massaged, then as much fluid as possible was withdrawn. This was repeated if necessary to collect at least 2 mL of fluid. The resulting single cell suspensions (uterus and peritoneal lavage) were counted using Countess II (Thermo Fisher Scientific), resuspended in flow staining buffer and placed on ice.

To analyze viability, all cells were stained with Live/Dead Blue (Thermo Fisher Scientific, Cat. #L23105) on ice for 30 minutes, followed by Fc receptor block (BD Biosciences, East Rutherford, New Jersey, Cat. #553141) on ice for 20 minutes. Antibodies against specific mouse antigens were utilized for cell-surface staining (Table B.2). Between 2-6x10^5 cells were stained using a cocktail of cell-surface antibodies for 30 minutes on ice, washed three times in flow staining buffer, and fixed in 1% paraformaldehyde prior to analysis. All samples were analyzed using spectral flow cytometry, Cytek® Aurora (Cytek Biosciences, CA) at Michigan State University Flow Cytometry Core. The flow cytometric analysis software Kaluza (Beckman Coulter, Indianapolis, IN) was used to for analysis and generation of gating strategy.

3.5.8 Statistical Analysis

To assess statistical significance of parametric data, we used student's t-test. For non-parametric data, we used the Mann-Whitney U test. All statistical tests were two-tailed when applicable, and a value of $p<0.05$ was considered statistically significant. Statistical analyses were performed using the Instat 3 package from GraphPad (San Diego, CA). Statistical test results (p-values) are presented with the results in the text and symbolically in the figures, with explanations in figure legends. The value of n for each experiment, representing number of animals unless noted as number of implantation sites, is reported in the appropriate figure legend.

3.6 Data Availability

The data that support the findings of this study are available in the chapter, Appendix B, and the publicly accessible GEO database under series GSE196489.

3.7 Acknowledgments

Research reported in this chapter was supported in part by the Eunice Kennedy Shriver National Institute of Child Health & Human Development of the National Institutes of Health under Award Numbers R01HD084478 to J.W.J., F31HD101207 to R.M.M., and T32HD087166, MSU AgBio Research, and Michigan State University. The content is solely the responsibility of the authors and does not necessarily represent the official views of the National Institutes of Health. We thank the Van Andel Genomics Core for providing RNA-sequencing facilities and services.

CHAPTER 4

ENDOMETRIAL ARID1A LOSS IN A MOUSE MODEL OF ENDOMETRIOSIS-RELATED INFERTILITY

Portions of this chapter are modified from a previously published work (Yoo et al. 2022): Jung-Yoon Yoo, Tae Hoon Kim, Jung-Ho Shin, Ryan M. Marquardt, Ulrich Müller, Asgerally T. Fazleabas, Steven L. Young, Bruce A. Lessey, Ho-Geun Yoon, and Jae-Wook Jeong (2022). Loss of MIG-6 results in endometrial progesterone resistance via ERBB2. *Nature Communications* 13, 1101. This article is an open access article distributed under the terms and conditions of the Creative Commons Attribution (CC BY) license (http://creativecommons.org/licenses/by/4.0/). The remaining sections unpublished at the time of dissertation submission are in collaboration with Tae Hoon Kim and Jae-Wook Jeong at the Department of Obstetrics, Gynecology & Reproductive Biology in the Michigan State University College of Human Medicine.

4.1 Abstract

Female subfertility is highly associated with endometriosis. Increasing evidence suggests epigenetic and chromatin structure dysregulation as an important factor in the development of endometrial diseases. ARID1A displays loss of function mutations in some deep infiltrating and ovarian endometriotic lesions and shows decreased expression in endometrial samples from infertile women with endometriosis. We report in this chapter that uterine *ARID1A* ablation drives increased endometriosis lesion incidence in a mouse model of endometriosis that shows similar pathophysiology to the human condition. In addition, endometriosis recipients in our syngeneic mouse model of endometriosis exhibit implantation and decidualization defects which follow decreased endometrial stromal expression of ARID1A. Together, our results demonstrate that ARID1A loss: (1) leads to increased endometriosis lesion development; (2) occurs in the

endometrial stroma after lesion formation; and (3) is associated with endometriosis-related implantation and decidualization failure in a mouse model of endometriosis.

4.2 Introduction

Critical for fertility, the uterine endometrium's epithelial and stromal compartments undergo dynamic hormonally controlled molecular and morphological changes to prepare for embryo implantation and development. However, this dynamic balance is often lost in cases of gynecological disease. Endometriosis affects about 10% of all women of reproductive age, and the incidence increases to 50-60% of women with chronic pelvic pain and infertility (Eskenazi and Warner 1997; Bulun 2009). Retrograde menstruation is the most widely accepted theory of endometriosis pathogenesis, but since most women experience this phenomenon, either the properties of endometrial cells shed into the peritoneum or their environment must be different in women who develop endometriosis (de Ziegler, Borghese, and Chapron 2010; Zondervan et al. 2018). Severe endometriosis can compromise fertility by directly diminishing ovarian reserve through endometriomas or by distorting pelvic anatomy, but these mechanisms do not explain the fertility defects observed in mild cases of endometriosis when endometrial receptivity is apparently compromised (Holoch and Lessey 2010; de Ziegler, Borghese, and Chapron 2010). The endometrium is thus critical to study in the context of endometriosis-related infertility, but the in vivo pathophysiology of initial endometriosis lesion development and of pregnancy establishment are impossible to study directly in humans. This reality necessitates indirect experimental methods such as preclinical animal models.

Several animal models have been developed using rodents and non-human primates to study the mechanisms of endometriosis development and the relationship between endometriosis

lesions and symptoms (Sharpe-Timms and Stilley 2020). Mice are an especially attractive species for preclinical research because they are accessible and cost-effective due to their small size, rapid breeding, and receptivity to genetic manipulation (Saunders 2020).

ARID1A is a molecule of particular interest in endometrial dysfunction. Mutations in the *ARID1A* gene that cause loss of its expression were identified in endometriotic lesions (Anglesio et al. 2017), and ARID1A expression is reduced in eutopic endometrium from infertile women with endometriosis (Kim, Yoo, Wang, et al. 2015). Previous work utilized conditional uterine *Arid1a* knockout mice ($Pgr^{cre/+}Arid1a^{f/f}$) to show that uterine ARID1A loss causes infertility due to implantation and decidualization defects,

Here, we use uterine-specific *Arid1a* knock-out mice combined with a surgically induced mouse model of endometriosis to demonstrate that ARID1A loss results in increased lesion formation. We also show that wild type female mice induced with endometriosis lose endometrial stromal ARID1A expression on their way to developing compromised implantation and decidualization. Our findings provide insight into the etiology of female infertility and its relationship to the development of endometriosis.

4.3 Results

4.3.1 Development of a Mouse Model of Endometriosis in $Pgr^{cre/+}Rosa26^{mT/mG}$ Mice with a Double-Fluorescent Cre Reporter

Uncovering pathophysiological mechanisms of endometriosis-related infertility with animal models requires easy identification of lesions to distinguish them from the surrounding normal tissues. With this in mind, we developed a mouse model of endometriosis using *mT/mG* reporters. In $Pgr^{cre/+}Rosa26^{mTmG/+}$ mice, *Pgr*-positive uterine cells express mG, while *Pgr*-negative

cells express mT (Figure 4.1A, B). Using this model, we surgically induced endometriosis in *Pgr*$^{cre/+}$*Rosa26*$^{mTmG/+}$ mice by inoculating autologous endometrial tissue fragments into the peritoneal cavity after 3 days of E2 treatment (Figure 4.1C). This method leads to the development of endometriotic lesions similar to those in humans without the need for ovariectomy or unopposed E2 treatment (Figure 4.1D-F). To examine the responsiveness of our endometriosis model to E2 and P4, *Pgr*$^{cre/+}$*Rosa26*$^{mTmG/+}$ mice induced with endometriosis were treated with vehicle, E2, or E2+P4 for one month. While E2 treatment after endometriosis induction significantly increased the number of endometriotic lesions compared to the vehicle group, the addition of P4 suppressed the E2-induced increase in lesion number (Fig 4.1G, H; $p=0.0077$ and $p=0.0014$). Our mouse model thus closely mirrors human endometriosis as an E2-dependent and P4-suppressed disorder.

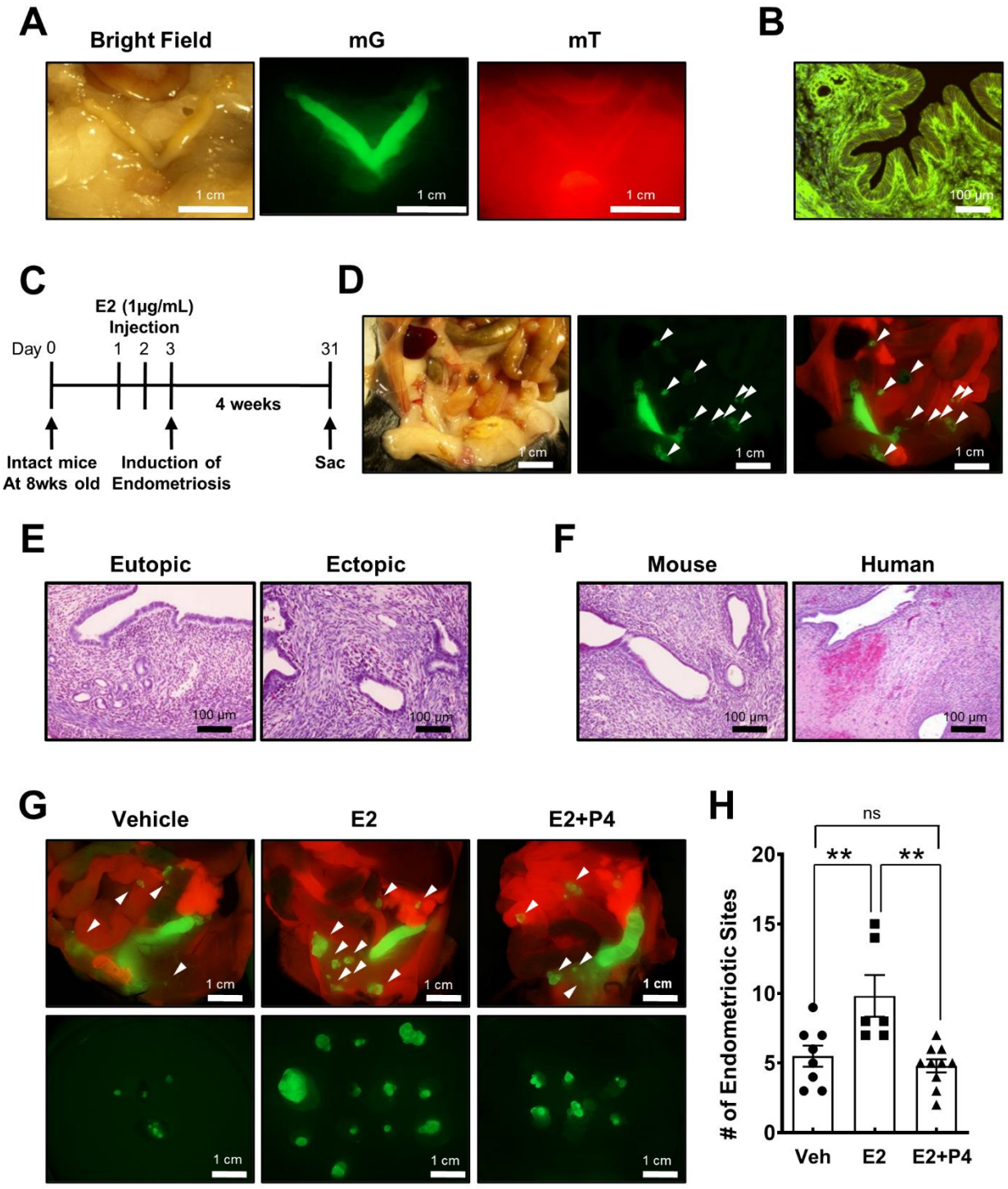

Figure 4.1 *Development of a mouse model of endometriosis in* $Pgr^{cre/+}Rosa26^{mTmG/+}$ *mice with a double-fluorescent Cre reporter*. **(A)** Double-fluorescence based on Cre-recombinase activity in $Pgr^{cre/+}Rosa26^{mTmG/+}$ mice. Scale bars=1 cm. **(B)** Green fluorescence photomicrograph of a uterine section from a $Pgr^{cre/+}Rosa26^{mTmG/+}$ mouse. Scale bar=100 µm. **(C)** Process schematic diagram of the mouse model of endometriosis based on *mT/mG* mice. **(D)** Fluorescence photomicrographs of endometriotic sites in $Pgr^{cre/+}Rosa26^{mTmG/+}$ mice. Scale bars=1 cm. **(E)** H&E

Figure 4.1 (cont'd)
staining of eutopic endometrium and ectopic lesions in the mouse model of endometriosis. Scale bar=100 μm. **(F)** H&E staining of ectopic lesions from the mouse model of endometriosis and women with endometriosis. Scale bar=100 μm. **(G, H)** Fluorescence photomicrographs (G) and average total number (H) of endometriosis lesions in $Pgr^{cre/+}Rosa26^{mTmG/+}$ mice treated with vehicle, E2, and E2+P4 for 1 month (n=8 for vehicle, n=6 for E2, and n=10 for E2+P4 treatment). Arrowheads indicate lesions attached outside of the uterus. Data are represented as mean ± SEM; **, $p<0.01$; ns, $p>0.05$. Scale bar=1 cm.

4.3.2 ARID1A Deficiency Increases Endometriosis Lesion Incidence

To assess the effect of ARID1A deficiency in endometriosis development, we induced endometriosis in control ($Pgr^{cre/+}Rosa26^{mTmG/mTmG}$) and $Pgr^{cre/+}Arid1a^{f/f}Rosa26^{mTmG/mTmG}$ mice. After one month, we found that uterine tissue with *Arid1a* deleted exhibited a significantly increased number of endometriotic lesions compared to controls ($p=0.0132$; Figure 4.2). This finding suggests that ARID1A loss is capable of driving an increase in endometriosis lesion formation.

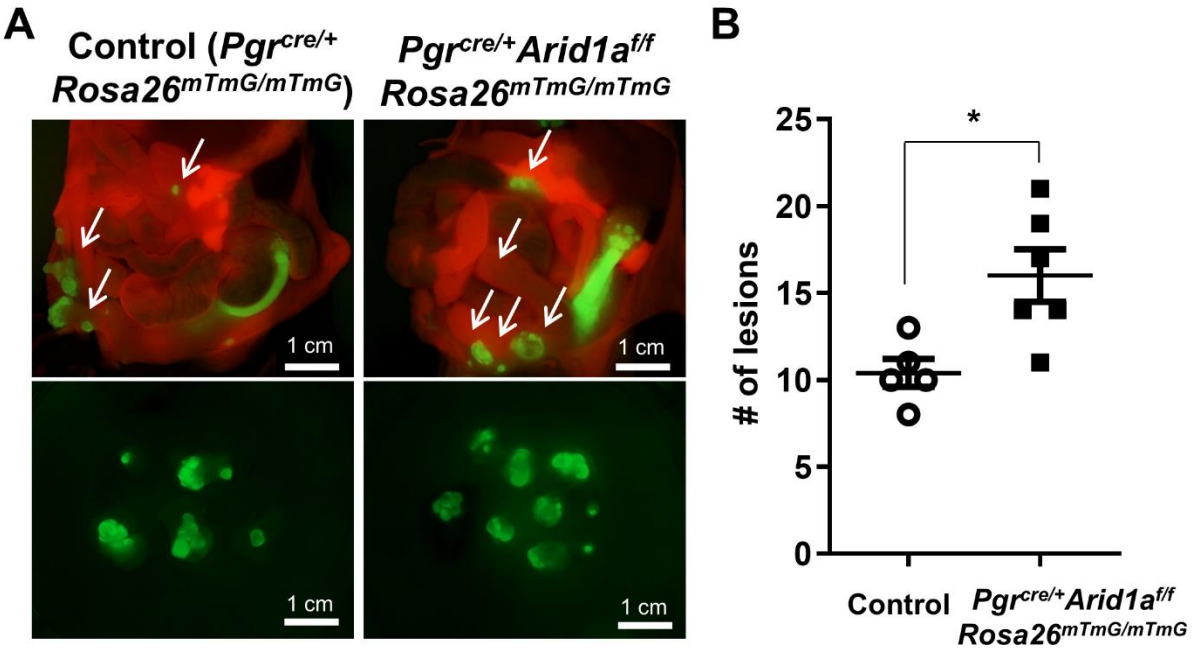

Figure 4.2 *ARID1A deficiency increases endometriosis lesion incidence*. **(A)** Endometriosis was surgically induced in control ($Pgr^{cre/+}Rosa26^{mTmG/mTmG}$) and $Pgr^{cre/+}Arid1a^{f/f}Rosa26^{mTmG/mTmG}$ mice. Endometriotic lesions were visualized by mG (green) expression in control and $Pgr^{cre/+}Arid1a^{f/f}Rosa26^{mTmG/mTmG}$ mice as shown in fluorescence photomicrographs. Arrows indicate lesions attached outside the uterus. Scale bars=1 cm. **(B)** Average total number of

Figure 4.2 (cont'd)
endometriosis lesions in control and *Pgr*$^{cre/+}$*Arid1a*$^{f/f}$*Rosa26*$^{mTmG/mTmG}$ mice (control n=5, *Pgr*$^{cre/+}$*Arid1a*$^{f/f}$*Rosa26*$^{mTmG/mTmG}$ n=6). Data are represented as mean ± SEM; *, p<0.05.

4.3.3 Endometrial ARID1A Attenuation in Mice Induced with Endometriosis

To determine whether endometrial ARID1A expression loss is caused by endometriosis lesion development, we examined ARID1A levels in eutopic endometrium from intact *Pgr*$^{cre/+}$*Rosa26*$^{mTmG/+}$ mice with endometriosis induced by syngeneic tissue transfer from a littermate donor. ARID1A protein expression was significantly reduced in eutopic endometrial stroma (p<0.01, p<0.05) but not epithelium (p=0.589) from the mice with endometriosis compared to controls at both 1 month and 3 months post-induction (Figure 4.3).

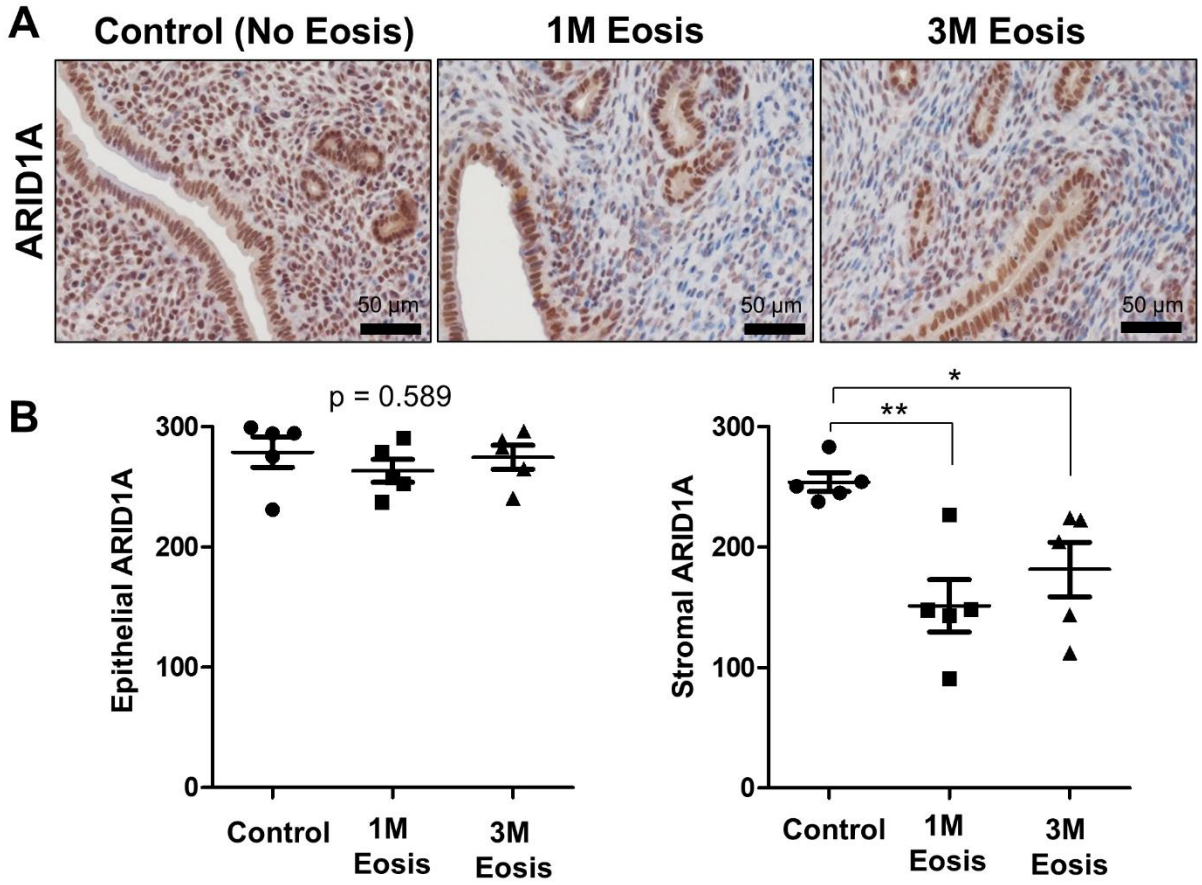

Figure 4.3 *Endometrial ARID1A attenuation in mice induced with endometriosis.* **(A)** Representative photomicrographs of ARID1A immunohistochemical staining in uterine sections from the endometriosis mouse model (n=5/group). Scale bars=50 µm. **(B)** Immunohistochemical

Figure 4.3 (cont'd)
H-score for epithelial (left) and stromal (right) ARID1A staining strength in the sample sets represented in part (A) (n=5/group). Data are represented as mean ± SEM; **, $p<0.01$; *, $p<0.05$.

4.3.4 Defects of Implantation and Decidualization in Mice Induced with Endometriosis

Next, we assessed whether endometriosis in mice causes infertility by assessing implantation and decidualization success (Figure 4.4A). One month after endometriosis induction, the number of implantation sites in mice with endometriosis was not changed compared to the sham group. However, 63.6% (7 out of 11) of mice with endometriosis experienced implantation failure 3 months after endometriosis induction (Figure 4.4B). We found that no significant correlation exists between the number of implantation sites and the number of endometriosis lesions (Figure C.1). We next examined the impact of endometriosis on decidualization using an artificial decidualization model (Finn and Martin 1972). One month after endometriosis induction, mice with endometriosis displayed a uterine horn that responded well to artificial decidualization; however, after 3 month of endometriosis development, the mice with endometriosis exhibited a significant defect in decidual response compared to control and sham mice (Figure 4.4C; $p=0.0001$). Our results suggest that endometriosis development causes implantation failure and a defect of decidualization, as has been hypothesized in humans (Lessey and Kim 2017).

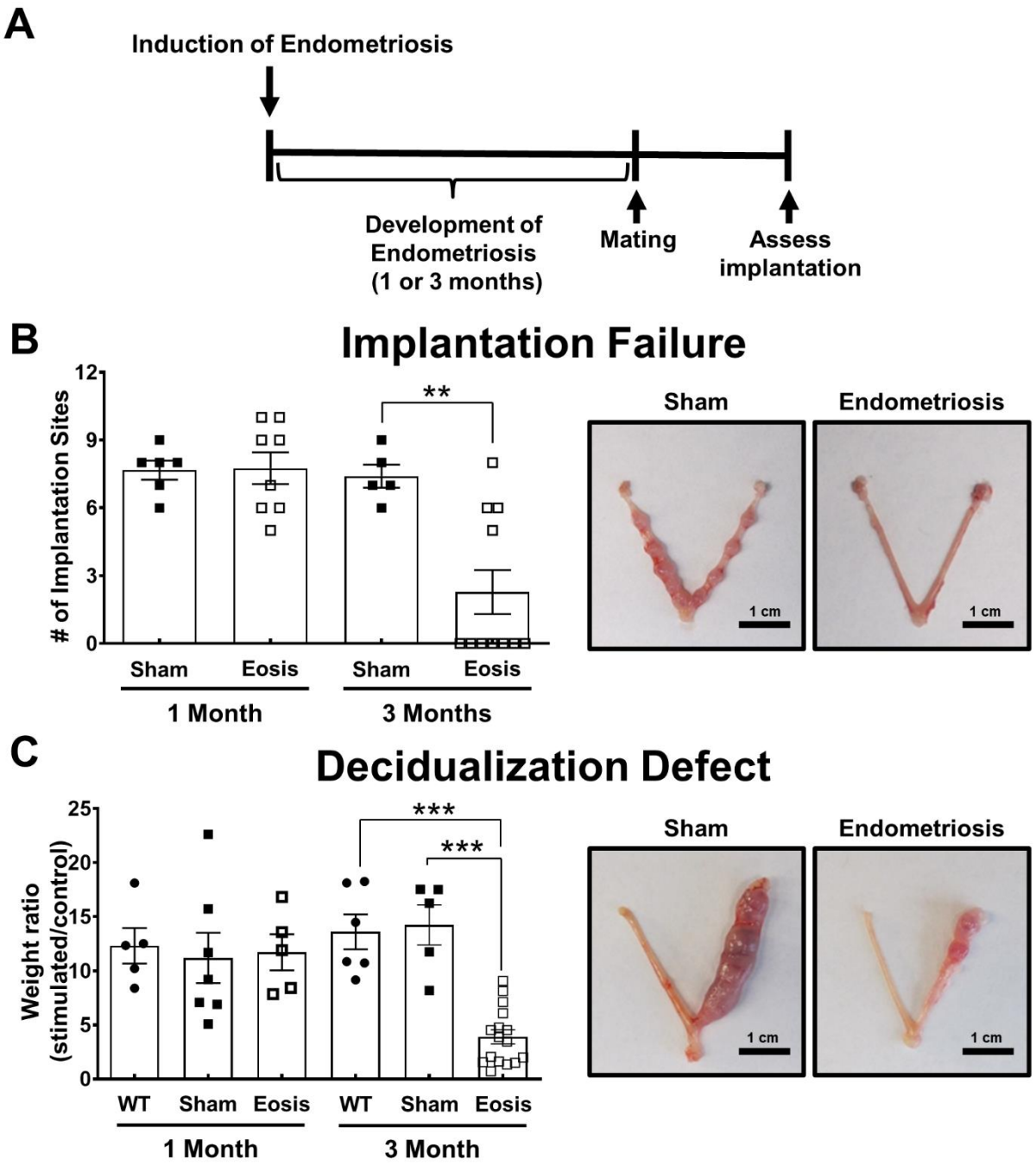

Figure 4.4 *Defects of implantation and decidualization in mice induced with endometriosis*. **(A)** Experimental design to investigate endometriosis-related infertility. **(B)** Average number and uterine images of implantation sites at GD 7.5 in mice with endometriosis (Eosis) at 1 and 3 months after endometriosis induction (n=6 for sham and n=8 for endometriosis at 1 month and n=5 for sham and for n=11 endometriosis at 3 months). Data are represented as mean ± SEM; ** $p<0.01$. Scale bars=1 cm **(C)** Average ratio of stimulated uterine weight to control weight and uterine images of mice with endometriosis after artificially induced decidualization (n=5 for wild type, n=7 for sham, and n = 5 for endometriosis at 1 month and n=6 for wild type, n=5 for sham, and n=16 for endometriosis at 3 months). Data are represented as mean ± SEM; ***, $p<0.001$. Scale bars=1 cm.

4.4 Discussion

Improving fertility rates where they are impacted by uterine disease requires unraveling the molecular mechanisms of implantation. ARID1A is linked to endometriosis-related infertility because it's expression is reduced in the endometrium of infertile women with endometriosis, and deletion of uterine *Arid1a* in mice causes fertility problems due to uterine dysfunction as we saw in Chapter 2 and previous studies (Kim, Yoo, Wang, et al. 2015; Marquardt et al. 2021).

To experimentally explore this linkage, we developed a mouse model of endometriosis based on $Pgr^{cre/+}$ and *mT/mG* reporters that produces endometriotic lesions highly similar to those in humans. A mouse model in which excised human endometrial fragments are introduced into the peritoneum of immunocompromised mice is widely used, but it is limited by lack of a normal immune system, which is thought to be important in endometriosis pathophysiology (Grummer 2006; Giudice and Kao 2004; Bruner-Tran et al. 2018). In contrast, the mouse model of induced endometriosis is a versatile model that has been used to study how the immune system (Lin et al. 2006), hormones (Fang et al. 2004; Fang et al. 2002) and environmental factors (Foster et al. 1997; Cummings, Metcalf, and Birnbaum 1996) affect endometriosis. The availability of a large number of transgenic mice in which specific genes can be either eliminated or overexpressed make this induced endometriosis model ideal for studying specific pathways in development and progression of endometriosis and other diseases (Bruner-Tran et al. 2018). However, current mouse models of endometriosis that involve ovariectomy and E2 treatment are impractical for studies of physiological functions that require natural fluctuations in ovarian steroid hormones, such as fertility. Our mouse model alleviates the need to apply ovariectomy and E2 treatment to enlarge endometriotic lesions because fluorescence reporter genes allow us to clearly visualize endometriotic lesions like those found in humans and quantitatively examine them. Moreover,

similarities between our mouse model and human endometriosis include: 1) development and progression of disease; 2) steroid hormone regulation; 3) fertility defect with implantation failure; and 4) endometrial ARID1A deficiency.

Because fertility cannot be studied in an autologous surgical model of endometriosis due to removal of a uterine horn, we applied a syngeneic mouse model to examine the effect of endometriotic lesions on the eutopic endometrium. Several groups have used syngeneic mouse models of endometriosis in which the uterus of one mouse is removed, minced and injected intraperitoneally into recipient mice (Bruner-Tran et al. 2018). Syngeneic murine models have several potential advantages over the rodent surgical model: 1) peritoneal seeding of uterine fragments is more similar to retrograde menstruation in women; 2) either the donor or recipient animal can receive therapeutic intervention or be otherwise manipulated prior to induction of disease; and 3) a large number of transgenic mice in which specific genes can be either eliminated or overexpressed are available. These advantages make syngeneic murine models ideal for studying the role of specific pathways in development and progression of endometriosis and other diseases.

Our finding that *Arid1a* deletion led to increased endometriosis lesion development is consistent with previous data from our group in a similar mouse model (Kim, Kim, et al. 2021). Additionally, that study reported that deletion of PGR in the uterus led to a similar increase in lesion number (Kim, Kim, et al. 2021). Furthermore, ARID1A and PGR colocalized and directly interacted in both mouse and human endometrium, and their expression levels correlated in endometrial samples from women with endometriosis (Kim, Kim, et al. 2021). Combined with the knowledge that uterine *Arid1a* knockout mice experience disrupted endometrial PGR signaling,

these data suggest that ARID1A loss may lead to increased lesion development and subfertility in our endometriosis mouse model by causing P4 resistance and E2 dominance.

Curiously, endometriosis induction in our mouse model led to attenuation of endometrial stromal ARID1A but not epithelial ARID1A. In women, ARID1A downregulation occurs in both cell types, so the cause for this discrepancy remains unclear. The studies described in Chapter 2 and Chapter 3 explore in detail the endometrial epithelial role of ARID1A, but its activity in the stroma remains elusive. Therefore, the present finding provides a unique opportunity to study the stroma-specific function of ARID1A in the endometrium.

In summary, our findings reveal that attenuation of ARID1A is sufficient to drive increased growth of endometriotic lesions and occurs in endometriosis-effected eutopic endometrium as a result of lesion development. Furthermore, endometrial ARID1A downregulation precedes the onset of endometriosis related implantation and decidualization defects in our mouse model. These findings support the hypothesis that ARID1A loss is both a cause and an effect of endometriosis pathophysiology in a vicious cycle that contributes to endometriosis-related infertility. Further study will be key to understanding the molecular mechanisms by which ARID1A is lost in lesions and how they drive increased lesion incidence, and answering these questions will provide the potential for new treatment strategies for uterine disease.

4.5 Materials and Methods

4.5.1 Human Endometrium Samples

Human endometrial samples were obtained from Michigan State University's Center for Women's Health Research Female Reproductive Tract Biorepository, the University of North Carolina, and the Greenville Hospital System in accordance with the guidelines set by the

Institutional Review Boards of Michigan State University (Grand Rapids, MI), the University of North Carolina (Chapel Hill, NC), and Greenville Health System (Greenville, SC), respectively. Written informed consent was obtained from all participants. The study design and conduct complied with all relevant regulations regarding the use of human study participants and was conducted in accordance with the criteria set by the Declaration of Helsinki. Tubal ligation was a source for normal subjects as it allows us to rule out endometriosis laparoscopically. All patients did not have uterine leiomyoma and adenomyosis. Samples used for histology were fixed in 10% buffered formalin prior to embedding in paraffin wax.

4.5.2 Animals and Tissue Collection

Mice were maintained in a designated animal care facility according to Michigan State University's Institutional Guidelines for the care and use of laboratory animals. All mouse procedures were approved by the Institutional Animal Care and Use Committee of Michigan State University. All housing and breeding were done in a designated animal care facility at Michigan State University with controlled humidity and temperature conditions and a 12 hour light/dark cycle. Access to water and food (Envigo 8640 rodent diet) was ad libitum. Mice utilized for experiments were 8 to 12 weeks old mice from mixed background C57BL/6 and 129P2/OlaHsd strains. No statistical method was used to pre-select the sample size. Animal numbers for each study type were determined by the investigators on the basis of our previous results (Kim et al. 2019; Yoo et al. 2018) with the standard disease models that were used or from pilot studies. For all animal studies, animals were randomly distributed among different conditions by the investigator as the animals did not show any size or appearance differences at the onset of the experiments. No animals were excluded, and the investigator was not blinded to group allocation

during the experiment. *Arid1a* conditional knockout mice were generated by initially crossing $Pgr^{cre/+}$ (Soyal et al. 2005) males with $Arid1a^{f/f}$ (Gao et al. 2008) (generously provided by Dr. Zhong Wang, University of Michigan) females and then selecting $Pgr^{cre/+}Arid1a^{f/f}$ males and $Arid1a^{f/f}$ females from the F2 generation for continuous breeding.

4.5.3 Induction of Endometriosis

Eight-week-old female mice which have conditional double-fluorescent Cre reporter gene ($Pgr^{cre/+}Rosa26^{mTmG/mTmG}$, $Pgr^{cre/+}Arid1a^{f/f}Rosa26^{mTmG/mTmG}$) were injected with 1 μg/mL of E2 per day for three days and had a surgical procedure to induce endometriosis. Under anesthesia, a midline abdominal incision was made to expose the uterus in female mice, and one of uterine horns was ligated and removed. In a Petri dish containing PBS (pH 7.5), the uterine horn was opened longitudinally with scissors. The excised uterine horn was cut into small fragments of about 1 mm^3 and then injected back into the peritoneum of the same mouse. The abdominal incision and wound were closed with sutures and the skin was closed with surgical wound clips. After a designated time, the mice were sacrificed, and endometriosis-like lesions were removed using a fluorescence microscope and counted. Uterine tissues were processed at the time of dissection by fixing with 4% (vol/vol) paraformaldehyde for histology and immunostaining. For the study of steroid hormone regulation, control $Pgr^{cre/+}Rosa26^{mTmG/+}$ mice induced with endometriosis were injected with vehicle (sesame oil; Veh), E2 (0.1 μg/mouse), or E2 plus P4 (1 mg/mouse) for one month before the mice were sacrificed, and endometriosis-like lesions were removed using a fluorescence microscope and counted.

4.5.4 Endometriosis-Related Infertility Analysis

Endometriosis was induced in 8-week-old control female mouse recipients (fertile) receiving endometrial fragments from donor *Pgr*$^{cre/+}$*Rosa26*$^{mTmG/+}$ mice. A sham surgery group was included as a control. Either 1 or 3 months after endometriosis induction, the mice with endometriotic lesions were assessed for implantation and decidualization. Pregnant uterine samples were obtained by mating the mice with fertile breeder male mice, with the morning of a vaginal plug designated as GD 0.5. Mice were sacrificed at GD 7.5. Uterine tissues were immediately processed at the time of dissection by fixing with 4% (vol/vol) paraformaldehyde for histology. To artificially induce decidualization, we mechanically stimulated one horn following hormonal preparation as previously described (Kim, Yoo, Wang, et al. 2015).

4.5.5 Histology and Immunohistochemistry Analysis

Fixed, paraffin-embedded tissues were cut at 5 μm, mounted on slides, deparaffinized, and rehydrated in a graded alcohol series. For H&E staining, slides were sequentially submerged in hematoxylin, 0.25% HCL, 1% lithium carbonate, and eosin, followed by dehydration and mounting. Immunohistochemistry analysis was performed as previously described (Kim, Yoo, Kim, et al. 2015). Briefly, dewaxed hydrated paraffin-embedded tissue sections were pre-incubated with 10% NGS (#S-1000; Vector Laboratories) in PBS and then incubated with an anti-ARID1A primary antibody (SC-98441; Santa Cruz) in PBS supplemented with 10% NGS overnight at 4°C. The sections were then incubated with secondary antibody conjugated to horseradish peroxidase (1:1000 dilution; #43-4324; Invitrogen) for one hour at room temperature. Immunoreactivity was detected using DAB (Vector Laboratories) and analyzed using microscopy software from NIS Elements, Inc. (Nikon). A semi-quantitative grading system (H-score) was

calculated to compare the IHC staining intensities. The H-score was calculated using the following equation: H-score = $\sum$ Pi (i), where i=intensity of staining with a value of 1, 2, or 3 (weak, moderate, or strong, respectively) and Pi is the percentage of stained cells for each intensity, varying from 0 to 100%. The overall score ranged from 0 to 300 (Ishibashi et al. 2003). For fluorescence imaging of tissue sections, frozen, OCT-embedded tissue samples were cut at 10 µM and mounted on slides before coverslipping for imaging.

4.5.6 Statistical Analysis

No statistical method was used to predetermine sample size for in vivo studies. Based on prior experience, experiments normally used five mice per group to achieve adequate statistical power. For all animal experiments, block randomization was used to ensure a balance in sample size across groups. For all animal experiments, over three biological replicates were analyzed for each condition, and results are presented as the mean ± SEM. For data with only two groups, two-tailed unpaired t-test was used. For data containing more than two groups, an ordinary one-way ANOVA test was used, followed by Tukey test for pairwise t-test. $p<0.05$ was considered statistically significant. All statistical analyses were performed using Prism version 9.2.0 or InStat 3 from GraphPad.

4.6 Data Availability

The data that support the findings of this study are available within the chapter and Appendix C.

4.7 Acknowledgments

This work was supported by the National Research Foundation of Korea grant funded by the Korean Government (MIST) (No. 2018R1A5A2025079 to H.-G.Y.), and SRI and Bayer Discovery/Innovation Grant (to T.H.K.), as well as by the Eunice Kennedy Shriver National Institute of Child Health & Human Development of the National Institutes of Health under Award Numbers R01HD084478 and R01HD101243 (to J.W.J) and F31HD101207 and T32HD087166 (to R.M.M.). The content is solely the responsibility of the authors and does not necessarily represent the official views of the National Institutes of Health.

CHAPTER 5

A MOUSE MODEL OF ENDOMETRIOSIS WITH NANOPARTICLE LABELING FOR IN VIVO PHOTOACOUSTIC IMAGING

This chapter is not published at the time of dissertation submission. The following study is in collaboration with Md Nafiujjaman, Seock-Jin Chung, Kay Hadrick, and Taeho Kim at the Department of Biomedical Engineering in the Michigan State University College of Engineering and Tae Hoon Kim and Jae-Wook Jeong at the Department of Obstetrics, Gynecology & Reproductive Biology in the Michigan State University College of Human Medicine.

5.1 Abstract

Endometriosis is a condition of the female reproductive tract characterized by endometrium-like tissue growing outside the uterus. Though it is a common cause of pelvic pain and infertility, there is currently no reliable noninvasive method to diagnose the presence of endometriosis without surgery, and the pathophysiological mechanisms that lead to the occurrence of symptoms require further inquiry. Due to patient heterogeneity and delayed diagnosis, animal models are commonly used to study the development of endometriosis, but these are costly due to the large number of animals needed to test various treatments and experimental conditions at multiple endpoints. Here, we describe a method for synthesis of multimodal imaging gold-fluorescein isothiocyanate (FITC) nanoparticles with preclinical application via induction of nanoparticle-labeled endometriosis-like lesions in mice. Labeling donor endometrial tissue fragments with gold-FITC nanoparticles prior to induction of endometriosis in recipients enables in vivo detection of the gold-labeled lesions with photoacoustic imaging. The same imaging method can be used to visualize embryos noninvasively in pregnant mice. Furthermore, the

conjugated FITC dye on the gold nanoparticles allows easy isolation of labeled lesion tissue under a fluorescence dissection microscope. After dissection, the presence of gold-FITC nanoparticles and endometrium-like histology of lesions can be verified through fluorescence imaging, gold enhancement, and immunostaining. This method for in vivo imaging of endometriosis-like lesions and fluorescence-guided dissection will permit new experimental possibilities for the longitudinal study of endometriosis development and progression as well as endometriosis-related infertility.

5.2 Introduction

Endometriosis affects an estimated 1-in-10 women of reproductive age, equating to 176 million globally, but estimated delays from symptom onset to diagnosis range from 4 to 11 years (Adamson, Kennedy, and Hummelshoj 2010; Agarwal et al. 2019; Zondervan et al. 2018). With regard to pathophysiology, endometriosis is a condition of the female reproductive tract where non-malignant lesions composed of endometrium-like glands and stroma take root and grow outside the uterus, frequently leading to chronic pelvic pain and fertility problems (Zondervan et al. 2018). Definitive diagnosis requires invasive laparoscopic visualization of lesions because no clinically reliable biomarkers are available, and only limited subtypes of endometriosis such as ovarian endometrioma or deep infiltrating endometriosis can be detected using noninvasive ultrasonography or magnetic resonance imaging (Zondervan et al. 2018; Saunders and Horne 2021; Guerriero et al. 2013). This lack of noninvasive diagnostic tools combined with heterogeneity in symptoms and lesion location among patients contributes to the marked delays in diagnosis and treatment (Agarwal et al. 2019). Furthermore, the delay in diagnosis makes it difficult to directly study the early stages of endometriosis development and discern how it leads to infertility and pain in patients.

To mechanistically study endometriosis development and the relationship between lesion presence and symptoms, several animal models have been developed utilizing rodents and non-human primates (Sharpe-Timms and Stilley 2020). Mice, in particular, are attractive as an accessible and cost-effective species for modeling endometriosis due to their small size, rapid breeding, and receptivity to genetic manipulation (Saunders 2020). A variety of approaches have been used to induce endometriosis-like lesions in mice that involve either heterologous transfer of human endometrial tissue to immunocompromised mice (Martinez et al. 2019; Tamura et al. 2015) or homologous murine uterine tissue transfer. Such homologous models have used autologous (Kim, Kim, et al. 2021; Kim, Yu, et al. 2014) or syngeneic (Kim et al. 2019; Ferrero et al. 2017; Dorning et al. 2021) transfer of either sutured (Bilotas et al. 2015; Mishra et al. 2020; Rosa et al. 2019) or injected (Fattori et al. 2020) uterine tissue. Some models utilize inductions performed after ovariectomy with exogenous hormone treatment to prepare the tissue (Greaves, Cousins, et al. 2014), whereas some use intact, untreated mice (Richards et al. 2020). Each method comes with unique benefits and limitations with regard to mimicking human endometriosis etiology and histology, identification of lesions, and maintenance of a functionally intact reproductive system (Simitsidellis, Gibson, and Saunders 2018).

Several past studies utilizing endometriosis mouse models have incorporated reporter systems for detection of endometriosis lesions. For example, genetically encoded fluorescence or bioluminescence reporters (Becker et al. 2006; Dorning et al. 2021; Kim, Young, et al. 2021) and ex vivo adenoviral vector-mediated fluorescent labeling (Ferrero et al. 2017; Martinez et al. 2019) have been successfully applied for in vivo imaging or post-mortem endometriosis lesion analysis. However, conventional optical imaging suffers from low imaging depth, thus limiting whole tomographic imaging in preclinical studies (Ntziachristos 2010). Therefore, the majority of these

studies resort to mouse models that place the lesions subcutaneously or just beneath the peritoneal wall, except the work of Dorning et al., which achieved bioluminescent imaging in intraperitoneal injection models of endometriosis (Ntziachristos 2010; Dorning et al. 2021).

Photoacoustic (PA) imaging is an emerging imaging tool to noninvasively detect and longitudinally track the targeted cells or tissues in vivo (Kim et al. 2017). In contrast to conventional optical imaging, PA imaging can substantially increase the signal penetration depth based on the 'light in/sound out' approach (Zackrisson, van de Ven, and Gambhir 2014). In PA imaging, the signals are generated by the ultrasonic pressure waves, which are emitted by the thermoelastic expansion under near-infrared (NIR) light illumination (680-980 nm) (Wang and Hu 2012; Wang 2009). Since ultrasonic waves propagate much farther through the tissue than light, PA imaging can achieve deeper tissue penetration for imaging (up to several centimeters). As a hybrid imaging technique, PA imaging offers excellent temporal (100 ms) and spatial (50-150 μm) resolution with concurrent anatomical data from B-mode ultrasound imaging (Kim et al. 2017). The ultrasound imaging component in the tool can also be used to analyze pregnancy, fetal gestational staging, and functional changes during pregnancy development (Bayer et al. 2017; Basak et al. 2019).

Since PA imaging is a multi-spectral imaging technique, this tool can facilitate the imaging of target-specific signals via exogenous nanoparticle contrast agents alongside mapping with endogenous chromophores such as hemoglobin (Shvedova et al. 2015). The quantification of total hemoglobin can allow imaging for angiogenic endometriosis lesion vasculature (Rocha, Reis, and Taylor 2013), and the addition of an exogenous contrast agent is beneficial to attain sensitive target-specific signals. Ideal photoacoustic contrast agents can be made with NIR light (680–980 nm) absorbing compounds, including small-molecule dye (e.g., indocyanine green, methylene

blue), metallic nanoparticles (e.g., gold nanorods, carbon nanotubes), or organic nanostructures (porphyrin). The contrast agents can efficiently convert the irradiated light energy to heat in PA imaging to produce intense PA signals for detection (Weber, Beard, and Bohndiek 2016). Among them, gold nanorods are the most available exogenous imaging agent because they feature strong NIR light absorption (high molar extinction coefficient), inert nature, biocompatibility, and in vivo stability (Kim, Zhang, et al. 2018). In addition, silica-coated gold nanorods have been reported to amplify the labelling efficacy to achieve sufficient particle loading in the targeted tissues (Jokerst, Thangaraj, et al. 2012; Chen et al. 2011). Therefore, gold nanoparticles have been extensively used for PA molecular imaging of cells (Jokerst, Thangaraj, et al. 2012), proteins (Zhang and Kang 2011), and tumor tissues (Jokerst, Cole, et al. 2012).

In this work, we utilized gold nanoparticles conjugated with a FITC dye as a contrast agent with sensitive PA signal to discriminate the endometriosis lesion-specific signals from endogenous tissues in mice. The multimodal imaging nanoparticles incorporating a fluorescent FITC dye on the particle surface were designed to be used dually for in vivo PA imaging and for fluorescence-guided tissue isolation by fluorescence dissection microscope. Upon ex vivo labelling of donor uterine tissue with the nanoparticles followed by transfer to the recipient mice, we monitored the distribution and retention of the labelled tissue by PA imaging. Furthermore, we optimized the treated particle dosages without inducing toxicity or perturbing the functionality of labelled endometriosis-like lesion tissues. Finally, we validated their utility for in vivo detection and fluorescence-guided dissection with histological confirmation.

5.3 Results

5.3.1 Gold Nanoparticle Synthesis

To generate an exogenous contrast agent suitable for distinguishing labeled tissue via PA imaging, we colloidally synthesized gold nanorods using seed-mediated growth methods by employing surfactants as directing agents (Nikoobakht and El-Sayed 2003). We then coated the particles with silica shells via the silica sol-gel process and attached them with a distal fluorescein tag (FITC) using simple silane chemistry (Jokerst, Thangaraj, et al. 2012). Transmission electron microscopy (TEM) showed the distinctive rod structure of gold particles (width: 12−14 nm, length: 50−55 nm), and the silica shells were distinctively detected on the surface of the gold nanorods (Figure 5.1A). The UV−vis absorption spectrum of the nanoparticles showed a maximal absorbance peak at 780 nm with a broad and intense absorption in NIR, generating strong PA signals (Figure 5.1B). The fluorescent FITC dye attached to the particles was detected by the fluorescent mode in microplate readers (excitation wavelength: 460 nm, emission wavelength: 516 nm), and the gold-FITC particles exhibited the typical emissions of fluorescein at 516 nm under UV excitation (Figure 5.1C, D).

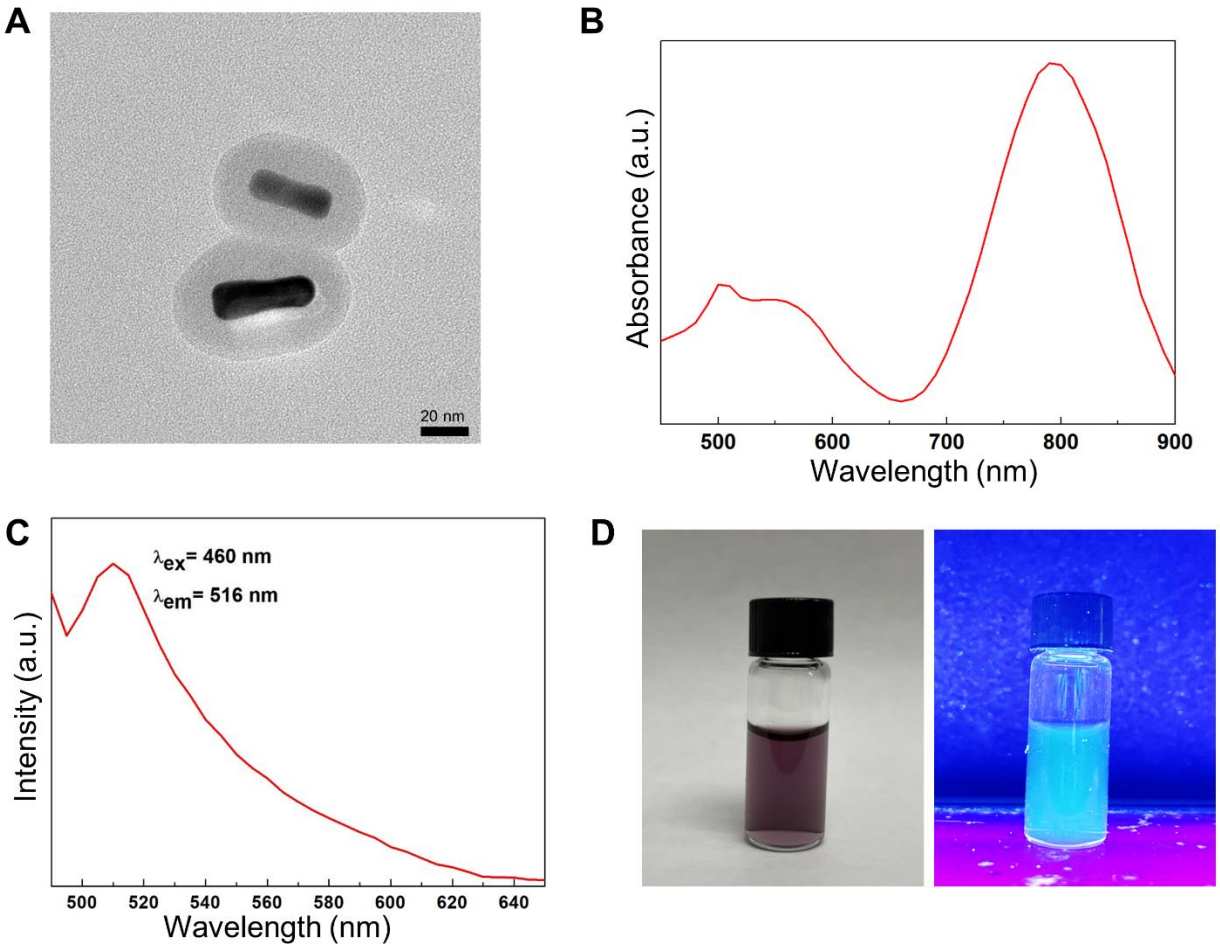

Figure 5.1 *Physical characterization of gold-FITC nanoparticles (FITC dye attached silica-coated gold nanorods).* **(A)** TEM images of gold-FITC nanoparticles. Uniform and discrete gold nanorods (13 × 52 nm) were synthesized and successfully coated with silica shells. The overall size and morphology of particles were maintained after FITC dye attachment. Scale bar = 20 nm. **(B)** UV−visible spectra of gold-FITC nanoparticles dispersed in deionized water (1 mg/mL). The maximal absorbance peak is at 780 nm, and the particle can emit strong PA signals under near-infrared (NIR) laser light illumination. **(C)** Photoluminescence spectra of gold-FITC nanoparticles (λ_{ex}=460 nm). The FITC dye attachment was successfully characterized by PL spectrum. **(D)** Fluorescence emission of the gold-FITC nanoparticles dispersed in water under UV light.

5.3.2 Optimization of Uterine Tissue Labeling

In order to determine optimal gold-FITC nanoparticle tissue labeling conditions for use in a mouse model of endometriosis based on syngeneic uterine tissue transfer, we tested various incubation times and concentrations with uterine tissue fragments. Tissue donor mice were treated with E2 for 3 days to synchronize the hormonal state of the uterine tissue. Beginning with a

nanoparticle solution of approximately 300 µg Au/mL and 15 µg FITC/mL, we made a 20% dilution of the nanoparticles in supplemented tissue media and incubated tissue fragments for one hour, two hours, or three hours. Tissues were washed three times before imaging to clear unattached particles. Gross visualization of tissue fragments under fluorescence microscopy and independent fluorescence quantitation showed significantly increasing fluorescent intensity with increasing incubation time (Figure 5.2A, B). Examination of tissue sections by fluorescence microscopy revealed that FITC signal was located at the exterior border of tissue fragments (Figure 5.2C). Furthermore, a gold enhancement assay confirmed that gold molecules were also located at the exterior border of tissue fragments, matching the location of FITC signal (Figure 5.2D). Due to concerns about tissue viability, we did not extend the incubation longer than 3 hours and proceeded with this condition to further experiments.

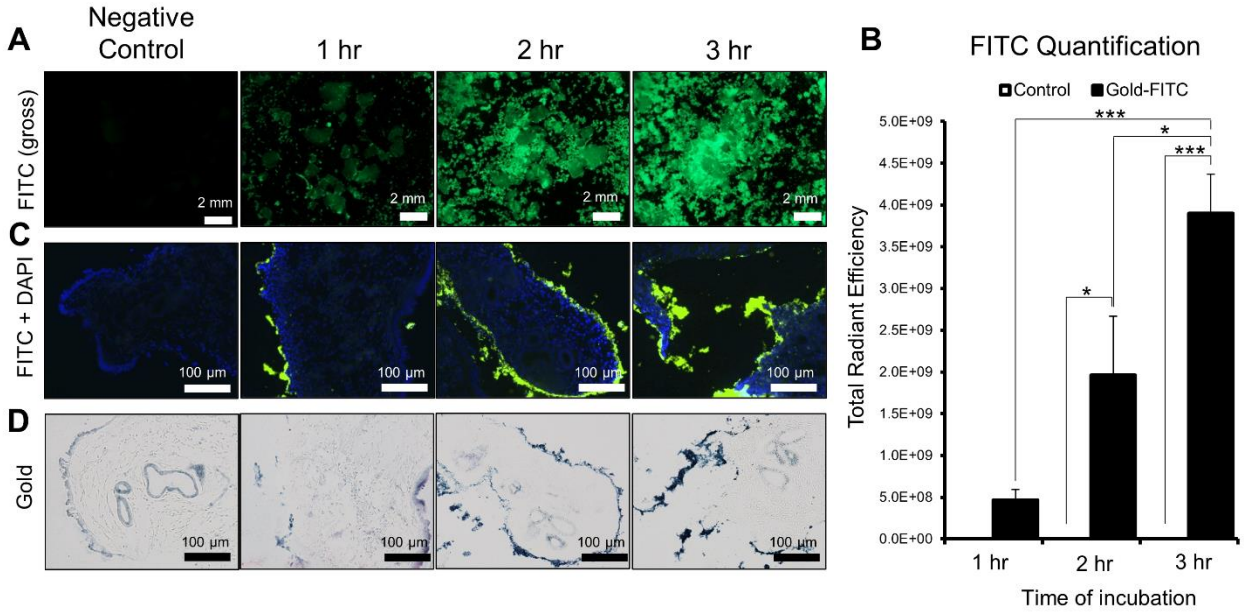

Figure 5.2 *Incubation time-dependence of uterine tissue labeling*. **(A)** Representative images of gross fluorescence imaging of chopped uterine tissue incubated with gold-FITC nanoparticle diluted to 20% in tissue media for 1 hour, 2 hours, or 3 hours. Scale bar = 2 mm. **(B)** Quantification of total FITC fluorescent intensity from chopped, labeled tissue as shown in (A) and measured by IVIS. The graphs represent the mean ± SEM (n=3; *, $p<0.05$, ***, $p<0.001$). **(C)** Representative fluorescence images of nanoparticle-labeled tissue sections from (A) showing localization of gold-FITC nanoparticles (green) and counterstained with DAPI (blue). Scale bar = 100 µm. **(D)**

Figure 5.2 (cont'd)
Representative images of gold enhancement performed on nanoparticle-labeled tissue sections from (A) showing localization of gold-FITC nanoparticles (black). Scale bars = 100 µm.

To determine the dependence of successful tissue labeling on nanoparticle concentration, we performed a dose-comparison with 0%, 5%, 10%, 20%, and 40% of nanoparticles in media for the three-hour incubation period with uterine tissue fragments. Fluorescence microscopy and quantitation of fluorescent intensity demonstrated the dose-dependency of nanoparticle tissue labeling (Figure 5.3A, B). Histological examination again showed that both fluorescent dye and gold particles were located on the outside edge of the tissue fragments (Figure 5.3C, D). We determined the labeling coverage to be sufficient at a 20% dilution (60 µg Au/mL, 3 µg FITC/mL) for use in further experiments.

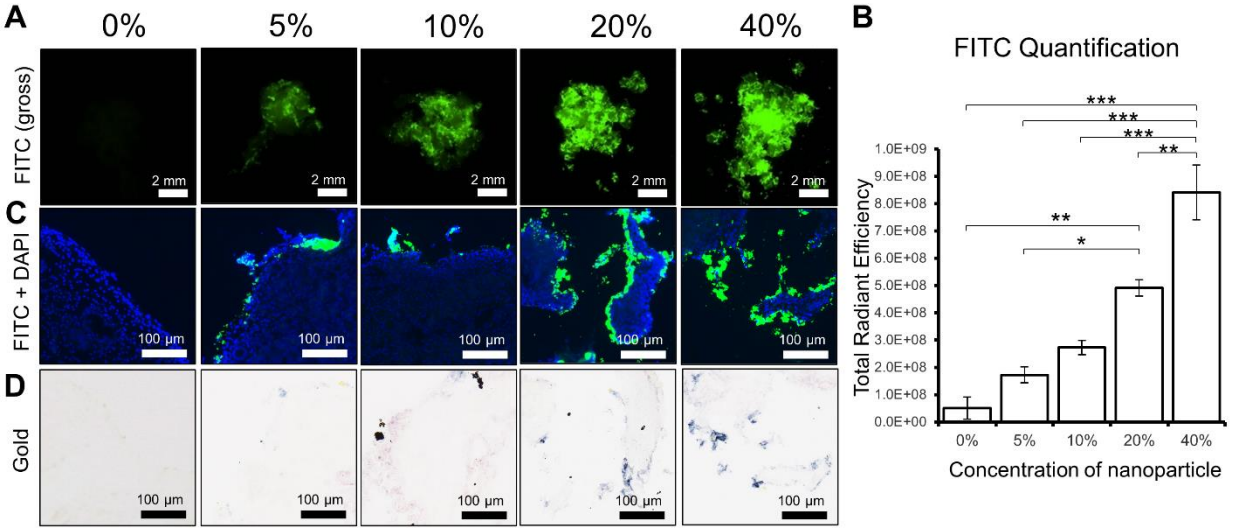

Figure 5.3 *Nanoparticle concentration-dependence of uterine tissue labeling*. **(A)** Representative images of gross fluorescence imaging of chopped uterine tissue incubated with gold-FITC nanoparticle diluted to 0% (negative control), 5%, 10%, 20%, or 40% in tissue media for 3 hours. Scale bar = 2 mm. **(B)** Quantification of total FITC fluorescent intensity from chopped, labeled tissue as shown in (A) and measured by IVIS. The graphs represent the mean ± SEM (n=3; *, $p<0.05$, **, $p<0.01$, ***, $p<0.001$). **(C)** Representative fluorescence images of nanoparticle-labeled tissue sections from (A) showing localization of gold-FITC nanoparticles (green) and counterstained with DAPI (blue). Scale bar = 100 µm. **(D)** Representative images of gold enhancement performed on nanoparticle-labeled tissue sections from (A) showing localization of gold-FITC nanoparticles (black). Scale bar = 100 µm.

5.3.3 In Vivo Imaging of Endometriosis-Like Lesions and Pregnancy Development

To monitor the establishment of endometriosis-like lesions in mice in vivo, we induced endometriosis in intact, untreated wild-type mice using syngeneic uterine tissue transfer after ex vivo incubation with gold-FITC nanoparticles in media or with vehicle (media only) according to the previously determined conditions (Figure 5.4). After allowing time for endometriosis lesion establishment in the recipient mice (4 weeks), we performed noninvasive, full-body photoacoustic (PA) imaging followed by fluorescence-guided lesion isolation.

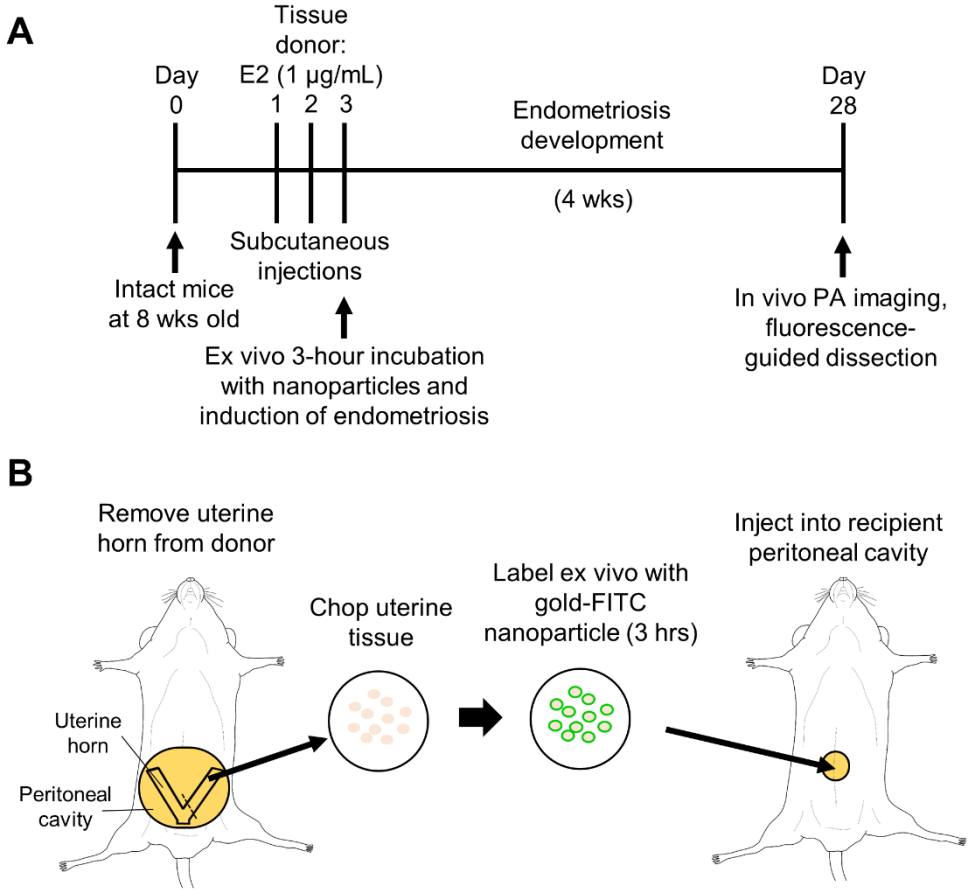

Figure 5.4 *Induction of endometriosis with nanoparticle-labeled uterine tissue*. **(A)** Schematic diagram showing the experimental design and conditions for endometriosis induction in mice with gold-FITC nanoparticle-labeled uterine tissue and for data collection. **(B)** Diagram illustrating the surgical procedure for endometriosis induction in mice with gold-FITC nanoparticle labeled uterine tissue.

In mice induced with gold-FITC nanoparticle-labeled endometriosis lesions, regions outlined in gold signal (yellow) were detected colocalized with oxyhemoglobin (HbO_2; red) and deoxyhemoglobin (Hb; blue) signal, but similar areas were not seen in controls by PA imaging with concurrent ultrasound (Figure 5.5A). This observation indicates an anatomically distinct area of gold nanoparticle-labeled tissue with increased blood supply as would be expected in endometriosis-like lesions (Moses et al. 2020; Moses et al. 2021). Nanoparticle labeling enabled the PA detection of endometriosis lesion-specific signals, where we detected the statistically significant increase of the gold signals in the region of labeled tissue compared to unlabeled control tissues (P=0.0004; Figure 5.5B). In contrast, the presence of the nanoparticle did not significantly affect local oxygen saturation (SO_2), a ratio of oxyhemoglobin to total Hb (p=0.9538; Figure D.1). Upon dissection, FITC-positive endometriosis-like lesions were clearly visible in the peritoneal cavity of mice induced with gold-FITC nanoparticle-labeled lesions but not in controls (Figure 5.5C).

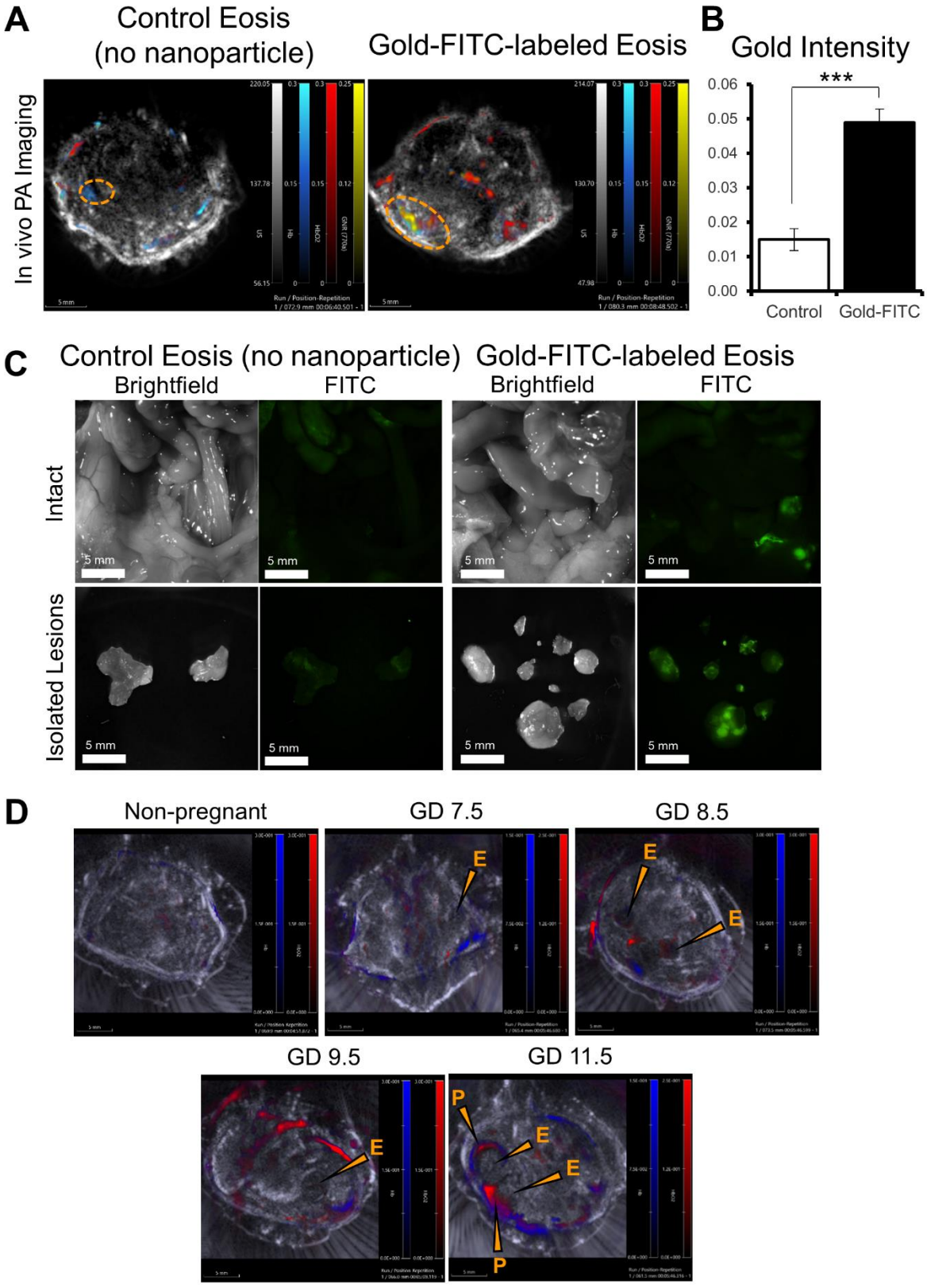

Figure 5.5 *In vivo imaging of endometriosis-like lesions and pregnancy development*. **(A)** Representative in vivo photoacoustic (PA) images from control endometriosis mice (no

Figure 5.5 (cont'd)
nanoparticle; left) and mice with gold-FITC nanoparticle-labeled lesions (right) showing PA signal detection for gold (yellow), Hb (blue), and HbO_2 (red) four weeks after induction. The orange segmented circle (left panel) indicates a region containing an unlabeled lesion identified after dissection. The orange segmented circle (right panel) indicates lesion identified by PA signal and confirmed by dissection. Scale bar = 5 mm. **(B)** Mean intensities of gold PA signals from each group. We plotted gold PA signals from ROIs drawn around the endometriosis-like lesions of at least three mice. The graphs represent the mean ± SEM (control n=4, gold-FITC nanoparticle n=3; ***, $p<0.001$). PA signals were co-registered with mouse anatomy by B-mode ultrasound (grey). **(C)** Brightfield (left) and FITC fluorescent (right) images taken of control endometriosis mice (no nanoparticle) and mice with gold-FITC nanoparticle-labeled lesions after opening the peritoneal cavity (top) and then dissecting lesions (bottom) four weeks after induction. Strong green fluorescence indicates the presence of gold-FITC nanoparticles. Scale bar = 5 mm. **(D)** Noninvasive PA imaging of murine pregnancy to image in real-time the placental and fetal development. Representative images from in vivo PA imaging of non-pregnant and gestation day (GD) 7.5-11.5 wild-type mice. Identification of embryo and placental regions (indicated by arrowheads; E = embryo, P = placenta) was based on PA signal detection of Hb (blue) and HbO_2 (red) combined with ultrasound-derived anatomical structures (grey). Scale bar = 5 mm.

In addition to the visualization of nanoparticle-labeled endometriosis-like lesions, PA imaging combined with ultrasound imaging can also be used to detect implanted embryos and associated functional changes (e.g., vasculature, placental oxygenation) at various stages of pregnancy development (Bayer et al. 2017; Basak et al. 2019). Using the same noninvasive PA imaging platform as applied for the detection of endometriosis lesions, we detected the presence of embryos as early as GD 7.5 and on subsequent days of pregnancy based on ultrasound-derived anatomical structures (grey) and hemoglobin photoacoustic signals (Figure 5.5D; oxyhemoglobin, red; deoxyhemoglobin, blue). This method allows longitudinal study of pregnancy progression that is amenable to combination with monitoring of nanoparticle-labeled endometriosis lesions.

5.3.4 Histological Analysis of Endometriosis-Like Lesions

Bona fide endometriosis lesion tissue contains endometrial epithelial glands and stroma (Zondervan et al. 2018). To assess the histology of FITC-positive endometriosis lesions isolated

from endometriosis model mice, we performed immunostaining for E-cadherin and vimentin on tissue sections. E-cadherin-positive gland-like structures surrounded by vimentin-positive stromal cells with similar structures and staining strength to the eutopic endometrium were observed, confirming endometriosis-like tissue identity (Figure 5.6A, B). Furthermore, we performed fluorescence imaging and gold enhancement on tissue sections from the endometriosis-like lesions and detected the presence of both FITC signal and gold particles in the lesions labeled with gold-FITC nanoparticles (Figure 5.6C, D).

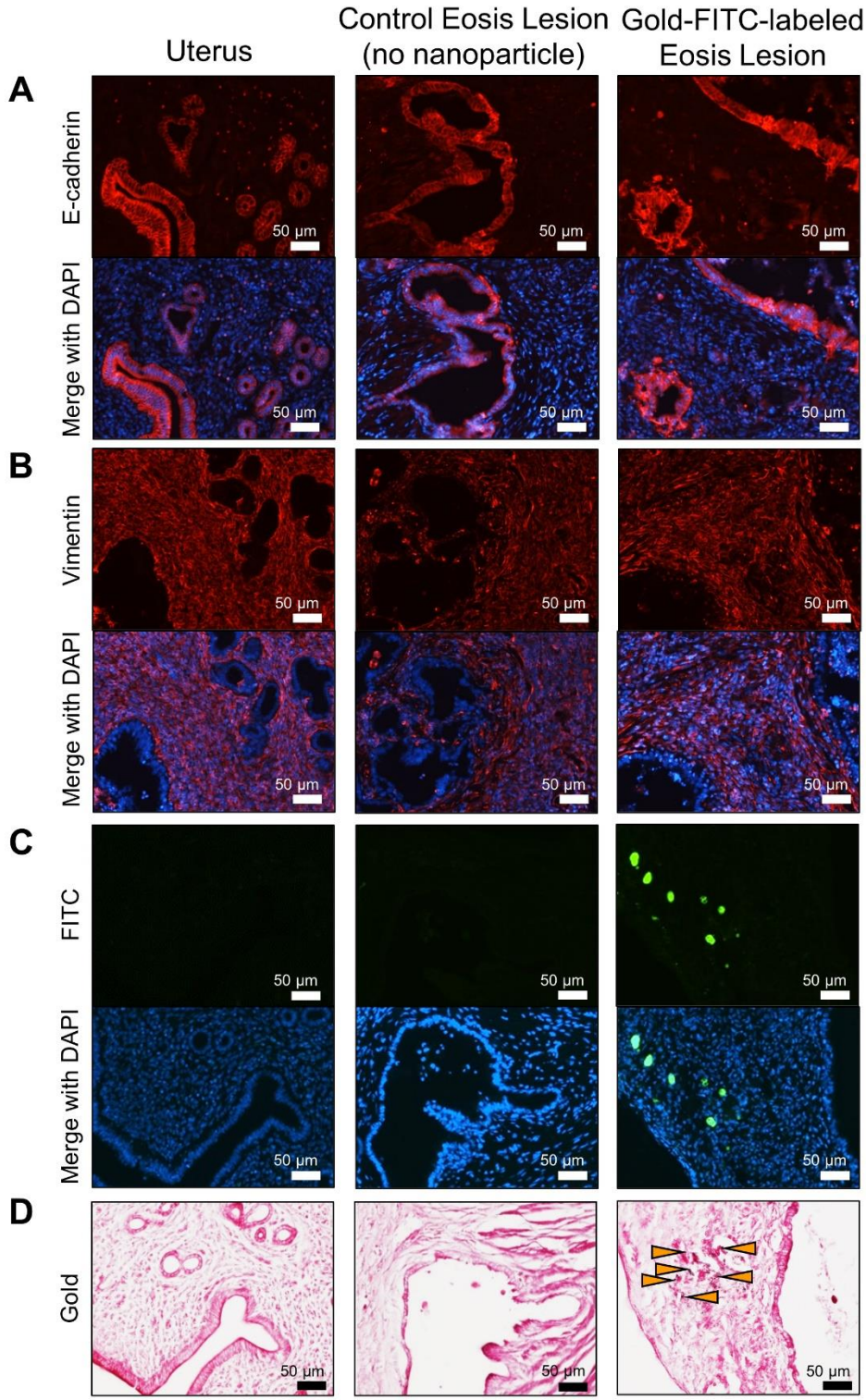

Figure 5.6 *Histological characterization of endometriosis-like lesions*. **(A)** Representative images showing immunofluorescence staining of E-cadherin (Texas Red) counterstained with DAPI (blue) demonstrating the presence of gland-like epithelial structures in control and gold-FITC nanoparticle-labeled endometriosis-like lesions that are similar to those in the wildtype uterus. Samples were collected four weeks after endometriosis induction. **(B)** Representative images

Figure 5.6 (cont'd)
showing immunofluorescence staining of vimentin (Texas Red) counterstained with DAPI (blue) demonstrating the presence of vimentin-negative gland-like epithelial structures and surrounding vimentin-positive stromal cells in control and gold-FITC nanoparticle-labeled endometriosis-like lesions that are similar to those in the wildtype uterus. Samples were collected four weeks after endometriosis induction. **(C)** Representative fluorescence images from tissue sections of wildtype uterus, control endometriosis-like lesions (no nanoparticle), and gold-FITC nanoparticle-labeled endometriosis-like lesions showing the localization of gold-FITC nanoparticles (green) in the interior of the lesion tissue. Counterstained with DAPI (blue). Samples were collected four weeks after endometriosis induction. **(D)** Representative images of gold enhancement performed on tissue sections of wildtype uterus, control endometriosis-like lesions (no nanoparticle), and gold-FITC nanoparticle-labeled endometriosis-like lesions from (A) showing localization of gold-FITC nanoparticles (black; indicated by arrowheads). Scale bars = 50 μm.

5.4 Discussion

Preclinical animal models are essential tools for gaining a mechanistic understanding of endometriosis development and its relationship to infertility and pain. They also enable preclinical proof of concept studies for future clinical diagnostics and treatment options. A wide variety of mouse models of endometriosis have been used for this purpose, but many of these have been limited by a lack of close similarity to human endometriosis pathophysiology and a need to use large numbers of mice to collect endpoint data without a way to monitor endometriosis development over time (Grummer 2006). Here, we present a reproductively intact mouse model of endometriosis based on syngeneic transfer of uterine tissue tagged with gold nanoparticles conjugated to FITC dye and amenable to noninvasive detection.

The benefits of this model are at least six-fold. First, the primary advance made by our model for endometriosis research is the novel application of PA imaging with an exogenous contrast agent for in vivo imaging of internally located endometriosis-like lesions in mice with the added benefit of pregnancy monitoring via endogenous PA signals and B-mode ultrasound. To our knowledge, this is the first reported endometriosis mouse model for in vivo imaging of lesions located deep in the peritoneal cavity that is not based on optical imaging, which is limited by

penetration depth and lacks anatomical information. Photoacoustic, high-resolution ultrasound, and magnetic resonance imaging have each been applied to endometriosis mouse models previously, but these models involved suturing the donor endometrial tissue close to the surface of the animal, either subcutaneously or to the peritoneal wall (Ding et al. 2015; Laschke et al. 2010; Korbel, Menger, and Laschke 2010; Hsu et al. 2020; Chang et al. 2020; Schreinemacher et al. 2012; Silveira et al. 2013). Our model incorporates both endogenous PA signals (e.g., hemoglobin) and an exogenous contrast agent to locate endometriosis-like lesion tissue anywhere within the peritoneal cavity and also visualize developing embryos in the case of pregnant mice. The PA signals are combined with ultrasound imaging to provide concurrent anatomical data.

Second, our exogenous gold nanoparticle contrast agent is conjugated to a FITC fluorescent dye, which enables identification of labeled tissues in multiple-length scales by fluorescent imaging (macroscopic/microscopic) in addition to PA imaging (macroscopic). This property is useful for fluorescence-guided dissection and isolation of lesions at the experiment endpoint as well as locating the nanoparticles in the tissue via histological analysis.

Third, our use of an inert, biocompatible exogenous nanoparticle contrast agent rather than a genetically incorporated reporter alleviates the need for the time-consuming establishment of new genetically modified mouse lines. Rather, our system can be applied to any wild-type or genetically modified mouse of interest. Still, combining the current model for PA imaging with bioluminescence would be beneficial to track the viability of implanted tissues, which is a limitation of nanoparticle imaging markers.

Fourth, our model is applied to recipient mice without surgical or hormonal disruption of reproductive function. Since suboptimal fertility is one of the major dysfunctions associated with endometriosis, the ability to study the effects of endometriosis and potential therapies on an intact

reproductive tract is crucial. Additionally, chronic E2 treatment in other endometriosis models frequently produces cystic lesions that do not represent the typical endometriosis lesion histology in women (Cummings and Metcalf 1995; Han et al. 2012).

Fifth, our model is based on the injection of finely chopped uterine tissue into the peritoneal cavity of the recipient mouse rather than suturing larger pieces of tissue. This injection method more closely mirrors the mechanism of human endometriosis etiology that is most commonly accepted, retrograde menstruation, where menstrual endometrial tissue flows backward into the peritoneal cavity via the fallopian tubes (Zondervan et al. 2018).

Sixth, our model is simple to employ. There is no need for major survival surgery in the recipient that would require a great degree of surgical skill, and there is only a simple three-day intraperitoneal E2 injection required to prepare the donor mouse rather than a lengthy and complicated hormonal regimen. These strengths highlight the utility of our new model as a tool for the field.

In addition to the many benefits of our model, there are also important limitations to consider. Of course, synthesis of the gold-FITC nanoparticles as a contrast agent is required since they are not commercially available at this time. PA imaging systems are also currently less accessible than optical imagers, but this may change with the increased adoption of PA imaging methods in various fields of study (Steinberg et al. 2019). Furthermore, an inert exogenous label like our gold-FITC nanoparticle will dissipate over time in living tissue as cells divide, die, and are recycled. This leads to diminished signal intensity, the possibility of off-target signals, and the inability to determine tissue viability based on signal presence or intensity. Moreover, though signal penetration for PA imaging is greatly improved over optical imaging, imaging depth could limit the application of this system in larger animals and in the clinic.

There are several exciting potential applications of the model we present in this work with regard to preclinical animal experiments and future clinical studies. We view this model as an excellent candidate for the longitudinal study of the effects of endometriosis lesion number, size, and location on fertility outcomes. It also has potential as a method for drug candidate screening as it allows imaging lesion number and size before, during, and after treatment. Combined longitudinal in vivo data regarding fertility outcomes and lesion response to drug treatments would also be possible. Furthermore, we see no reason our nanoparticle-based imaging method could not also be applied to other endometriosis mouse models to compare treatment efficacy in multiple models and increase the rigor and reproducibility of preclinical findings. Additionally, past studies have shown the feasibility of in vivo imaging using intravenously injectable contrast agents that preferentially home to endometriosis lesions based on locally increased angiogenesis (Moses et al. 2020; Xu et al. 2011; Becker et al. 2006). Our nanoparticle-based contrast agent could potentially be applied through this avenue for short term noninvasive PA imaging.

Finally, this work contributes to a growing body of research suggesting the utility of PA imaging either with or without exogenous contrast agents for noninvasive clinical imaging (Zackrisson, van de Ven, and Gambhir 2014; Steinberg et al. 2019). Traditional ultrasound has already been applied as a tool for detection and surveillance of endometriosis, and Doppler ultrasound can even estimate blood flow (Moro, Leombroni, and Testa 2019). Therefore, it is easy to envision how the incorporation of PA imaging technology would be a feasible and useful addition to the clinical arsenal of noninvasive endometriosis imaging. The ‘light in/sound out’ approach of PA imaging has the potential improve the imaging depth and resolution to identify and monitor lesion development more precisely (Zackrisson, van de Ven, and Gambhir 2014). Additionally, detection of endogenous chromophores such as hemoglobin and exogenous contrast

agents like indocyanine green and methylene blue could enhance the ability for clinicians to noninvasively determine the lesion type and molecular and cellular characteristics (Steinberg et al. 2019).

Though there is still need for further preclinical development, the future possibility of implementation of portable PA imaging as an additional tool for noninvasive clinical diagnosis of endometriosis is exciting. Women suffering from endometriosis may someday finally be diagnosed and treated without waiting for years and without the need for invasive laparoscopy.

5.5 Materials and Methods

5.5.1 Preparation of Silica Coated Gold Nanorods (AuNRs@silica)

AuNRs were synthesized by the seed-mediated growth method with some modifications from the previous report (Nikoobakht and El-Sayed 2003). First, the gold seed solution was prepared by adding cold sodium borohydride ($NaBH_4$; 0.01 M; Sigma Aldrich, St. Louis, MO, Cat. #71320) to an aqueous solution of 5 mL of hexadecyltrimethylammonium bromide (CTAB; 0.2 M, Sigma Aldrich, Cat. #H6269) and 5 mL of gold(III) chloride ($AuCl_3$; 0.005 M; >99%, Sigma Aldrich, Cat. #334049). The growth solution was prepared by adding 3.5 mL of L-Ascorbic acid (0.089 M; Sigma Aldrich, Cat. #A7506) to an aqueous solution containing 12 mL of silver nitrate (4 mM; $AgNO_3$; (≥99.0%, Sigma Aldrich, Cat. #209139), 250 mL of CTAB (0.2 M), and 250 mL of $AuCl_3$ (0.001 M). Next, 0.6 mL of the gold seed solution was added into the growth solution, and the reaction mixture became dark blue/purple/brown overtime. After 6 hours of reaction time, the mixture was then washed three times with distilled water by centrifugation (12,000 rpm, 20 min) to remove any extra CTAB. For silica coating, tetraethyl orthosilicate (TEOS; 6 μL, 99.0%, Sigma Aldrich, Cat. #86578) was added to the diluted stock of AuNRs (2.2

nM) in 10mL of DI water with the addition of 100 μL of 0.1 N sodium hydroxide (NaOH; Sigma Aldrich, Cat. #221465). The mixture solution was then vigorously stirred for 1 hour to ensure the complete coating of silica shells, washed with centrifugation (12,000 rpm, 20 min), re-dispersed in distilled water, and sonicated for resuspension.

5.5.2 Fluorescent Dye (FITC) Conjugation on AuNRs@silica Particles

10 mg of FITC (Sigma Aldrich, Cat. #46905) was reacted with 44 μL of 3-aminopropyltriethoxysilane (APTES; 99%, Sigma Aldrich, Cat. #440140; molar ratio of FITC:APTES = 1:10) in 0.75 mL of ethanol under dark conditions for 2 days. 50 μL of the prepared FITC-APTES was added into the AuNRs@silica nanoparticle solution in ethanol and was stirred for 3 hours. The particle suspension AuNRs@silica(FITC) nanoparticles were washed 3 times with ethanol to remove the unreacted species and dispersed in aqueous solution.

5.5.3 Characterization of Particles

TEM imaging was performed by using a 2200FS transmission electron microscope (JEOL, Japan). TEM specimens were prepared by dropping a small amount of nanoparticle suspension in ethanol onto carbon-coated Cu grids. ICP-OES (PerkinElmer Optima 3000DV) was used to quantify the amount of gold elements from the particles by using a gold standard solution (Sigma Aldrich, Cat. #38168). The hydrodynamic diameter and zeta potentials of nanoparticles were measured by DLS (Zetasizer ZS 90, Malvern Instruments). The UV−visible absorption and fluorescent spectrum of the FITC attached particles were analyzed with a microplate reader (SpectraMax; Molecular Devices).

5.5.4 Animals and Tissue Collection

All mouse procedures were approved by Michigan State University's IACUC. All housing and breeding were done in a designated animal care facility at Michigan State University with controlled humidity and temperature conditions and a 12 hour light/dark cycle. Access to water and food (Envigo 8640 rodent diet) was ad libitum. Mice utilized for experiments were 8 to 12 weeks old wildtype mice from mixed background C57BL/6 and 129P2/OlaHsd strains. For breeding, one male mouse was normally housed with one female mouse. One male was occasionally placed with two females to increase breeding success, in which case females were separated with their pups until weaning. After weaning at P21-P28, male and female littermates were housed separately at 5 mice/cage maximum until use in experiments or further breeding. All tissues collected for histological analysis were fixed for 6 hours in 4% (vol/vol) paraformaldehyde (Fisher Scientific, Hampton, NH, Cat. #04042-500) followed cryopreservation in a series of sucrose solutions increasing from 10% to 15% to 20% sucrose in Hanks' Balanced Salt Solution (HBSS; Gibco, Grand Island, NY, Cat. #14170-112) before freezing in Tissue-Tek OCT compound (Sakura Finetek USA, Torrance, CA, Cat. # 4583).

5.5.5 Induction of Endometriosis

Induction of endometriosis was modified from previously described methods (Kim et al. 2019; Kim, Kim, et al. 2021). Intact wildtype tissue donor mice were injected with 100 µL of 1 µg/mL E2 (Sigma Aldrich, Cat. #E8875) in sesame oil daily for 3 days to prepare the donor uterine tissue. Approximately 6 hours after the final injection, the mouse was euthanized, and the uterus was removed. For each recipient mouse, one uterine horn was opened longitudinally with scissors and cut into small fragments of about 1 mm^3 in a petri dish with a scalpel. Tissue fragments were

placed into 500 µL RPMI-1640 media (Gibco, Cat. #11835-030) supplemented with 10% fetal bovine serum (FBS; Gibco, Cat # 16000044), 0.1 mM sodium pyruvate (Gibco, Cat. #11360-070), and 1% penicillin streptomycin (P/S; Gibco, Cat #15140) with gold-FITC nanoparticles (60 µg Au/mL, 3 µg FITC/mL). Mixtures were incubated for 3 hours at 37˚C, 5% CO_2 before washing 3 times in media to remove free floating nanoparticles before transferring to the recipient mouse. Under anesthesia, a small midline abdominal incision was made in the recipient mouse, and nanoparticle-labeled tissue was injected into the peritoneal cavity. The abdominal incision was closed with sutures for the peritoneum and wound clips for the skin.

5.5.6 Photoacoustic Imaging

Photoacoustic imaging was performed using the inVision 512-echo preclinical multispectral optoacoustic tomographic imaging (MSOT) system (iThera Medical, Munich, Germany). The transmit central frequency of the transducer is set to be 5 MHz. MSOT functions to visualize images by irradiating the pulsed laser lights in multiple wavelengths (680-980 nm) and detecting the propagated ultrasound waves emitted from photo-absorbing molecules–oxyhemoglobin (HbO_2), deoxyhemoglobin (Hb), and imaging agents–from the tissue. Under isoflurane anesthesia, the mouse was shaved 360˚ around the abdominal area, all remaining hair in this region was removed with commercial hair removal cream, and warm ultrasound gel was applied. The mouse was then placed in a mouse holder with a thin polyethylene membrane to ensure acoustic coupling. Next, the assembled mouse holder was submerged in warm water in the imaging chamber. During imaging, the anesthetic isoflurane and oxygen were supplied through a breathing mask. Imaging took place with the movement of the imaging stage in a given scanning site (abdominal area). All acquisition was performed using 10 averages per illumination

wavelength, with chosen wavelengths (680, 700, 730, 760, 800, and 850 nm) and step sizes of scanning (0.3 mm). The imaging took less than 20 minutes per mouse. The acquired images were reconstructed using a back-projection algorithm, and linear spectral unmixing was applied as implemented in the ViewMSOT software (iTheraMedical). The multispectral data analysis fit to the pixel-to-pixel intensities across different wavelengths to create component images for each individual absorber (gold, Hb, and HbO_2) from the composites. In PA imaging, all layers in a multispectral image are autoscaled using imaging threshold tool to eliminate the visualization of low signals. SO_2 was calculated as a ratio of oxyhemoglobin to total Hb. PA imaging at specific times of pregnancy was performed using wildtype female mice after mating with wildtype male mice and defining morning of identification of a vaginal plug as GD 0.5. Pregnancy was visually confirmed by dissection after completing in vivo imaging.

5.5.7 Fluorescence Imaging and Immunostaining

Fluorescence-guided dissection and brightfield imaging were performed with a Nikon fluorescence dissection microscope and NIS-Elements imaging software (Nikon Instruments, Melville, NY). Quantitation of fluorescence intensity was performed using the IVIS Spectrum in vivo imaging system and Living Image software (PerkinElmer, Waltham, MA). Measurements were made based on normalized Radiant Efficiency units from manual regions of interest after adaptive fluorescence background subtraction. For fluorescence imaging of tissue sections, frozen, OCT-embedded tissue samples were cut at 10 μM and mounted on slides before coverslipping with DAPI mounting media (Vector Laboratories, Burlingame, CA, Cat. #H-1800) for imaging. For immunostaining, frozen tissue sections were fixed in 4% (vol/vol) paraformaldehyde (Fisher Scientific, Cat. #04042-500), immersed in 0.3% hydrogen peroxide in methanol, and washed in

1/40 Triton-X 100 (Fisher Scientific, Cat. #BP151-500) before blocking with 10% NGS; Vector Laboratories, Cat. #S-1000) in pH 7.5 PBS and incubating with primary antibodies diluted in 10% NGS in PBS overnight at 4°C. Primary antibodies were used at the following dilutions: 1:1000 for anti-E-Cadherin (CS-3195, Cell Signaling Technology, Danvers, MA) and 1:10,000 for anti-Vimentin (ab92547, Abcam, Cambridge, United Kingdom). An appropriate species-specific fluorescently tagged secondary antibody (Donkey anti-Rabbit IgG Alexa Fluor 594; Invitrogen, Carlsbad, CA, Cat. # A-21207) was then used before mounting and coverslipping with DAPI mounting media for imaging. Imaging was performed with a Nikon epi-fluorescence microscope and NIS-Elements imaging software (Nikon Instruments).

5.5.8 Gold Enhancement

Gold enhancement for microscopic visualization was performed with the GoldEnhance LM kit (Nanoprobes, Inc, Yaphank, NY, Cat. #2112-28) on frozen, OCT-embedded tissue samples cut at 10 μM and mounted on slides. The kit was used according to the manufacturer's instructions.

5.5.9 Statistical Analysis

To assess statistical significance, we used one-way ANOVA followed by Tukey's post hoc test for multiple group comparisons. A value of $p < 0.05$ was considered statistically significant. Statistical analyses were performed using the InStat 3 package from GraphPad (San Diego, CA).

5.6 Data Availability

The data that support the findings of this study are available within the chapter and Appendix D.

5.7 Acknowledgments

Research reported in this chapter was supported in part by the Eunice Kennedy Shriver National Institute of Child Health & Human Development of the National Institutes of Health under Award Numbers R01HD084478, R01HD101243, and R01HD102170 to J.W.J., F31HD101207 to R.M.M. and T32HD087166; MSU AgBio Research, and Michigan State University. M.N. would like to thank Hyeonjoo Woo for assistance on TEM analysis. T.K. acknowledges funding from Departmental Start-Up Grant, Michigan State University. The content is solely the responsibility of the authors and does not necessarily represent the official views of the National Institutes of Health.

CHAPTER 6

CONCLUSION

6.1 Summary

The work comprising the body of this dissertation explored the pathophysiological consequences of the endometrial ARID1A loss associated with endometriosis. We analyzed the effect of ARID1A loss in endometriotic lesions on disease development, the impact of lesion growth on the eutopic endometrial environment, and the resulting fallout of ARID1A loss in the eutopic endometrium related to fertility outcomes. Most of the focus here was placed on the function of ARID1A in endometrial epithelial cells due to previous studies identifying them as a key cell type regulated by ARID1A (Anglesio et al. 2017; Kim, Yoo, Wang, et al. 2015; Wilson et al. 2019).

After introducing the broad landscape of hormone regulation of the endometrium and what was previously known of ARID1A's involvement in endometrial dysfunction in Chapter 1, Chapter 2 defined the essential role of ARID1A in endometrial gland development and function for pregnancy success (Marquardt et al. 2021). There, we showed that ARID1A directly regulates the *Foxa2* gene in mice during early pregnancy to facilitate LIF secretion. When *Arid1a* is attenuated in the endometrial epithelium, severe subfertility results due to implantation failure, incomplete decidualization, and a non-receptive endometrium. Without sufficient FOXA2 and LIF expression, STAT3 is not activated and EGR1 is not sufficiently expressed to allow healthy pregnancy establishment. Furthermore, a translational study of infertile women with endometriosis revealed that FOXA2 is down regulated in their endometrial tissue in correlation with ARID1A.

In a baboon model of endometriosis, we observed that experimental induction of lesion growth led to simultaneous reduction of endometrial ARID1A and FOXA2.

In Chapter 3, we performed RNA-sequencing analysis on the endometrial epithelial-specific *Arid1a* knockout mouse uterus during early pregnancy, which led to the finding that in addition to its role in gland function, epithelial ARID1A is also a critical player in regulation of inflammation and immune homeostasis. When ARID1A was attenuated in the endometrial epithelium, proinflammatory gene expression spiked along with uterus-specific infiltration of proinflammatory macrophages and a decrease of uDCs at GD 3.5. At GD 7.5, implantation size was significantly reduced alongside diminished uNK cell numbers.

Chapter 4 described the development of a hormone-responsive mouse model of endometriosis with a double-fluorescent Cre reporter that mimics important histological and pathophysiological aspects of human endometriosis while allowing for genetic manipulation and easy visualization of disease progression (Yoo et al. 2022). Using this model, we showed that uterus-specific deletion of *Arid1a* caused increased lesion incidence. In a syngeneic adaptation of our model, induction of endometriosis caused wild type females to experience diminished endometrial stromal ARID1A expression, which preceded the onset of implantation and decidualization defects at 3 months after induction of disease.

Finally, we reported in Chapter 5 a method for in vivo PA imaging of endometriosis lesion development and pregnancy progression in mice based on nanoparticle labeling. Using custom gold-FITC nanoparticles as an exogenous contrast agent, we labeled endometriosis donor uterine tissue before using it to induce lesion growth in the recipient. This enabled us to visualize the location of lesions in intact, anesthetized recipients based on PA detection of gold signals. At time of dissection, the FITC component of the nanoparticle allowed fluorescence-guided lesion

removal. We successfully used the same PA imaging system to identify and track in vivo fetal growth during early and mid-pregnancy, providing a powerful new tool to study endometriosis-related infertility in mice without the need for dissection to monitor lesion growth and pregnancy progression.

6.2 Conclusions

This dissertation contributes to a growing body of knowledge of the molecular dysregulation that underpins endometriosis-related infertility. Though steroid hormone regulation of the endometrium has been extensively studied in the context of both healthy uterine function and gynecological disease (reviewed in Chapter 1), important questions have persisted regarding how endometriosis lesion development is connected to fertility problems arising from a non-receptive endometrium. Several recent studies have highlighted the importance of epigenetic and chromatin structure regulators in endometrial health and in pathologies such as endometriosis (Kim et al. 2019; Kim, Young, et al. 2021; Brunty et al. 2021; Joshi et al. 2021; Wilson et al. 2020; Samadieh et al. 2019). The work herein delineates the physiological function of the chromatin remodeler ARID1A in the endometrium and elucidates the impact of ARID1A loss in endometriosis-related infertility.

The bulk of our study centered on the role of endometrial epithelial ARID1A in early pregnancy (Figure 6.1). Our findings demonstrate the need for sufficient ARID1A expression in the endometrial epithelium to support functional glands and show that gland dysregulation is a key consequence of ARID1A loss in endometriosis that may be a translationally relevant mechanism of compromised fertility. Without ARID1A, glands do not express FOXA2 at sufficient levels to potentiate LIF secretion, which is necessary to activate signaling pathways critical for implantation

and decidualization (Kelleher, DeMayo, and Spencer 2019). In addition, the excessive uterine inflammation that results from epithelial ARID1A loss likely excludes pro-pregnancy uDCs and uNKs while promoting an influx of proinflammatory macrophages. Excessive proinflammatory cytokine expression leads to a hostile endometrial environment that may be another contributor to implantation failure (Winger and Reed 2008; Ledee-Bataille et al. 2004; Wilson et al. 2004).

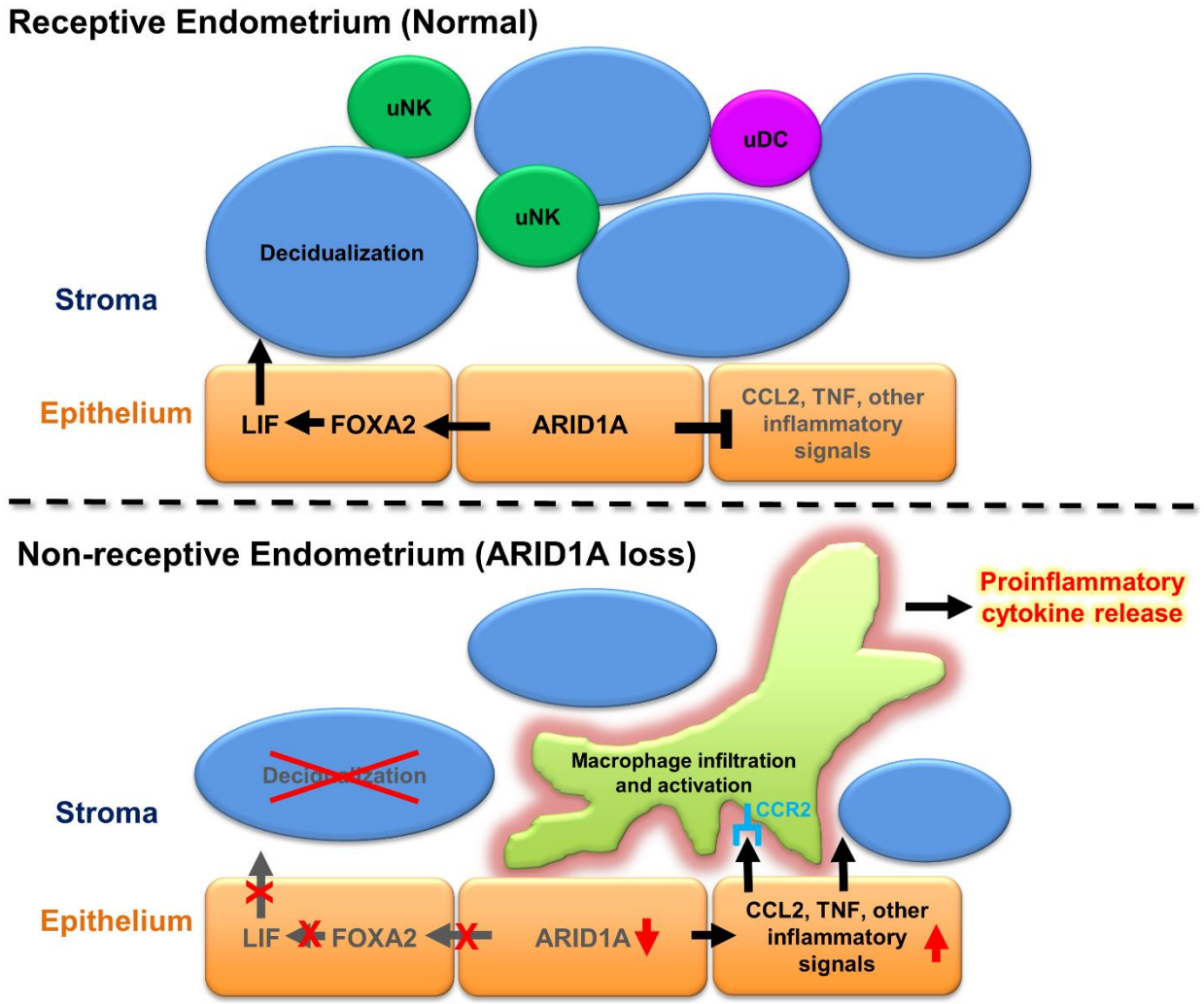

Figure 6.1 *Proposed model for the multifaceted role of endometrial epithelial ARID1A in uterine fertility function and dysfunction*. In normal uterine function (top), ARID1A facilitates glandular FOXA2-LIF signaling for decidualization and inhibits excessive production of proinflammatory cytokines. When epithelial ARID1A expression is attenuated in endometriosis conditions (bottom), endometrial gland function is compromised and proinflammatory cytokines recruit macrophages, which further promote inflammation and exclude pro-pregnancy immune cells. Together, these disruptions in the normal uterine environment lead to a non-receptive endometrium, implantation failure, and defective decidualization.

ARID1A directly interacts with PGR in the endometrium, and deletion of *Arid1a* in all uterine compartments of $Pgr^{cre/+}Arid1a^{f/f}$ mice leads to suppressed epithelial PGR signaling during early pregnancy (Kim, Yoo, Wang, et al. 2015; Kim, Kim, et al. 2021), which led us to expect a similar result in mice with epithelial-specific ARID1A loss. However, epithelial PGR loss was not a major phenotype of $Ltf^{iCre/+}Arid1a^{f/f}$ mice. Though this finding could be due in part to inefficient *Ltf-iCre* activity, it also suggests an important role for stromal ARID1A in coordinating epithelial PGR signaling, which is particularly interesting given our finding of stromal-specific ARID1A attenuation in a mouse model of endometriosis-related infertility. Overall, the epithelial and stromal cell-specific relationships between ARID1A and PGR's regulation of the endometrium is a topic requiring more detailed inquiry.

Our finding that endometrial epithelial ARID1A loss causes uterine inflammation is also interesting given the increase in endometriosis lesion formation in $Pgr^{cre/+}Arid1a^{f/f}$ mice induced with endometriosis. The relationship between endometriosis lesions and inflammation is widely acknowledged, though complex (Vallve-Juanico, Houshdaran, and Giudice 2019). Depending on their type and origin, immune cells can either lead to clearance of endometriotic lesions or protect their survival (Hogg et al. 2021). Therefore, further study of the connection between ARID1A loss, inflammation, and lesion development is warranted.

As to the prevailing molecular mechanism of ARID1A loss in endometriosis, no definitive conclusion can be drawn based on the available data. Inactivating somatic mutations can cause ARID1A expression loss in endometrial cancer and in non-cancerous deep infiltrating endometriotic lesions (Mathur 2018; Anglesio et al. 2017), likely due to common causes of DNA mutations such as endogenous replication errors, exposure to ionizing radiation, or reactive oxygen species. However, *ARID1A* mutations are far too rare in the endometrium to be the primary drivers

of the quite common population-wide incidence of endometriosis (Lac et al. 2019; Suda et al. 2018). Thus, endometrial attenuation of ARID1A expression more likely results from epigenetic, transcriptional, or post-transcriptional changes. The PGR-regulated transcription factor SOX17 has been identified as a possible upstream regulator of ARID1A expression in the endometrium, but this is a topic in need of further study (Wang et al. 2018).

The initial event that causes the development of endometriotic lesions remains unknown in most cases, and this dissertation does not conclusively answer that question. However, our data do provide clues about the process. Most menstruating women experience retrograde menstruation, so a molecular proclivity to attachment and proliferation may explain why only some women's free-flowing endometrial cells form lesions (de Ziegler, Borghese, and Chapron 2010; Giudice and Kao 2004; Zondervan et al. 2018). In this vein, ARID1A expression may be lost first in the eutopic endometrium, predisposing it to lesion formation in the peritoneum when retrograde menstruation occurs. This hypothesis is supported by our finding that endometriotic lesion incidence increases in endometriosis model mice with *Arid1a* knockout seed tissue compared to ARID1A-expressing tissue. Another possibility is that lesion development may happen first and then confer ARID1A loss and endometrial non-receptivity to the eutopic endometrium through an unknown mechanism potentially involving inflammatory cytokine secretion (Kyama et al. 2009). This concept is supported by our data showing that endometrial ARID1A expression decreases following endometriosis induction in baboons and mice. It is also, of course, possible that lesion development and ARID1A loss share a common cause rather than a direct relationship in the human disease. Figure 6.2 graphically summarizes the proposed contributions of ARID1A loss to endometriosis-related infertility based on this dissertation work together with the experimental models that provided the data for each aspect of the model.

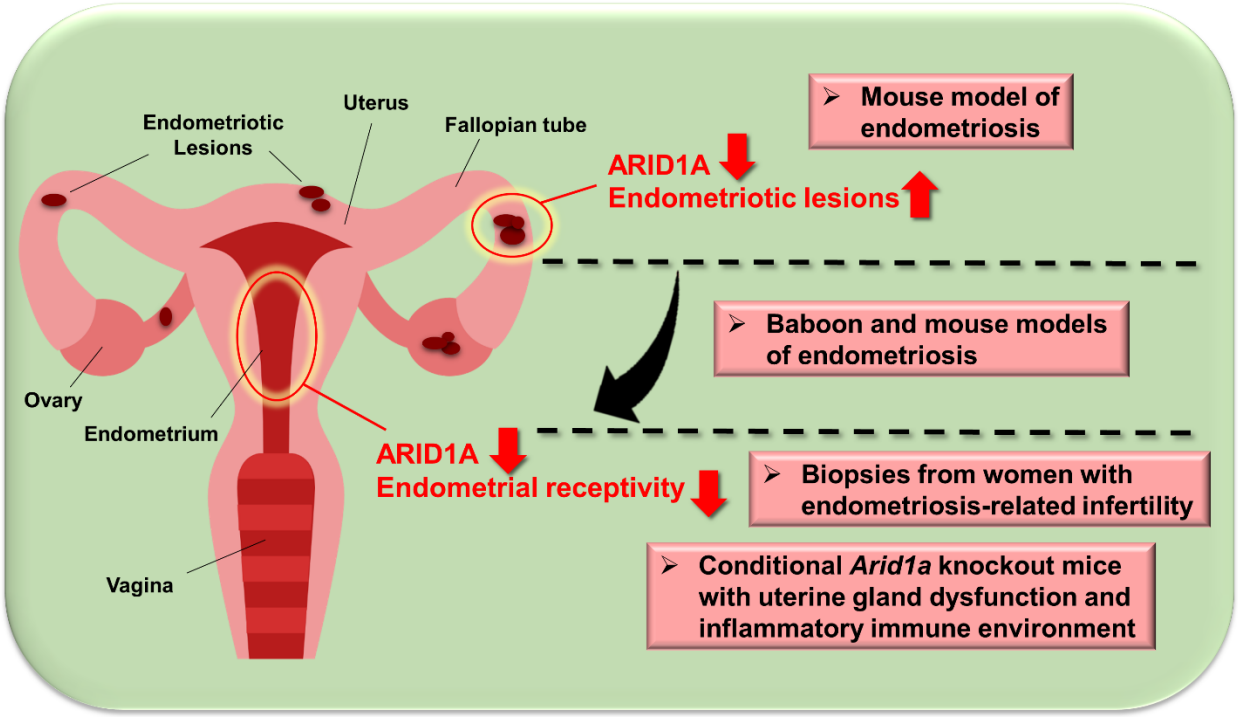

Figure 6.2 *Summary of the contributions of ARID1A loss to endometriosis-related infertility*. ARID1A loss leads to increased lesion development. Lesion development causes downregulation of ARID1A in the eutopic endometrium. Attenuated endometrial ARID1A causes gland dysfunction and uterine inflammation, resulting in compromised receptivity to pregnancy. The boxes on the right indicate the experimental models that led to each finding.

Taken together, the studies reported in this dissertation make the case that endometrial ARID1A loss contributes to endometriosis-related infertility by exacerbating endometriotic lesion development and compromising the ability of the uterus to receive an implanting embryo. A continually deepening understanding of endometrial function and dysfunction at the molecular level through studies like these is necessary to empower the development of targeted treatment options for women suffering the effects of endometriosis who desire to maintain or restore their fertility.

6.3 Future Directions

6.3.1 Effect of ARID1A Loss on In Vivo Chromatin Dynamics During Pregnancy

The data reported here have contributed to our knowledge of the role of ARID1A in endometriosis-related infertility and opened up new lines of inquiry that will lead to fruitful future studies. While we showed the consequences of endometrial epithelial *Arid1a* deletion on pregnancy physiology and gene expression in Chapters 2 and 3, understanding the direct molecular mechanisms by which ARID1A controls gene expression during pregnancy in vivo would be very interesting. To address this gap in knowledge, it would be beneficial to consider the molecular function of ARID1A in SWI/SNF chromatin remodeling. Performing ATAC-seq (Assay for Transposase-Accessible Chromatin using sequencing) on GD 3.5 control and $Ltf^{iCre/+}Arid1a^{f/f}$ mouse uteri would reveal the effect of ARID1A loss in early pregnancy on genome-wide chromatin accessibility. Furthermore, ARID1A ChIP-seq on the same sample type would reveal genomic loci with which ARID1A physically interacts in this context. For even more information, ChIP-seq targeting epigenetic marks such as the active enhancer mark H3K27ac would demonstrate the influence of ARID1A on chromatin state at genome regions of interest. These new datasets could be compared to our RNA-seq data (see Chapter 3) to infer the effects of direct ARID1A-DNA interactions on chromatin accessibility, enhancer activity, and transcriptional output of specific genes throughout the genome. If possible, isolating endometrial epithelium from the mice at this stage would sharpen interpretation of the data by removing the confounding influence of stromal cells. However, this procedure is technically difficult and brings the added difficulty of low cell populations for bioinformatic analysis.

6.3.2 Physiological and Molecular Mechanisms of Immune Dysregulation Resulting from ARID1A Loss in Endometriosis-Related Infertility

Our finding in Chapter 3 of dramatically increased proinflammatory uterine conditions in the GD 3.5 *Ltf*$^{iCre/+}$*Arid1a*$^{f/f}$ mouse opens exciting new experimental possibilities. For example, more thorough characterization of the altered proinflammatory macrophage population would provide clues to the direct effects of these cells on the pregnant uterus as well as the mechanism that causes their infiltration into the uterus. One way to assess this would be by sorting the cells and performing RNA-seq analysis to compare their gene expression patterns in controls versus *Ltf*$^{iCre/+}$*Arid1a*$^{f/f}$ mice. A more broad and comprehensive method to assess the gene expression landscape of all the cell types involved in this condition would be single-cell RNA-seq, which would have the benefit of showing concurrent gene expression data from immune cells, epithelial cells, and stromal cells.

Additionally, more detailed study at other stages of pregnancy and in non-pregnant *Ltf*$^{iCre/+}$*Arid1a*$^{f/f}$ mice would be informative. For example, what is the preceding and subsequent behavior of the infiltrating proinflammatory macrophages that are increased in *Ltf*$^{iCre/+}$*Arid1a*$^{f/f}$ uteri at pre-implantation? Analyzing their spaciotemporal activity before onset of pregnancy and then during implantation and beyond would provide insight into whether these cells infiltrate specifically during pregnancy and whether they are directly involved in causing the failure to establish and maintain healthy implantation sites.

The data gleaned from the above-mentioned experiments could be supplemented with an analysis of the secreted cytokine environment in the uterus at the same stages of pregnancy via ELISA (enzyme-linked immunosorbent assay)-based cytokine screening, which would help in evaluating the functional importance of the changes we found in mRNA expression of various

cytokines in *Ltf*$^{iCre/+}$*Arid1a*$^{f/f}$ uteri. Furthermore, a lipopolysaccharide (LPS) challenge intended to provoke systemic immune response in *Ltf*$^{iCre/+}$*Arid1a*$^{f/f}$ mice would reveal if the excessive uterine inflammation we observed in pregnancy is replicable in an immune challenge outside the context of pregnancy. Based on the combined results, experiments could be designed to evaluate the efficacy of anti-inflammatory drugs or antibody-based therapies for restoring uterine immune homeostasis and pregnancy success after ARID1A loss.

Increased knowledge of the inflammatory signals prompted by endometrial ARID1A loss would also be valuable for evaluating the endometriotic lesion environment. Given that we observed increased lesion formation in our endometriosis mouse model, ARID1A-loss-induced secretion of inflammatory factors by the uterine cells injected back into the peritoneal cavity may influence the process of lesion formation. Additionally, evaluation of the cytokine landscapes of the lesion and peritoneal environments could provide clues as to how lesion formation enacts its deleterious effects on implantation and decidualization in our mouse model of endometriosis-related infertility. To add an additional dimension to this analysis, post-mating in vivo imaging of mice induced with endometriosis using our nanoparticle-based PA imaging model would show in real time the impact of the lesion number, size, and location on the formation, maintenance, and growth of implantation sites.

6.3.3 Mechanisms of ARID1A Regulation of PGR Function in Pregnancy and Endometriosis

Previously published work identified physical protein interaction between ARID1A and PGR as well as a role for ARID1A in modulating endometrial PGR signaling (Kim, Yoo, Wang, et al. 2015; Kim, Kim, et al. 2021). As discussed above, the studies included in this dissertation have contributed limited but interesting information about this relationship. Given our findings of

only minor PGR signaling disruption in *Ltf*$^{iCre/+}$*Arid1a*$^{f/f}$ uteri at pre-implantation (Chapter 2) and of endometrial stromal-specific ARID1A reduction after endometriosis induction in our mouse model of endometriosis-related infertility (Chapter 4), future studies should focus on an evaluation of the role of endometrial stromal ARID1A in modulating PGR activity. Analysis of genomic regions of ARID1A and PGR co-occupancy combined with RNA-seq of primary stromal cells from healthy controls and endometriosis patients would provide insight on cell-autonomous ARID1A-PGR co-regulation of gene expression. Use of endometrial assembloids (Rawlings et al. 2021), consisting of both epithelial and stromal cells in culture, would provide an exciting opportunity for in vitro manipulations (such as cell type-specific *ARID1A* siRNA knockdown prior to co-culture) with follow-up analysis of epithelial-stromal signaling crosstalk. This could be a viable system for analyzing the effects of stromal ARID1A loss on epithelial PGR signaling, which appears to be important based on combined findings from *Pgr*$^{cre/+}$*Arid1a*$^{f/f}$ (Kim, Yoo, Wang, et al. 2015) and *Ltf*$^{iCre/+}$*Arid1a*$^{f/f}$ (Marquardt et al. 2021) mice (see Chapter 2). Furthermore, development and generation of an efficient and specific endometrial stromal Cre-expressing mouse to cross with *Arid1a*$^{f/f}$ mice would provide an optimal opportunity for assessing the in vivo stromal-specific function of ARID1A in pregnancy and in our endometriosis mouse model.

6.3.4 Cause of Endometrial ARID1A Loss in Endometriosis-Related Infertility

This dissertation research has investigated what happens as a consequence of ARID1A loss in the endometrium in the context of endometriosis. However, the initial cause for the downregulation of ARID1A remains unclear. In various cancers, inactivating mutations that cause loss of *ARID1A* expression are common (Mathur 2018). These types of cancer-associated mutations have also been identified in non-malignant deeply infiltrating endometriotic lesions

(Anglesio et al. 2017) and ovarian endometriomas (Suda et al. 2018), but they are relatively rare and appear to be later somatic events after initial lesion formation rather than drivers of lesion establishment. Since *ARID1A* mutations in benign endometrial tissue are uncommon and no more frequent in endometriosis cases than in controls (Suda et al. 2018; Lac et al. 2019), the decrease of endometrial ARID1A in women with endometriosis is likely independent of DNA sequence changes. Therefore, downregulation of ARID1A is probably due to changes at the epigenetic, transcriptional, or post-transcriptional level. One study suggests that the transcription factor SOX17 may transcriptionally promote *Arid1a* expression (Wang et al. 2018), implying that decreased SOX17 in endometriosis may be a cause for decreased ARID1A. Another study observed hypermethylation of the *ARID1A* promoter in women with endometriosis which was recapitulated in vitro by treatment with reactive oxygen species (Xie et al. 2017). These interesting initial findings should prompt further inquiry into the mechanism of ARID1A downregulation in endometriosis-related infertility. Since direct therapeutic targeting of ARID1A is likely to be difficult or impossible due to its pleiotropic functions, understanding what precipitates ARID1A attenuation may lead to more straightforward clinical application through the development of drug therapies designed to indirectly reverse or prevent ARID1A loss.

APPENDICES

APPENDIX A

SUPPLEMENTARY MATERIAL FOR CHAPTER 2

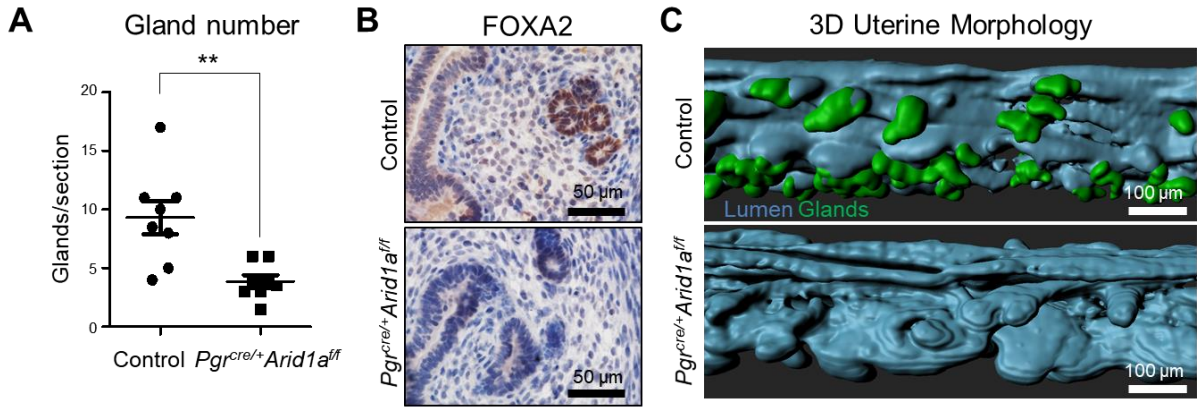

Figure A.1 *Endometrial glands are dysregulated during postnatal development in* $Pgr^{cre/+}Arid1a^{f/f}$ *mice*. **(A)** Endometrial gland counts in control and $Pgr^{cre/+}Arid1a^{f/f}$ mice at 4 weeks of age. The graph represents the mean ± SEM of the number of glands per uterine tissue section (n=8; **, p<0.01). **(B)** Representative images of FOXA2 IHC in control and $Pgr^{cre/+}Arid1a^{f/f}$ mouse uterine sections at 4 weeks of age (n=3). **(C)** Three-dimensional uterine morphology of control and $Pgr^{cre/+}Arid1a^{f/f}$ uterine horns at 3 weeks of age based on whole-mount immunofluorescence for E-cadherin and FOXA2, where the 3D luminal structure (blue) is constructed by subtracting the FOXA2 (green) from the E-cadherin signal (Control, n=3; $Pgr^{cre/+}Arid1a^{f/f}$, n=2).

A

Six Month Fertility Trial

Genotype	Number of Litters	Number of Pups	Average Pups/Litter ± SEM	Average Litters/Mouse ± SEM
Control (n=6)	32	200	6.25 ± 0.21	5.33 ± 0.21
$Ltf^{iCre/+}Arid1a^{f/f}$ (n=6)	2	3	1.5 ± 0.5	0.33 ± 0.33

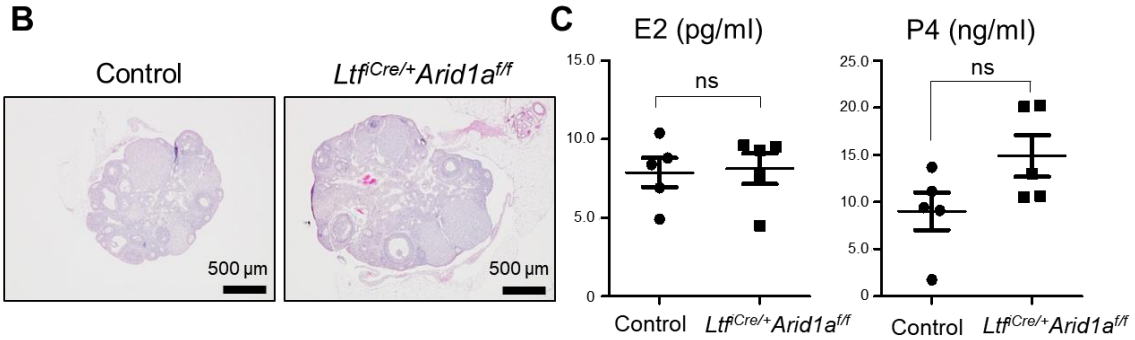

Figure A.2 *Endometrial epithelial-specific Arid1a loss results in severe sub-fertility but normal ovarian function*. **(A)** Resulting numbers of litters and pups found in a fertility trial where female control or $Ltf^{iCre/+}Arid1a^{f/f}$ mice were housed in breeding cages with wildtype male mice for six months. **(B)** Representative images of hematoxylin and eosin-stained ovary cross-sections from control and $Ltf^{iCre/+}Arid1a^{f/f}$ mice at GD 3.5 (n=3). **(C)** Quantification of serum P4 and E2 levels in control and $Ltf^{iCre/+}Arid1a^{f/f}$ mice at GD 3.5. The graphs represent the mean ± SEM (n=5; ns, p>0.05).

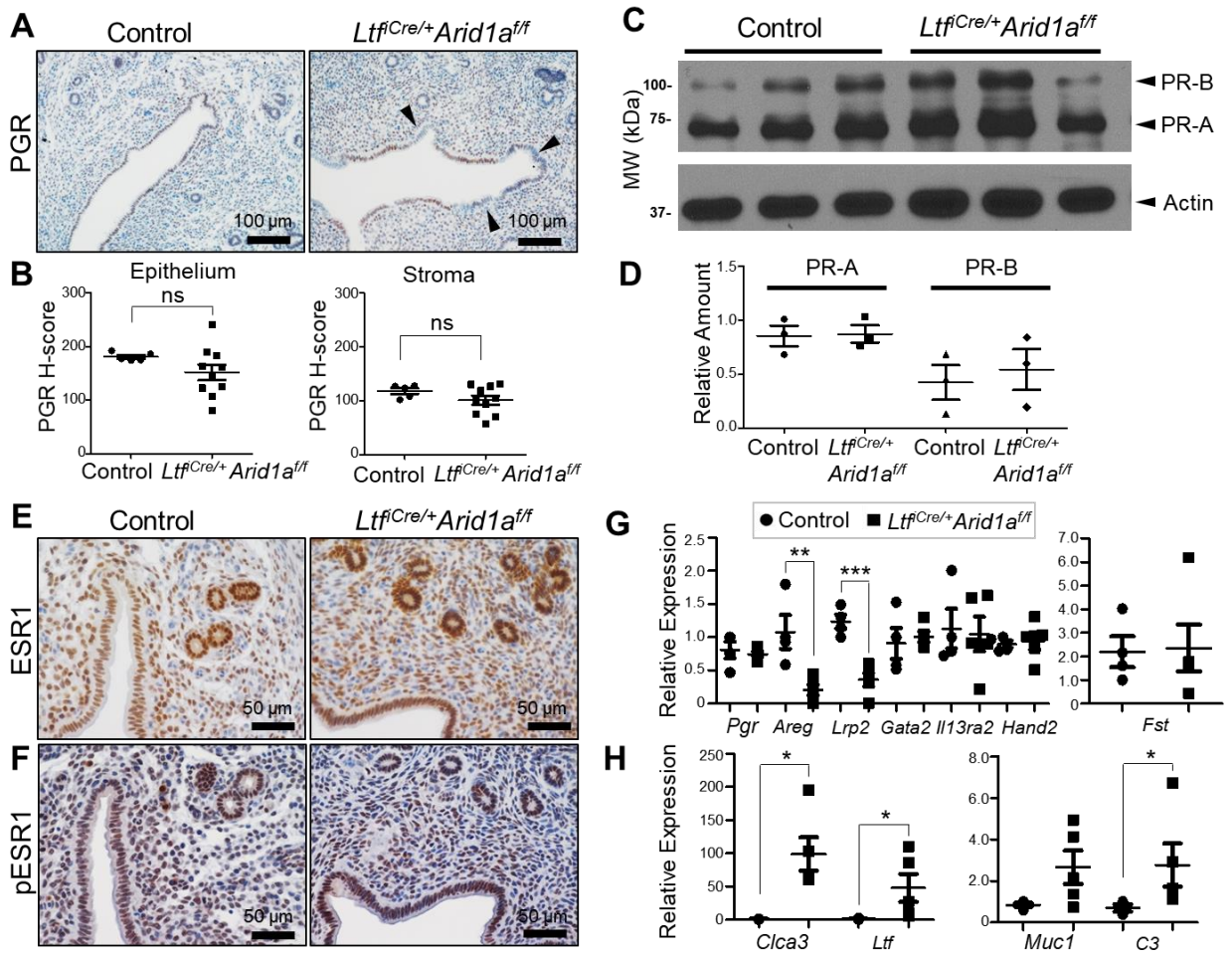

Figure A.3 *P4 and E2 signaling exhibit minor changes in GD 3.5 Ltf*$^{iCre/+}$*Arid1a*$^{f/f}$ *mice.* **(A)** Representative images of PGR IHC in control and *Ltf*$^{iCre/+}$*Arid1a*$^{f/f}$ mouse uterine tissue sections (control, n=3; *Ltf*$^{iCre/+}$*Arid1a*$^{f/f}$, n=10). Arrowheads indicate patches of PGR-negative cells in the luminal epithelium. **(B)** Semi-quantitative H-scores of epithelial and stromal PGR staining strength. The graphs represent the mean ± SEM (control, n=3, 5 tissue regions; *Ltf*$^{iCre/+}$*Arid1a*$^{f/f}$, n=10; ns, p>0.05). **(C)** Western blot of PGR (PR-A and PR-B) in protein isolated from total uterine tissue of control and *Ltf*$^{iCre/+}$*Arid1a*$^{f/f}$ mouse uteri (n=3). Western blotting was performed at previously described (Kim, Yoo, et al. 2014). **(D)** Quantification of band intensity of PR-A and PR-B relative to actin in control and *Ltf*$^{iCre/+}$*Arid1a*$^{f/f}$ uteri (n=3, p>0.05). **(E)** Representative images of ESR1 IHC in control and *Ltf*$^{iCre/+}$*Arid1a*$^{f/f}$ mouse uterine tissue sections (n=3). **(F)** Representative images of pESR1 IHC in control and *Ltf*$^{iCre/+}$*Arid1a*$^{f/f}$ mouse uterine tissue sections (n=3). **(G)** Relative expression of P4 target gene mRNA normalized to *Rpl7* in whole uterine tissue preparations. The graphs represent the mean ± SEM (control, n=4; *Ltf*$^{iCre/+}$*Arid1a*$^{f/f}$, n=5; **, p<0.01; ***, p<0.001). **(H)** Relative expression of E2 target gene mRNA normalized to *Rpl7* in whole uterine tissue preparations. The graphs represent the mean ± SEM (control, n=4; *Ltf*$^{iCre/+}$*Arid1a*$^{f/f}$, n=5; *, p<0.05).

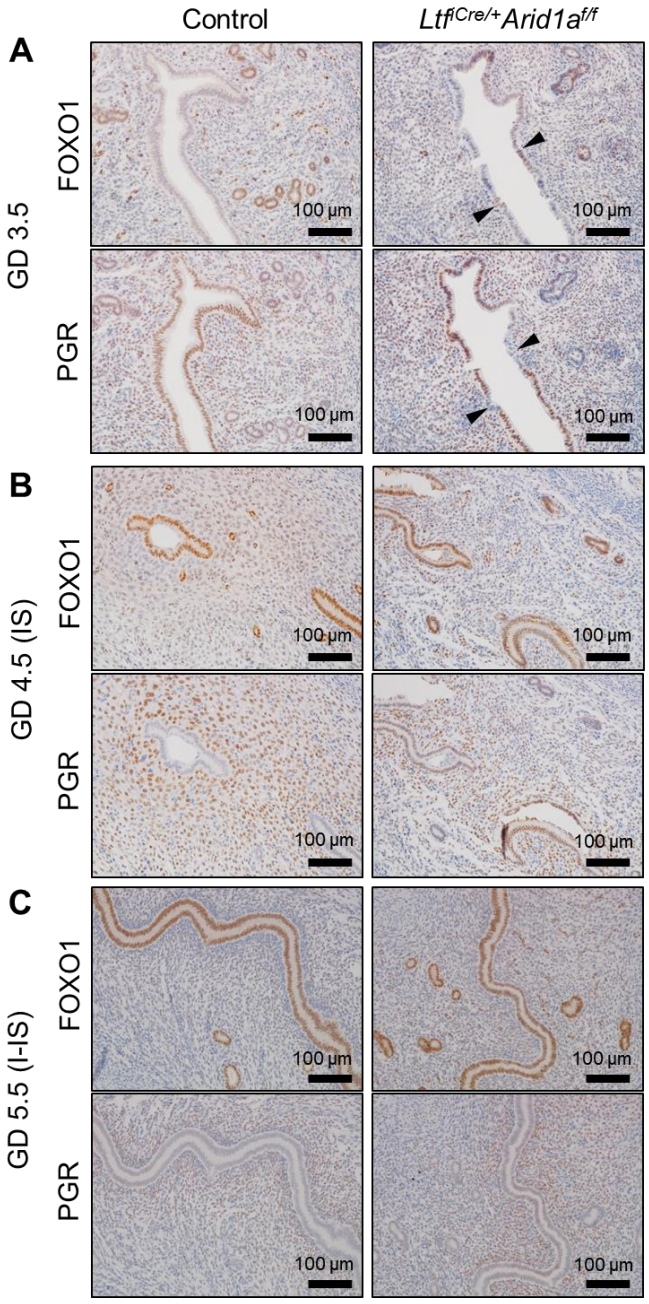

Figure A.4 *FOXO1 and PGR are not notably altered in the Ltf$^{iCre/+}$Arid1a$^{f/f}$ uterus during early pregnancy*. **(A)** Representative images of FOXO1 (upper panel) and PGR (lower panel) IHC in control and *Ltf*$^{iCre/+}$*Arid1a*$^{f/f}$ mouse serial uterine tissue sections at GD 3.5 (n=3). Arrowheads indicate patches of FOXO1-positive/PGR-negative cells in the luminal epithelium. **(B)** Representative images of FOXO1 (upper panel) and PGR (lower panel) IHC in control and *Ltf*$^{iCre/+}$*Arid1a*$^{f/f}$ mouse serial uterine tissue sections surrounding implantation sites at GD 4.5 (n=3, 6 IS). **(C)** Representative images of FOXO1 (upper panel) and PGR (lower panel) IHC in control and *Ltf*$^{iCre/+}$*Arid1a*$^{f/f}$ mouse serial uterine tissue sections at inter-implantation site regions at GD 5.5 (control, n=3; *Ltf*$^{iCre/+}$*Arid1a*$^{f/f}$, n=5).

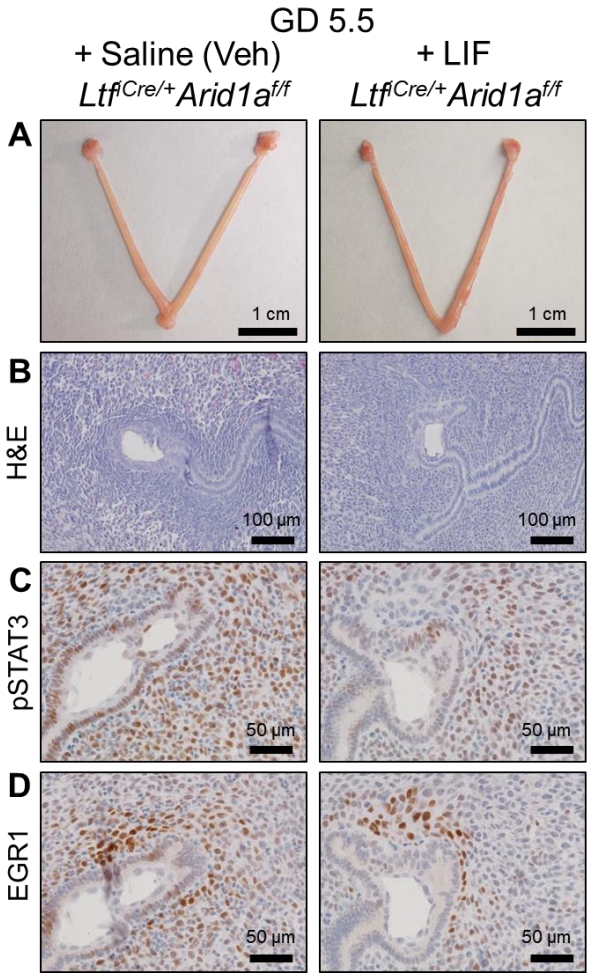

Figure A.5 *LIF repletion at GD 3.5 does not rescue implantation in Ltf$^{iCre/+}$Arid1a$^{f/f}$ mice.*
(A) No implantation sites were grossly visible at GD 5.5 in uteri from vehicle or LIF-treated *Ltf$^{iCre/+}$Arid1a$^{f/f}$* mice (n=3). Attempted rescue of implantation by LIF repletion was performed as described previously (Kelleher et al. 2018). Briefly, *Ltf$^{iCre/+}$Arid1a$^{f/f}$* mice received i.p. injections of 10 µg recombinant mouse LIF (BioLegend, San Diego, CA) in saline or vehicle (saline only) on GD 3.5 at 1000 and 1800 hours. Implantation sites were analyzed on the morning of GD 5.5 morphologically and histologically. **(B)** Representative images of hematoxylin and eosin-stained uterine tissue sections from control and *Ltf$^{iCre/+}$Arid1a$^{f/f}$* mice at GD 5.5 (Veh-treated n=3, 7 IS; LIF-treated n=3, 9 IS). **(C)** Representative images of pSTAT3 IHC in saline (vehicle) and LIF-treated *Ltf$^{iCre/+}$Arid1a$^{f/f}$* mouse uteri. **(D)** Representative images of EGR1 IHC in saline (vehicle) and LIF-treated *Ltf$^{iCre/+}$Arid1a$^{f/f}$* mouse uteri.

Table A.1 *Genes dysregulated in both $Pgr^{cre/+}Arid1a^{f/f}$ and $Pgr^{cre/+}Foxa2^{f/f}$ uteri at GD 3.5*

A2m	Cd38	Dsg2	Gstm1	Lcn2
Abcb1a	Cdc14a	Dsp	Gstm2	Ldlr
Abcg2	Cdh1	Ebf1	Gzma	Lgr6
Accn1	Cdh5	Egfl6	Gzmb	Lox
Acer2	Ceacam1	Egln3	H19	Lpar3
Acot1	Cfi	Egr1	Has2	Lrig1
Adamts16	Cftr	Elf3	Hmcn1	Lrp2
Adcy1	Chaf1b	Eltd1	Hmga2	Lrrn1
Adcy4	Chrdl1	Enpp1	Hmgcll1	Ltf
Aff3	Chst11	Entpd2	Hmgcs1	Macc1
Ak5	Cited4	Epcam	Hmgn3	Mad2l1
Akr1c14	Ckmt1	Epsti1	Hspa8	Mal2
Akr1c19	Cks2	Esam	Idi1	Mall
Alcam	Clca1 /// Clca2	F2r	Igfbp3	Maob
Aldh1a1	Clca3	Fam176a	Il15ra	Matn2
Alox12e	Clcn5	Fam20c	Il17rb	Me1
Ampd3	Cldn8	Fam43a	Il2rb	Melk
Anln	Cln5	Fcrls	Inhbb	Mfap4
Aplnr	Cnn3	Fdft1	Insig1	Mfsd4
Arl4c	Col14a1	Fdps	Itgax	Mid1
Atp1b1	Col4a6	Fkbp5	Jam2	Mme
Atp8a1	Col6a4	Fmod	Kbtbd11	Mmp11
Avil	Cpm	Foxf1a	Kbtbd8	Mogat2
AW112010	Crabp1	Fut9	Kcnd2	Mpzl2
B3gnt5	Csrnp3	Gabrp	Kif23	Mt1
Bcat1	Ctgf	Galnt12	Kit	Muc1
Bhlhe40	Ctsd	Galnt3	Klra3 /// Klra9	Muc4
Capn5	Ctsw	Gfpt2	Klra8	Mug1
Capn6	Cxcl15	Ggt5	Klrd1	Mvd
Caprin2	Cxcl17	Gimap4	Klrg1	Myb
Car2	Cyp1b1	Gimap6	Krt19	Mycn
Car4	Cyp27a1	Gjb2	Krt23	Myd88
Cbr2	Cyp2e1	Glis3	Krt7	Myl4
Cbs	Cyyr1	Glul	Krt8	Myo3b
Ccl11	D630045J12Rik	Gm106	Lad1	Myo6
Ccnb1	Dhcr24	Gpld1	Lamb3	Ncam1
Cd109	Dio2	Gpx2	Lamc3	Nfil3
Cd24a	Dkk3	Greb1	Lass3	Ngfr

Table A.1 (cont'd)

Nkg7	Rab25	Slc44a3	Tshz2
Npl	Rab27b	Slc44a4	Tspan1
Nrk	Racgap1	Slc7a11	Tspan7
Nsdhl	Rad18	Sned1	Ttc9
Nudt19	Ramp3	Sorcs2	Ttr
Odz4	Rasip1	Sorl1	Uox
Ogn	Rbp1	Spink12	Vwf
Oit1	Rdh9	Spink3	Wfdc1
Osgin2	Rgs2	Spock2	Wfdc2
Oxtr	Rgs5	Spp1	Wfdc3
Padi1	Ripply3	Sprr2f	LOC100503611 /// Wnt4
Padi2	Rnf150	Sqle	Wnt7a
Padi4	Rnf180	St14	Xcl1
Paox	Rnf186	Stc2	Zbtb16
Parvb	Rps6ka5	Steap4	Zmpste24
Pcdh19	S100g	Sult1a1	
Pdgfd	Sc4mol	Sv2b	
Pdk4	Scd1	Syn2	
Penk	Sdc1	Tac2	
Perp	Selp	Tacstd2	
Pknox2	Sema3a	Tdo2	
Pkp2	Sema7a	Tek	
Pla2g10	Sfn	Tfrc	
Plk1	Sftpd	Tgfbrap1	
Plod2	Sh3gl2	Tie1	
Pls1	Sh3rf2	Tjp3	
Plxnb1	Six4	Tle1	
Pof1b	Slain1	Tmem158	
Ppap2c	Slc16a12	Tmem20	
Prap1	Slc16a6	Tmem30b	
Prss22	Slc25a48	Tmem40	
Prss28	Slc26a7	Tmem45b	
Psat1	Slc28a3	Tmem54	
Ptger2	Slc29a1	Tmprss4	
Ptger4	Slc2a3	Tnfrsf21	
Ptn	Slc2a4	Trib2	
Ptprg	Slc40a1	Trpc4	

Table A.2 *Primary antibody list*

Target	Company	Catalog #
ARID1A (IF)	Abnova	H00008289-M02
ARID1A (IHC)	Santa Cruz	SC-98441
ARID1A (ChIP)	Abnova	MAB15809
COX-2	Cayman	160106
E-cadherin (IHC)	Cell Signaling	3195
E-cadherin (3D, IF)	Clontech	M108
EGR1	Cell Signaling	4153
FOXA2 (IHC)	Seven Hills	WRAB-FOXA2
FOXA2 (3D, IF)	Novus Biologicals	NBP1-95426
FOXO1	Cell Signaling	2880
Ki67	BD Pharmingen	550609
PGR	Cell Signaling	8757
ESR1	Vector	VP-E613
pESR1	Abcam	ab31477
STAT3	Cell Signaling	4904
pSTAT3	Cell Signaling	9145

Table A.3 *SYBR Green RT-qPCR primer list*

Gene	Forward primer	Reverse primer
Areg	CTGTTGCTGCTGGTCTTA	TCCTCTGAGTAGTCGTAGTC
Arid1a	CTGTTGCCATGCATGTTGCT	TGAGGGTTGATCATGCCAGC
Clca3	ACTAAGGTGGCCTACCTCCAA	GGAGGTGACAGTCAAGGTGAGA
Cxcl15	CAAGGCTGGTCCATGCTCC	TGCTATCACTTCCTTTCTGTTGC
C3	GCGTCTCCATCAAGATTCCAGCCA	CACCACCGTTTCCCCGAAGTTTG
Egr1	ACCCTATGAGCACCTGACCAC	TATAGGTGATGGGAGGCAACC
Fst	GCAGCCGGAACTAGAAGTACA	ACACAGTAGGCATTATTGGTCTG
Hand2	TCCAAGATCAAGACACTGCG	TCTTCTTGATCTCCGCCTTG
Lrp2	CCAGAA AATGTGGAA AACCA	TTCGAAGTTCGTTGTCTGCTT
Ltf	GAGAAGATGCTGGCTTCACC	CACCAATACACAGGGCACAG
Muc1	GGCATTCGGGCTCCTTTCTT	TGGAGTGGTAGTCGATGCTAAG
Rpl7	TCAATGGAGTAAGCCCAAAG	CAAGAGACCGAGCAATCAAG
Spink3	TATAGTTCTTCTGGCTTTTGC	TCTATGCGTTTCCTGTTTTCA
Foxa2 #1 (ChIP)	AGGCAGCGATTTGCCTCT	TGCCCTGTTTGTTTTAGTTACG-3
Foxa2 #2 (ChIP)	AAGCCACCCTTGGAGAAACT	AGGGAGGAAACCCGAGATAA
Foxa2 #3 (ChIP)	CACAACAAACGACCAGCAAT	GCGGGAGAGAGAGAGGAAGT
Foxa2 #4 (ChIP)	TGTGTTCATGCCATTCATCC	CGAGCTCAGCCTAGGTGCTA
Negative control (ChIP)	GGCCATTCTAGCCAGAACAC	GTGTACCGGACCAGGAGAAA

Table A.4 *TaqMan RT-qPCR probe list*

Gene	Applied Biosystems Assay ID
Foxa2	00839704
Gapdh	99999915
Gata2	00492301
Il13ra2	00515166
Lif	00434761
Pgr	00435628

APPENDIX B

SUPPLEMENTARY MATERIAL FOR CHAPTER 3

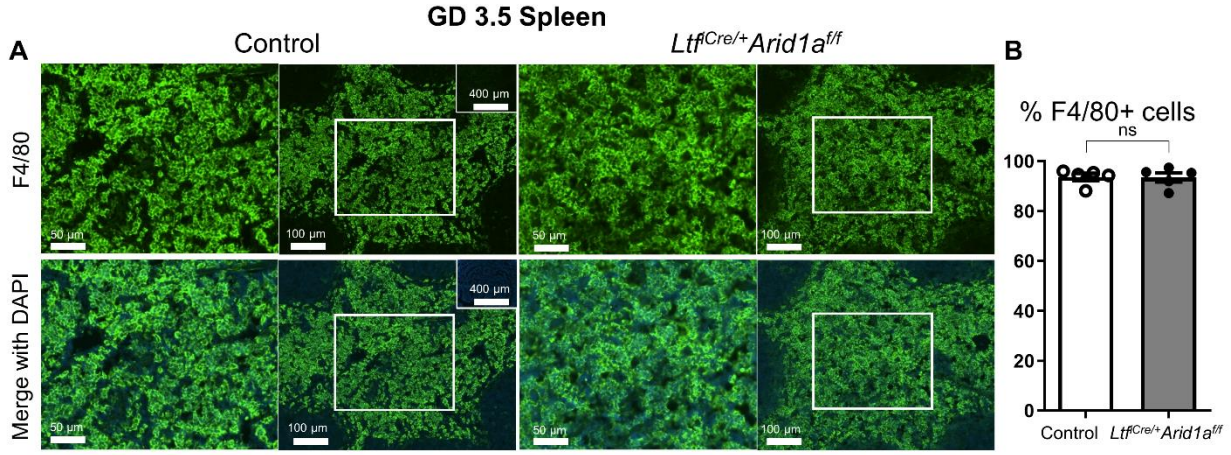

Figure B.1 *F4/80+ macrophage numbers are unchanged in the spleen tissue of Ltf$^{iCre/+}$Arid1a$^{f/f}$ mice at GD 3.5*. **(A)** Representative images of F4/80 immunofluorescence (green) counterstained with DAPI (blue) in control (left) and *Ltf$^{iCre/+}$Arid1a$^{f/f}$* (right) mouse spleen sections at GD 3.5 (n=5/genotype) Insets: no primary antibody negative controls. **(B)** The percentage of F4/80-positive spleen cells was counted in representative red pulp fields of approximately 500 cells per sample of control (n=5, empty bar) and *Ltf$^{iCre/+}$Arid1a$^{f/f}$* (n=5, grey bar) uteri at GD3.5. The graph represents the mean ± SEM. ns, p>0.05.

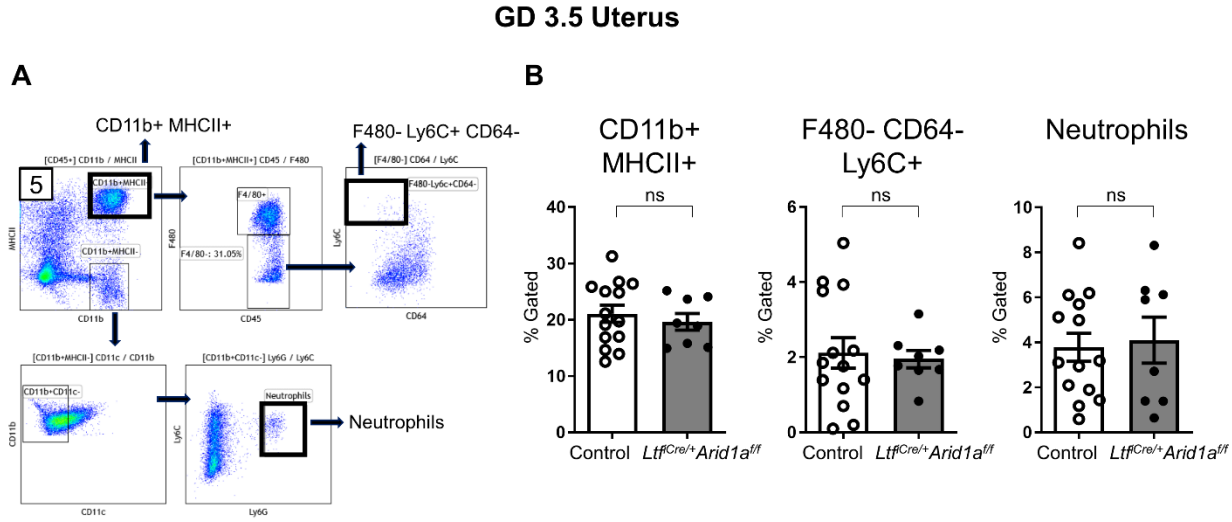

Figure B.2 *No change was detected in the proportions of CD11b+ MHCII+ cells, F4/80- CD64- Ly6C+ cells, or Neutrophils in Ltf$^{iCre/+}$Arid1a$^{f/f}$ uteri at GD 3.5*. **(A)** The flow gating strategy to identify CD11b+ MHCII+ cells, F4/80- CD64- Ly6C+ cells, and Neutrophils in the mouse uterus is shown. **(B)** The % Gated proportion of CD11b+ MHCII+ cells (left), F4/80- CD64- Ly6C+ cells (middle), and neutrophils (right) in control (n=14, empty bar) and *Ltf$^{iCre/+}$Arid1a$^{f/f}$* (n=8, grey bar) uteri at GD3.5 is shown. The graphs represent the mean ± SEM. ns, p>0.05.

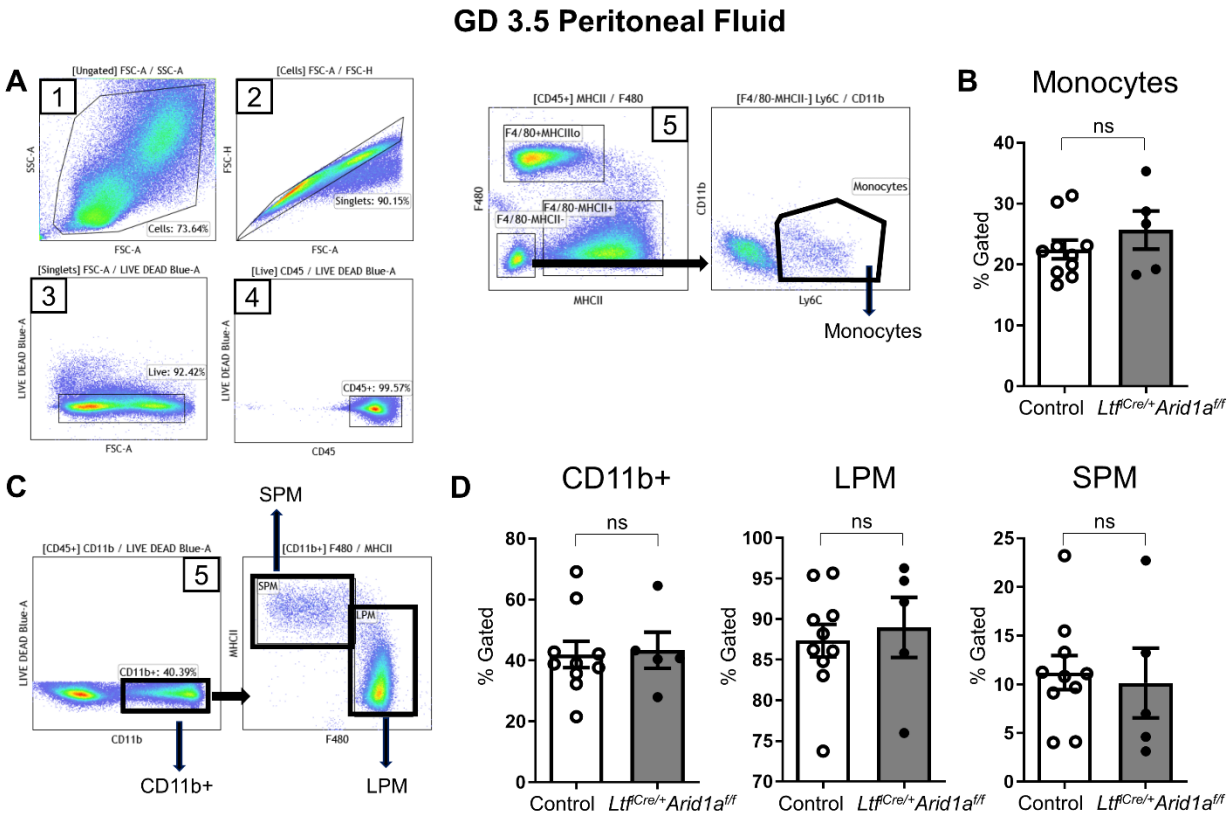

Figure B.3 *No change was detected in proportions of CD11b+ cells, large peritoneal macrophages (LPM), small peritoneal macrophages (SPM), or Ly6C+ monocytes in* $Ltf^{iCre/+}Arid1a^{f/f}$ *peritoneal fluid at GD3.5.* **(A)** The flow gating strategy to identify Ly6C+ monocytes in the peritoneal fluid is shown. **(B)** The % Gated proportion of Ly6C+ monocytes in control (n=14, empty bar) and $Ltf^{iCre/+}Arid1a^{f/f}$ (n=8, grey bar) peritoneal fluid at GD3.5 is shown. **(C)** The flow gating strategy to identify CD11b+ cells, LPM, and SPM in the peritoneal fluid is shown. **(D)** The % Gated proportion of CD11b+ cells (left), LPM (middle), and SPM (right) in control (n=14, empty bar) and $Ltf^{iCre/+}Arid1a^{f/f}$ (n=8, grey bar) peritoneal fluid at GD3.5 is shown. The graphs represent the mean ± SEM. ns, p>0.05.

Table B.1 *SYBR Green primers used for RT-qPCR*

Gene Name	Forward Primer (5' - 3')	Reverse Primer (5' - 3')
Klra7	TCACAGCACACAGGTAGAGG	AGCTGGAAATCTGGCAGGTC
Scara5	AGGAGGGAAAGCCAGGTAGC	CCCCTAGCTTCCCATCATCA
Dio2	CCTCTTCCTGGCGCTCTATG	TTCAGGATTGGAGACGTGCA
Myd88	CCCACTCGCAGTTTGTTGGA	TAGGGGGTCATCAAGGGTGG
Naip1	CAGCCACCTAAAATAAGCTCTGG	GGACCCATGTTGGTCACTCC
Il17rb	CCATCCCTCCAGATGACAAC	TGCTCCTTCCTTGCCTCCAAGTTA
Ccr2	GACAAGCACTTAGACCAGGC	ACCTTCGGAACTTCTCTCCA
Ccr4	CCATTCTGGGGCTACTACGC	ACCAGGTACATCCATGAAACGA
Tnfsf13b	ACACTGCCCAACAATTCCTG	TCGTCTCCGTTGCGTGAAATC
Csf3	GCAGACACAGTGCCTAAGCCA	CATCCAGCTGAAGCAAGTCCA
Il18	GACTCTTGCGTCAACTTCAAGG	CAGGCTGTCTTTTGTCAACGA
Tnf	GCCTCCCTCTCATCAGTTCT	CACTTGGTGGTTTGCTACGA
Il1a	CCATCCAACCCAGATCAGCA	GTTTCTGGCAACTCCTTCAGC
Csf2	CCTGGGCATTGTGGTCTACAG	GGCATGTCATCCAGGAGGTT
Il17a	GGAGAGCTTCATCTGTGTCTCTG	TTGGCCTCAGTGTTTGGACA
Il36a	CTACAGCTTGGGGAAGGGAACATA	CCCTTTAGAGCAGACAGCGATGAA

Table B.2 *Antibodies used for flow cytometry*

Antibody	Conjugate	Clone	Company	Cat. #
CD45	PE Cy5	30-F11	BioLegend	103110
CD11c	PE	N418	BioLegend	117307
CD11b	Percp Cy5.5	M1/70	BioLegend	101228
Ly6C	BV510	HK1.4	BioLegend	128033
Ly6G	BV711	1A8	BioLegend	127643
CD64	FITC	X54-5/7.1	BioLegend	136316
CD24	APC	M1/69	BioLegend	101813
F4/80	APC Cy7	BM8	BioLegend	127117
MHCII	EF450	M5/114.15.2	Invitrogen	48-5321-82
LD	Blue	--	Thermo Fisher	L23105

APPENDIX C

SUPPLEMENTARY MATERIAL FOR CHAPTER 4

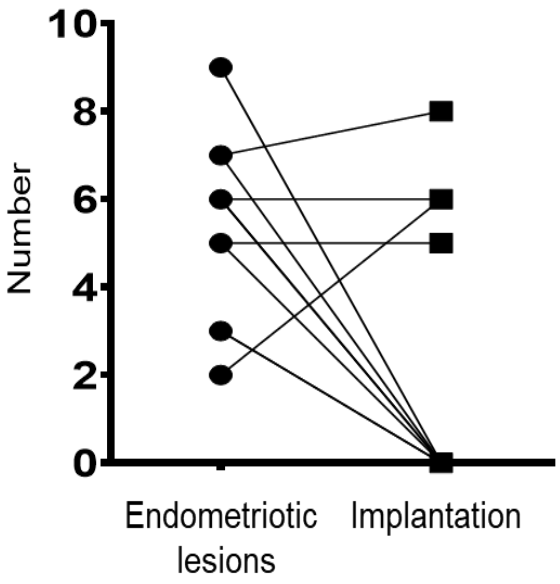

Figure C.1 *No correlation between number of endometriotic lesions and implantation sites at GD 7.5 three months after endometriosis induction (n=11)*. Three independent experiments were performed for correlation study with similar results.

APPENDIX D

SUPPLEMENTARY MATERIAL FOR CHAPTER 5

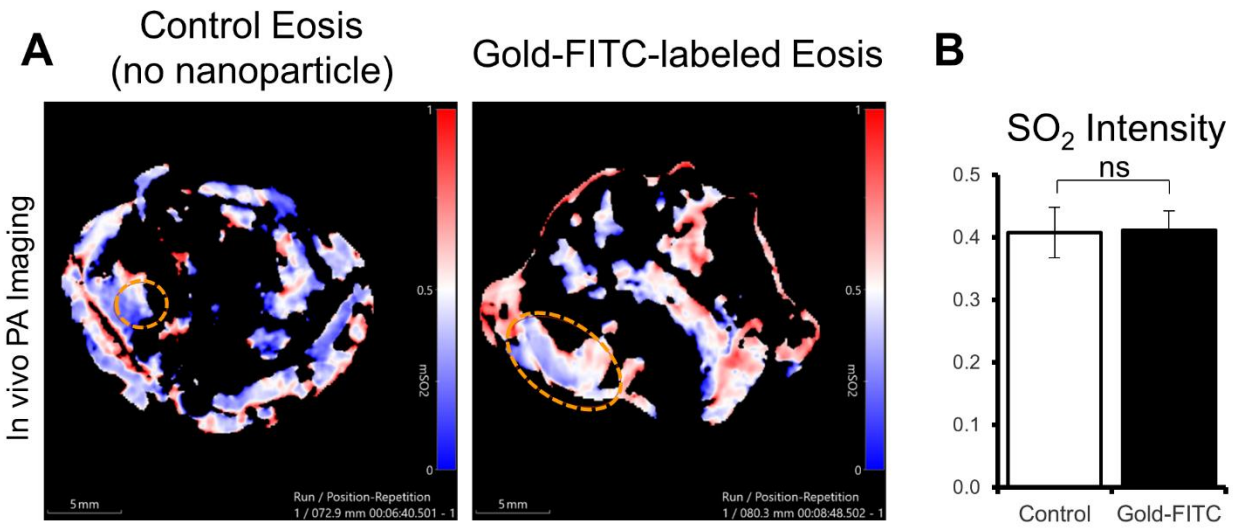

Figure D.1 *In vivo imaging of endometriosis-like lesions based on SO_2.* **(A)** Representative in vivo photoacoustic (PA) images from control endometriosis mice (no nanoparticle; left) and mice with gold-FITC nanoparticle-labeled lesions (right) showing PA signal detection for SO_2 (blue-red) four weeks after induction. The orange segmented circle (left panel) indicates a region containing an unlabeled lesion identified after dissection. The orange segmented circle (right panel) indicates lesion identified by PA signal and confirmed by dissection. **(B)** Mean intensities of SO_2 PA signals from each group. We plotted PA signals from ROIs drawn at the endometriotic lesions of at least three mice. The graphs represent the mean ± SEM (control n=4, gold-FITC nanoparticle n=3; ns, $p>0.05$). Scale bar = 5 mm.

APPENDIX E

AUTHOR CONTRIBUTIONS

The studies that comprise the chapters of this dissertation were collaborative works involving contributions from many talented scientists. This appendix lists the contributions of the dissertation author to each of the included studies that has multiple authors (Chapters 1-5). All authors of each study are listed at the beginning of the appropriate chapter.

Chapter 1: Conceptualization, literature search, figure preparation, and writing of the original draft

Chapter 2: Experimental design, investigation (mouse sample collections, histological analysis, immunohistochemistry, RT-qPCR), data analysis, figure preparation, and writing of the original draft

Chapter 3: Experimental design, data analysis, investigation (mouse sample collections, immunostaining, RT-qPCR, flow cytometry sample preparation), figure preparation, and writing of the original draft

Chapter 4: Data analysis, experiments contributing to the development of the model, and writing

Chapter 5: Experimental design, data analysis, investigation (mouse sample collections, optimization of tissue labeling, photoacoustic imaging, immunostaining, gold enhancement), figure preparation, and writing of the original draft

REFERENCES

REFERENCES

Adamson GD, Kennedy S, and Hummelshoj L. Creating Solutions in Endometriosis: Global Collaboration through the World Endometriosis Research Foundation. *Journal of Endometriosis* 2010: 2; 3-6.

Adesanya OO, Zhou J, Samathanam C, Powell-Braxton L, and Bondy CA. Insulin-like growth factor 1 is required for G2 progression in the estradiol-induced mitotic cycle. *Proc Natl Acad Sci U S A* 1999: 96; 3287-3291.

Agarwal SK, Chapron C, Giudice LC, Laufer MR, Leyland N, Missmer SA, Singh SS, and Taylor HS. Clinical diagnosis of endometriosis: a call to action. *Am J Obstet Gynecol* 2019: 220; 354 e351-354 e312.

Ahn SH, Edwards AK, Singh SS, Young SL, Lessey BA, and Tayade C. IL-17A Contributes to the Pathogenesis of Endometriosis by Triggering Proinflammatory Cytokines and Angiogenic Growth Factors. *J Immunol* 2015: 195; 2591-2600.

Ahn SH, Khalaj K, Young SL, Lessey BA, Koti M, and Tayade C. Immune-inflammation gene signatures in endometriosis patients. *Fertil Steril* 2016: 106; 1420-1431 e1427.

Akinrinmade OA, Chetty S, Daramola AK, Islam MU, Thepen T, and Barth S. CD64: An Attractive Immunotherapeutic Target for M1-type Macrophage Mediated Chronic Inflammatory Diseases. *Biomedicines* 2017: 5.

Al-Sabbagh M, Lam EW, and Brosens JJ. Mechanisms of endometrial progesterone resistance. *Mol Cell Endocrinol* 2012: 358; 208-215.

Angers S and Moon RT. Proximal events in Wnt signal transduction. *Nat Rev Mol Cell Biol* 2009: 10; 468-477.

Anglesio MS, Papadopoulos N, Ayhan A, Nazeran TM, Noe M, Horlings HM, Lum A, Jones S, Senz J, Seckin T, *et al.* Cancer-Associated Mutations in Endometriosis without Cancer. *N Engl J Med* 2017: 376; 1835-1848.

Arguni E, Arima M, Tsuruoka N, Sakamoto A, Hatano M, and Tokuhisa T. JunD/AP-1 and STAT3 are the major enhancer molecules for high Bcl6 expression in germinal center B cells. *Int Immunol* 2006: 18; 1079-1089.

Arici A, Engin O, Attar E, and Olive DL. Modulation of leukemia inhibitory factor gene expression and protein biosynthesis in human endometrium. *J Clin Endocrinol Metab* 1995: 80; 1908-1915.

Arora R, Fries A, Oelerich K, Marchuk K, Sabeur K, Giudice LC, and Laird DJ. Insights from imaging the implanting embryo and the uterine environment in three dimensions. *Development* 2016: 143; 4749-4754.

Ashkar AA, Black GP, Wei Q, He H, Liang L, Head JR, and Croy BA. Assessment of requirements for IL-15 and IFN regulatory factors in uterine NK cell differentiation and function during pregnancy. *J Immunol* 2003: 171; 2937-2944.

Attia GR, Zeitoun K, Edwards D, Johns A, Carr BR, and Bulun SE. Progesterone receptor isoform A but not B is expressed in endometriosis. *J Clin Endocrinol Metab* 2000: 85; 2897-2902.

Balmer NN, Richer JK, Spoelstra NS, Torkko KC, Lyle PL, and Singh M. Steroid receptor coactivator AIB1 in endometrial carcinoma, hyperplasia and normal endometrium: Correlation with clinicopathologic parameters and biomarkers. *Mod Pathol* 2006: 19; 1593-1605.

Barent RL, Nair SC, Carr DC, Ruan Y, Rimerman RA, Fulton J, Zhang Y, and Smith DF. Analysis of FKBP51/FKBP52 chimeras and mutants for Hsp90 binding and association with progesterone receptor complexes. *Mol Endocrinol* 1998: 12; 342-354.

Basak K, Luis Dean-Ben X, Gottschalk S, Reiss M, and Razansky D. Non-invasive determination of murine placental and foetal functional parameters with multispectral optoacoustic tomography. *Light Sci Appl* 2019: 8; 71.

Bayer CL, Wlodarczyk BJ, Finnell RH, and Emelianov SY. Ultrasound-guided spectral photoacoustic imaging of hemoglobin oxygenation during development. *Biomed Opt Express* 2017: 8; 757-763.

Becker CM, Wright RD, Satchi-Fainaro R, Funakoshi T, Folkman J, Kung AL, and D'Amato RJ. A novel noninvasive model of endometriosis for monitoring the efficacy of antiangiogenic therapy. *Am J Pathol* 2006: 168; 2074-2084.

Bedaiwy MA, Dahoud W, Skomorovska-Prokvolit Y, Yi L, Liu JH, Falcone T, Hurd WW, and Mesiano S. Abundance and Localization of Progesterone Receptor Isoforms in Endometrium in Women With and Without Endometriosis and in Peritoneal and Ovarian Endometriotic Implants. *Reprod Sci* 2015: 22; 1153-1161.

Benson GV, Lim H, Paria BC, Satokata I, Dey SK, and Maas RL. Mechanisms of reduced fertility in Hoxa-10 mutant mice: uterine homeosis and loss of maternal Hoxa-10 expression. *Development* 1996: 122; 2687-2696.

Bergqvist A, Ljungberg O, and Skoog L. Immunohistochemical analysis of oestrogen and progesterone receptors in endometriotic tissue and endometrium. *Hum Reprod* 1993: 8; 1915-1922.

Berkley KJ, Rapkin AJ, and Papka RE. The pains of endometriosis. *Science* 2005: 308; 1587-1589.

Bilotas M, Meresman G, Stella I, Sueldo C, and Baranao RI. Effect of aromatase inhibitors on ectopic endometrial growth and peritoneal environment in a mouse model of endometriosis. *Fertil Steril* 2010: 93; 2513-2518.

Bilotas MA, Olivares CN, Ricci AG, Baston JI, Bengochea TS, Meresman GF, and Baranao RI. Interplay between Endometriosis and Pregnancy in a Mouse Model. *PLoS One* 2015: 10; e0124900.

Bjorling DE, Beckman M, Clayton MK, and Wang ZY. Modulation of nerve growth factor in peripheral organs by estrogen and progesterone. *Neuroscience* 2002: 110; 155-167.

Boonyaratanakornkit V, Scott MP, Ribon V, Sherman L, Anderson SM, Maller JL, Miller WT, and Edwards DP. Progesterone receptor contains a proline-rich motif that directly interacts with SH3 domains and activates c-Src family tyrosine kinases. *Mol Cell* 2001: 8; 269-280.

Brighton PJ, Maruyama Y, Fishwick K, Vrljicak P, Tewary S, Fujihara R, Muter J, Lucas ES, Yamada T, Woods L, *et al.* Clearance of senescent decidual cells by uterine natural killer cells in cycling human endometrium. *Elife* 2017: 6.

Broi MGD, Rocha CVJ, Meola J, Martins WP, Carvalho FM, Ferriani RA, and Navarro PA. Expression of PGR, HBEGF, ITGAV, ITGB3 and SPP1 genes in eutopic endometrium of infertile women with endometriosis during the implantation window: a pilot study. *JBRA Assist Reprod* 2017: 21; 196-202.

Brosens JJ and Gellersen B. Death or survival--progesterone-dependent cell fate decisions in the human endometrial stroma. *J Mol Endocrinol* 2006: 36; 389-398.

Brown DM, Lee HC, Liu S, Quick CM, Fernandes LM, Simmen FA, Tsai SJ, and Simmen RCM. Notch-1 Signaling Activation and Progesterone Receptor Expression in Ectopic Lesions of Women With Endometriosis. *J Endocr Soc* 2018: 2; 765-778.

Brown J, Pan A, and Hart RJ. Gonadotrophin-releasing hormone analogues for pain associated with endometriosis. *Cochrane Database Syst Rev* 2010; CD008475.

Bruner-Tran KL, Mokshagundam S, Herington JL, Ding T, and Osteen KG. Rodent Models of Experimental Endometriosis: Identifying Mechanisms of Disease and Therapeutic Targets. *Curr Womens Health Rev* 2018: 14; 173-188.

Brunty S, Ray Wright K, Mitchell B, and Santanam N. Peritoneal Modulators of EZH2-miR-155 Cross-Talk in Endometriosis. *Int J Mol Sci* 2021: 22.

Bukulmez O, Hardy DB, Carr BR, Word RA, and Mendelson CR. Inflammatory status influences aromatase and steroid receptor expression in endometriosis. *Endocrinology* 2008: 149; 1190-1204.

Bulun SE. Endometriosis. *N Engl J Med* 2009: 360; 268-279.

Bulun SE, Yilmaz BD, Sison C, Miyazaki K, Bernardi L, Liu S, Kohlmeier A, Yin P, Milad M, and Wei J. Endometriosis. *Endocr Rev* 2019.

Burney RO, Talbi S, Hamilton AE, Vo KC, Nyegaard M, Nezhat CR, Lessey BA, and Giudice LC. Gene expression analysis of endometrium reveals progesterone resistance and candidate susceptibility genes in women with endometriosis. *Endocrinology* 2007: 148; 3814-3826.

Carter JE. Combined hysteroscopic and laparoscopic findings in patients with chronic pelvic pain. *J Am Assoc Gynecol Laparosc* 1994: 2; 43-47.

Casper RF. Progestin-only pills may be a better first-line treatment for endometriosis than combined estrogen-progestin contraceptive pills. *Fertil Steril* 2017: 107; 533-536.

Catalano RD, Johnson MH, Campbell EA, Charnock-Jones DS, Smith SK, and Sharkey AM. Inhibition of Stat3 activation in the endometrium prevents implantation: a nonsteroidal approach to contraception. *Proc Natl Acad Sci U S A* 2005: 102; 8585-8590.

Centore RC, Sandoval GJ, Soares LMM, Kadoch C, and Chan HM. Mammalian SWI/SNF Chromatin Remodeling Complexes: Emerging Mechanisms and Therapeutic Strategies. *Trends Genet* 2020: 36; 936-950.

Cetel NS, Rivier J, Vale W, and Yen SS. The dynamics of gonadotropin inhibition in women induced by an antagonistic analog of gonadotropin-releasing hormone. *J Clin Endocrinol Metab* 1983: 57; 62-65.

Cha J, Sun X, and Dey SK. Mechanisms of implantation: strategies for successful pregnancy. *Nat Med* 2012: 18; 1754-1767.

Chambers M, Rees A, Cronin JG, Nair M, Jones N, and Thornton CA. Macrophage Plasticity in Reproduction and Environmental Influences on Their Function. *Front Immunol* 2020: 11; 607328.

Chang LC, Chiang YF, Chen HY, Huang YJ, Liu AC, and Hsia SM. The Potential Effect of Fucoidan on Inhibiting Epithelial-to-Mesenchymal Transition, Proliferation, and Increase in Apoptosis for Endometriosis Treatment: In Vivo and In Vitro Study. *Biomedicines* 2020: 8.

Chen JR, Cheng JG, Shatzer T, Sewell L, Hernandez L, and Stewart CL. Leukemia inhibitory factor can substitute for nidatory estrogen and is essential to inducing a receptive uterus for implantation but is not essential for subsequent embryogenesis. *Endocrinology* 2000: 141; 4365-4372.

Chen YS, Frey W, Kim S, Kruizinga P, Homan K, and Emelianov S. Silica-coated gold nanorods as photoacoustic signal nanoamplifiers. *Nano Lett* 2011: 11; 348-354.

Chene G, Ouellet V, Rahimi K, Barres V, Provencher D, and Mes-Masson AM. The ARID1A pathway in ovarian clear cell and endometrioid carcinoma, contiguous endometriosis, and benign endometriosis. *Int J Gynaecol Obstet* 2015: 130; 27-30.

Cheng JG, Chen JR, Hernandez L, Alvord WG, and Stewart CL. Dual control of LIF expression and LIF receptor function regulate Stat3 activation at the onset of uterine receptivity and embryo implantation. *Proc Natl Acad Sci U S A* 2001: 98; 8680-8685.

Cho YJ, Lee JE, Park MJ, O'Malley BW, and Han SJ. Bufalin suppresses endometriosis progression by inducing pyroptosis and apoptosis. *J Endocrinol* 2018: 237; 255-269.

Collins MK, Tay CS, and Erlebacher A. Dendritic cell entrapment within the pregnant uterus inhibits immune surveillance of the maternal/fetal interface in mice. *J Clin Invest* 2009: 119; 2062-2073.

Colon-Caraballo M, Garcia M, Mendoza A, and Flores I. Human Endometriosis Tissue Microarray Reveals Site-specific Expression of Estrogen Receptors, Progesterone Receptor, and Ki67. *Appl Immunohistochem Mol Morphol* 2018.

Cooke PS, Buchanan DL, Young P, Setiawan T, Brody J, Korach KS, Taylor J, Lubahn DB, and Cunha GR. Stromal estrogen receptors mediate mitogenic effects of estradiol on uterine epithelium. *Proc Natl Acad Sci U S A* 1997: 94; 6535-6540.

Couse JF, Curtis SW, Washburn TF, Lindzey J, Golding TS, Lubahn DB, Smithies O, and Korach KS. Analysis of transcription and estrogen insensitivity in the female mouse after targeted disruption of the estrogen receptor gene. *Mol Endocrinol* 1995: 9; 1441-1454.

Crosignani PG, Luciano A, Ray A, and Bergqvist A. Subcutaneous depot medroxyprogesterone acetate versus leuprolide acetate in the treatment of endometriosis-associated pain. *Hum Reprod* 2006: 21; 248-256.

Croy BA, Zhang J, Tayade C, Colucci F, Yadi H, and Yamada AT. Analysis of uterine natural killer cells in mice. *Methods Mol Biol* 2010: 612; 465-503.

Cummings AM and Metcalf JL. Induction of endometriosis in mice: a new model sensitive to estrogen. *Reprod Toxicol* 1995: 9; 233-238.

Cummings AM, Metcalf JL, and Birnbaum L. Promotion of endometriosis by 2,3,7,8-tetrachlorodibenzo-p-dioxin in rats and mice: time-dose dependence and species comparison. *Toxicol Appl Pharmacol* 1996: 138; 131-139.

Curtis Hewitt S, Goulding EH, Eddy EM, and Korach KS. Studies using the estrogen receptor alpha knockout uterus demonstrate that implantation but not decidualization-associated signaling is estrogen dependent. *Biol Reprod* 2002: 67; 1268-1277.

Curtis SW, Clark J, Myers P, and Korach KS. Disruption of estrogen signaling does not prevent progesterone action in the estrogen receptor alpha knockout mouse uterus. *Proc Natl Acad Sci U S A* 1999: 96; 3646-3651.

Daftary GS, Troy PJ, Bagot CN, Young SL, and Taylor HS. Direct regulation of beta3-integrin subunit gene expression by HOXA10 in endometrial cells. *Mol Endocrinol* 2002: 16; 571-579.

Daikoku T, Ogawa Y, Terakawa J, Ogawa A, DeFalco T, and Dey SK. Lactoferrin-iCre: a new mouse line to study uterine epithelial gene function. *Endocrinology* 2014: 155; 2718-2724.

Daikoku T, Song H, Guo Y, Riesewijk A, Mosselman S, Das SK, and Dey SK. Uterine Msx-1 and Wnt4 signaling becomes aberrant in mice with the loss of leukemia inhibitory factor or Hoxa-10: evidence for a novel cytokine-homeobox-Wnt signaling in implantation. *Mol Endocrinol* 2004: 18; 1238-1250.

de Ziegler D, Borghese B, and Chapron C. Endometriosis and infertility: pathophysiology and management. *Lancet* 2010: 376; 730-738.

Deshmane SL, Kremlev S, Amini S, and Sawaya BE. Monocyte chemoattractant protein-1 (MCP-1): an overview. *J Interferon Cytokine Res* 2009: 29; 313-326.

Dimitriadis E, Stoikos C, Stafford-Bell M, Clark I, Paiva P, Kovacs G, and Salamonsen LA. Interleukin-11, IL-11 receptoralpha and leukemia inhibitory factor are dysregulated in endometrium of infertile women with endometriosis during the implantation window. *J Reprod Immunol* 2006: 69; 53-64.

Ding Y, Zhang M, Lang J, Leng J, Ren Q, Yang J, and Li C. In vivo study of endometriosis in mice by photoacoustic microscopy. *J Biophotonics* 2015: 8; 94-101.

Dobin A, Davis CA, Schlesinger F, Drenkow J, Zaleski C, Jha S, Batut P, Chaisson M, and Gingeras TR. STAR: ultrafast universal RNA-seq aligner. *Bioinformatics* 2013: 29; 15-21.

Dorning A, Dhami P, Panir K, Hogg C, Park E, Ferguson GD, Hargrove D, Karras J, Horne AW, and Greaves E. Bioluminescent imaging in induced mouse models of endometriosis reveals differences in four model variations. *Dis Model Mech* 2021: 14.

Dosiou C and Giudice LC. Natural killer cells in pregnancy and recurrent pregnancy loss: endocrine and immunologic perspectives. *Endocr Rev* 2005: 26; 44-62.

Dunselman GA, Vermeulen N, Becker C, Calhaz-Jorge C, D'Hooghe T, De Bie B, Heikinheimo O, Horne AW, Kiesel L, Nap A, *et al.* ESHRE guideline: management of women with endometriosis. *Hum Reprod* 2014: 29; 400-412.

Dyson MT, Roqueiro D, Monsivais D, Ercan CM, Pavone ME, Brooks DC, Kakinuma T, Ono M, Jafari N, Dai Y, *et al.* Genome-wide DNA methylation analysis predicts an epigenetic switch for GATA factor expression in endometriosis. *PLoS Genet* 2014: 10; e1004158.

Eskenazi B and Warner ML. Epidemiology of endometriosis. *Obstet Gynecol Clin North Am* 1997: 24; 235-258.

Eswarakumar VP, Lax I, and Schlessinger J. Cellular signaling by fibroblast growth factor receptors. *Cytokine Growth Factor Rev* 2005: 16; 139-149.

Evans-Hoeker E, Lessey BA, Jeong JW, Savaris RF, Palomino WA, Yuan L, Schammel DP, and Young SL. Endometrial BCL6 Overexpression in Eutopic Endometrium of Women With Endometriosis. *Reprod Sci* 2016: 23; 1234-1241.

Fahnenstich J, Nandy A, Milde-Langosch K, Schneider-Merck T, Walther N, and Gellersen B. Promyelocytic leukaemia zinc finger protein (PLZF) is a glucocorticoid- and progesterone-induced transcription factor in human endometrial stromal cells and myometrial smooth muscle cells. *Mol Hum Reprod* 2003: 9; 611-623.

Falconer H, Sundqvist J, Xu H, Vodolazkaia A, Fassbender A, Kyama C, Bokor A, and D'Hooghe TM. Analysis of common variations in tumor-suppressor genes on chr1p36 among Caucasian women with endometriosis. *Gynecol Oncol* 2012: 127; 398-402.

Fang Z, Yang S, Gurates B, Tamura M, Simpson E, Evans D, and Bulun SE. Genetic or enzymatic disruption of aromatase inhibits the growth of ectopic uterine tissue. *J Clin Endocrinol Metab* 2002: 87; 3460-3466.

Fang Z, Yang S, Lydon JP, DeMayo F, Tamura M, Gurates B, and Bulun SE. Intact progesterone receptors are essential to counteract the proliferative effect of estradiol in a genetically engineered mouse model of endometriosis. *Fertil Steril* 2004: 82; 673-678.

Fattori V, Franklin NS, Gonzalez-Cano R, Peterse D, Ghalali A, Madrian E, Verri WA, Jr., Andrews N, Woolf CJ, and Rogers MS. Nonsurgical mouse model of endometriosis-associated pain that responds to clinically active drugs. *Pain* 2020: 161; 1321-1331.

Fazleabas AT. A baboon model for inducing endometriosis. *Methods Mol Med* 2006: 121; 95-99.

Ferrero H, Buigues A, Martinez J, Simon C, Pellicer A, and Gomez R. A novel homologous model for noninvasive monitoring of endometriosis progression. *Biol Reprod* 2017: 96; 302-312.

Ferrero S, Evangelisti G, and Barra F. Current and emerging treatment options for endometriosis. *Expert Opin Pharmacother* 2018: 19; 1109-1125.

Filant J, Lydon JP, and Spencer TE. Integrated chromatin immunoprecipitation sequencing and microarray analysis identifies FOXA2 target genes in the glands of the mouse uterus. *FASEB J* 2014: 28; 230-243.

Finn CA and Martin L. Endocrine control of the timing of endometrial sensitivity to a decidual stimulus. *Biol Reprod* 1972: 7; 82-86.

Fleisch MC, Chou YC, Cardiff RD, Asaithambi A, and Shyamala G. Overexpression of progesterone receptor A isoform in mice leads to endometrial hyperproliferation, hyperplasia and atypia. *Mol Hum Reprod* 2009: 15; 241-249.

Flores VA, Vanhie A, Dang T, and Taylor HS. Progesterone Receptor Status Predicts Response to Progestin Therapy in Endometriosis. *J Clin Endocrinol Metab* 2018: 103; 4561-4568.

Foster WG, Ruka MP, Gareau P, Foster RA, Janzen EG, and Yang JZ. Morphologic characteristics of endometriosis in the mouse model: application to toxicology. *Can J Physiol Pharmacol* 1997: 75; 1188-1196.

Franco HL, Dai D, Lee KY, Rubel CA, Roop D, Boerboom D, Jeong JW, Lydon JP, Bagchi IC, Bagchi MK, *et al.* WNT4 is a key regulator of normal postnatal uterine development and progesterone signaling during embryo implantation and decidualization in the mouse. *FASEB J* 2011: 25; 1176-1187.

Franco HL, Rubel CA, Large MJ, Wetendorf M, Fernandez-Valdivia R, Jeong JW, Spencer TE, Behringer RR, Lydon JP, and Demayo FJ. Epithelial progesterone receptor exhibits pleiotropic roles in uterine development and function. *FASEB J* 2012: 26; 1218-1227.

Frank DA. STAT signaling in the pathogenesis and treatment of cancer. *Mol Med* 1999: 5; 432-456.

Fu L, Osuga Y, Morimoto C, Hirata T, Hirota Y, Yano T, and Taketani Y. Dienogest inhibits BrdU uptake with G0/G1 arrest in cultured endometriotic stromal cells. *Fertil Steril* 2008: 89; 1344-1347.

Gao J, Mazella J, Suwanichkul A, Powell DR, and Tseng L. Activation of the insulin-like growth factor binding protein-1 promoter by progesterone receptor in decidualized human endometrial stromal cells. *Mol Cell Endocrinol* 1999: 153; 11-17.

Gao X, Tate P, Hu P, Tjian R, Skarnes WC, and Wang Z. ES cell pluripotency and germ-layer formation require the SWI/SNF chromatin remodeling component BAF250a. *Proc Natl Acad Sci U S A* 2008: 105; 6656-6661.

Gellersen B and Brosens JJ. Cyclic decidualization of the human endometrium in reproductive health and failure. *Endocr Rev* 2014: 35; 851-905.

Giudice LC and Kao LC. Endometriosis. *Lancet* 2004: 364; 1789-1799.

Golson ML and Kaestner KH. Fox transcription factors: from development to disease. *Development* 2016: 143; 4558-4570.

Greaves E, Collins F, Esnal-Zufiaurre A, Giakoumelou S, Horne AW, and Saunders PT. Estrogen receptor (ER) agonists differentially regulate neuroangiogenesis in peritoneal endometriosis via the repellent factor SLIT3. *Endocrinology* 2014: 155; 4015-4026.

Greaves E, Cousins FL, Murray A, Esnal-Zufiaurre A, Fassbender A, Horne AW, and Saunders PT. A novel mouse model of endometriosis mimics human phenotype and reveals insights into the inflammatory contribution of shed endometrium. *Am J Pathol* 2014: 184; 1930-1939.

Greaves E, Grieve K, Horne AW, and Saunders PT. Elevated peritoneal expression and estrogen regulation of nociceptive ion channels in endometriosis. *J Clin Endocrinol Metab* 2014: 99; E1738-1743.

Greaves E, Temp J, Esnal-Zufiurre A, Mechsner S, Horne AW, and Saunders PT. Estradiol is a critical mediator of macrophage-nerve cross talk in peritoneal endometriosis. *Am J Pathol* 2015: 185; 2286-2297.

Gregory CW, Wilson EM, Apparao KB, Lininger RA, Meyer WR, Kowalik A, Fritz MA, and Lessey BA. Steroid receptor coactivator expression throughout the menstrual cycle in normal and abnormal endometrium. *J Clin Endocrinol Metab* 2002: 87; 2960-2966.

Grimaldi G, Christian M, Steel JH, Henriet P, Poutanen M, and Brosens JJ. Down-regulation of the histone methyltransferase EZH2 contributes to the epigenetic programming of decidualizing human endometrial stromal cells. *Mol Endocrinol* 2011: 25; 1892-1903.

Groves AM, Johnston CJ, Williams JP, and Finkelstein JN. Role of Infiltrating Monocytes in the Development of Radiation-Induced Pulmonary Fibrosis. *Radiat Res* 2018: 189; 300-311.

Grummer R. Animal models in endometriosis research. *Hum Reprod Update* 2006: 12; 641-649.

Gu Z, Eils R, and Schlesner M. Complex heatmaps reveal patterns and correlations in multidimensional genomic data. *Bioinformatics* 2016: 32; 2847-2849.

Gu Z, Gu L, Eils R, Schlesner M, and Brors B. circlize Implements and enhances circular visualization in R. *Bioinformatics* 2014: 30; 2811-2812.

Guerriero S, Spiga S, Ajossa S, Peddes C, Perniciano M, Soggiu B, De Cecco CN, Laghi A, Melis GB, and Saba L. Role of imaging in the management of endometriosis. *Minerva Ginecol* 2013: 65; 143-166.

Guimaraes-Young A, Neff T, Dupuy AJ, and Goodheart MJ. Conditional deletion of Sox17 reveals complex effects on uterine adenogenesis and function. *Dev Biol* 2016: 414; 219-227.

Haider S and Knofler M. Human tumour necrosis factor: physiological and pathological roles in placenta and endometrium. *Placenta* 2009: 30; 111-123.

Hamilton JA. GM-CSF-Dependent Inflammatory Pathways. *Front Immunol* 2019: 10; 2055.

Han SJ, DeMayo FJ, Xu J, Tsai SY, Tsai MJ, and O'Malley BW. Steroid receptor coactivator (SRC)-1 and SRC-3 differentially modulate tissue-specific activation functions of the progesterone receptor. *Mol Endocrinol* 2006: 20; 45-55.

Han SJ, Hawkins SM, Begum K, Jung SY, Kovanci E, Qin J, Lydon JP, DeMayo FJ, and O'Malley BW. A new isoform of steroid receptor coactivator-1 is crucial for pathogenic progression of endometriosis. *Nat Med* 2012: 18; 1102-1111.

Han SJ, Jeong J, Demayo FJ, Xu J, Tsai SY, Tsai MJ, and O'Malley BW. Dynamic cell type specificity of SRC-1 coactivator in modulating uterine progesterone receptor function in mice. *Mol Cell Biol* 2005: 25; 8150-8165.

Han SJ, Jung SY, Wu SP, Hawkins SM, Park MJ, Kyo S, Qin J, Lydon JP, Tsai SY, Tsai MJ, *et al.* Estrogen Receptor beta Modulates Apoptosis Complexes and the Inflammasome to Drive the Pathogenesis of Endometriosis. *Cell* 2015: 163; 960-974.

Han SJ and O'Malley BW. The dynamics of nuclear receptors and nuclear receptor coregulators in the pathogenesis of endometriosis. *Hum Reprod Update* 2014: 20; 467-484.

Hantak AM, Bagchi IC, and Bagchi MK. Role of uterine stromal-epithelial crosstalk in embryo implantation. *Int J Dev Biol* 2014: 58; 139-146.

Harada T, Kosaka S, Elliesen J, Yasuda M, Ito M, and Momoeda M. Ethinylestradiol 20 mug/drospirenone 3 mg in a flexible extended regimen for the management of endometriosis-associated pelvic pain: a randomized controlled trial. *Fertil Steril* 2017: 108; 798-805.

Harada T, Momoeda M, Taketani Y, Aso T, Fukunaga M, Hagino H, and Terakawa N. Dienogest is as effective as intranasal buserelin acetate for the relief of pain symptoms associated with endometriosis--a randomized, double-blind, multicenter, controlled trial. *Fertil Steril* 2009: 91; 675-681.

Harada T, Momoeda M, Taketani Y, Hoshiai H, and Terakawa N. Low-dose oral contraceptive pill for dysmenorrhea associated with endometriosis: a placebo-controlled, double-blind, randomized trial. *Fertil Steril* 2008: 90; 1583-1588.

Hawkins SM, Creighton CJ, Han DY, Zariff A, Anderson ML, Gunaratne PH, and Matzuk MM. Functional microRNA involved in endometriosis. *Mol Endocrinol* 2011: 25; 821-832.

Hayashi A, Tanabe A, Kawabe S, Hayashi M, Yuguchi H, Yamashita Y, Okuda K, and Ohmichi M. Dienogest increases the progesterone receptor isoform B/A ratio in patients with ovarian endometriosis. *J Ovarian Res* 2012: 5; 31.

Haydardedeoglu B and Zeyneloglu HB. The impact of endometriosis on fertility. *Womens Health (Lond)* 2015: 11; 619-623.

He S, Wu Z, Tian Y, Yu Z, Yu J, Wang X, Li J, Liu B, and Xu Y. Structure of nucleosome-bound human BAF complex. *Science* 2020: 367; 875-881.

Hewitt SC, Deroo BJ, Hansen K, Collins J, Grissom S, Afshari CA, and Korach KS. Estrogen receptor-dependent genomic responses in the uterus mirror the biphasic physiological response to estrogen. *Mol Endocrinol* 2003: 17; 2070-2083.

Hewitt SC and Korach KS. Estrogen Receptors: New Directions in the New Millennium. *Endocr Rev* 2018: 39; 664-675.

Hewitt SC, Li L, Grimm SA, Chen Y, Liu L, Li Y, Bushel PR, Fargo D, and Korach KS. Research resource: whole-genome estrogen receptor alpha binding in mouse uterine tissue revealed by ChIP-seq. *Mol Endocrinol* 2012: 26; 887-898.

Hewitt SC, Lierz SL, Garcia M, Hamilton KJ, Gruzdev A, Grimm SA, Lydon JP, DeMayo FJ, and Korach KS. A distal super enhancer mediates estrogen-dependent mouse uterine-specific gene transcription of Insulin-like growth factor 1 (Igf1). *J Biol Chem* 2019.

Hewitt SC, Winuthayanon W, and Korach KS. What's new in estrogen receptor action in the female reproductive tract. *J Mol Endocrinol* 2016: 56; R55-71.

Hirate Y, Suzuki H, Kawasumi M, Takase HM, Igarashi H, Naquet P, Kanai Y, and Kanai-Azuma M. Mouse Sox17 haploinsufficiency leads to female subfertility due to impaired implantation. *Sci Rep* 2016: 6; 24171.

Hirota Y, Tranguch S, Daikoku T, Hasegawa A, Osuga Y, Taketani Y, and Dey SK. Deficiency of immunophilin FKBP52 promotes endometriosis. *Am J Pathol* 2008: 173; 1747-1757.

Hogg C, Panir K, Dhami P, Rosser M, Mack M, Soong D, Pollard JW, Jenkins SJ, Horne AW, and Greaves E. Macrophages inhibit and enhance endometriosis depending on their origin. *Proc Natl Acad Sci U S A* 2021: 118.

Holoch KJ and Lessey BA. Endometriosis and infertility. *Clin Obstet Gynecol* 2010: 53; 429-438.

Hou Z, Mamillapalli R, and Taylor HS. Predictive biomarkers may allow precision therapy of endometriosis. *Journal of Endometriosis and Pelvic Pain Disorders* 2017: 9; 279-285.

Hsu YW, Chen HY, Chiang YF, Chang LC, Lin PH, and Hsia SM. The effects of isoliquiritigenin on endometriosis in vivo and in vitro study. *Phytomedicine* 2020: 77; 153214.

Huyen DV and Bany BM. Evidence for a conserved function of heart and neural crest derivatives expressed transcript 2 in mouse and human decidualization. *Reproduction* 2011: 142; 353-368.

Igarashi TM, Bruner-Tran KL, Yeaman GR, Lessey BA, Edwards DP, Eisenberg E, and Osteen KG. Reduced expression of progesterone receptor-B in the endometrium of women with endometriosis and in cocultures of endometrial cells exposed to 2,3,7,8-tetrachlorodibenzo-p-dioxin. *Fertil Steril* 2005: 84; 67-74.

Ignatiadis N, Klaus B, Zaugg JB, and Huber W. Data-driven hypothesis weighting increases detection power in genome-scale multiple testing. *Nat Methods* 2016: 13; 577-580.

Irizarry RA, Hobbs B, Collin F, Beazer-Barclay YD, Antonellis KJ, Scherf U, and Speed TP. Exploration, normalization, and summaries of high density oligonucleotide array probe level data. *Biostatistics* 2003: 4; 249-264.

Ishibashi H, Suzuki T, Suzuki S, Moriya T, Kaneko C, Takizawa T, Sunamori M, Handa M, Kondo T, and Sasano H. Sex steroid hormone receptors in human thymoma. *J Clin Endocrinol Metab* 2003: 88; 2309-2317.

Jackson KS, Brudney A, Hastings JM, Mavrogianis PA, Kim JJ, and Fazleabas AT. The altered distribution of the steroid hormone receptors and the chaperone immunophilin FKBP52 in a baboon model of endometriosis is associated with progesterone resistance during the window of uterine receptivity. *Reprod Sci* 2007: 14; 137-150.

Jeong JW, Kwak I, Lee KY, Kim TH, Large MJ, Stewart CL, Kaestner KH, Lydon JP, and DeMayo FJ. Foxa2 is essential for mouse endometrial gland development and fertility. *Biol Reprod* 2010: 83; 396-403.

Jeong JW, Lee HS, Franco HL, Broaddus RR, Taketo MM, Tsai SY, Lydon JP, and DeMayo FJ. beta-catenin mediates glandular formation and dysregulation of beta-catenin induces hyperplasia formation in the murine uterus. *Oncogene* 2009: 28; 31-40.

Jeong JW, Lee HS, Lee KY, White LD, Broaddus RR, Zhang YW, Vande Woude GF, Giudice LC, Young SL, Lessey BA, *et al.* Mig-6 modulates uterine steroid hormone responsiveness and exhibits altered expression in endometrial disease. *Proc Natl Acad Sci U S A* 2009: 106; 8677-8682.

Jeong JW, Lee KY, Han SJ, Aronow BJ, Lydon JP, O'Malley BW, and DeMayo FJ. The p160 steroid receptor coactivator 2, SRC-2, regulates murine endometrial function and regulates progesterone-independent and -dependent gene expression. *Endocrinology* 2007: 148; 4238-4250.

Jeong JW, Lee KY, Kwak I, White LD, Hilsenbeck SG, Lydon JP, and DeMayo FJ. Identification of murine uterine genes regulated in a ligand-dependent manner by the progesterone receptor. *Endocrinology* 2005: 146; 3490-3505.

Jokerst JV, Cole AJ, Van de Sompel D, and Gambhir SS. Gold nanorods for ovarian cancer detection with photoacoustic imaging and resection guidance via Raman imaging in living mice. *ACS Nano* 2012: 6; 10366-10377.

Jokerst JV, Thangaraj M, Kempen PJ, Sinclair R, and Gambhir SS. Photoacoustic imaging of mesenchymal stem cells in living mice via silica-coated gold nanorods. *ACS Nano* 2012: 6; 5920-5930.

Jolicoeur C, Boutouil M, Drouin R, Paradis I, Lemay A, and Akoum A. Increased expression of monocyte chemotactic protein-1 in the endometrium of women with endometriosis. *Am J Pathol* 1998: 152; 125-133.

Joshi NR, Kohan-Ghadr HR, Roqueiro DS, Yoo JY, Fru K, Hestermann E, Yuan L, Ho SM, Jeong JW, Young SL, *et al.* Genetic and epigenetic changes in the eutopic endometrium of women with endometriosis: association with decreased endometrial alphavbeta3 integrin expression. *Mol Hum Reprod* 2021: 27.

Joshi NR, Miyadahira EH, Afshar Y, Jeong JW, Young SL, Lessey BA, Serafini PC, and Fazleabas AT. Progesterone Resistance in Endometriosis Is Modulated by the Altered Expression of MicroRNA-29c and FKBP4. *J Clin Endocrinol Metab* 2017: 102; 141-149.

Juhasz-Boss I, Fischer C, Lattrich C, Skrzypczak M, Malik E, Ortmann O, and Treeck O. Endometrial expression of estrogen receptor beta and its splice variants in patients with and without endometriosis. *Arch Gynecol Obstet* 2011: 284; 885-891.

Kao LC, Germeyer A, Tulac S, Lobo S, Yang JP, Taylor RN, Osteen K, Lessey BA, and Giudice LC. Expression profiling of endometrium from women with endometriosis reveals candidate genes for disease-based implantation failure and infertility. *Endocrinology* 2003: 144; 2870-2881.

Kastner P, Krust A, Turcotte B, Stropp U, Tora L, Gronemeyer H, and Chambon P. Two distinct estrogen-regulated promoters generate transcripts encoding the two functionally different human progesterone receptor forms A and B. *EMBO J* 1990: 9; 1603-1614.

Kato N, Iwase A, Ishida C, Nagai T, Mori M, Bayasula, Nakamura T, Osuka S, Ganiyeva U, Qin Y, *et al*. Upregulation of Fibroblast Growth Factors Caused by Heart and Neural Crest Derivatives Expressed 2 Suppression in Endometriotic Cells: A Possible Therapeutic Target in Endometriosis. *Reprod Sci* 2018; 1933719118802053.

Kelleher AM, Behura SK, Burns GW, Young SL, DeMayo FJ, and Spencer TE. Integrative analysis of the forkhead box A2 (FOXA2) cistrome for the human endometrium. *FASEB J* 2019: 33; 8543-8554.

Kelleher AM, DeMayo FJ, and Spencer TE. Uterine Glands: Developmental Biology and Functional Roles in Pregnancy. *Endocr Rev* 2019: 40; 1424-1445.

Kelleher AM, Milano-Foster J, Behura SK, and Spencer TE. Uterine glands coordinate on-time embryo implantation and impact endometrial decidualization for pregnancy success. *Nat Commun* 2018: 9; 2435.

Kelleher AM, Peng W, Pru JK, Pru CA, DeMayo FJ, and Spencer TE. Forkhead box a2 (FOXA2) is essential for uterine function and fertility. *Proc Natl Acad Sci U S A* 2017: 114; E1018-E1026.

Kettel LM, Murphy AA, Morales AJ, Ulmann A, Baulieu EE, and Yen SS. Treatment of endometriosis with the antiprogesterone mifepristone (RU486). *Fertil Steril* 1996: 65; 23-28.

Kettel LM, Murphy AA, Morales AJ, and Yen SS. Clinical efficacy of the antiprogesterone RU486 in the treatment of endometriosis and uterine fibroids. *Hum Reprod* 1994: 9 Suppl 1; 116-120.

Kim BG, Yoo JY, Kim TH, Shin JH, Langenheim JF, Ferguson SD, Fazleabas AT, Young SL, Lessey BA, and Jeong JW. Aberrant activation of signal transducer and activator of transcription-3 (STAT3) signaling in endometriosis. *Hum Reprod* 2015: 30; 1069-1078.

Kim HI, Kim TH, Yoo JY, Young SL, Lessey BA, Ku BJ, and Jeong JW. ARID1A and PGR proteins interact in the endometrium and reveal a positive correlation in endometriosis. *Biochem Biophys Res Commun* 2021: 550; 151-157.

Kim HR, Kim YS, Yoon JA, Lyu SW, Shin H, Lim HJ, Hong SH, Lee DR, and Song H. Egr1 is rapidly and transiently induced by estrogen and bisphenol A via activation of nuclear estrogen receptor-dependent ERK1/2 pathway in the uterus. *Reprod Toxicol* 2014: 50; 60-67.

Kim HR, Kim YS, Yoon JA, Yang SC, Park M, Seol DW, Lyu SW, Jun JH, Lim HJ, Lee DR, *et al.* Estrogen induces EGR1 to fine-tune its actions on uterine epithelium by controlling PR signaling for successful embryo implantation. *FASEB J* 2018: 32; 1184-1195.

Kim JJ, Taylor HS, Lu Z, Ladhani O, Hastings JM, Jackson KS, Wu Y, Guo SW, and Fazleabas AT. Altered expression of HOXA10 in endometriosis: potential role in decidualization. *Mol Hum Reprod* 2007: 13; 323-332.

Kim T, Lemaster JE, Chen F, Li J, and Jokerst JV. Photoacoustic Imaging of Human Mesenchymal Stem Cells Labeled with Prussian Blue-Poly(l-lysine) Nanocomplexes. *ACS Nano* 2017: 11; 9022-9032.

Kim T, Zhang Q, Li J, Zhang L, and Jokerst JV. A Gold/Silver Hybrid Nanoparticle for Treatment and Photoacoustic Imaging of Bacterial Infection. *ACS Nano* 2018: 12; 5615-5625.

Kim TH, Yoo JY, Choi KC, Shin JH, Leach RE, Fazleabas AT, Young SL, Lessey BA, Yoon HG, and Jeong JW. Loss of HDAC3 results in nonreceptive endometrium and female infertility. *Sci Transl Med* 2019: 11.

Kim TH, Yoo JY, Kim HI, Gilbert J, Ku BJ, Li J, Mills GB, Broaddus RR, Lydon JP, Lim JM, *et al.* Mig-6 suppresses endometrial cancer associated with Pten deficiency and ERK activation. *Cancer Res* 2014: 74; 7371-7382.

Kim TH, Yoo JY, Wang Z, Lydon JP, Khatri S, Hawkins SM, Leach RE, Fazleabas AT, Young SL, Lessey BA, *et al.* ARID1A Is Essential for Endometrial Function during Early Pregnancy. *PLoS Genet* 2015: 11; e1005537.

Kim TH, Young SL, Sasaki T, Deaton JL, Schammel DP, Palomino AW, Jeong JW, and Lessey BA. Role of SIRT1 and Progesterone Resistance in Normal and Abnormal Endometrium. *J Clin Endocrinol Metab* 2021.

Kim TH, Yu Y, Luo L, Lydon JP, Jeong JW, and Kim JJ. Activated AKT pathway promotes establishment of endometriosis. *Endocrinology* 2014: 155; 1921-1930.

Klemmt PA, Carver JG, Kennedy SH, Koninckx PR, and Mardon HJ. Stromal cells from endometriotic lesions and endometrium from women with endometriosis have reduced decidualization capacity. *Fertil Steril* 2006: 85; 564-572.

Klotz DM, Hewitt SC, Ciana P, Raviscioni M, Lindzey JK, Foley J, Maggi A, DiAugustine RP, and Korach KS. Requirement of estrogen receptor-alpha in insulin-like growth factor-1 (IGF-1)-induced uterine responses and in vivo evidence for IGF-1/estrogen receptor cross-talk. *J Biol Chem* 2002: 277; 8531-8537.

Kommagani R, Szwarc MM, Kovanci E, Gibbons WE, Putluri N, Maity S, Creighton CJ, Sreekumar A, DeMayo FJ, Lydon JP, *et al.* Acceleration of the glycolytic flux by steroid receptor coactivator-2 is essential for endometrial decidualization. *PLoS Genet* 2013: 9; e1003900.

Kommagani R, Szwarc MM, Vasquez YM, Peavey MC, Mazur EC, Gibbons WE, Lanz RB, DeMayo FJ, and Lydon JP. The Promyelocytic Leukemia Zinc Finger Transcription Factor Is Critical for Human Endometrial Stromal Cell Decidualization. *PLoS Genet* 2016: 12; e1005937.

Koopman LA, Kopcow HD, Rybalov B, Boyson JE, Orange JS, Schatz F, Masch R, Lockwood CJ, Schachter AD, Park PJ, *et al.* Human decidual natural killer cells are a unique NK cell subset with immunomodulatory potential. *J Exp Med* 2003: 198; 1201-1212.

Korbel C, Menger MD, and Laschke MW. Size and spatial orientation of uterine tissue transplants on the peritoneum crucially determine the growth and cyst formation of endometriosis-like lesions in mice. *Hum Reprod* 2010: 25; 2551-2558.

Kovacic B, Hoelbl-Kovacic A, Fischhuber KM, Leitner NR, Gotthardt D, Casanova E, Sexl V, and Muller M. Lactotransferrin-Cre reporter mice trace neutrophils, monocytes/macrophages and distinct subtypes of dendritic cells. *Haematologica* 2014: 99; 1006-1015.

Krege JH, Hodgin JB, Couse JF, Enmark E, Warner M, Mahler JF, Sar M, Korach KS, Gustafsson JA, and Smithies O. Generation and reproductive phenotypes of mice lacking estrogen receptor beta. *Proc Natl Acad Sci U S A* 1998: 95; 15677-15682.

Krishnarajah S, Ingelfinger F, Friebel E, Cansever D, Amorim A, Andreadou M, Bamert D, Litscher G, Lutz M, Mayoux M, *et al.* Single-cell profiling of immune system alterations in lymphoid, barrier and solid tissues in aged mice. *Nature Aging* 2022: 2; 74-89.

Krizsan-Agbas D, Pedchenko T, Hasan W, and Smith PG. Oestrogen regulates sympathetic neurite outgrowth by modulating brain derived neurotrophic factor synthesis and release by the rodent uterus. *Eur J Neurosci* 2003: 18; 2760-2768.

Kulak J, Jr., Fischer C, Komm B, and Taylor HS. Treatment with bazedoxifene, a selective estrogen receptor modulator, causes regression of endometriosis in a mouse model. *Endocrinology* 2011: 152; 3226-3232.

Kumagami A, Ito A, Yoshida-Komiya H, Fujimori K, and Sato A. Expression patterns of the steroid receptor coactivator family in human ovarian endometriosis. *J Obstet Gynaecol Res* 2011: 37; 1269-1276.

Kumar R, Clerc AC, Gori I, Russell R, Pellegrini C, Govender L, Wyss JC, Golshayan D, and Canny GO. Lipoxin A(4) prevents the progression of de novo and established endometriosis in a mouse model by attenuating prostaglandin E(2) production and estrogen signaling. *PLoS One* 2014: 9; e89742.

Kumar R, Vicari M, Gori I, Achtari C, Fiche M, Surbeck I, Damnon F, and Canny GO. Compartmentalized secretory leukocyte protease inhibitor expression and hormone responses along the reproductive tract of postmenopausal women. *J Reprod Immunol* 2011: 92; 88-96.

Kurihara I, Lee DK, Petit FG, Jeong J, Lee K, Lydon JP, DeMayo FJ, Tsai MJ, and Tsai SY. COUP-TFII mediates progesterone regulation of uterine implantation by controlling ER activity. *PLoS Genet* 2007: 3; e102.

Kurita T, Lee KJ, Cooke PS, Lydon JP, and Cunha GR. Paracrine regulation of epithelial progesterone receptor and lactoferrin by progesterone in the mouse uterus. *Biol Reprod* 2000: 62; 831-838.

Kyama CM, Mihalyi A, Simsa P, Falconer H, Fulop V, Mwenda JM, Peeraer K, Tomassetti C, Meuleman C, and D'Hooghe TM. Role of cytokines in the endometrial-peritoneal cross-talk and development of endometriosis. *Front Biosci (Elite Ed)* 2009: 1; 444-454.

Lac V, Nazeran TM, Tessier-Cloutier B, Aguirre-Hernandez R, Albert A, Lum A, Khattra J, Praetorius T, Mason M, Chiu D, *et al.* Oncogenic mutations in histologically normal endometrium: the new normal? *J Pathol* 2019: 249; 173-181.

Laird SM, Tuckerman EM, Saravelos H, and Li TC. The production of tumour necrosis factor alpha (TNF-alpha) by human endometrial cells in culture. *Hum Reprod* 1996: 11; 1318-1323.

Large MJ and DeMayo FJ. The regulation of embryo implantation and endometrial decidualization by progesterone receptor signaling. *Mol Cell Endocrinol* 2012: 358; 155-165.

Laschke MW, Korbel C, Rudzitis-Auth J, Gashaw I, Reinhardt M, Hauff P, Zollner TM, and Menger MD. High-resolution ultrasound imaging: a novel technique for the noninvasive in vivo analysis of endometriotic lesion and cyst formation in small animal models. *Am J Pathol* 2010: 176; 585-593.

Ledee-Bataille N, Olivennes F, Kadoch J, Dubanchet S, Frydman N, Chaouat G, and Frydman R. Detectable levels of interleukin-18 in uterine luminal secretions at oocyte retrieval predict failure of the embryo transfer. *Hum Reprod* 2004: 19; 1968-1973.

Lee CH, Kim TH, Lee JH, Oh SJ, Yoo JY, Kwon HS, Kim YI, Ferguson SD, Ahn JY, Ku BJ, *et al.* Extracellular signal-regulated kinase 1/2 signaling pathway is required for endometrial decidualization in mice and human. *PLoS One* 2013: 8; e75282.

Lee DK, Kurihara I, Jeong JW, Lydon JP, DeMayo FJ, Tsai MJ, and Tsai SY. Suppression of ERalpha activity by COUP-TFII is essential for successful implantation and decidualization. *Mol Endocrinol* 2010: 24; 930-940.

Lee JH, Kim TH, Oh SJ, Yoo JY, Akira S, Ku BJ, Lydon JP, and Jeong JW. Signal transducer and activator of transcription-3 (Stat3) plays a critical role in implantation via progesterone receptor in uterus. *FASEB J* 2013: 27; 2553-2563.

Lee K, Jeong J, Kwak I, Yu CT, Lanske B, Soegiarto DW, Toftgard R, Tsai MJ, Tsai S, Lydon JP, *et al.* Indian hedgehog is a major mediator of progesterone signaling in the mouse uterus. *Nat Genet* 2006: 38; 1204-1209.

Lee KY, Jeong JW, Wang J, Ma L, Martin JF, Tsai SY, Lydon JP, and DeMayo FJ. Bmp2 is critical for the murine uterine decidual response. *Mol Cell Biol* 2007: 27; 5468-5478.

Lessey BA, Castelbaum AJ, Sawin SW, Buck CA, Schinnar R, Bilker W, and Strom BL. Aberrant integrin expression in the endometrium of women with endometriosis. *J Clin Endocrinol Metab* 1994: 79; 643-649.

Lessey BA and Kim JJ. Endometrial receptivity in the eutopic endometrium of women with endometriosis: it is affected, and let me show you why. *Fertil Steril* 2017: 108; 19-27.

Lessey BA, Palomino WA, Apparao KB, Young SL, and Lininger RA. Estrogen receptor-alpha (ER-alpha) and defects in uterine receptivity in women. *Reprod Biol Endocrinol* 2006: 4 Suppl 1; S9.

Li Q, Kannan A, DeMayo FJ, Lydon JP, Cooke PS, Yamagishi H, Srivastava D, Bagchi MK, and Bagchi IC. The antiproliferative action of progesterone in uterine epithelium is mediated by Hand2. *Science* 2011: 331; 912-916.

Li Q, Kannan A, Wang W, Demayo FJ, Taylor RN, Bagchi MK, and Bagchi IC. Bone morphogenetic protein 2 functions via a conserved signaling pathway involving Wnt4 to regulate uterine decidualization in the mouse and the human. *J Biol Chem* 2007: 282; 31725-31732.

Li R, Wang X, Huang Z, Balaji J, Kim TH, Wang T, Zhou L, Deleon A, Cook ME, Marbrey MW, *et al.* The role of epithelial progesterone receptor isoforms in embryo implantation. *iScience* 2021: 24; 103487.

Liang XH, Deng WB, Li M, Zhao ZA, Wang TS, Feng XH, Cao YJ, Duan EK, and Yang ZM. Egr1 protein acts downstream of estrogen-leukemia inhibitory factor (LIF)-STAT3 pathway and plays a role during implantation through targeting Wnt4. *J Biol Chem* 2014: 289; 23534-23545.

Liang Y, Li Y, Liu K, Chen P, and Wang D. Expression and Significance of WNT4 in Ectopic and Eutopic Endometrium of Human Endometriosis. *Reprod Sci* 2016: 23; 379-385.

Lim H, Ma L, Ma WG, Maas RL, and Dey SK. Hoxa-10 regulates uterine stromal cell responsiveness to progesterone during implantation and decidualization in the mouse. *Mol Endocrinol* 1999: 13; 1005-1017.

Lin A, Yin J, Cheng C, Yang Z, and Yang H. Decreased expression of FOXA2 promotes eutopic endometrial cell proliferation and migration in patients with endometriosis. *Reprod Biomed Online* 2018: 36; 181-187.

Lin SC, Li YH, Wu MH, Chang YF, Lee DK, Tsai SY, Tsai MJ, and Tsai SJ. Suppression of COUP-TFII by proinflammatory cytokines contributes to the pathogenesis of endometriosis. *J Clin Endocrinol Metab* 2014: 99; E427-437.

Lin YJ, Lai MD, Lei HY, and Wing LY. Neutrophils and macrophages promote angiogenesis in the early stage of endometriosis in a mouse model. *Endocrinology* 2006: 147; 1278-1286.

Lockhat FB, Emembolu JO, and Konje JC. The efficacy, side-effects and continuation rates in women with symptomatic endometriosis undergoing treatment with an intra-uterine administered progestogen (levonorgestrel): a 3 year follow-up. *Hum Reprod* 2005: 20; 789-793.

Love MI, Anders S, Kim V, and Huber W. RNA-Seq workflow: gene-level exploratory analysis and differential expression. *F1000Res* 2015: 4; 1070.

Love MI, Huber W, and Anders S. Moderated estimation of fold change and dispersion for RNA-seq data with DESeq2. *Genome Biol* 2014: 15; 550.

Lubahn DB, Moyer JS, Golding TS, Couse JF, Korach KS, and Smithies O. Alteration of reproductive function but not prenatal sexual development after insertional disruption of the mouse estrogen receptor gene. *Proc Natl Acad Sci U S A* 1993: 90; 11162-11166.

Lucas ES, Vrljicak P, Muter J, Diniz-da-Costa MM, Brighton PJ, Kong CS, Lipecki J, Fishwick KJ, Odendaal J, Ewington LJ, *et al.* Recurrent pregnancy loss is associated with a pro-senescent decidual response during the peri-implantation window. *Commun Biol* 2020: 3; 37.

Lydon JP, DeMayo FJ, Funk CR, Mani SK, Hughes AR, Montgomery CA, Jr., Shyamala G, Conneely OM, and O'Malley BW. Mice lacking progesterone receptor exhibit pleiotropic reproductive abnormalities. *Genes Dev* 1995: 9; 2266-2278.

Macer ML and Taylor HS. Endometriosis and infertility: a review of the pathogenesis and treatment of endometriosis-associated infertility. *Obstet Gynecol Clin North Am* 2012: 39; 535-549.

Maeda D and Shih Ie M. Pathogenesis and the role of ARID1A mutation in endometriosis-related ovarian neoplasms. *Adv Anat Pathol* 2013: 20; 45-52.

Mai H, Liao Y, Luo S, Wei K, Yang F, and Shi H. Histone deacetylase HDAC2 silencing prevents endometriosis by activating the HNF4A/ARID1A axis. *J Cell Mol Med* 2021: 25; 9972-9982.

Mantena SR, Kannan A, Cheon YP, Li Q, Johnson PF, Bagchi IC, and Bagchi MK. C/EBPbeta is a critical mediator of steroid hormone-regulated cell proliferation and differentiation in the uterine epithelium and stroma. *Proc Natl Acad Sci U S A* 2006: 103; 1870-1875.

Maridas DE, Hey-Cunningham AJ, Ng CHM, Markham R, Fraser IS, and Berbic M. Peripheral and endometrial dendritic cell populations during the normal cycle and in the presence of endometriosis. *J Endometr Pelvic Pain Disord* 2014: 6; 67-119.

Marquardt RM, Kim TH, Shin JH, and Jeong JW. Progesterone and Estrogen Signaling in the Endometrium: What Goes Wrong in Endometriosis? *Int J Mol Sci* 2019: 20.

Marquardt RM, Kim TH, Yoo JY, Teasley HE, Fazleabas AT, Young SL, Lessey BA, Arora R, and Jeong JW. Endometrial epithelial ARID1A is critical for uterine gland function in early pregnancy establishment. *FASEB J* 2021: 35; e21209.

Martin M. Cutadapt removes adapter sequences from high-throughput sequencing reads. *EMBnet.journal* 2011: 17.

Martinez J, Bisbal V, Marin N, Cano A, and Gomez R. Noninvasive Monitoring of Lesion Size in a Heterologous Mouse Model of Endometriosis. *J Vis Exp* 2019.

Mathur R. ARID1A loss in cancer: Towards a mechanistic understanding. *Pharmacol Ther* 2018.

Matsumoto H, Zhao X, Das SK, Hogan BL, and Dey SK. Indian hedgehog as a progesterone-responsive factor mediating epithelial-mesenchymal interactions in the mouse uterus. *Dev Biol* 2002: 245; 280-290.

Matsuzaki S, Murakami T, Uehara S, Canis M, Sasano H, and Okamura K. Expression of estrogen receptor alpha and beta in peritoneal and ovarian endometriosis. *Fertil Steril* 2001: 75; 1198-1205.

McLaren J, Prentice A, Charnock-Jones DS, Millican SA, Muller KH, Sharkey AM, and Smith SK. Vascular endothelial growth factor is produced by peritoneal fluid macrophages in endometriosis and is regulated by ovarian steroids. *J Clin Invest* 1996: 98; 482-489.

Migliaccio A, Di Domenico M, Castoria G, de Falco A, Bontempo P, Nola E, and Auricchio F. Tyrosine kinase/p21ras/MAP-kinase pathway activation by estradiol-receptor complex in MCF-7 cells. *EMBO J* 1996: 15; 1292-1300.

Millard CJ, Watson PJ, Fairall L, and Schwabe JW. An evolving understanding of nuclear receptor coregulator proteins. *J Mol Endocrinol* 2013: 51; T23-36.

Mishra A, Galvankar M, Singh N, and Modi D. Spatial and temporal changes in the expression of steroid hormone receptors in mouse model of endometriosis. *J Assist Reprod Genet* 2020: 37; 1069-1081.

Moberg C, Bourlev V, Ilyasova N, and Olovsson M. Endometrial expression of LIF and its receptor and peritoneal fluid levels of IL-1alpha and IL-6 in women with endometriosis

are associated with the probability of pregnancy. *Arch Gynecol Obstet* 2015: 292; 429-437.

Moberg C, Bourlev V, Ilyasova N, and Olovsson M. Levels of oestrogen receptor, progesterone receptor and alphaB-crystallin in eutopic endometrium in relation to pregnancy in women with endometriosis. *Hum Fertil (Camb)* 2015: 18; 30-37.

Monsivais D, Dyson MT, Yin P, Coon JS, Navarro A, Feng G, Malpani SS, Ono M, Ercan CM, Wei JJ, *et al.* ERbeta- and prostaglandin E2-regulated pathways integrate cell proliferation via Ras-like and estrogen-regulated growth inhibitor in endometriosis. *Mol Endocrinol* 2014: 28; 1304-1315.

Montagna P, Capellino S, Villaggio B, Remorgida V, Ragni N, Cutolo M, and Ferrero S. Peritoneal fluid macrophages in endometriosis: correlation between the expression of estrogen receptors and inflammation. *Fertil Steril* 2008: 90; 156-164.

Mori M, Bogdan A, Balassa T, Csabai T, and Szekeres-Bartho J. The decidua-the maternal bed embracing the embryo-maintains the pregnancy. *Semin Immunopathol* 2016: 38; 635-649.

Moro F, Leombroni M, and Testa AC. Ultrasound Imaging in Endometriosis. *Obstet Gynecol Clin North Am* 2019: 46; 643-659.

Morotti M, Vincent K, and Becker CM. Mechanisms of pain in endometriosis. *Eur J Obstet Gynecol Reprod Biol* 2017: 209; 8-13.

Morotti M, Vincent K, Brawn J, Zondervan KT, and Becker CM. Peripheral changes in endometriosis-associated pain. *Hum Reprod Update* 2014: 20; 717-736.

Moses AS, Demessie AA, Taratula O, Korzun T, Slayden OD, and Taratula O. Nanomedicines for Endometriosis: Lessons Learned from Cancer Research. *Small* 2021: 17; e2004975.

Moses AS, Taratula OR, Lee H, Luo F, Grenz T, Korzun T, Lorenz AS, Sabei FY, Bracha S, Alani AWG, *et al.* Nanoparticle-Based Platform for Activatable Fluorescence Imaging and Photothermal Ablation of Endometriosis. *Small* 2020: 16; e1906936.

Mousazadeh S, Ghaheri A, Shahhoseini M, Aflatoonian R, and Afsharian P. The Effect of Imbalanced Progesterone Receptor-A/-B Ratio on Gelatinase Expressions in Endometriosis. *Int J Fertil Steril* 2019: 13; 127-134.

Mukherjee A, Soyal SM, Fernandez-Valdivia R, Gehin M, Chambon P, Demayo FJ, Lydon JP, and O'Malley BW. Steroid receptor coactivator 2 is critical for progesterone-dependent uterine function and mammary morphogenesis in the mouse. *Mol Cell Biol* 2006: 26; 6571-6583.

Mulac-Jericevic B, Lydon JP, DeMayo FJ, and Conneely OM. Defective mammary gland morphogenesis in mice lacking the progesterone receptor B isoform. *Proc Natl Acad Sci U S A* 2003: 100; 9744-9749.

Mulac-Jericevic B, Mullinax RA, DeMayo FJ, Lydon JP, and Conneely OM. Subgroup of reproductive functions of progesterone mediated by progesterone receptor-B isoform. *Science* 2000: 289; 1751-1754.

Muneyyirci-Delale O and Karacan M. Effect of norethindrone acetate in the treatment of symptomatic endometriosis. *Int J Fertil Womens Med* 1998: 43; 24-27.

Murrieta-Coxca JM, Gomez-Chavez F, Baeza-Martinez DA, Cancino-Diaz ME, Cancino-Diaz JC, Perez-Tapia SM, Reyes-Maldonado E, and Rodriguez-Martinez S. Estrous Cycle and Gestational Age-Dependent Expression of Members of the Interleukin-36 Subfamily in a Semi-Allogeneic Model of Infected and Non-Infected Murine Pregnancy. *Front Immunol* 2016: 7; 376.

Nanjappa MK, Mesa AM, Medrano TI, Jefferson WN, DeMayo FJ, Williams CJ, Lydon JP, Levin ER, and Cooke PS. The histone methyltransferase EZH2 is required for normal uterine development and function in mice. *Biol Reprod* 2019.

Neff R, Rush CM, Smith B, Backes FJ, Cohn DE, and Goodfellow PJ. Functional characterization of recurrent FOXA2 mutations seen in endometrial cancers. *Int J Cancer* 2018: 143; 2955-2961.

Nikoobakht B and El-Sayed MA. Preparation and Growth Mechanism of Gold Nanorods (NRs) Using Seed-Mediated Growth Method. *Chemistry of Materials* 2003: 15; 1957-1962.

Noble LS, Simpson ER, Johns A, and Bulun SE. Aromatase expression in endometriosis. *J Clin Endocrinol Metab* 1996: 81; 174-179.

Noyes RW, Hertig AT, and Rock J. Dating the endometrial biopsy. *Am J Obstet Gynecol* 1975: 122; 262-263.

Ntziachristos V. Going deeper than microscopy: the optical imaging frontier in biology. *Nat Methods* 2010: 7; 603-614.

Nyholt DR, Low SK, Anderson CA, Painter JN, Uno S, Morris AP, MacGregor S, Gordon SD, Henders AK, Martin NG, *et al.* Genome-wide association meta-analysis identifies new endometriosis risk loci. *Nat Genet* 2012: 44; 1355-1359.

O'Brien JE, Peterson TJ, Tong MH, Lee EJ, Pfaff LE, Hewitt SC, Korach KS, Weiss J, and Jameson JL. Estrogen-induced proliferation of uterine epithelial cells is independent of estrogen receptor alpha binding to classical estrogen response elements. *J Biol Chem* 2006: 281; 26683-26692.

Osinski M, Wirstlein P, Wender-Ozegowska E, Mikolajczyk M, Jagodzinski PP, and Szczepanska M. HSD3B2, HSD17B1, HSD17B2, ESR1, ESR2 and AR expression in infertile women with endometriosis. *Ginekol Pol* 2018: 89; 125-134.

Parameswaran N and Patial S. Tumor necrosis factor-alpha signaling in macrophages. *Crit Rev Eukaryot Gene Expr* 2010: 20; 87-103.

Parasar P, Ozcan P, and Terry KL. Endometriosis: Epidemiology, Diagnosis and Clinical Management. *Curr Obstet Gynecol Rep* 2017: 6; 34-41.

Park M, Kim HR, Kim YS, Yang SC, Yoon JA, Lyu SW, Lim HJ, Hong SH, and Song H. Estrogen-induced transcription factor EGR1 regulates c-Kit transcription in the mouse uterus to maintain uterine receptivity for embryo implantation. *Mol Cell Endocrinol* 2018: 470; 75-83.

Patel B, Elguero S, Thakore S, Dahoud W, Bedaiwy M, and Mesiano S. Role of nuclear progesterone receptor isoforms in uterine pathophysiology. *Hum Reprod Update* 2015: 21; 155-173.

Patel BG, Rudnicki M, Yu J, Shu Y, and Taylor RN. Progesterone resistance in endometriosis: origins, consequences and interventions. *Acta Obstet Gynecol Scand* 2017: 96; 623-632.

Pawar S, Laws MJ, Bagchi IC, and Bagchi MK. Uterine Epithelial Estrogen Receptor-alpha Controls Decidualization via a Paracrine Mechanism. *Mol Endocrinol* 2015: 29; 1362-1374.

Pei T, Liu C, Liu T, Xiao L, Luo B, Tan J, Li X, Zhou G, Duan C, and Huang W. miR-194-3p Represses the Progesterone Receptor and Decidualization in Eutopic Endometrium From Women With Endometriosis. *Endocrinology* 2018: 159; 2554-2562.

Pellegrini C, Gori I, Achtari C, Hornung D, Chardonnens E, Wunder D, Fiche M, and Canny GO. The expression of estrogen receptors as well as GREB1, c-MYC, and cyclin D1, estrogen-regulated genes implicated in proliferation, is increased in peritoneal endometriosis. *Fertil Steril* 2012: 98; 1200-1208.

Plaks V, Birnberg T, Berkutzki T, Sela S, BenYashar A, Kalchenko V, Mor G, Keshet E, Dekel N, Neeman M, *et al.* Uterine DCs are crucial for decidua formation during embryo implantation in mice. *J Clin Invest* 2008: 118; 3954-3965.

Prentice A, Randall BJ, Weddell A, McGill A, Henry L, Horne CH, and Thomas EJ. Ovarian steroid receptor expression in endometriosis and in two potential parent epithelia: endometrium and peritoneal mesothelium. *Hum Reprod* 1992: 7; 1318-1325.

Raab JR, Resnick S, and Magnuson T. Genome-Wide Transcriptional Regulation Mediated by Biochemically Distinct SWI/SNF Complexes. *PLoS Genet* 2015: 11; e1005748.

Rahmioglu N, Nyholt DR, Morris AP, Missmer SA, Montgomery GW, and Zondervan KT. Genetic variants underlying risk of endometriosis: insights from meta-analysis of eight genome-wide association and replication datasets. *Hum Reprod Update* 2014: 20; 702-716.

Ratsep MT, Felker AM, Kay VR, Tolusso L, Hofmann AP, and Croy BA. Uterine natural killer cells: supervisors of vasculature construction in early decidua basalis. *Reproduction* 2015: 149; R91-102.

Rawlings TM, Makwana K, Taylor DM, Mole MA, Fishwick KJ, Tryfonos M, Odendaal J, Hawkes A, Zernicka-Goetz M, Hartshorne GM, *et al.* Modelling the impact of decidual senescence on embryo implantation in human endometrial assembloids. *Elife* 2021: 10.

Renaud SJ, Scott RL, Chakraborty D, Rumi MA, and Soares MJ. Natural killer-cell deficiency alters placental development in rats. *Biol Reprod* 2017: 96; 145-158.

Reske JJ, Wilson MR, Holladay J, Siwicki RA, Skalski H, Harkins S, Adams M, Risinger JI, Hostetter G, Lin K, *et al.* Co-existing TP53 and ARID1A mutations promote aggressive endometrial tumorigenesis. *PLoS Genet* 2021: 17; e1009986.

Richards EG, Rehmer JM, Mathes MA, Esakov EL, Braley C, Joehlin-Price A, Chiesa-Vottero A, and Reizes O. A Syngeneic Murine Model of Endometriosis using Naturally Cycling Mice. *J Vis Exp* 2020.

Richards RG, Walker MP, Sebastian J, and DiAugustine RP. Insulin-like growth factor-1 (IGF-1) receptor-insulin receptor substrate complexes in the uterus. Altered signaling response to estradiol in the IGF-1(m/m) mouse. *J Biol Chem* 1998: 273; 11962-11969.

Richter ON, Dorn C, Rosing B, Flaskamp C, and Ulrich U. Tumor necrosis factor alpha secretion by peritoneal macrophages in patients with endometriosis. *Arch Gynecol Obstet* 2005: 271; 143-147.

Robertson SA, Mayrhofer G, and Seamark RF. Uterine epithelial cells synthesize granulocyte-macrophage colony-stimulating factor and interleukin-6 in pregnant and nonpregnant mice. *Biol Reprod* 1992: 46; 1069-1079.

Rocha-Junior CV, Da Broi MG, Miranda-Furtado CL, Navarro PA, Ferriani RA, and Meola J. Progesterone Receptor B (PGR-B) Is Partially Methylated in Eutopic Endometrium From Infertile Women With Endometriosis. *Reprod Sci* 2019; 1933719119828078.

Rocha AL, Reis FM, and Taylor RN. Angiogenesis and endometriosis. *Obstet Gynecol Int* 2013: 2013; 859619.

Rocha MG, e Silva JC, Ribeiro da Silva A, Candido Dos Reis FJ, Nogueira AA, and Poli-Neto OB. TRPV1 expression on peritoneal endometriosis foci is associated with chronic pelvic pain. *Reprod Sci* 2011: 18; 511-515.

Rosa ESA, Rosa ESJC, Mamillapalli R, and Taylor HS. Dose-Dependent Decreased Fertility in Response to the Burden of Endometriosis in a Murine Model. *Reprod Sci* 2019; 1933719119859438.

Rosario GX and Stewart CL. The Multifaceted Actions of Leukaemia Inhibitory Factor in Mediating Uterine Receptivity and Embryo Implantation. *Am J Reprod Immunol* 2016: 75; 246-255.

Roulis M, Armaka M, Manoloukos M, Apostolaki M, and Kollias G. Intestinal epithelial cells as producers but not targets of chronic TNF suffice to cause murine Crohn-like pathology. *Proc Natl Acad Sci U S A* 2011: 108; 5396-5401.

Rubel CA, Franco HL, Jeong JW, Lydon JP, and DeMayo FJ. GATA2 is expressed at critical times in the mouse uterus during pregnancy. *Gene Expr Patterns* 2012: 12; 196-203.

Rubel CA, Jeong JW, Tsai SY, Lydon JP, and Demayo FJ. Epithelial-stromal interaction and progesterone receptors in the mouse uterus. *Semin Reprod Med* 2010: 28; 27-35.

Rubel CA, Lanz RB, Kommagani R, Franco HL, Lydon JP, and DeMayo FJ. Research resource: Genome-wide profiling of progesterone receptor binding in the mouse uterus. *Mol Endocrinol* 2012: 26; 1428-1442.

Rubel CA, Wu SP, Lin L, Wang T, Lanz RB, Li X, Kommagani R, Franco HL, Camper SA, Tong Q, *et al.* A Gata2-Dependent Transcription Network Regulates Uterine Progesterone Responsiveness and Endometrial Function. *Cell Rep* 2016: 17; 1414-1425.

Sakaguchi H, Fujimoto J, Sun WS, and Tamaya T. Clinical implications of steroid receptor coactivator (SRC)-3 in uterine endometrial cancers. *J Steroid Biochem Mol Biol* 2007: 104; 237-240.

Samadieh Y, Favaedi R, Ramezanali F, Afsharian P, Aflatoonian R, and Shahhoseini M. Epigenetic Dynamics of HOXA10 Gene in Infertile Women With Endometriosis. *Reprod Sci* 2019: 26; 88-96.

Sapkota Y, Steinthorsdottir V, Morris AP, Fassbender A, Rahmioglu N, De Vivo I, Buring JE, Zhang F, Edwards TL, Jones S, *et al.* Meta-analysis identifies five novel loci associated with endometriosis highlighting key genes involved in hormone metabolism. *Nat Commun* 2017: 8; 15539.

Saunders PTK. What Have We Learned from Animal Models of Endometriosis and How Can We Use the Knowledge Gained to Improve Treatment of Patients? *Adv Anat Embryol Cell Biol* 2020: 232; 99-111.

Saunders PTK and Horne AW. Endometriosis: Etiology, pathobiology, and therapeutic prospects. *Cell* 2021: 184; 2807-2824.

Schofield G and Kimber SJ. Leukocyte subpopulations in the uteri of leukemia inhibitory factor knockout mice during early pregnancy. *Biol Reprod* 2005: 72; 872-878.

Schreinemacher MH, Backes WH, Slenter JM, Xanthoulea S, Delvoux B, van Winden L, Beets-Tan RG, Evers JL, Dunselman GA, and Romano A. Towards endometriosis diagnosis by gadofosveset-trisodium enhanced magnetic resonance imaging. *PLoS One* 2012: 7; e33241.

Schulke L, Berbic M, Manconi F, Tokushige N, Markham R, and Fraser IS. Dendritic cell populations in the eutopic and ectopic endometrium of women with endometriosis. *Hum Reprod* 2009: 24; 1695-1703.

Selak V, Farquhar C, Prentice A, and Singla A. Danazol for pelvic pain associated with endometriosis. *Cochrane Database Syst Rev* 2007; CD000068.

Sharpe-Timms KL and Stilley JAW. Introduction to Preclinical Evidence from Animal Models of Endometriosis. *Adv Anat Embryol Cell Biol* 2020: 232; 1-8.

Shen F, Yan C, Liu M, Feng Y, and Chen Y. Decreased expression of mucin-1 in endometriosis endometrium correlated with progesterone receptor B involved in infertility. *Arch Gynecol Obstet* 2015: 291; 439-445.

Shimizu Y, Mita S, Takeuchi T, Notsu T, Mizuguchi K, and Kyo S. Dienogest, a synthetic progestin, inhibits prostaglandin E2 production and aromatase expression by human endometrial epithelial cells in a spheroid culture system. *Steroids* 2011: 76; 60-67.

Shvedova AA, Kisin ER, Yanamala N, Tkach AV, Gutkin DW, Star A, Shurin GV, Kagan VE, and Shurin MR. MDSC and TGFbeta Are Required for Facilitation of Tumor Growth in the Lungs of Mice Exposed to Carbon Nanotubes. *Cancer Res* 2015: 75; 1615-1623.

Silveira CG, Finas D, Hunold P, Koster F, Stroschein K, Canny GO, Moldenhauer G, Altevogt P, Rody A, and Hornung D. L1 cell adhesion molecule as a potential therapeutic target in murine models of endometriosis using a monoclonal antibody approach. *PLoS One* 2013: 8; e82512.

Simitsidellis I, Gibson DA, and Saunders PTK. Animal models of endometriosis: Replicating the aetiology and symptoms of the human disorder. *Best Pract Res Clin Endocrinol Metab* 2018: 32; 257-269.

Smith K, Alnifaidy R, Wei Q, and Nieman LK. Endometrial Indian hedgehog expression is decreased in women with endometriosis. *Fertil Steril* 2011: 95; 2738-2741 e2731-2733.

Smuc T, Pucelj MR, Sinkovec J, Husen B, Thole H, and Lanisnik Rizner T. Expression analysis of the genes involved in estradiol and progesterone action in human ovarian endometriosis. *Gynecol Endocrinol* 2007: 23; 105-111.

Song H and Lim H. Evidence for heterodimeric association of leukemia inhibitory factor (LIF) receptor and gp130 in the mouse uterus for LIF signaling during blastocyst implantation. *Reproduction* 2006: 131; 341-349.

Song H, Lim H, Das SK, Paria BC, and Dey SK. Dysregulation of EGF family of growth factors and COX-2 in the uterus during the preattachment and attachment reactions of the blastocyst with the luminal epithelium correlates with implantation failure in LIF-deficient mice. *Mol Endocrinol* 2000: 14; 1147-1161.

Soyal SM, Mukherjee A, Lee KY, Li J, Li H, DeMayo FJ, and Lydon JP. Cre-mediated recombination in cell lineages that express the progesterone receptor. *Genesis* 2005: 41; 58-66.

Sroyraya M, Songkoomkrong S, Changklungmoa N, Poljaroen J, Weerakiet S, Sophonsritsuk A, Wongkularb A, Lertvikool S, Tingthanatikul Y, and Sobhon P. Differential expressions of estrogen and progesterone receptors in endometria and cyst walls of ovarian endometrioma from women with endometriosis and their responses to depo-medroxyprogesterone acetate treatment. *Mol Cell Probes* 2018: 40; 27-36.

Stefkovich ML, Arao Y, Hamilton KJ, and Korach KS. Experimental models for evaluating non-genomic estrogen signaling. *Steroids* 2018: 133; 34-37.

Steinberg I, Huland DM, Vermesh O, Frostig HE, Tummers WS, and Gambhir SS. Photoacoustic clinical imaging. *Photoacoustics* 2019: 14; 77-98.

Stewart CL, Kaspar P, Brunet LJ, Bhatt H, Gadi I, Kontgen F, and Abbondanzo SJ. Blastocyst implantation depends on maternal expression of leukaemia inhibitory factor. *Nature* 1992: 359; 76-79.

Stratton P, Sinaii N, Segars J, Koziol D, Wesley R, Zimmer C, Winkel C, and Nieman LK. Return of chronic pelvic pain from endometriosis after raloxifene treatment: a randomized controlled trial. *Obstet Gynecol* 2008: 111; 88-96.

Straub RH. The complex role of estrogens in inflammation. *Endocr Rev* 2007: 28; 521-574.

Strowitzki T, Faustmann T, Gerlinger C, and Seitz C. Dienogest in the treatment of endometriosis-associated pelvic pain: a 12-week, randomized, double-blind, placebo-controlled study. *Eur J Obstet Gynecol Reprod Biol* 2010: 151; 193-198.

Su RW, Strug MR, Joshi NR, Jeong JW, Miele L, Lessey BA, Young SL, and Fazleabas AT. Decreased Notch pathway signaling in the endometrium of women with endometriosis impairs decidualization. *J Clin Endocrinol Metab* 2015: 100; E433-442.

Suda K, Nakaoka H, Yoshihara K, Ishiguro T, Tamura R, Mori Y, Yamawaki K, Adachi S, Takahashi T, Kase H, *et al.* Clonal Expansion and Diversification of Cancer-Associated Mutations in Endometriosis and Normal Endometrium. *Cell Rep* 2018: 24; 1777-1789.

Sun X, Bartos A, Whitsett JA, and Dey SK. Uterine deletion of Gp130 or Stat3 shows implantation failure with increased estrogenic responses. *Mol Endocrinol* 2013: 27; 1492-1501.

Sun X, Chuang JC, Kanchwala M, Wu L, Celen C, Li L, Liang H, Zhang S, Maples T, Nguyen LH, *et al.* Suppression of the SWI/SNF Component Arid1a Promotes Mammalian Regeneration. *Cell Stem Cell* 2016: 18; 456-466.

Surveyor GA, Gendler SJ, Pemberton L, Das SK, Chakraborty I, Julian J, Pimental RA, Wegner CC, Dey SK, and Carson DD. Expression and steroid hormonal control of Muc-1 in the mouse uterus. *Endocrinology* 1995: 136; 3639-3647.

Suzuki A, Horiuchi A, Oka K, Miyamoto T, Kashima H, and Shiozawa T. Immunohistochemical detection of steroid receptor cofactors in ovarian endometriosis: involvement of down-regulated SRC-1 expression in the limited growth activity of the endometriotic epithelium. *Virchows Arch* 2010: 456; 433-441.

Symons LK, Miller JE, Kay VR, Marks RM, Liblik K, Koti M, and Tayade C. The Immunopathophysiology of Endometriosis. *Trends Mol Med* 2018: 24; 748-762.

Szwarc MM, Hai L, Gibbons WE, Mo Q, Lanz RB, DeMayo FJ, and Lydon JP. Early growth response 1 transcriptionally primes the human endometrial stromal cell for decidualization. *J Steroid Biochem Mol Biol* 2019: 189; 283-290.

Szwarc MM, Hai L, Gibbons WE, White LD, Mo Q, Kommagani R, Lanz RB, DeMayo FJ, O'Malley BW, and Lydon JP. Retinoid signaling controlled by SRC-2 in decidualization revealed by transcriptomics. *Reproduction* 2018: 156; 387-395.

Szwarc MM, Lydon JP, and O'Malley BW. Steroid receptor coactivators as therapeutic targets in the female reproductive system. *J Steroid Biochem Mol Biol* 2015: 154; 32-38.

Takamoto N, Zhao B, Tsai SY, and DeMayo FJ. Identification of Indian hedgehog as a progesterone-responsive gene in the murine uterus. *Mol Endocrinol* 2002: 16; 2338-2348.

Takano M, Lu Z, Goto T, Fusi L, Higham J, Francis J, Withey A, Hardt J, Cloke B, Stavropoulou AV, *et al.* Transcriptional cross talk between the forkhead transcription factor forkhead box O1A and the progesterone receptor coordinates cell cycle regulation and differentiation in human endometrial stromal cells. *Mol Endocrinol* 2007: 21; 2334-2349.

Tamura K, Takashima H, Fumoto K, Kajihara T, Uchino S, Ishihara O, Yoshie M, Kusama K, and Tachikawa E. Possible Role of alpha1-Antitrypsin in Endometriosis-Like Grafts From a Mouse Model of Endometriosis. *Reprod Sci* 2015: 22; 1088-1097.

Tamura M, Deb S, Sebastian S, Okamura K, and Bulun SE. Estrogen up-regulates cyclooxygenase-2 via estrogen receptor in human uterine microvascular endothelial cells. *Fertil Steril* 2004: 81; 1351-1356.

Taylor HS, Bagot C, Kardana A, Olive D, and Arici A. HOX gene expression is altered in the endometrium of women with endometriosis. *Hum Reprod* 1999: 14; 1328-1331.

Taylor HS, Giudice LC, Lessey BA, Abrao MS, Kotarski J, Archer DF, Diamond MP, Surrey E, Johnson NP, Watts NB, *et al.* Treatment of Endometriosis-Associated Pain with Elagolix, an Oral GnRH Antagonist. *N Engl J Med* 2017: 377; 28-40.

Ticconi C, Di Simone N, Campagnolo L, and Fazleabas A. Clinical consequences of defective decidualization. *Tissue Cell* 2021: 72; 101586.

Tokushige N, Markham R, Russell P, and Fraser IS. Effects of hormonal treatment on nerve fibers in endometrium and myometrium in women with endometriosis. *Fertil Steril* 2008: 90; 1589-1598.

Tomassetti C and D'Hooghe T. Endometriosis and infertility: Insights into the causal link and management strategies. *Best Pract Res Clin Obstet Gynaecol* 2018: 51; 25-33.

Tosti C, Biscione A, Morgante G, Bifulco G, Luisi S, and Petraglia F. Hormonal therapy for endometriosis: from molecular research to bedside. *Eur J Obstet Gynecol Reprod Biol* 2017: 209; 61-66.

Tranguch S, Cheung-Flynn J, Daikoku T, Prapapanich V, Cox MB, Xie H, Wang H, Das SK, Smith DF, and Dey SK. Cochaperone immunophilin FKBP52 is critical to uterine receptivity for embryo implantation. *Proc Natl Acad Sci U S A* 2005: 102; 14326-14331.

Tranguch S, Wang H, Daikoku T, Xie H, Smith DF, and Dey SK. FKBP52 deficiency-conferred uterine progesterone resistance is genetic background and pregnancy stage specific. *J Clin Invest* 2007: 117; 1824-1834.

Tsai SJ, Wu MH, Chen HM, Chuang PC, and Wing LY. Fibroblast growth factor-9 is an endometrial stromal growth factor. *Endocrinology* 2002: 143; 2715-2721.

Tsudo T, Harada T, Iwabe T, Tanikawa M, Nagano Y, Ito M, Taniguchi F, and Terakawa N. Altered gene expression and secretion of interleukin-6 in stromal cells derived from endometriotic tissues. *Fertil Steril* 2000: 73; 205-211.

Vallejo G, La Greca AD, Tarifa-Reischle IC, Mestre-Citrinovitz AC, Ballare C, Beato M, and Saragueta P. CDC2 mediates progestin initiated endometrial stromal cell proliferation: a PR signaling to gene expression independently of its binding to chromatin. *PLoS One* 2014: 9; e97311.

Vallve-Juanico J, Houshdaran S, and Giudice LC. The endometrial immune environment of women with endometriosis. *Hum Reprod Update* 2019: 25; 564-591.

Vasquez YM and DeMayo FJ. Role of nuclear receptors in blastocyst implantation. *Semin Cell Dev Biol* 2013: 24; 724-735.

Vasquez YM, Mazur EC, Li X, Kommagani R, Jiang L, Chen R, Lanz RB, Kovanci E, Gibbons WE, and DeMayo FJ. FOXO1 is required for binding of PR on IRF4, novel transcriptional regulator of endometrial stromal decidualization. *Mol Endocrinol* 2015: 29; 421-433.

Vasquez YM, Wang X, Wetendorf M, Franco HL, Mo Q, Wang T, Lanz RB, Young SL, Lessey BA, Spencer TE, *et al.* FOXO1 regulates uterine epithelial integrity and progesterone receptor expression critical for embryo implantation. *PLoS Genet* 2018: 14; e1007787.

Vercellini P, Buggio L, Frattaruolo MP, Borghi A, Dridi D, and Somigliana E. Medical treatment of endometriosis-related pain. *Best Pract Res Clin Obstet Gynaecol* 2018: 51; 68-91.

Vercellini P, Cortesi I, and Crosignani PG. Progestins for symptomatic endometriosis: a critical analysis of the evidence. *Fertil Steril* 1997: 68; 393-401.

Vercellini P, Somigliana E, Daguati R, Vigano P, Meroni F, and Crosignani PG. Postoperative oral contraceptive exposure and risk of endometrioma recurrence. *Am J Obstet Gynecol* 2008: 198; 504 e501-505.

Verma A and Konje JC. Successful treatment of refractory endometriosis-related chronic pelvic pain with aromatase inhibitors in premenopausal patients. *Eur J Obstet Gynecol Reprod Biol* 2009: 143; 112-115.

Wada-Hiraike O, Hiraike H, Okinaga H, Imamov O, Barros RP, Morani A, Omoto Y, Warner M, and Gustafsson JA. Role of estrogen receptor beta in uterine stroma and epithelium: Insights from estrogen receptor beta-/- mice. *Proc Natl Acad Sci U S A* 2006: 103; 18350-18355.

Wang H and Dey SK. Roadmap to embryo implantation: clues from mouse models. *Nat Rev Genet* 2006: 7; 185-199.

Wang LV. Multiscale photoacoustic microscopy and computed tomography. *Nat Photonics* 2009: 3; 503-509.

Wang LV and Hu S. Photoacoustic tomography: in vivo imaging from organelles to organs. *Science* 2012: 335; 1458-1462.

Wang W, Li Q, Bagchi IC, and Bagchi MK. The CCAAT/enhancer binding protein beta is a critical regulator of steroid-induced mitotic expansion of uterine stromal cells during decidualization. *Endocrinology* 2010: 151; 3929-3940.

Wang X, Khatri S, Broaddus R, Wang Z, and Hawkins SM. Deletion of Arid1a in Reproductive Tract Mesenchymal Cells Reduces Fertility in Female Mice. *Biol Reprod* 2016: 94; 93.

Wang X, Li X, Wang T, Wu SP, Jeong JW, Kim TH, Young SL, Lessey BA, Lanz RB, Lydon JP, *et al.* SOX17 regulates uterine epithelial-stromal cross-talk acting via a distal enhancer upstream of Ihh. *Nat Commun* 2018: 9; 4421.

Wang X, Wu SP, and DeMayo FJ. Hormone dependent uterine epithelial-stromal communication for pregnancy support. *Placenta* 2017: 60 Suppl 1; S20-S26.

Wang Y, Hoang L, Ji JX, and Huntsman DG. SWI/SNF Complex Mutations in Gynecologic Cancers: Molecular Mechanisms and Models. *Annu Rev Pathol* 2020: 15; 467-492.

Weber J, Beard PC, and Bohndiek SE. Contrast agents for molecular photoacoustic imaging. *Nat Methods* 2016: 13; 639-650.

Wetendorf M and DeMayo FJ. Progesterone receptor signaling in the initiation of pregnancy and preservation of a healthy uterus. *Int J Dev Biol* 2014: 58; 95-106.

Wetendorf M, Wu SP, Wang X, Creighton CJ, Wang T, Lanz RB, Blok L, Tsai SY, Tsai MJ, Lydon JP, *et al.* Decreased epithelial progesterone receptor A at the window of receptivity is required for preparation of the endometrium for embryo attachment. *Biol Reprod* 2017: 96; 313-326.

Wickham H. ggplot2 : Elegant Graphics for Data Analysis. Use R!,. 2016. Springer International Publishing : Imprint: Springer,, Cham, pp 1 online resource (XVI, 260 pages 232 illustrations, 140 illustrations in color.

Wiegand KC, Shah SP, Al-Agha OM, Zhao Y, Tse K, Zeng T, Senz J, McConechy MK, Anglesio MS, Kalloger SE, *et al.* ARID1A mutations in endometriosis-associated ovarian carcinomas. *N Engl J Med* 2010: 363; 1532-1543.

Wilcox AJ, Baird DD, and Weinberg CR. Time of implantation of the conceptus and loss of pregnancy. *N Engl J Med* 1999: 340; 1796-1799.

Wilson MR, Reske JJ, Holladay J, Neupane S, Ngo J, Cuthrell N, Wegener M, Rhodes M, Adams M, Sheridan R, *et al.* ARID1A Mutations Promote P300-Dependent Endometrial Invasion through Super-Enhancer Hyperacetylation. *Cell Rep* 2020: 33; 108366.

Wilson MR, Reske JJ, Holladay J, Wilber GE, Rhodes M, Koeman J, Adams M, Johnson B, Su RW, Joshi NR, *et al.* ARID1A and PI3-kinase pathway mutations in the endometrium drive epithelial transdifferentiation and collective invasion. *Nat Commun* 2019: 10; 3554.

Wilson R, Moor J, Jenkins C, Miller H, Walker JJ, McLean MA, Norman J, and McInnes IB. Abnormal first trimester serum interleukin 18 levels are associated with a poor outcome in women with a history of recurrent miscarriage. *Am J Reprod Immunol* 2004: 51; 156-159.

Wing LY, Chuang PC, Wu MH, Chen HM, and Tsai SJ. Expression and mitogenic effect of fibroblast growth factor-9 in human endometriotic implant is regulated by aberrant production of estrogen. *J Clin Endocrinol Metab* 2003: 88; 5547-5554.

Winger EE and Reed JL. Treatment with tumor necrosis factor inhibitors and intravenous immunoglobulin improves live birth rates in women with recurrent spontaneous abortion. *Am J Reprod Immunol* 2008: 60; 8-16.

Winuthayanon W, Hewitt SC, Orvis GD, Behringer RR, and Korach KS. Uterine epithelial estrogen receptor alpha is dispensable for proliferation but essential for complete biological and biochemical responses. *Proc Natl Acad Sci U S A* 2010: 107; 19272-19277.

Winuthayanon W, Lierz SL, Delarosa KC, Sampels SR, Donoghue LJ, Hewitt SC, and Korach KS. Juxtacrine Activity of Estrogen Receptor alpha in Uterine Stromal Cells is Necessary for Estrogen-Induced Epithelial Cell Proliferation. *Sci Rep* 2017: 7; 8377.

Wolfler MM, Kuppers M, Rath W, Buck VU, Meinhold-Heerlein I, and Classen-Linke I. Altered expression of progesterone receptor isoforms A and B in human eutopic endometrium in endometriosis patients. *Ann Anat* 2016: 206; 1-6.

Wu MH, Lu CW, Chuang PC, and Tsai SJ. Prostaglandin E2: the master of endometriosis? *Exp Biol Med (Maywood)* 2010: 235; 668-677.

Wu SP, Li R, and DeMayo FJ. Progesterone Receptor Regulation of Uterine Adaptation for Pregnancy. *Trends Endocrinol Metab* 2018: 29; 481-491.

Wu Y, Strawn E, Basir Z, Halverson G, and Guo SW. Promoter hypermethylation of progesterone receptor isoform B (PR-B) in endometriosis. *Epigenetics* 2006: 1; 106-111.

Xie H, Chen P, Huang HW, Liu LP, and Zhao F. Reactive oxygen species downregulate ARID1A expression via its promoter methylation during the pathogenesis of endometriosis. *Eur Rev Med Pharmacol Sci* 2017: 21; 4509-4515.

Xu H, Becker CM, Lui WT, Chu CY, Davis TN, Kung AL, Birsner AE, D'Amato RJ, Wai Man GC, and Wang CC. Green tea epigallocatechin-3-gallate inhibits angiogenesis and suppresses vascular endothelial growth factor C/vascular endothelial growth factor receptor 2 expression and signaling in experimental endometriosis in vivo. *Fertil Steril* 2011: 96; 1021-1028.

Xu J, Liao L, Ning G, Yoshida-Komiya H, Deng C, and O'Malley BW. The steroid receptor coactivator SRC-3 (p/CIP/RAC3/AIB1/ACTR/TRAM-1) is required for normal growth, puberty, female reproductive function, and mammary gland development. *Proc Natl Acad Sci U S A* 2000: 97; 6379-6384.

Xu J, Qiu Y, DeMayo FJ, Tsai SY, Tsai MJ, and O'Malley BW. Partial hormone resistance in mice with disruption of the steroid receptor coactivator-1 (SRC-1) gene. *Science* 1998: 279; 1922-1925.

Xue Q, Lin Z, Cheng YH, Huang CC, Marsh E, Yin P, Milad MP, Confino E, Reierstad S, Innes J, *et al.* Promoter methylation regulates estrogen receptor 2 in human endometrium and endometriosis. *Biol Reprod* 2007: 77; 681-687.

Yang H, Kang K, Cheng C, Mamillapalli R, and Taylor HS. Integrative Analysis Reveals Regulatory Programs in Endometriosis. *Reprod Sci* 2015: 22; 1060-1072.

Yang H, Zhou Y, Edelshain B, Schatz F, Lockwood CJ, and Taylor HS. FKBP4 is regulated by HOXA10 during decidualization and in endometriosis. *Reproduction* 2012: 143; 531-538.

Yang Q, Wang Y, Pei G, Deng X, Jiang H, Wu J, Zhou C, Guo Y, Yao Y, Zeng R, *et al.* Bone marrow-derived Ly6C(-) macrophages promote ischemia-induced chronic kidney disease. *Cell Death Dis* 2019: 10; 291.

Yao Z, Shen X, Capodanno I, Donnelly M, Fenyk-Melody J, Hausamann J, Nunes C, Strauss J, and Vakerich K. Validation of rat endometriosis model by using raloxifene as a positive control for the evaluation of novel SERM compounds. *J Invest Surg* 2005: 18; 177-183.

Yin X, Pavone ME, Lu Z, Wei J, and Kim JJ. Increased activation of the PI3K/AKT pathway compromises decidualization of stromal cells from endometriosis. *J Clin Endocrinol Metab* 2012: 97; E35-43.

Yoo JY, Jeong JW, Fazleabas AT, Tayade C, Young SL, and Lessey BA. Protein Inhibitor of Activated STAT3 (PIAS3) Is Down-Regulated in Eutopic Endometrium of Women with Endometriosis. *Biol Reprod* 2016: 95; 11.

Yoo JY, Kim TH, Fazleabas AT, Palomino WA, Ahn SH, Tayade C, Schammel DP, Young SL, Jeong JW, and Lessey BA. KRAS Activation and over-expression of SIRT1/BCL6 Contributes to the Pathogenesis of Endometriosis and Progesterone Resistance. *Sci Rep* 2017: 7; 6765.

Yoo JY, Kim TH, Lee JH, Dunwoodie SL, Ku BJ, and Jeong JW. Mig-6 regulates endometrial genes involved in cell cycle and progesterone signaling. *Biochem Biophys Res Commun* 2015: 462; 409-414.

Yoo JY, Kim TH, Shin JH, Marquardt RM, Muller U, Fazleabas AT, Young SL, Lessey BA, Yoon HG, and Jeong JW. Loss of MIG-6 results in endometrial progesterone resistance via ERBB2. *Nat Commun* 2022: 13; 1101.

Yoo JY, Shin H, Kim TH, Choi WS, Ferguson SD, Fazleabas AT, Young SL, Lessey BA, Ha UH, and Jeong JW. CRISPLD2 is a target of progesterone receptor and its expression is decreased in women with endometriosis. *PLoS One* 2014: 9; e100481.

Yoo JY, Yang WS, Lee JH, Kim BG, Broaddus RR, Lim JM, Kim TH, and Jeong JW. MIG-6 negatively regulates STAT3 phosphorylation in uterine epithelial cells. *Oncogene* 2018: 37; 255-262.

Yu YR, O'Koren EG, Hotten DF, Kan MJ, Kopin D, Nelson ER, Que L, and Gunn MD. A Protocol for the Comprehensive Flow Cytometric Analysis of Immune Cells in Normal and Inflamed Murine Non-Lymphoid Tissues. *PLoS One* 2016: 11; e0150606.

Zackrisson S, van de Ven S, and Gambhir SS. Light in and sound out: emerging translational strategies for photoacoustic imaging. *Cancer Res* 2014: 74; 979-1004.

Zanatta A, Pereira RM, Rocha AM, Cogliati B, Baracat EC, Taylor HS, Motta EL, and Serafini PC. The relationship among HOXA10, estrogen receptor alpha, progesterone receptor, and progesterone receptor B proteins in rectosigmoid endometriosis: a tissue microarray study. *Reprod Sci* 2015: 22; 31-37.

Zeitoun K, Takayama K, Sasano H, Suzuki T, Moghrabi N, Andersson S, Johns A, Meng L, Putman M, Carr B, *et al.* Deficient 17beta-hydroxysteroid dehydrogenase type 2

expression in endometriosis: failure to metabolize 17beta-estradiol. *J Clin Endocrinol Metab* 1998: 83; 4474-4480.

Zhang K and Kang JU. Real-time intraoperative 4D full-range FD-OCT based on the dual graphics processing units architecture for microsurgery guidance. *Biomed Opt Express* 2011: 2; 764-770.

Zhang L, Patterson AL, Zhang L, Teixeira JM, and Pru JK. Endometrial stromal beta-catenin is required for steroid-dependent mesenchymal-epithelial cross talk and decidualization. *Reprod Biol Endocrinol* 2012: 10; 75.

Zhang Q, Dong P, Liu X, Sakuragi N, and Guo SW. Enhancer of Zeste homolog 2 (EZH2) induces epithelial-mesenchymal transition in endometriosis. *Sci Rep* 2017: 7; 6804.

Zhao H, Kalish F, Schulz S, Yang Y, Wong RJ, and Stevenson DK. Unique roles of infiltrating myeloid cells in the murine uterus during early to midpregnancy. *J Immunol* 2015: 194; 3713-3722.

Zhao Y and Chegini N. The expression of granulocyte macrophage-colony stimulating factor (GM-CSF) and receptors in human endometrium. *Am J Reprod Immunol* 1999: 42; 303-311.

Zhong Z, Wen Z, and Darnell JE, Jr. Stat3: a STAT family member activated by tyrosine phosphorylation in response to epidermal growth factor and interleukin-6. *Science* 1994: 264; 95-98.

Zhou M, Fu J, Xiao L, Yang S, Song Y, Zhang X, Feng X, Sun H, Xu W, and Huang W. miR-196a overexpression activates the MEK/ERK signal and represses the progesterone receptor and decidualization in eutopic endometrium from women with endometriosis. *Hum Reprod* 2016: 31; 2598-2608.

Zhu A, Ibrahim JG, and Love MI. Heavy-tailed prior distributions for sequence count data: removing the noise and preserving large differences. *Bioinformatics* 2019: 35; 2084-2092.

Zhu L and Pollard JW. Estradiol-17beta regulates mouse uterine epithelial cell proliferation through insulin-like growth factor 1 signaling. *Proc Natl Acad Sci U S A* 2007: 104; 15847-15851.

Zondervan KT, Becker CM, Koga K, Missmer SA, Taylor RN, and Vigano P. Endometriosis. *Nat Rev Dis Primers* 2018: 4; 9.

Zondervan KT, Becker CM, and Missmer SA. Endometriosis. *N Engl J Med* 2020: 382; 1244-1256.